AD-A069 020 SCIENCE APPLICATIONS INC ANN ARBOR MICH F/G 20/6
SPECTROSCOPIC DATA BASE FOR DF LASER TRANSMISSION MODELING.(U)
DEC 77 D R WOODS, D H LESLIE, J L MANNING N00173-76-C-0152 NL
UNCLASSIFIED SAI-77-912-AA

1 OF 2
AD A069020

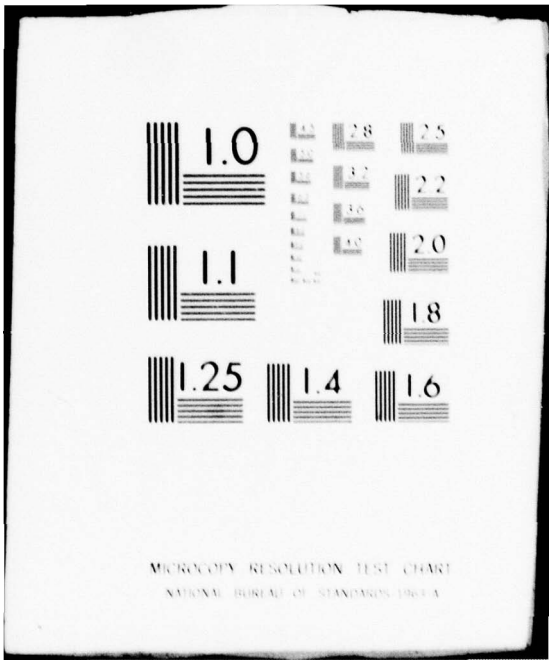
1.0
1.1
1.25
1.4
1.6
2.8
3.2
3.6
4.0
2.5
2.2
2.0
1.8
MICROCOPY RESOLUTION TEST CHART
NATIONAL BUREAU OF STANDARDS 1963-A

SAI-77-012-AA
December 1977

LEVEL

SPECTROSCOPIC DATA BASE FOR DF LASER TRANSMISSION MODELING

NRL #
539458

Prepared for:

Naval Research Laboratory
Washington, D.C. 20375

Contract #N00173-76-C-0152

Submitted by:

D.R. Woods
D.H. Leslie
J.L. Manning
R.E. Meredith

SCIENCE APPLICATIONS, INC.
15 Research Dr., P.O. Box 7329, Ann Arbor, MI 48107
(313) 662-3261

Unclassified

SECURITY CLASSIFICATION OF THIS PAGE (When Data Entered)

REPORT DOCUMENTATION PAGE		READ INSTRUCTIONS BEFORE COMPLETING FORM
1. REPORT NUMUER	2. GOVT ACCESSION NO.	3. RECIPIENT'S CATALOG NUMBER
4. TITLE (and Subtitle) SPECTROSCOPIC DATA BASE FOR DF LASER TRANSMISSION MODELING.		5. TYPE OF REPORT & PERIOD COVERED Final Report,
		6. PERFORMING ORG. REPORT NUMBER SAI-77-012-AA
7. AUTHOR(s) D.R. Woods, D.H. Leslie, J.L. Manning R.E. Meredith		8. CONTRACT OR GRANT NUMBER(s) N00173-76-C-0152
9. PERFORMING ORGANIZATION NAME AND ADDRESS Science Applications, Inc. P.O. Box 7329 Ann Arbor, MI 48107		10. PROGRAM ELEMENT, PROJECT, TASK AREA & WORK UNIT NUMBERS
11. CONTROLLING OFFICE NAME AND ADDRESS Naval Research Laboratory Washington, D.C. 20375		12. REPORT DATE December 1977
		13. NUMBER OF PAGES 162
14. MONITORING AGENCY NAME & ADDRESS(if different from Controlling Office) (12) 168 p.		15. SECURITY CLASS. (of this report) Unclassified
		15a. DECLASSIFICATION/DOWNGRADING SCHEDULE

16. DISTRIBUTION STATEMENT (of this Report)

DISTRIBUTION STATEMENT A
Approved for public release
Distribution Unlimited

17. DISTRIBUTION STATEMENT (of the abstract entered in Block 20, if different from Report)

18. SUPPLEMENTARY NOTES

19. KEY WORDS (Continue on reverse side if necessary and identify by block number)

approx. 2 micrometers

20. ABSTRACT (Continue on reverse side if necessary and identify by block number)

High resolution ($\leq .05/cm^{-1}$) molecular line absorption measurements have been performed in the 3-5 μm spectral region. This data completes the measurements activities directed toward developing field verified predictive modeling of DF laser atmospheric molecular absorption.

Some 181 HDO line profile measurement sets are presented for the path length and partial pressure combinations required to determine the air broadened HDO line parameters. Also, synthetic atmospheric

DD FORM 1 JAN 73 1473 EDITION OF 1 NOV 65 IS OBSOLETE

Unclassified

SECURITY CLASSIFICATION OF THIS PAGE (When Data Entered)

molecular absorption spectra have been generated for the several molecular absorbers (N_2O, CH_4, HDO, CO_2) known to be important in the DF laser region.

During the course of the DF transmission modeling effort, it became apparent that the line of sight molecular content should depend on the location and environmental conditions. To monitor the HDO molecular content, a Gas Filter Correlation Spectrometer (GFCS) was designed, constructed and delivered to NRL. Since the variability of HDO in the real atmosphere was shown by NRL to be quite dramatic and important, a design study to expand the GFCS capability was initiated. This study is included in this report.

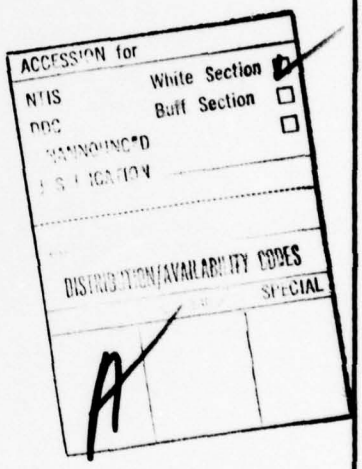

CONTENTS

LIST OF ILLUSTRATIONS

LIST OF TABLES

1
INTRODUCTION

For the past four years spectroscopic measurements and modeling activities directed to developing a more precise understanding of laser transmission have been in progress [1-4]. The measurements objectives of this work has been to develop a spectroscopic data base from which atmospheric absorption line strength, width and position parameters may be extracted. The long term objective has been to use this data base to develop modeling algorithms to predict atmospheric molecular absorption at laser frequencies. It has long been known [2,5] that molecular absorption may change by orders of magnitude in a spectral interval of less than a wavenumber, and that a precise line parameter data base is required for satisfactory predictive modeling.

Measurements have been restricted to high resolution ($\leq .05$ cm^{-1}) molecular line absorption in the .9 μm, 3-5 μm, and 10-11 μm spectral regions. Most recently, these activities have been restricted to the 3.0-5.0 μm region where the DF laser operates.

The investigation reported here completes the measurements activities directed toward developing field verified predictive modeling of DF laser atmospheric molecular absorption. In this report, some 181 HDO line profile measurement sets are presented for the path length and partial pressure combinations required to determine the air broadened HDO line parameters. Also, synthetic atmospheric molecular absorption spectra have been generated for the several molecular absorbers (N_2O, CH_4, HDO, CO_2) known to be important in the DF laser region.

The DF transmission algorithms have been presented in a companion report [4]. Comparisons between field data [6,7] and predictive modeling developed here have been made.

During the course of the DF transmission modeling effort, it became apparent that the line of sight molecular content should depend on the location and environmental conditions, in general, and that techniques must be developed to monitor molecular content during laser transmission measurements. Since HDO had been identified as the most important line absorber, and since its natural abundance and its variability with local conditions was not understood, a Gas Filter Correlation Spectrometer (GFCS) was designed, constructed and delivered to NRL to be used to monitor actual line of sight HDO content [8]. Since the variability of HDO in the real atmosphere was shown by NRL to be quite dramatic and important, a design study to expand the GFCS capability was initiated. This study is included in Section 5 of this report.

A status summary of DF transmission modeling is included in Section 6.

2
ATMOSPHERIC TRANSMISSION CALCULATIONS

It is required that accurate transmission algorithms be developed for all DF laser lines from which significant power is extracted in the high energy laser (HEL) devices. For this reason, synthetic atmospheric transmission spectra have been calculated using the SAI developed code SYNSPC [4] to establish the importance of each absorber, and to identify discrepancies with laboratory or NRL field data. In this section, a calculation of composite transmission for the Mid-Latitude Summer (MLS) model atmosphere [9] and individual components are described. The components considered are CO_2, N_2O, HDO, and CH_4. In all cases, the N_2 continuum is included since it is a non variable component at sea level.

2.1 CALCULATIONS FOR THE MLS MODEL ATMOSPHERE

Synthetic transmission spectra for the Midlattitude Summer Model Atmosphere were calculated for the nominal 5 km path used by NRL for their long path measurements. Plots using the SAI SYNSPC code are given in Figures 1a - 1q. The SYNSPC code has been described in the companion report [4]. Since the motivation for these calculations is identification of absorption features and determination of transmission magnitudes, infinite resolution is assumed. The nominal concentrations for mixed gases are used, as indicated by the information format above each plot. The .03% value for the HDO/H_2O ratio is used, although tentative NRL data indicates that this ratio is variable, and sensitive to meteorological conditions. The N_2 continuum is that measured by Burch [10]. In addition to CO_2 line absorption, it is well known that CO_2 line wing absorption is sub-Lorentzian, and that the use of Lorentz shapes under predicts transmission most importantly at wavelengths shorter than the CO_2 band head. In these calculations, Lorentz shapes have been used.

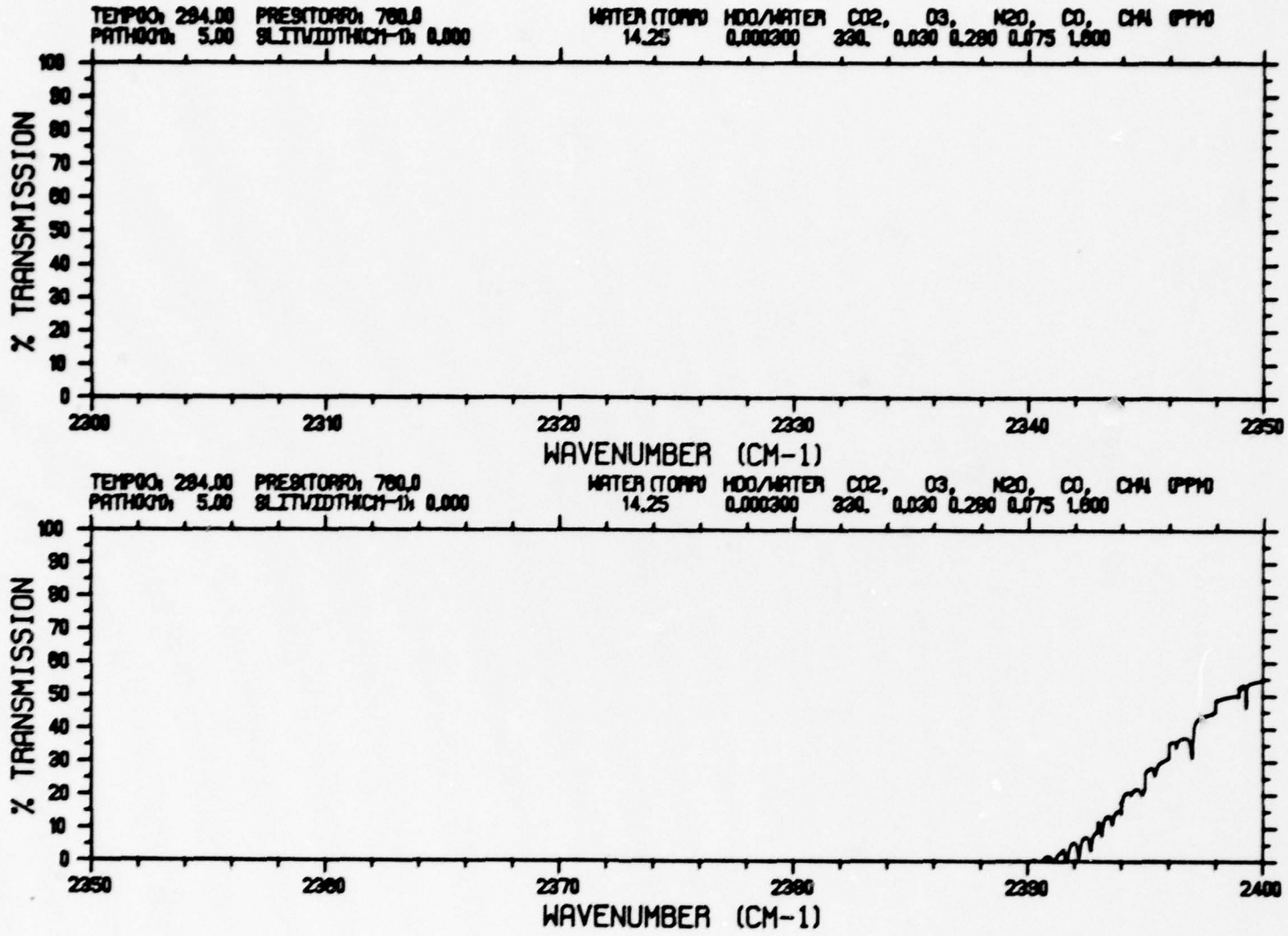

FIGURE 1a. ATMOSPHERIC TRANSMISSION FOR THE MIDLATITUDE SUMMER ATMOSPHERIC MODEL FOR THE INDICATED CONDITIONS, BETWEEN 2300 CM^{-1} AND 4000 CM^{-1}

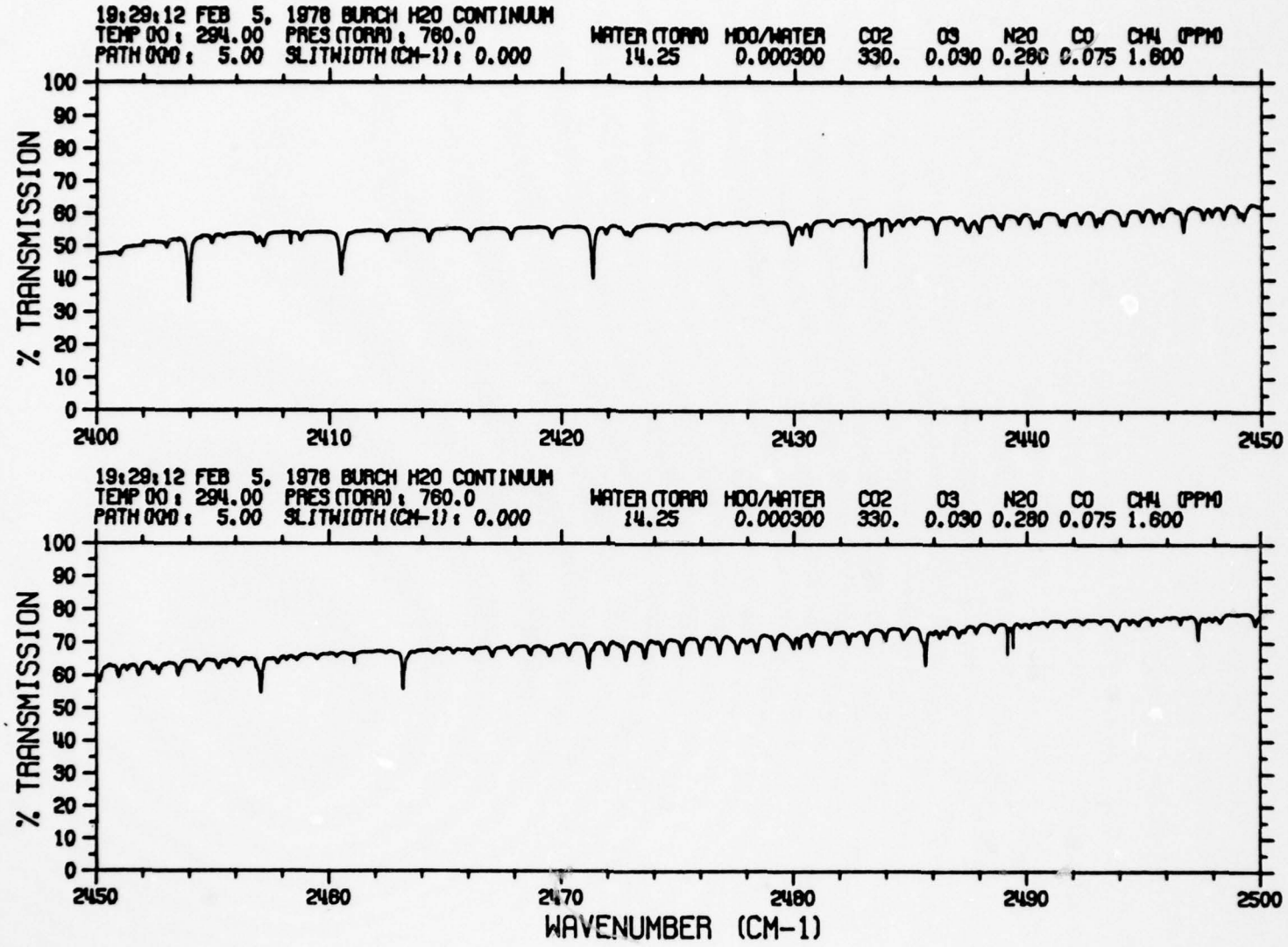

FIGURE 1b. FIGURE 1 CONTINUED

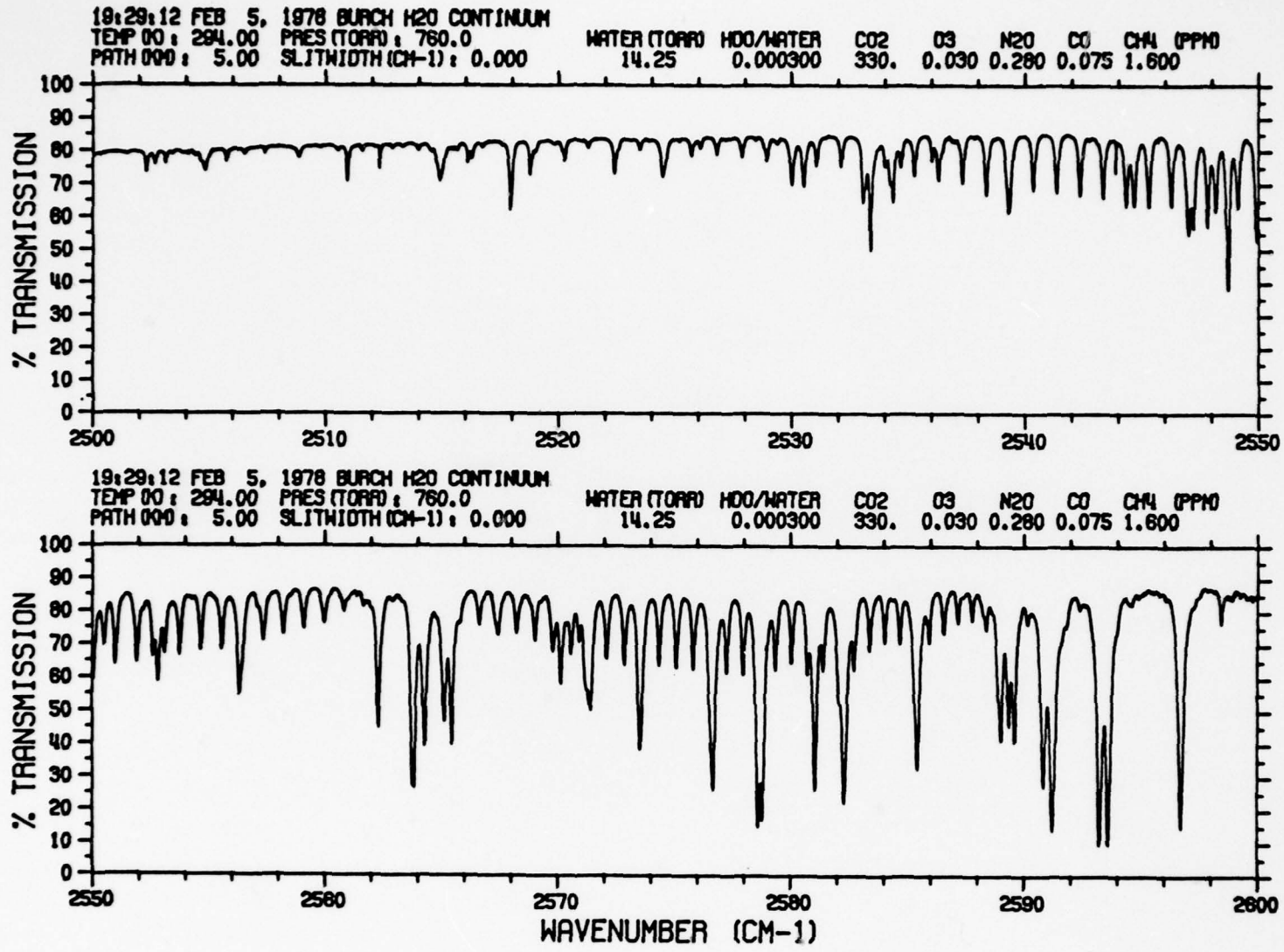

FIGURE 1c. FIGURE 1 CONTINUED

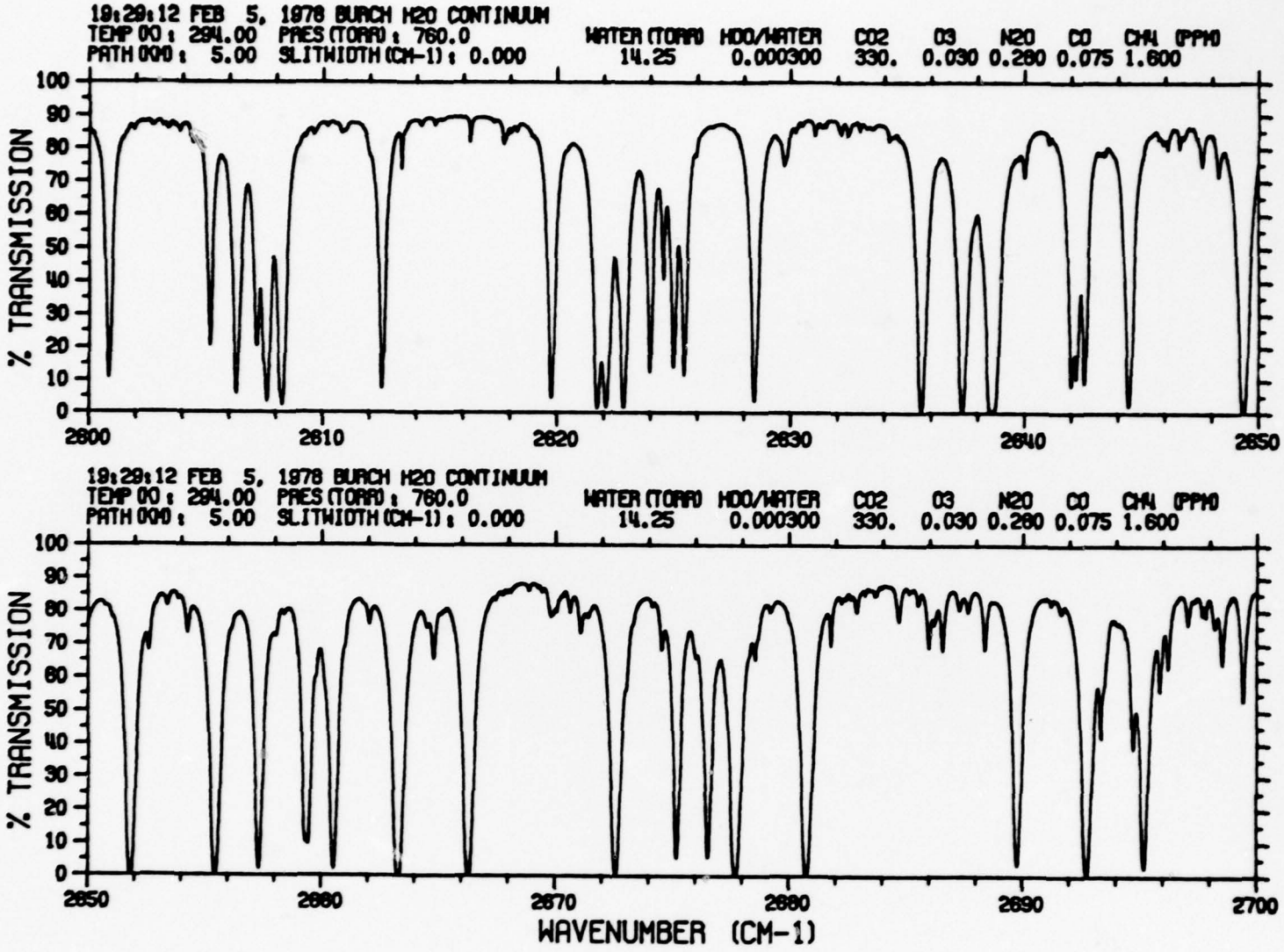

FIGURE 1d. FIGURE 1 CONTINUED

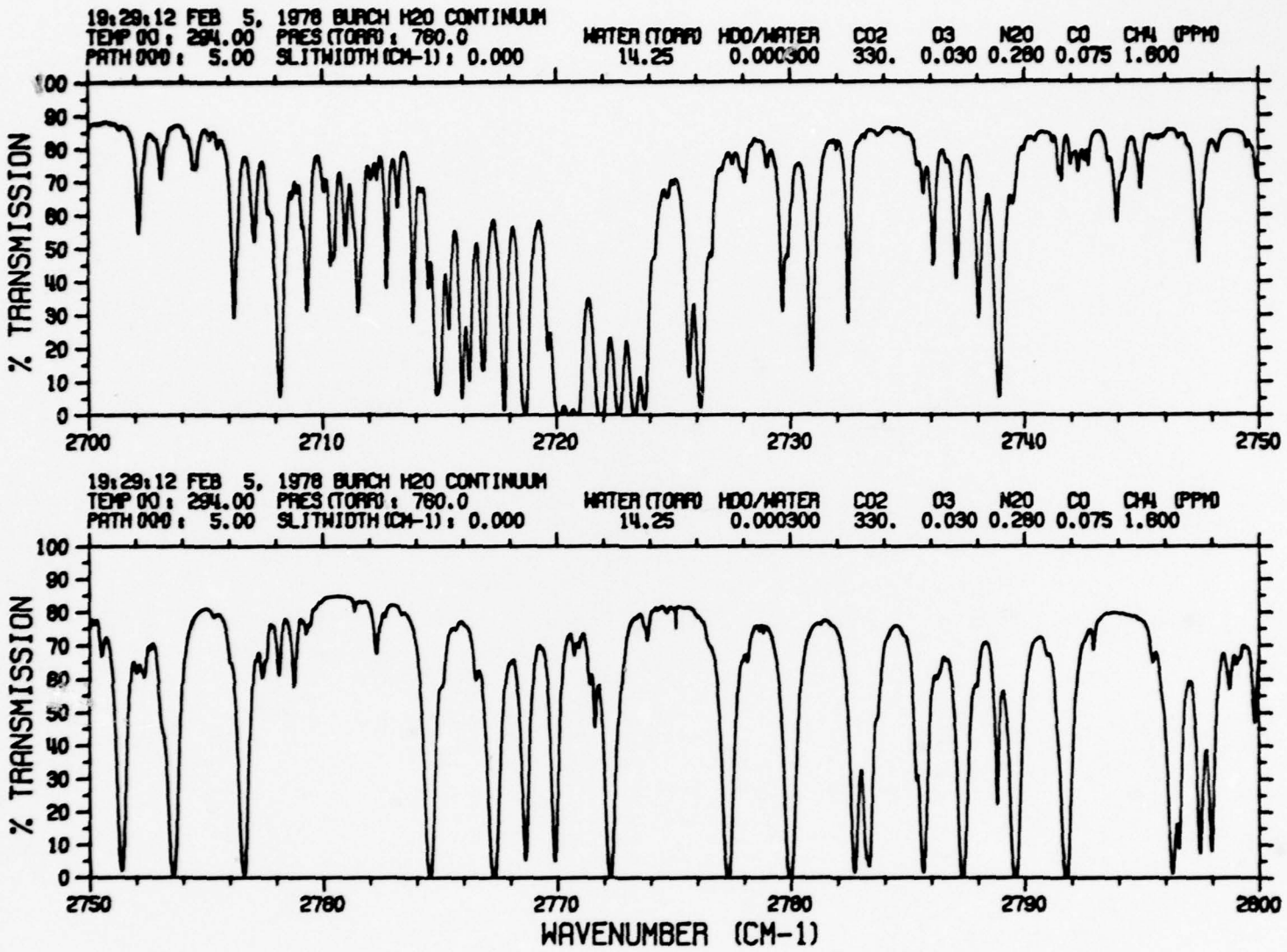

FIGURE 1e. FIGURE 1 CONTINUED

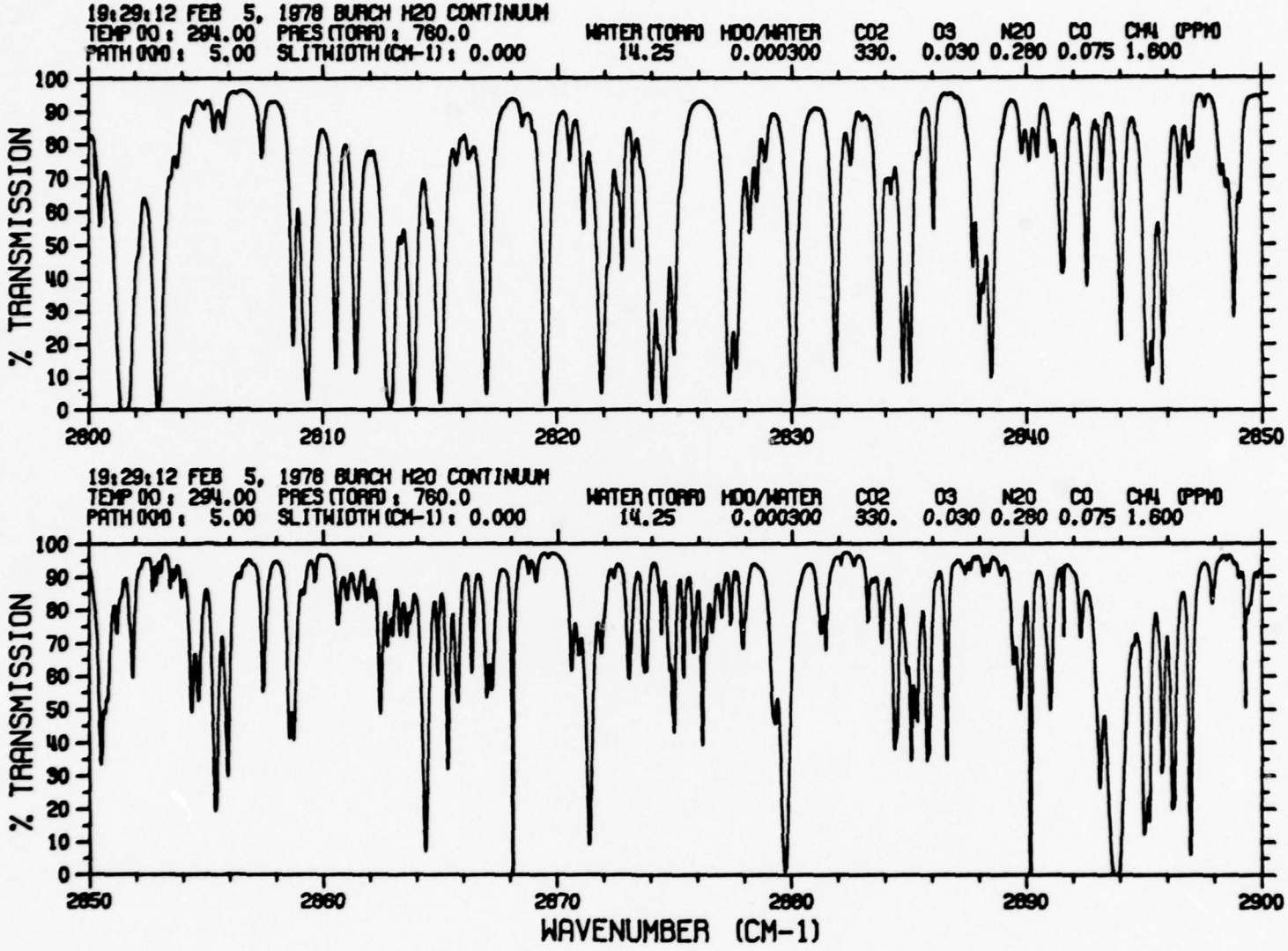

FIGURE 1f. FIGURE 1 CONTINUED

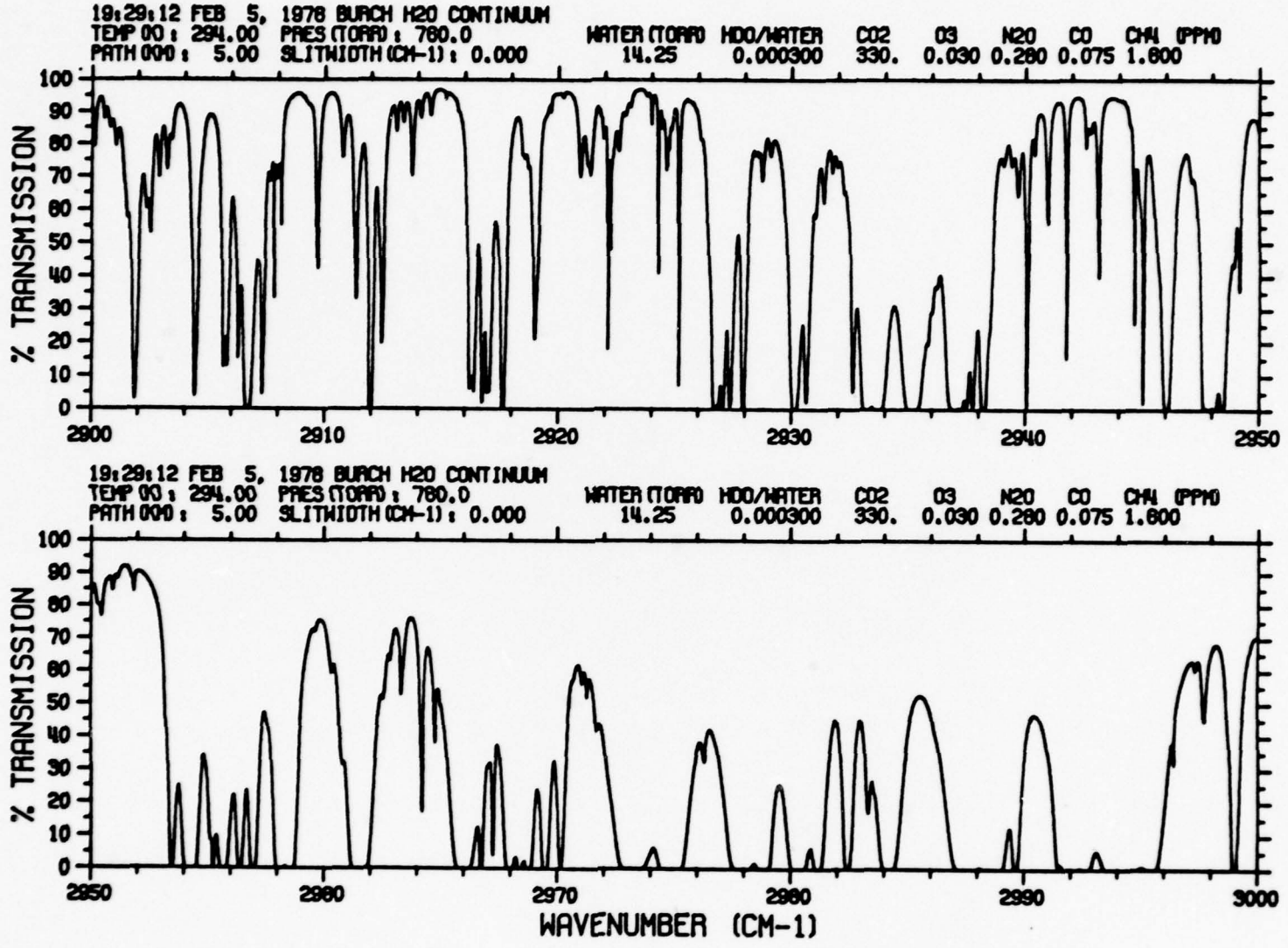

FIGURE 1g. FIGURE 1 CONTINUED

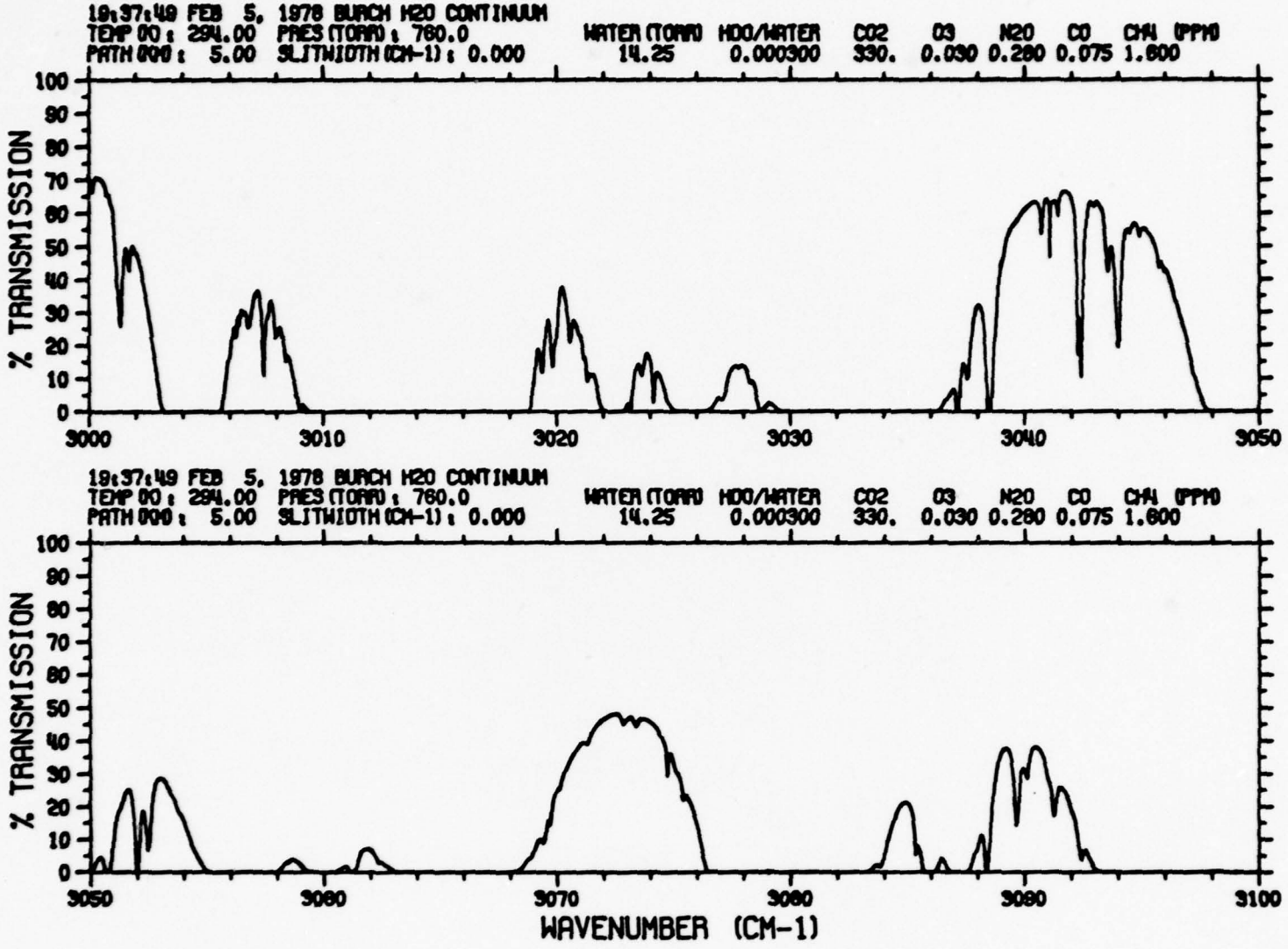

FIGURE 1h. FIGURE 1 CONTINUED

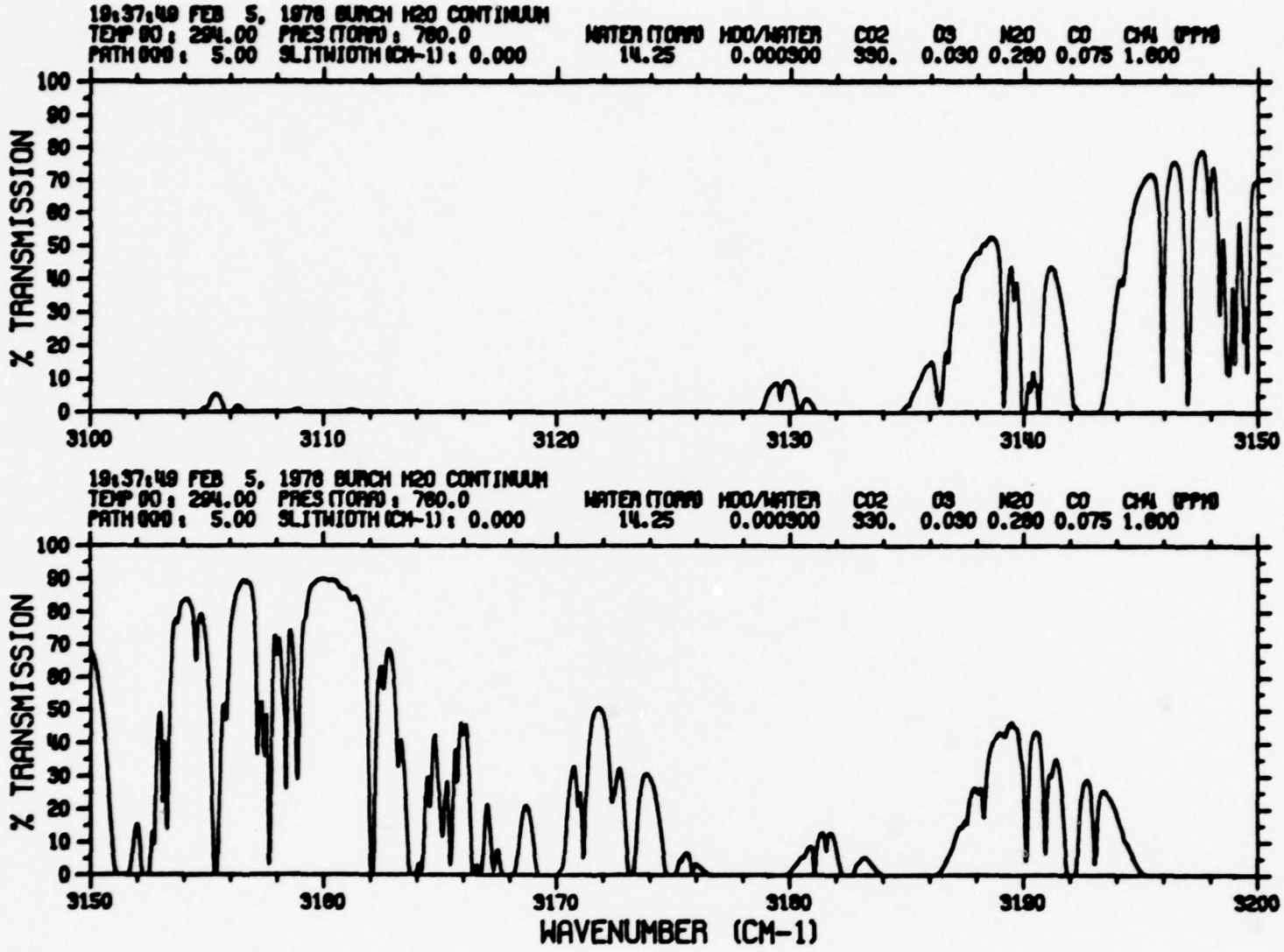

FIGURE 1i. FIGURE 1 CONTINUED

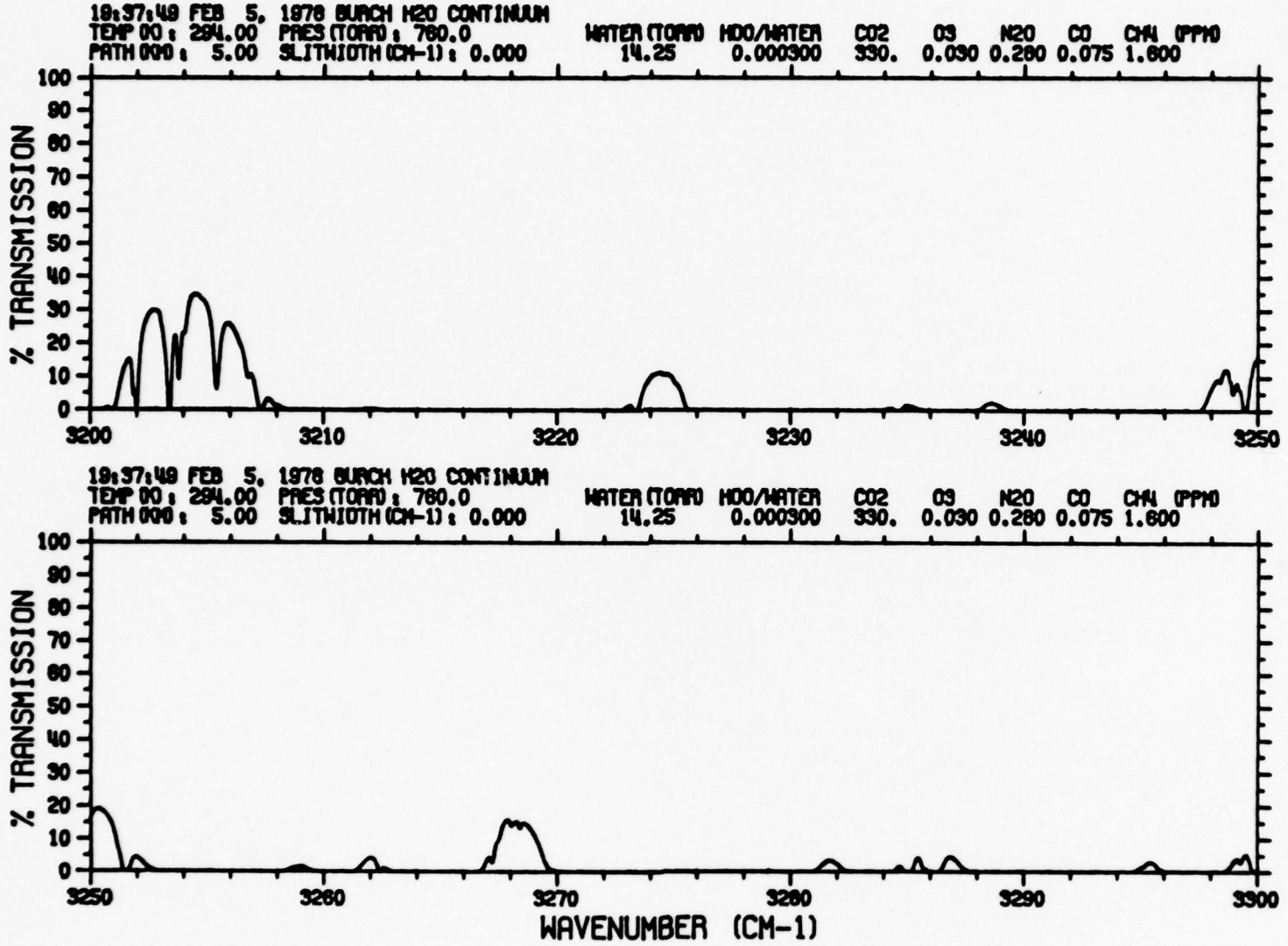

FIGURE 1j. FIGURE 1 CONTINUED

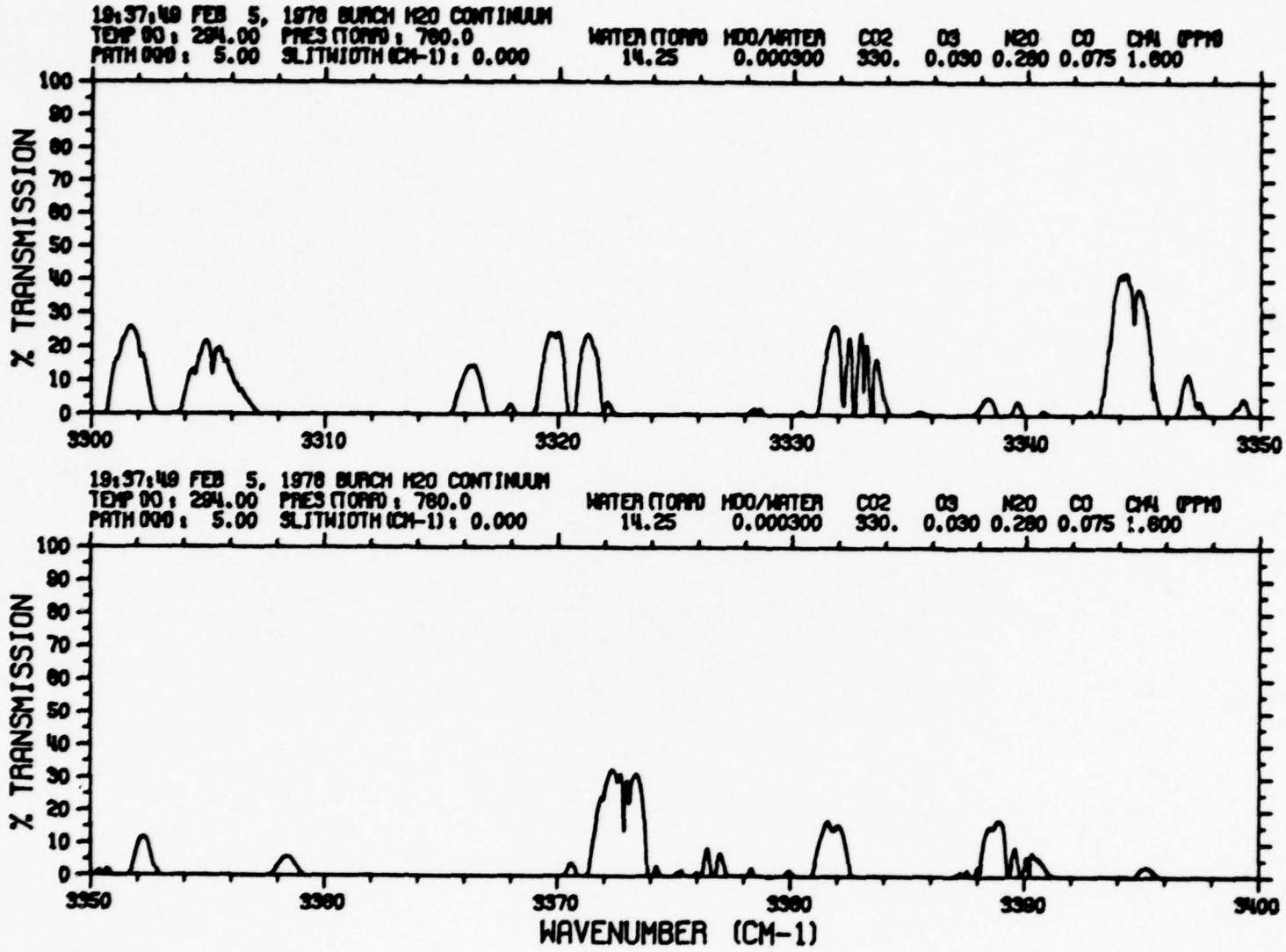

FIGURE 1k. FIGURE 1 CONTINUED

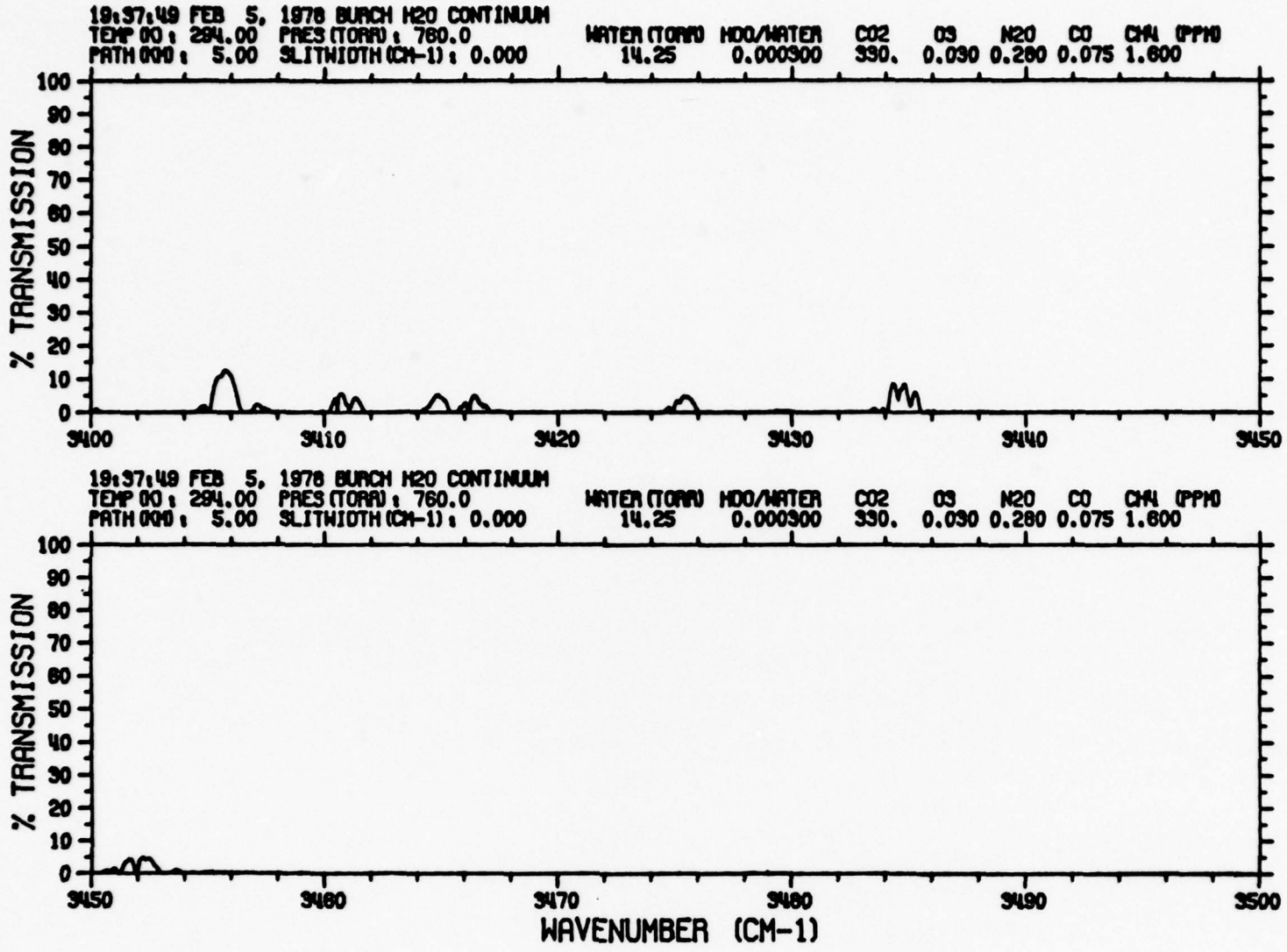

FIGURE 11. FIGURE 1 CONTINUED

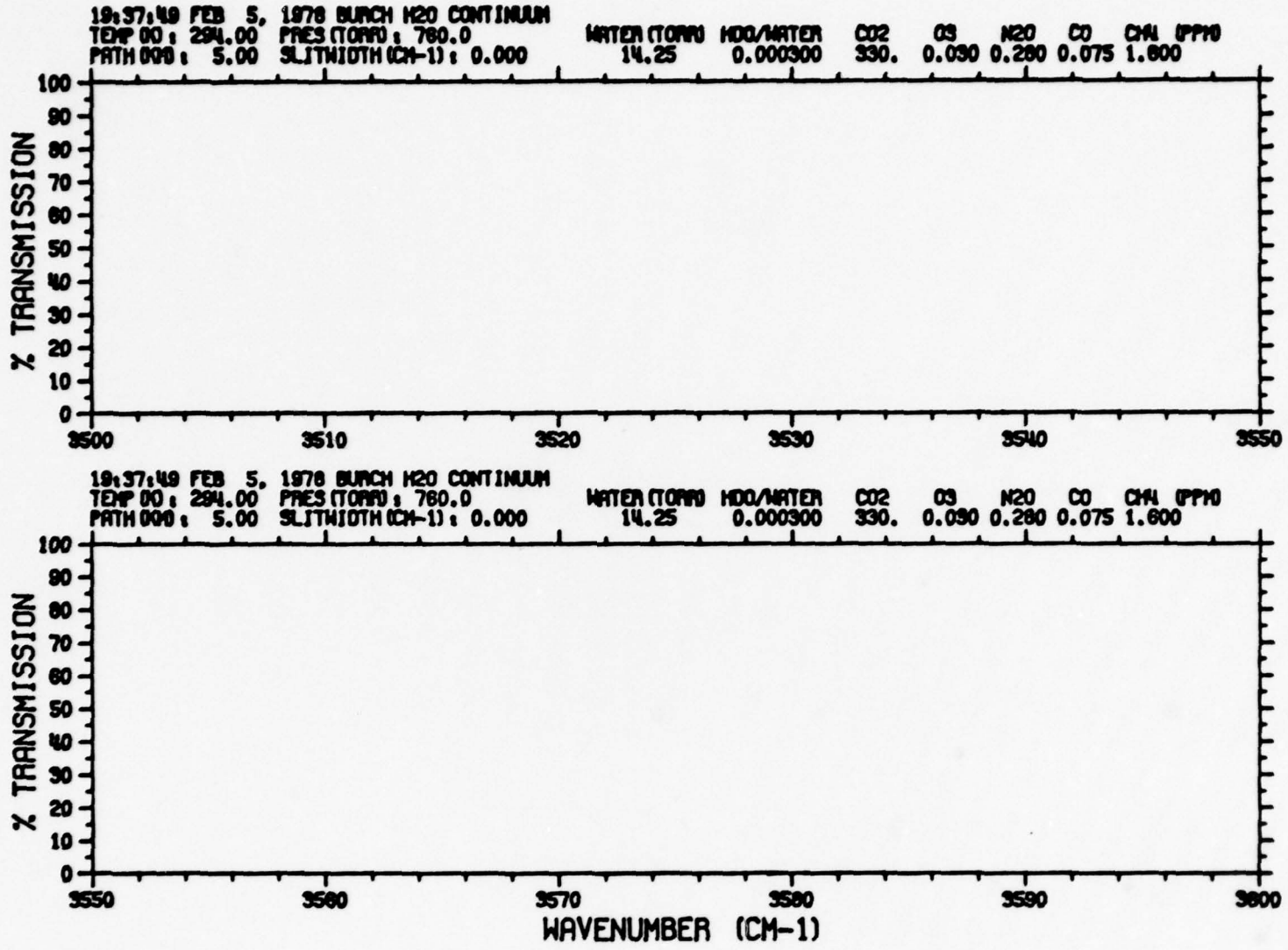

FIGURE 1m. FIGURE 1 CONTINUED

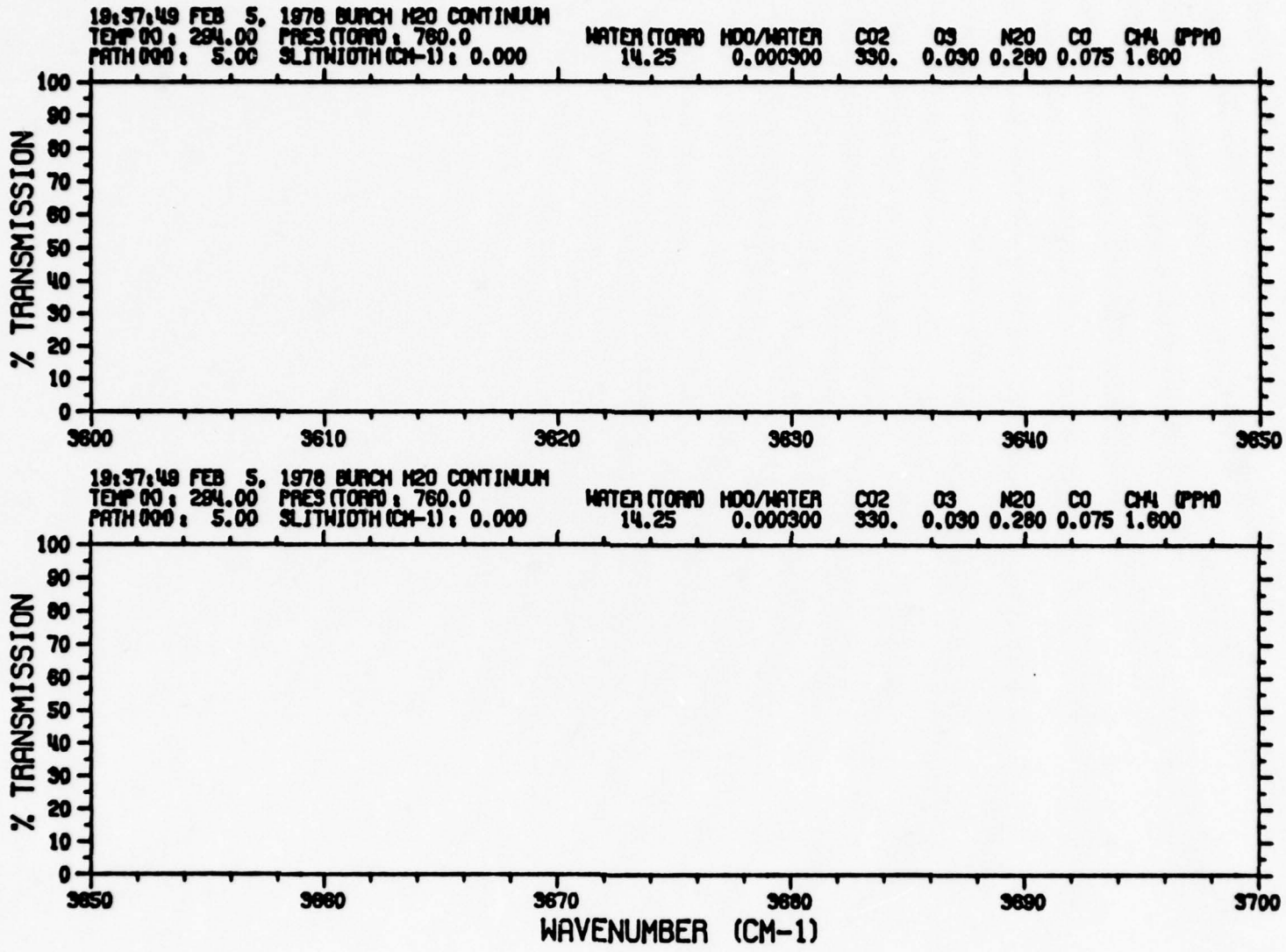

FIGURE 1n. FIGURE 1 CONTINUED

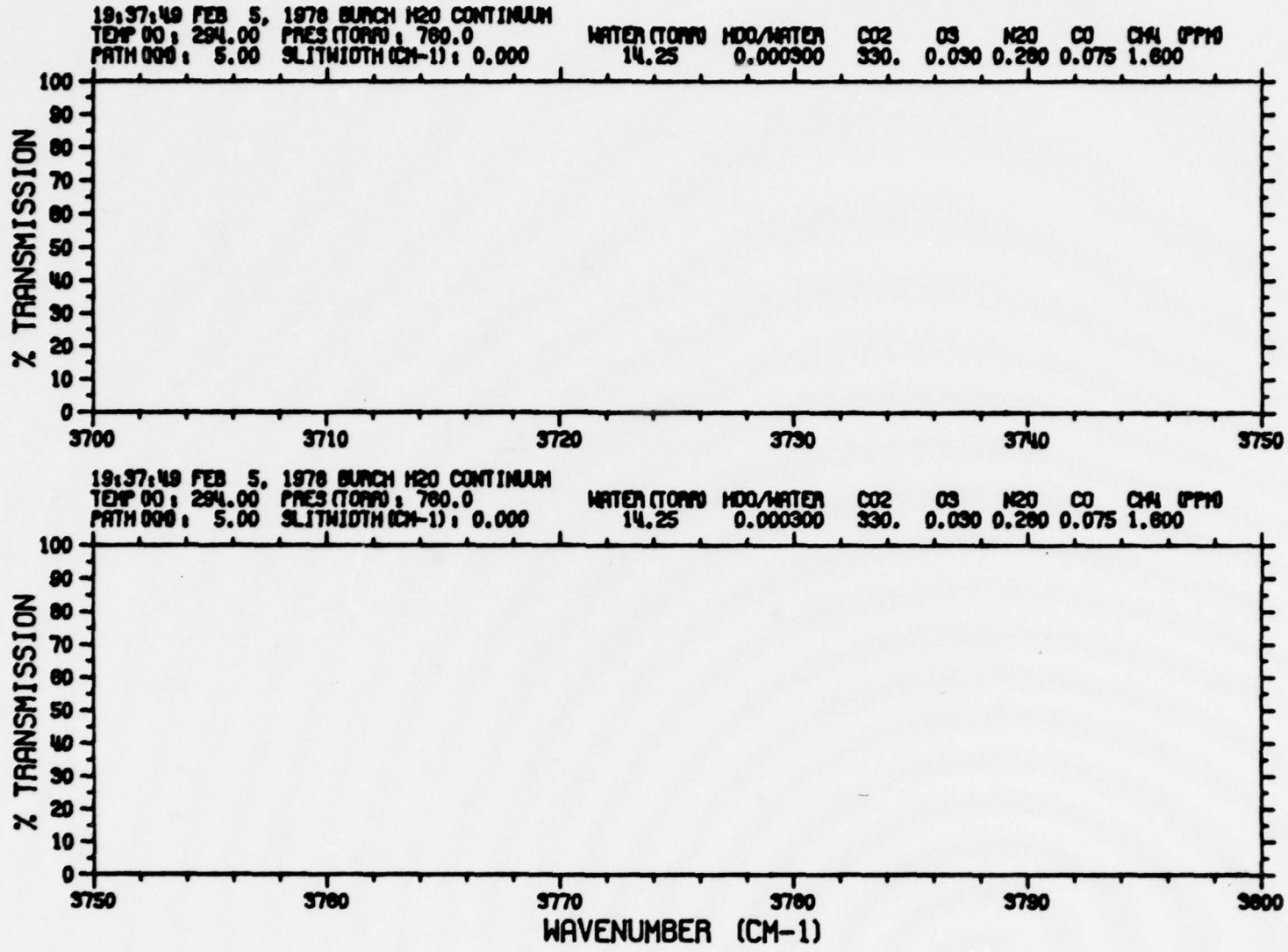

FIGURE 1o. FIGURE 1 CONTINUED

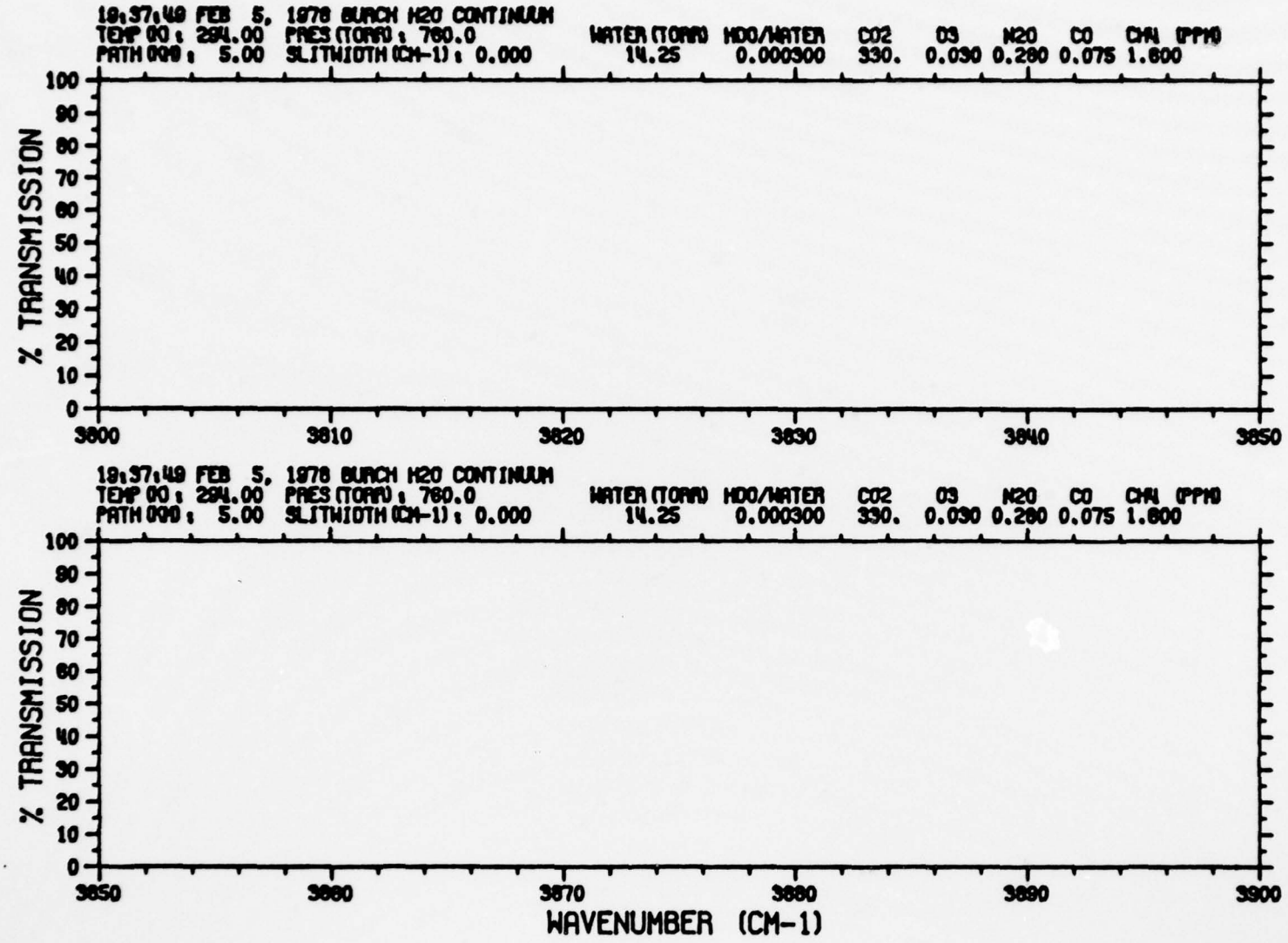

FIGURE 1p. FIGURE 1 CONTINUED

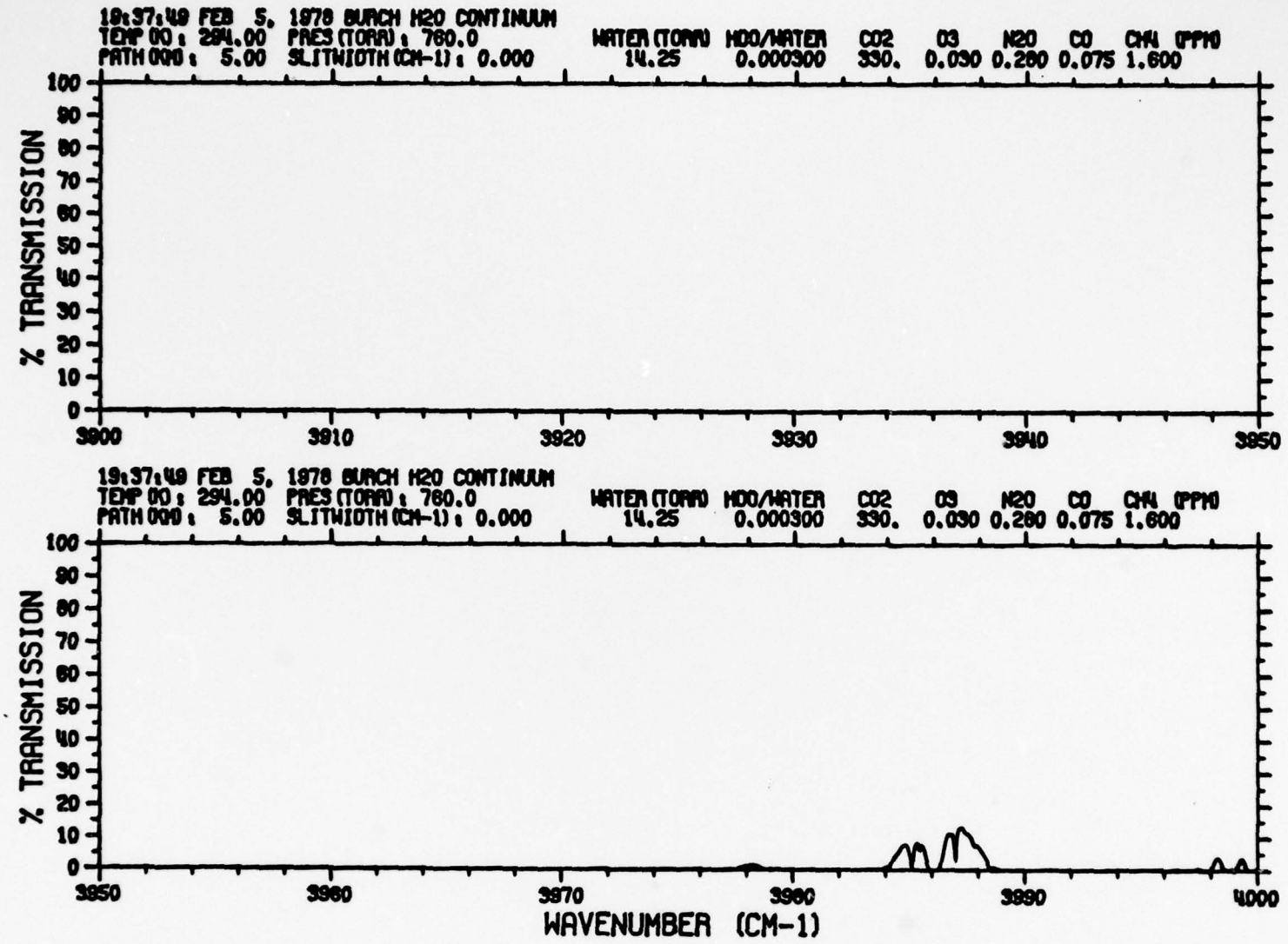

FIGURE 1q. FIGURE 1 CONTINUED

2.2 CO_2 TRANSMISSION SPECTRA

The CO_2 component of the atmospheric transmission shown in Figure 1 has been calculated spearately. These results are shown in Figures 2a - 2n. N_2 continuum is included.

The CO_2 continuum absoprtion caused by the Lorentz wing is evident. Also, the spectral region between ~2.390 cm^{-1} and ~2406 cm^{-1} is seen to have a small computational error. This error causes the unrealistic appearance of the line absorption superimposed on the continuum and wing absorption. The cause of this effect has been determined, and corrections to the code will be made.

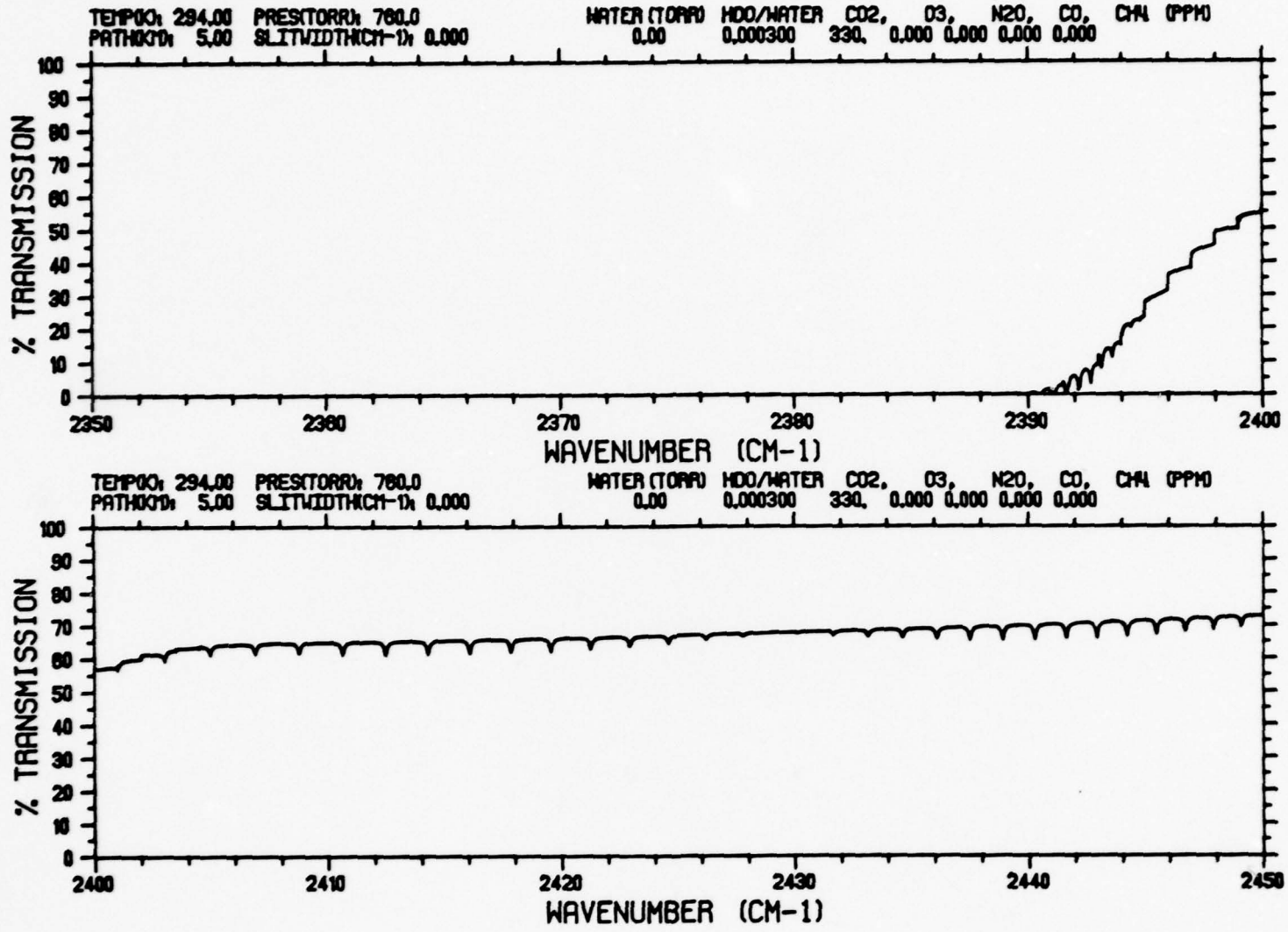

FIGURE 2a. ATMOSPHERIC TRANSMISSION FOR THE CO_2 AND N_2 COMPONENT OF FIGURE 1

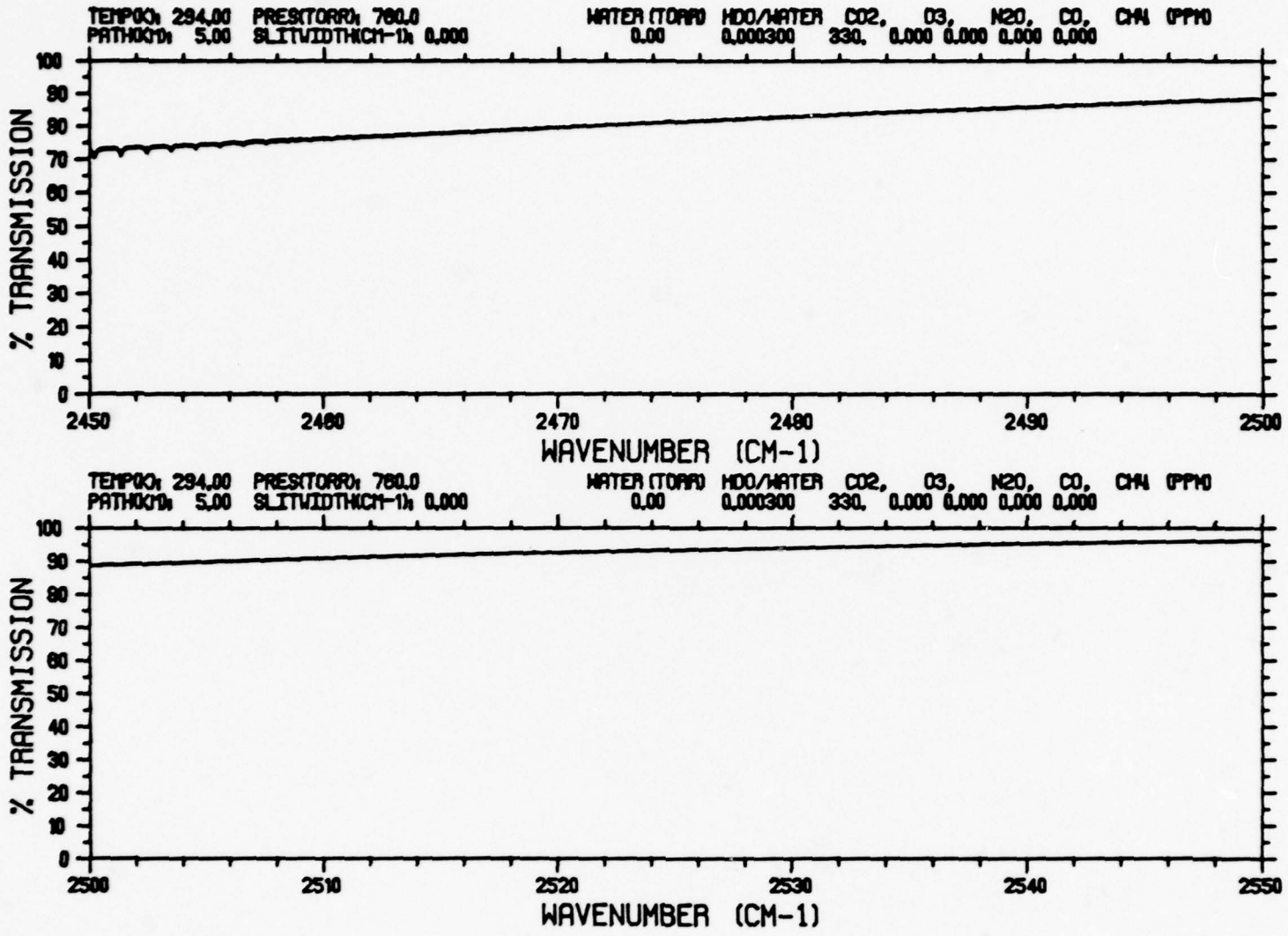

FIGURE 2b. FIGURE 2 CONTINUED

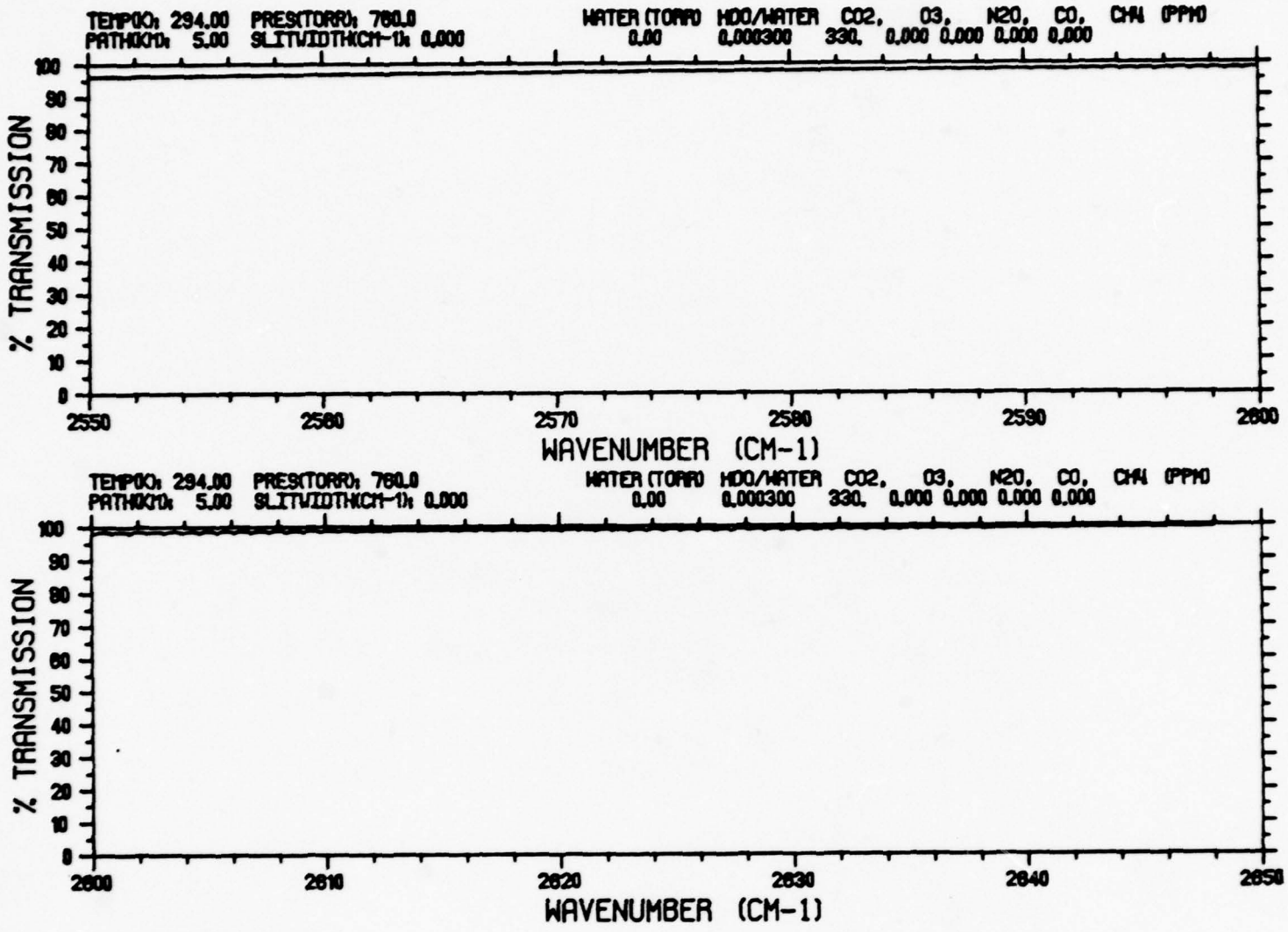

FIGURE 2c. FIGURE 2 CONTINUED

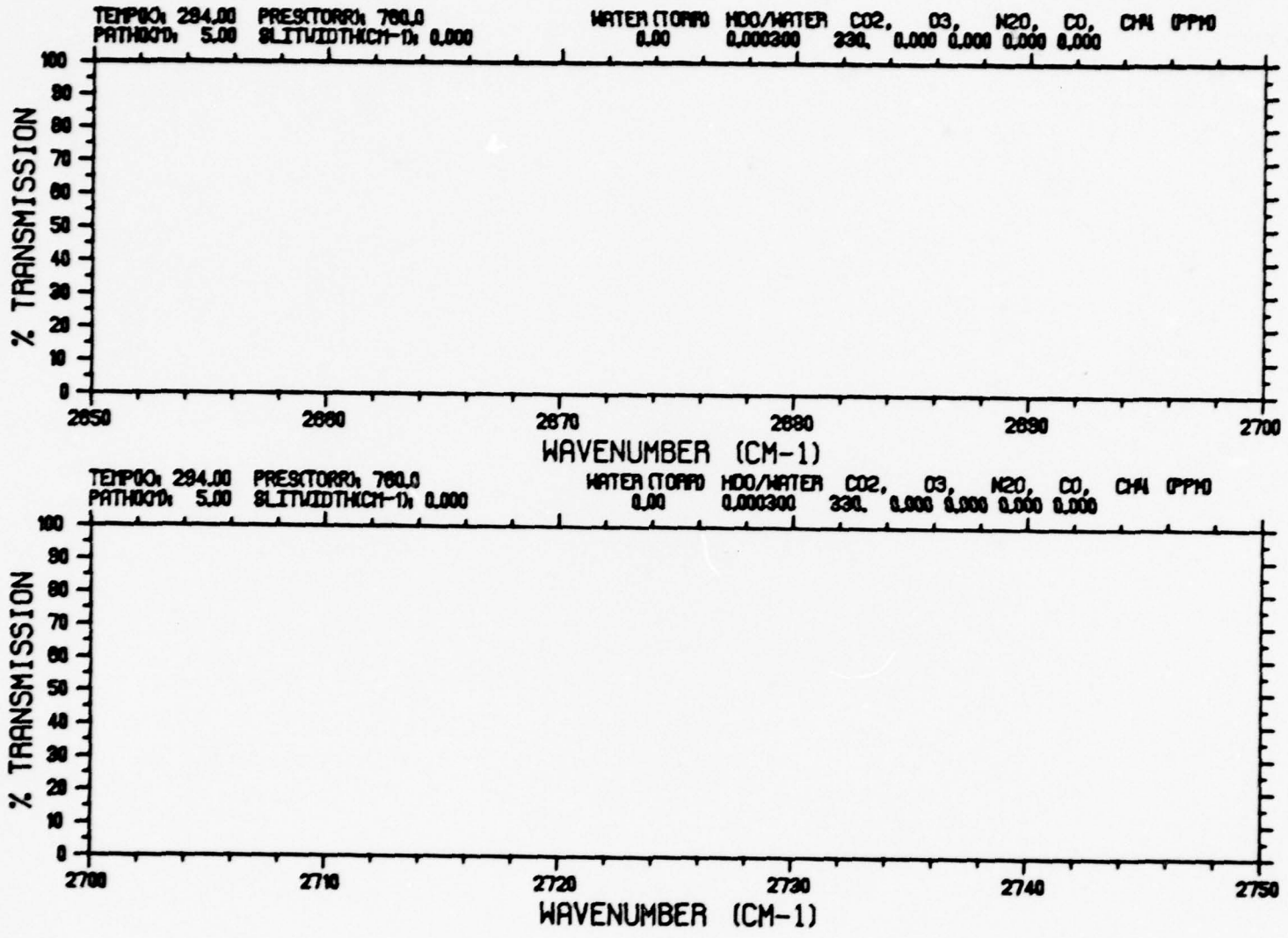

FIGURE 2d. FIGURE 2 CONTINUED

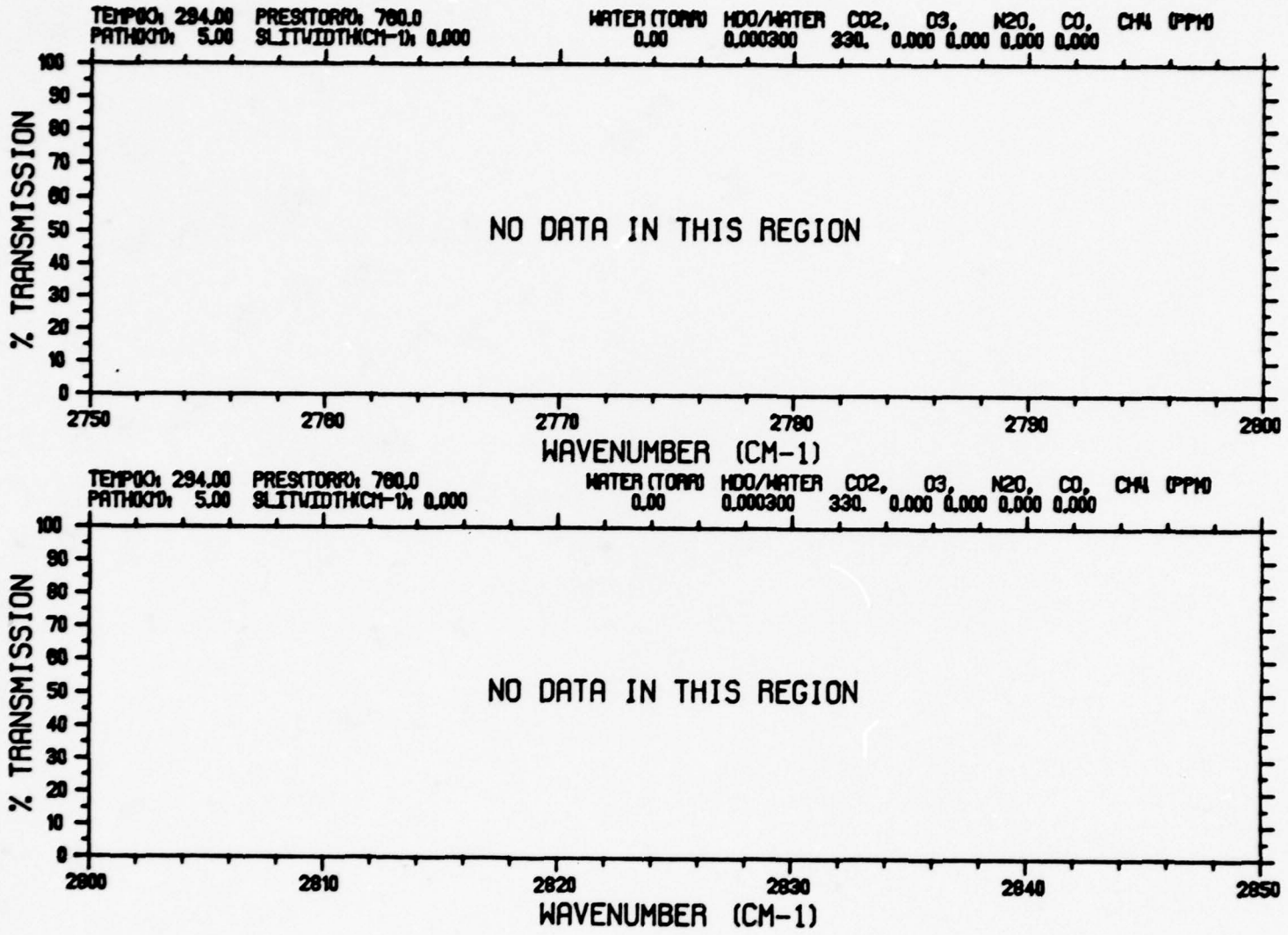

FIGURE 2e. FIGURE 2 CONTINUED

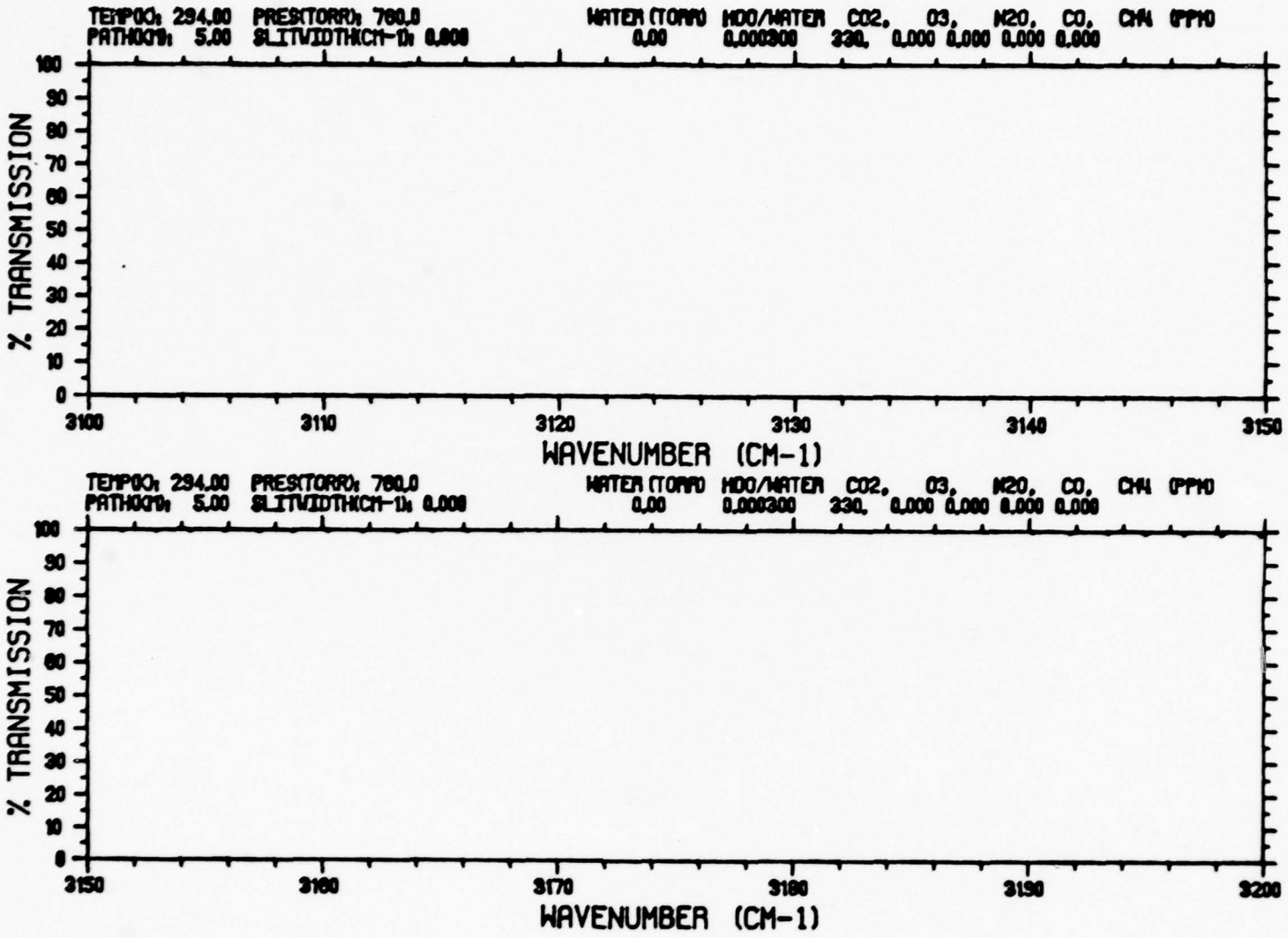

FIGURE 2f. FIGURE 2 CONTINUED

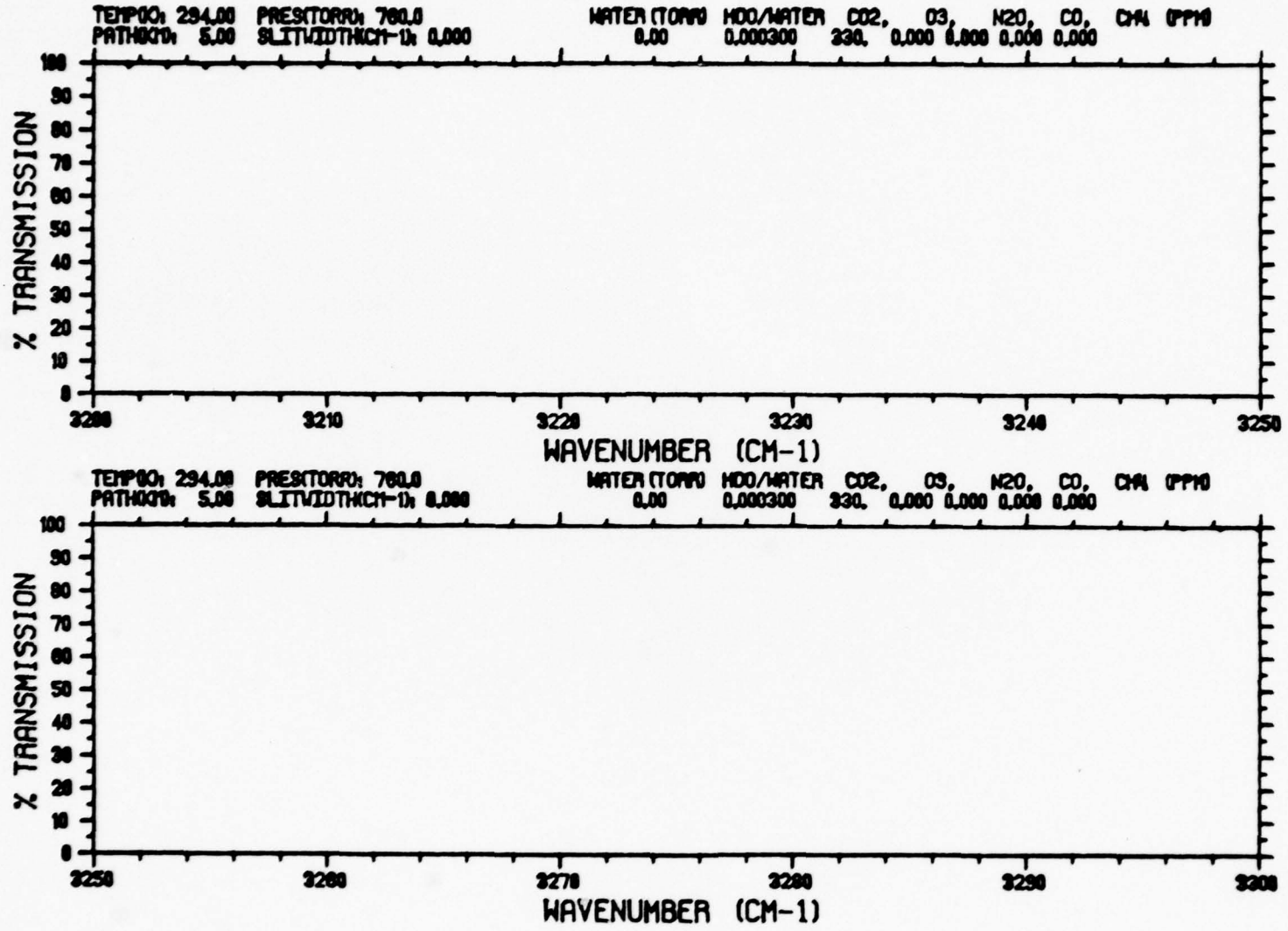

FIGURE 2g. FIGURE 2 CONTINUED

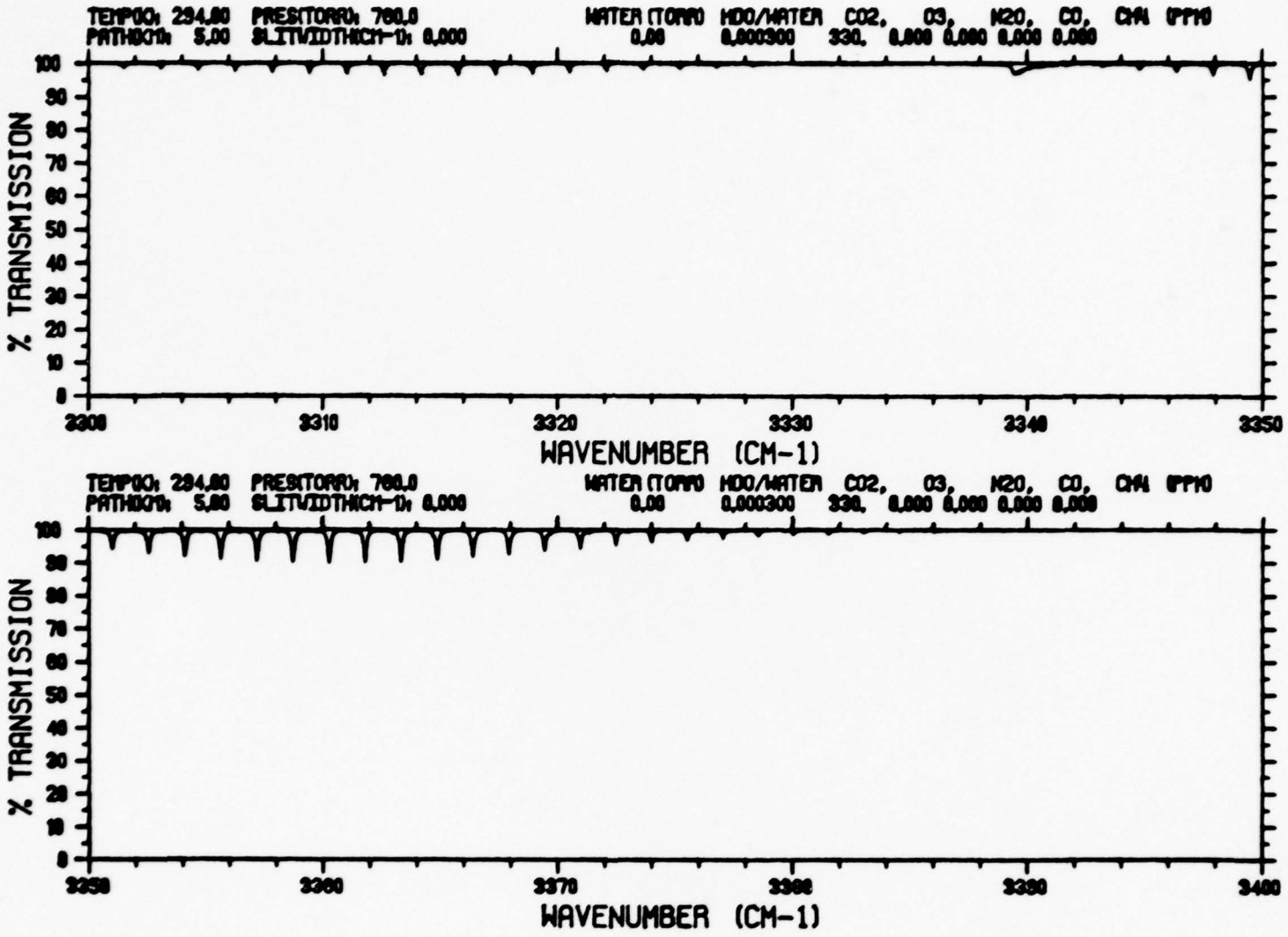

FIGURE 2h. FIGURE 2 CONTINUED

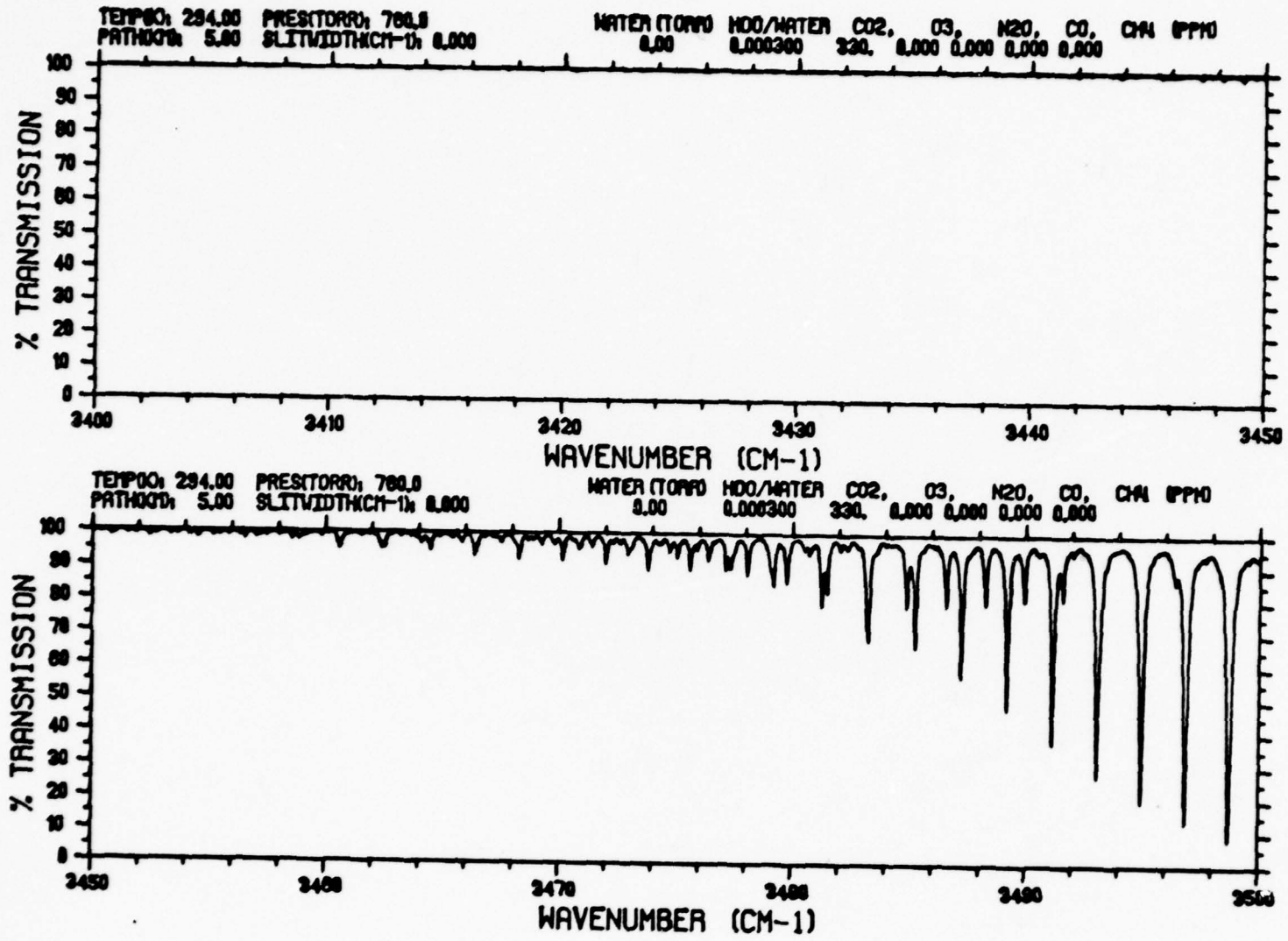

FIGURE 2i. FIGURE 2 CONTINUED

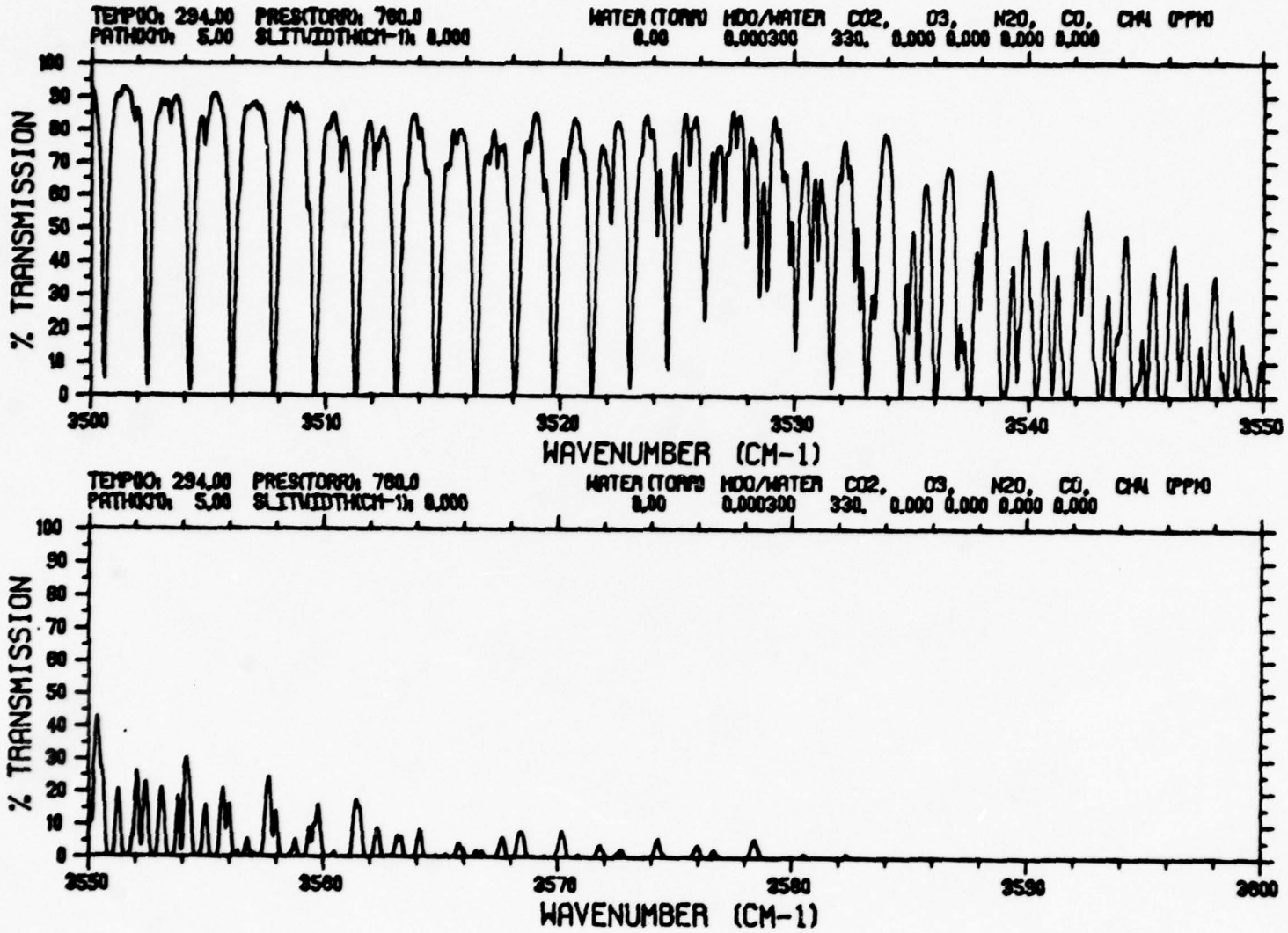

FIGURE 2j. FIGURE 2 CONTINUED

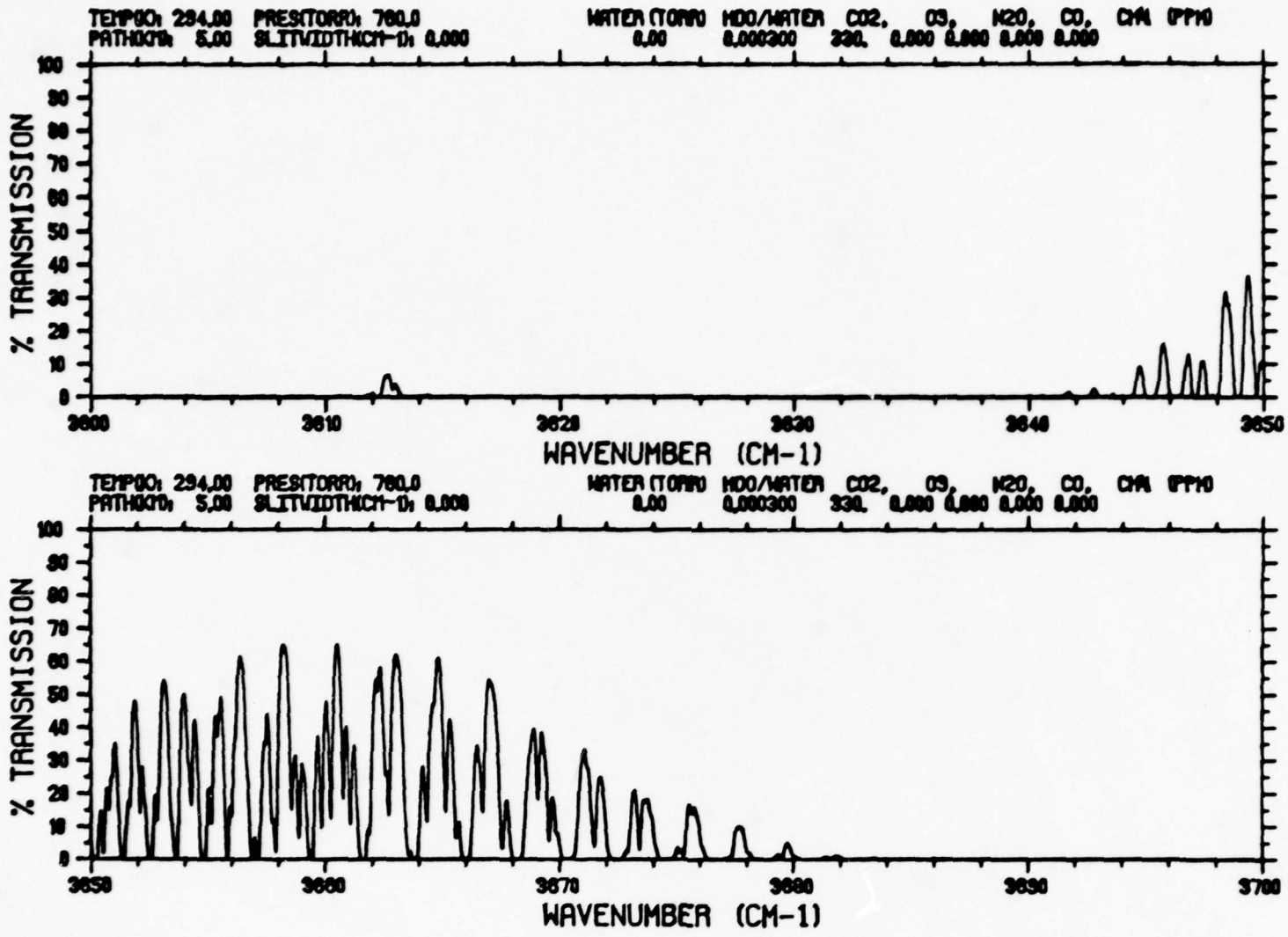

FIGURE 2k. FIGURE 2 CONTINUED

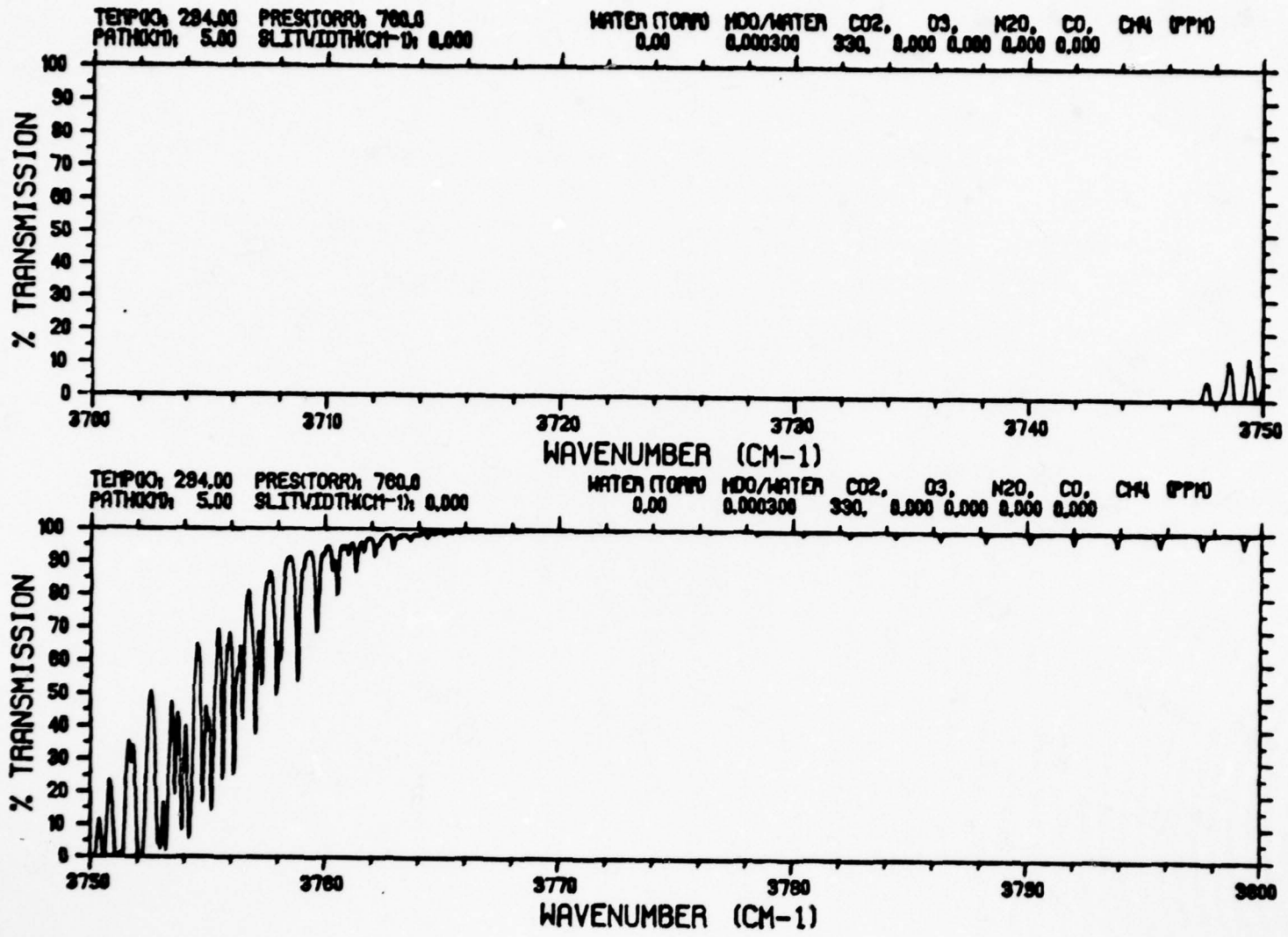

FIGURE 21. FIGURE 2 CONTINUED

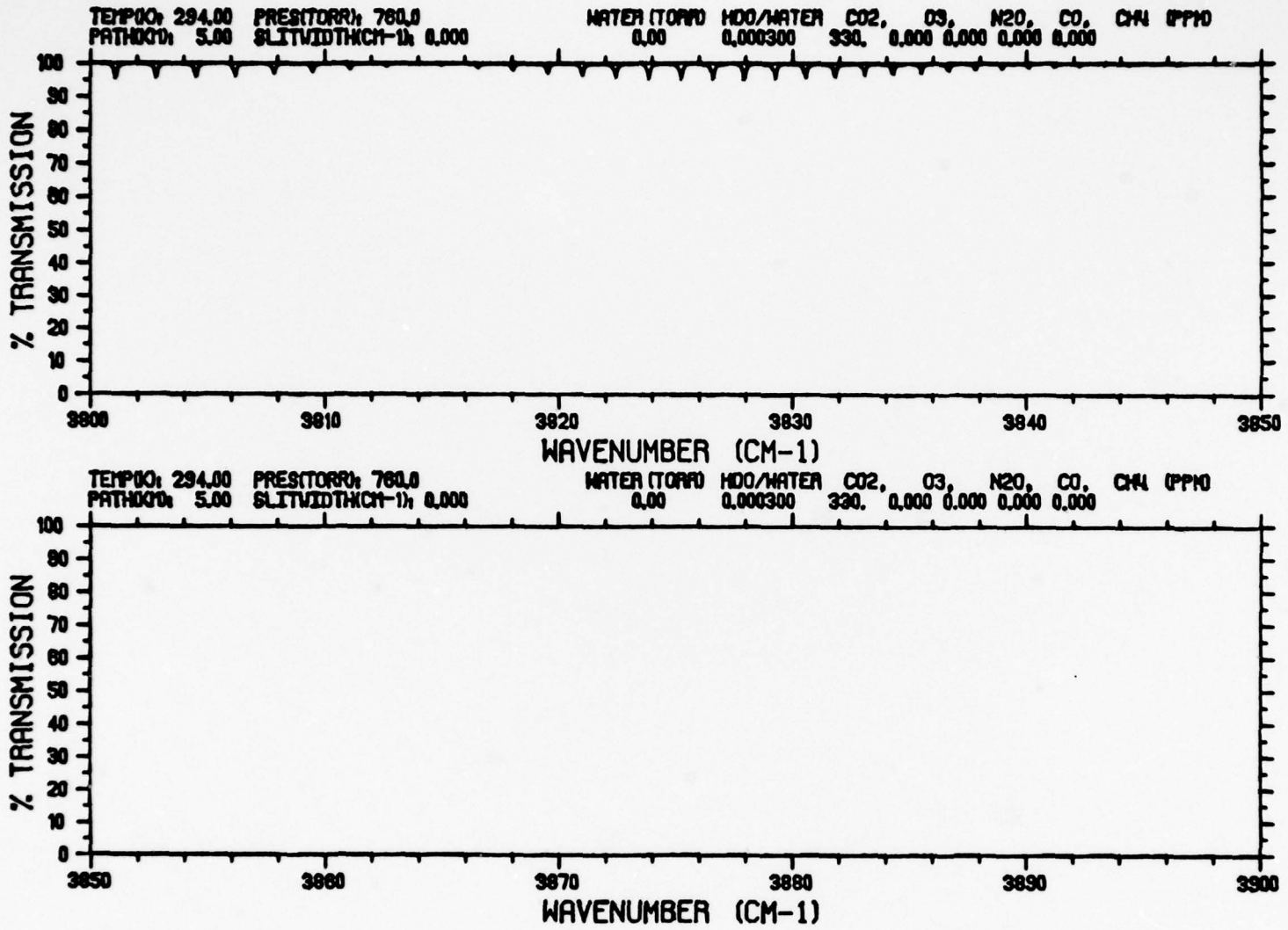

FIGURE 2m. FIGURE 2 CONTINUED

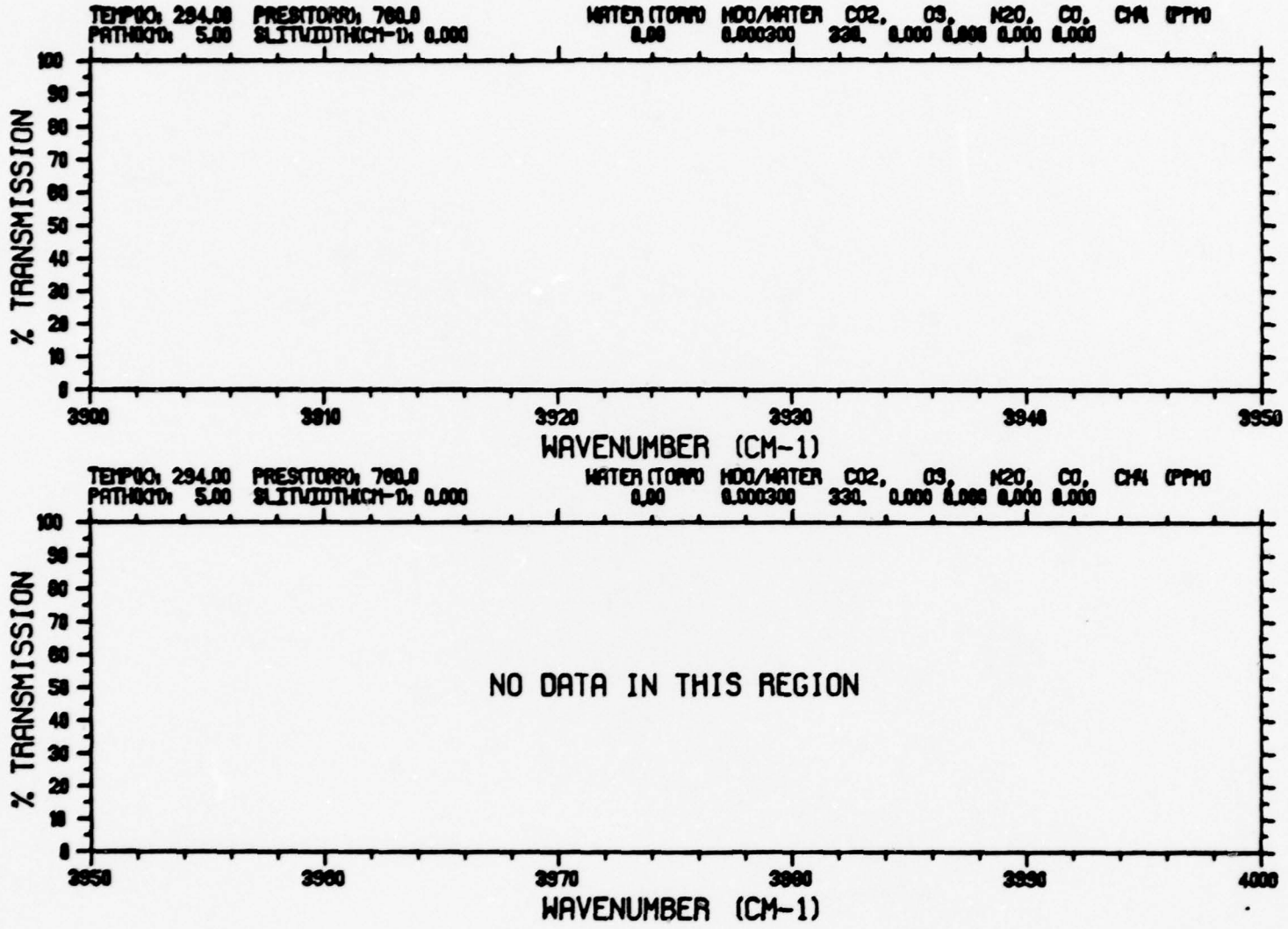

FIGURE 2n. FIGURE 2 CONTINUED

2.3 N_2O TRANSMISSION SPECTRA

Transmission plots of the N_2O component of the atmospheric transmission shown in Figure 1 are shown in Figures 3a - 3k. As was the case for the CO_2 calculations, the Burch N_2 continuum is included in the N_2O calculations. Several panels have been omitted since there is no detectable absorption by N_2O in the region.

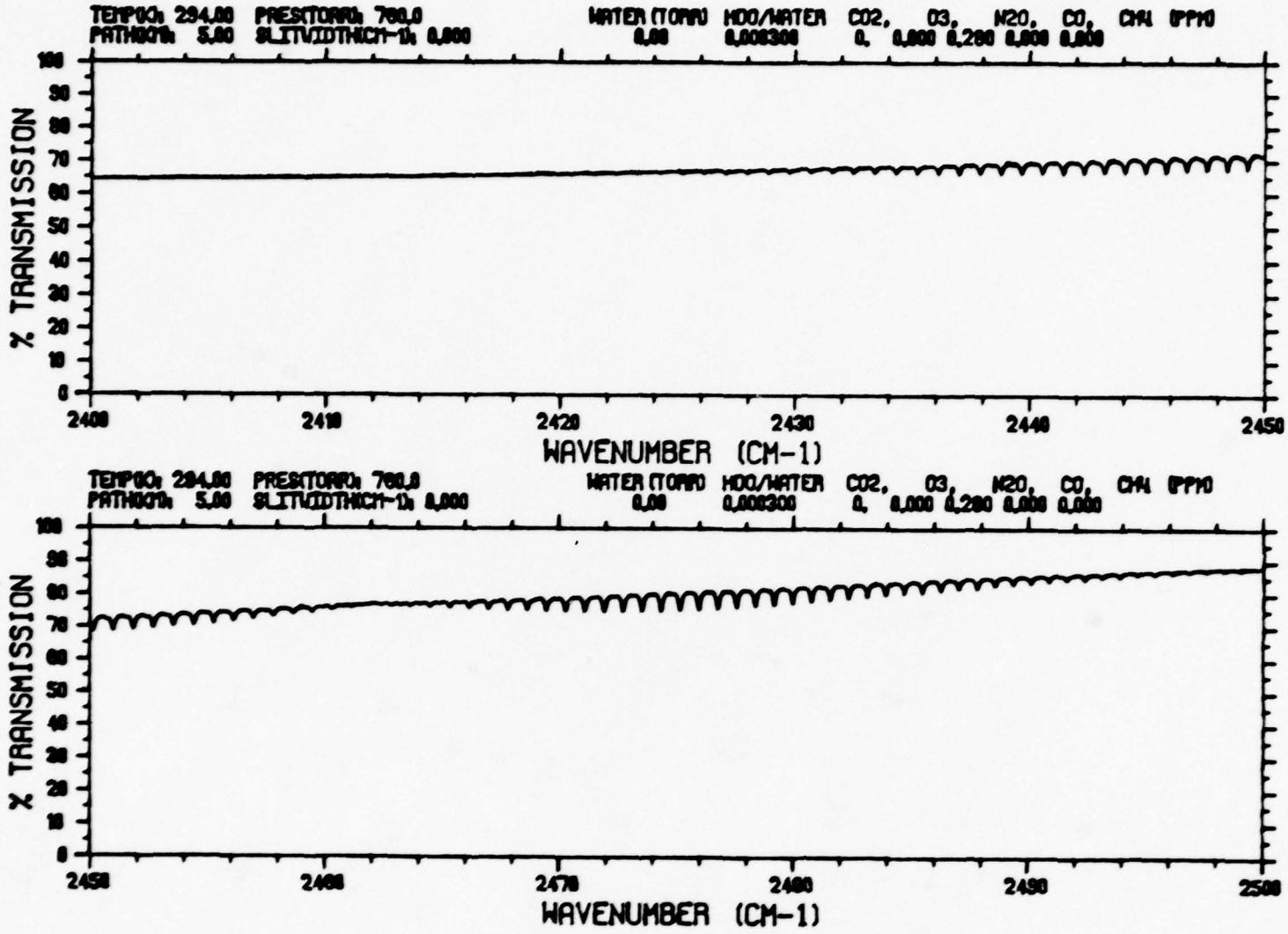

FIGURE 3a. ATMOSPHERIC TRANSMISSION FOR THE N_2O and N_2 COMPONENT FOR THE INDICATED CONDITIONS.

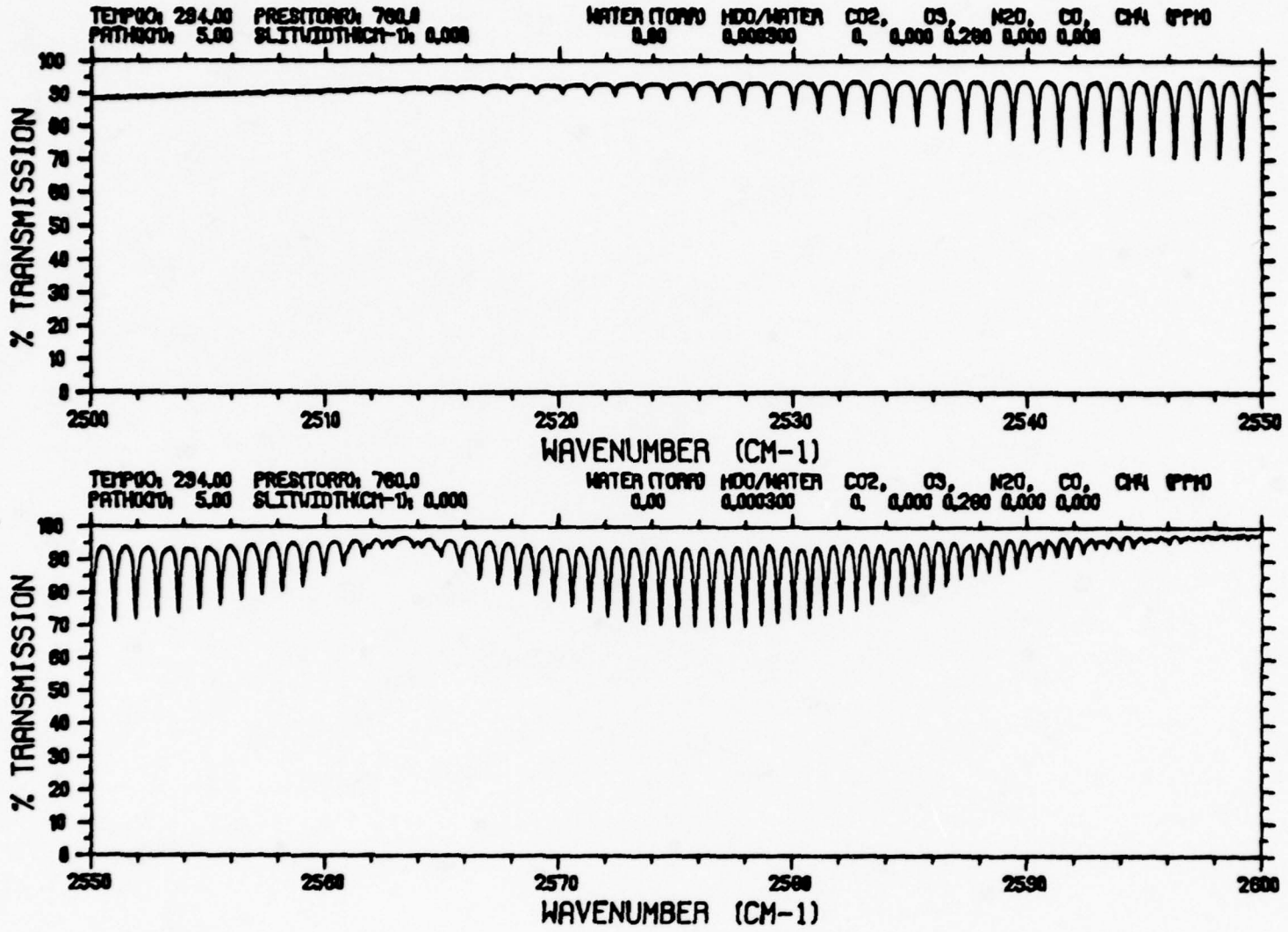

FIGURE 3b. FIGURE 3 CONTINUED

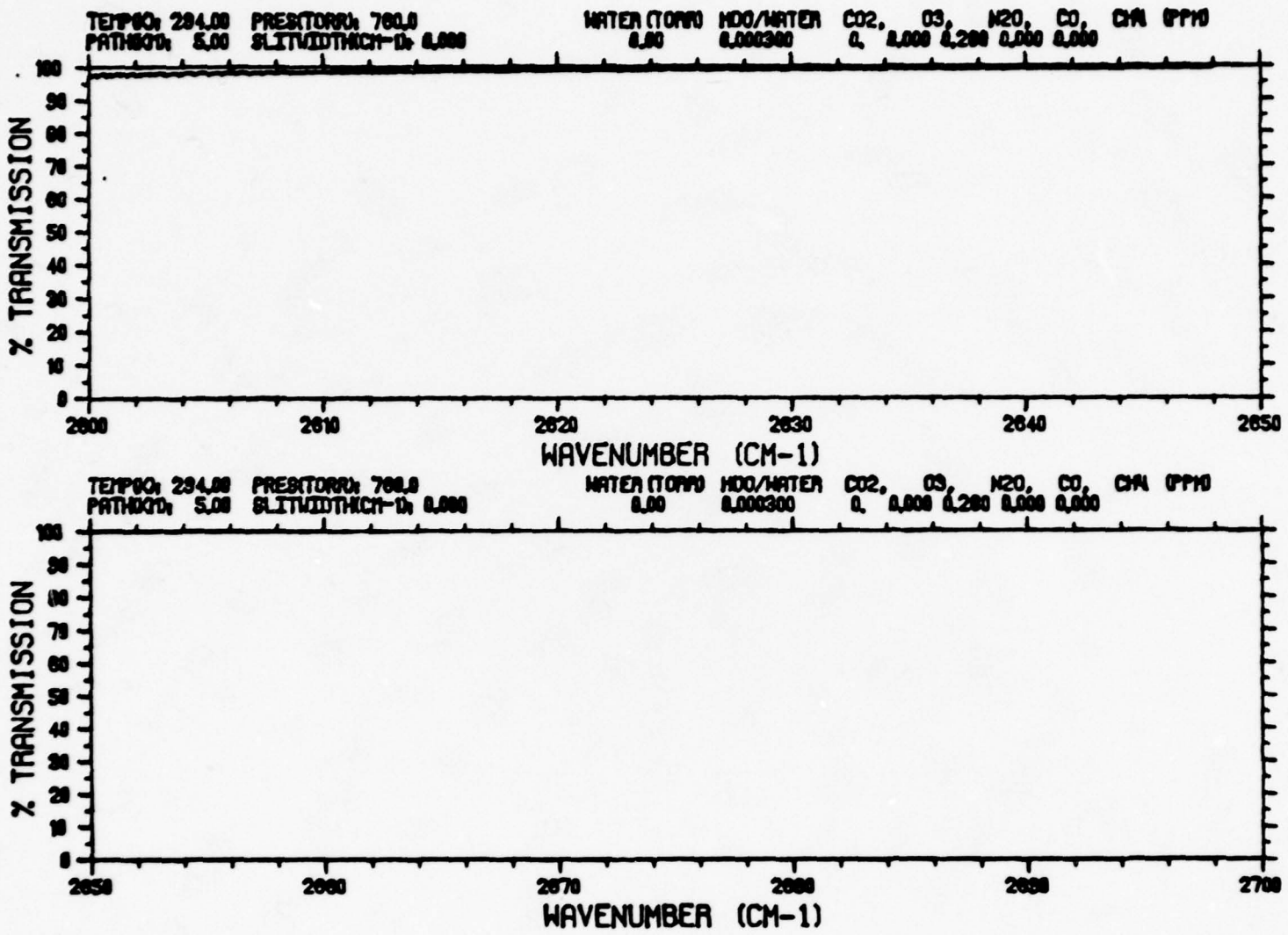

FIGURE 3c. FIGURE 3 CONTINUED

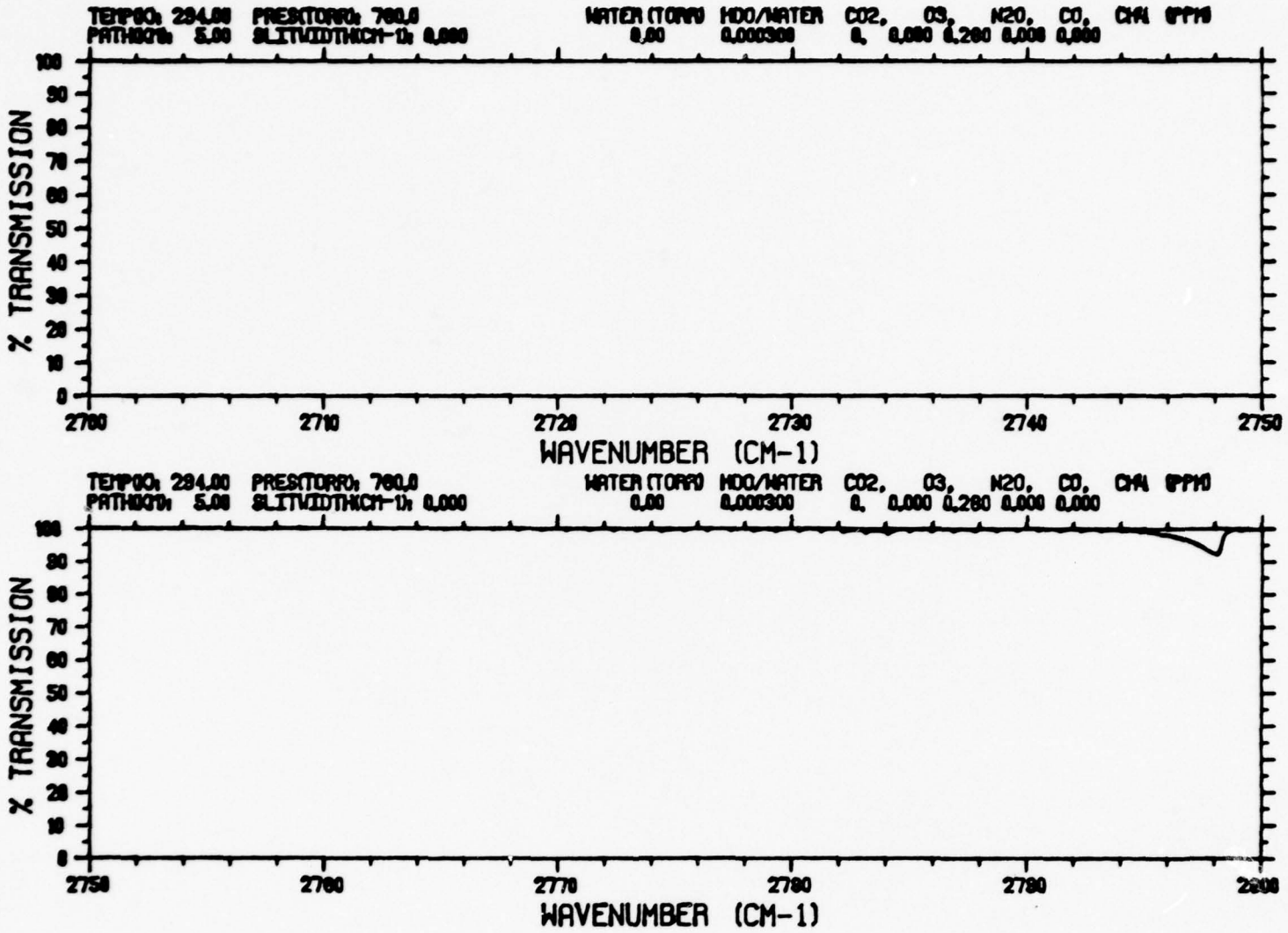

FIGURE 3d. FIGURE 3 CONTINUED

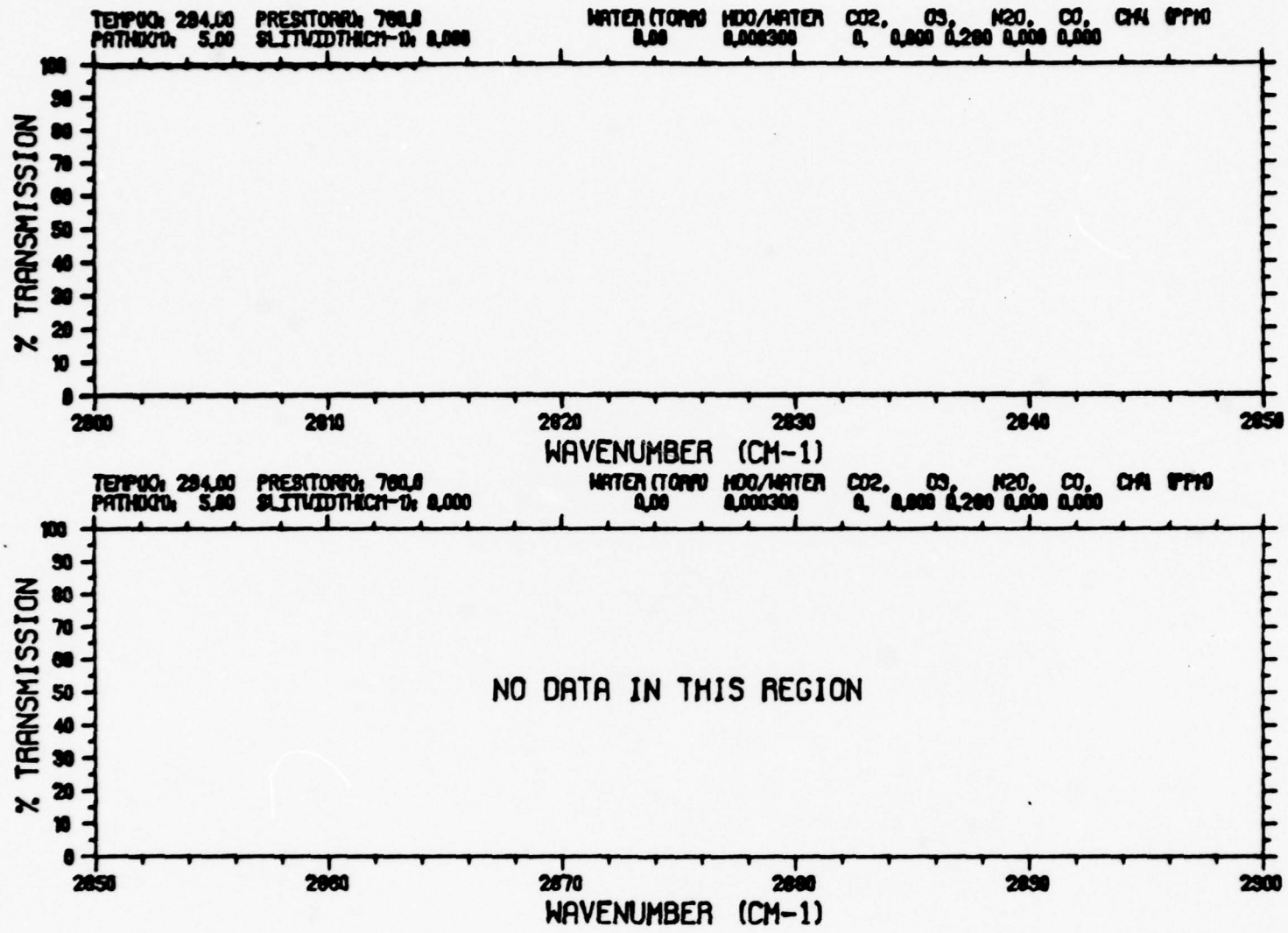

FIGURE 3e. FIGURE 3 CONTINUED

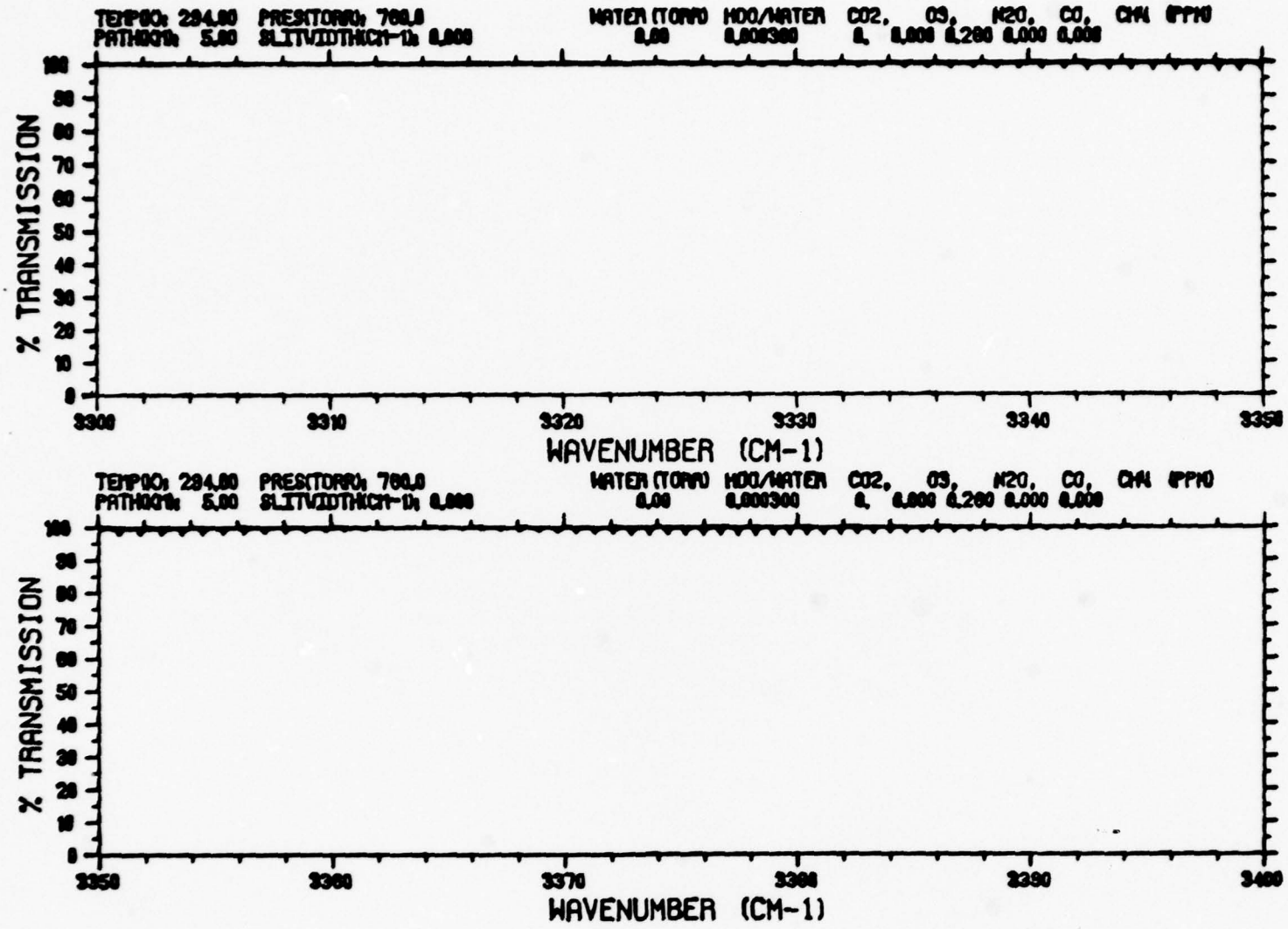

FIGURE 3f. FIGURE 3 CONTINUED

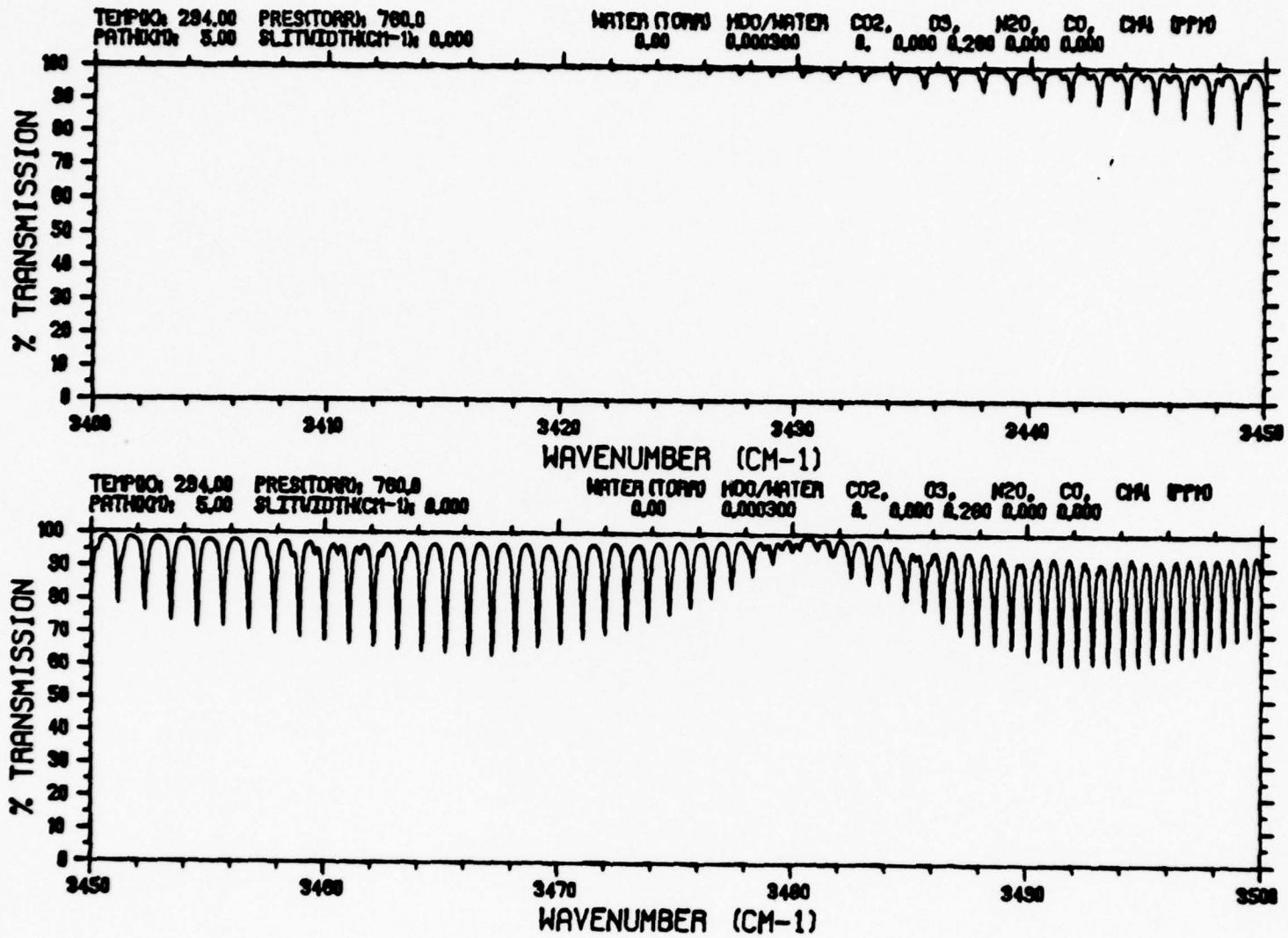

FIGURE 3g. FIGURE 3 CONTINUED

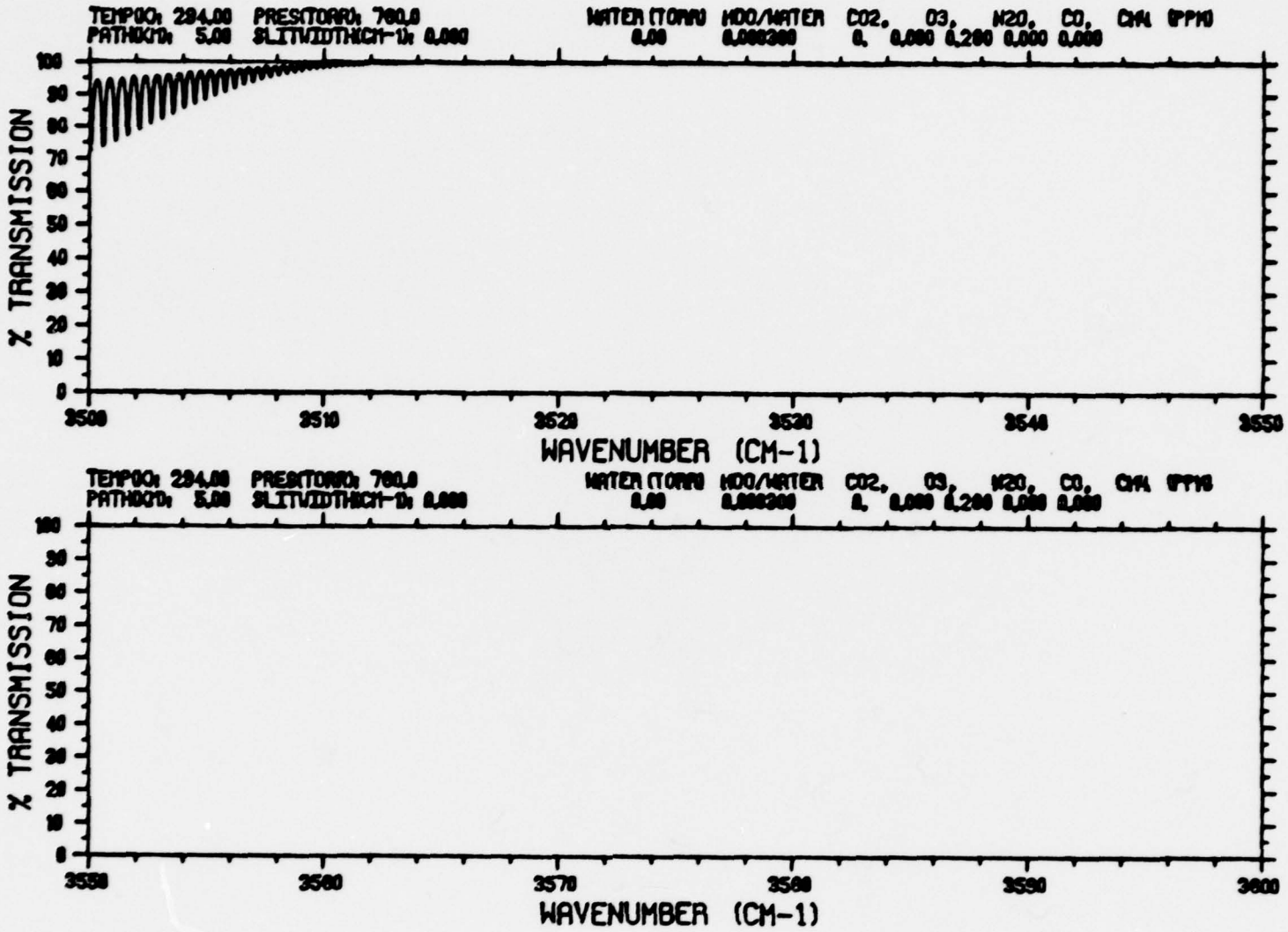

FIGURE 3h. FIGURE 3 CONTINUED

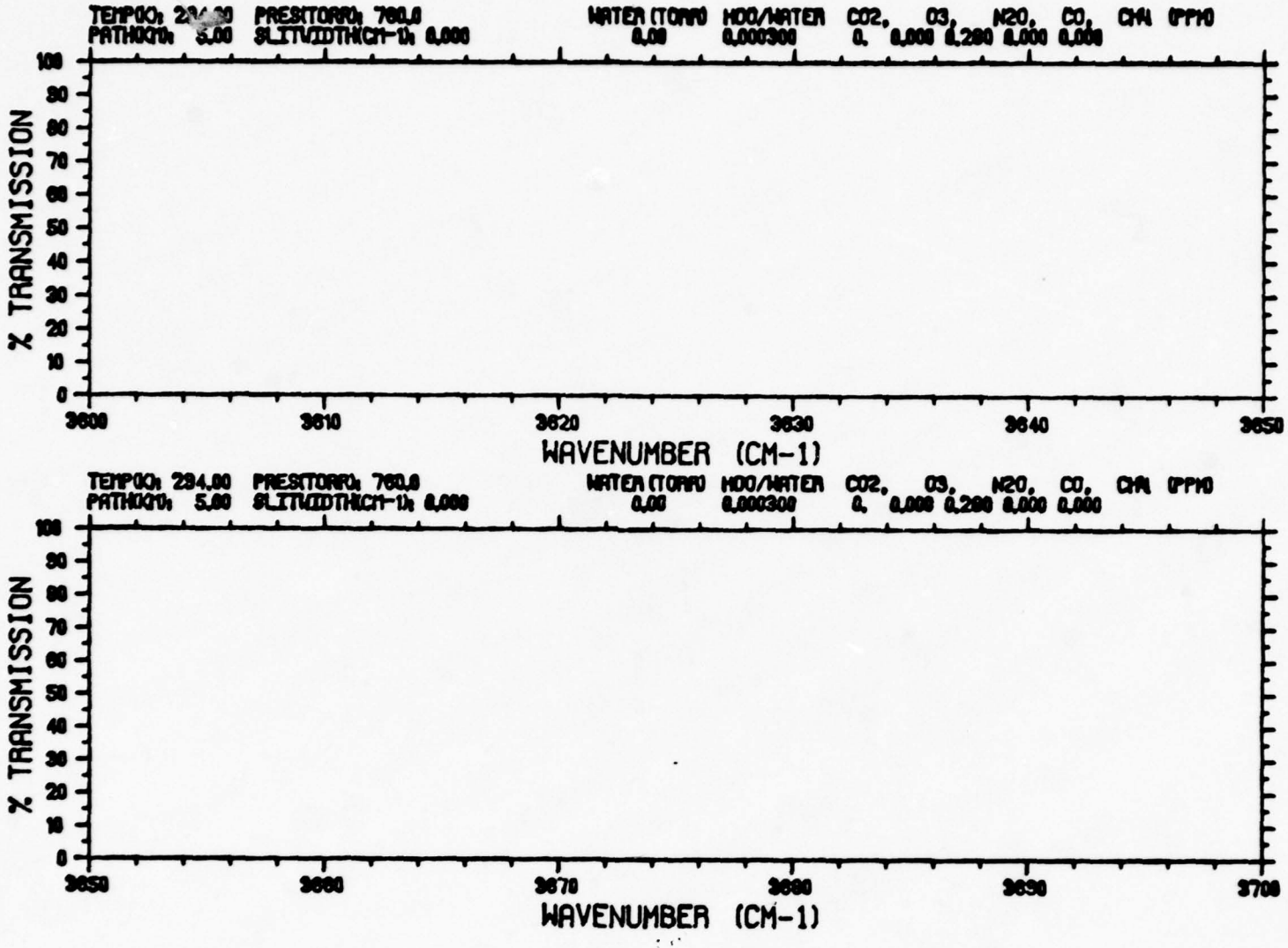

FIGURE 3i. FIGURE 3 CONTINUED

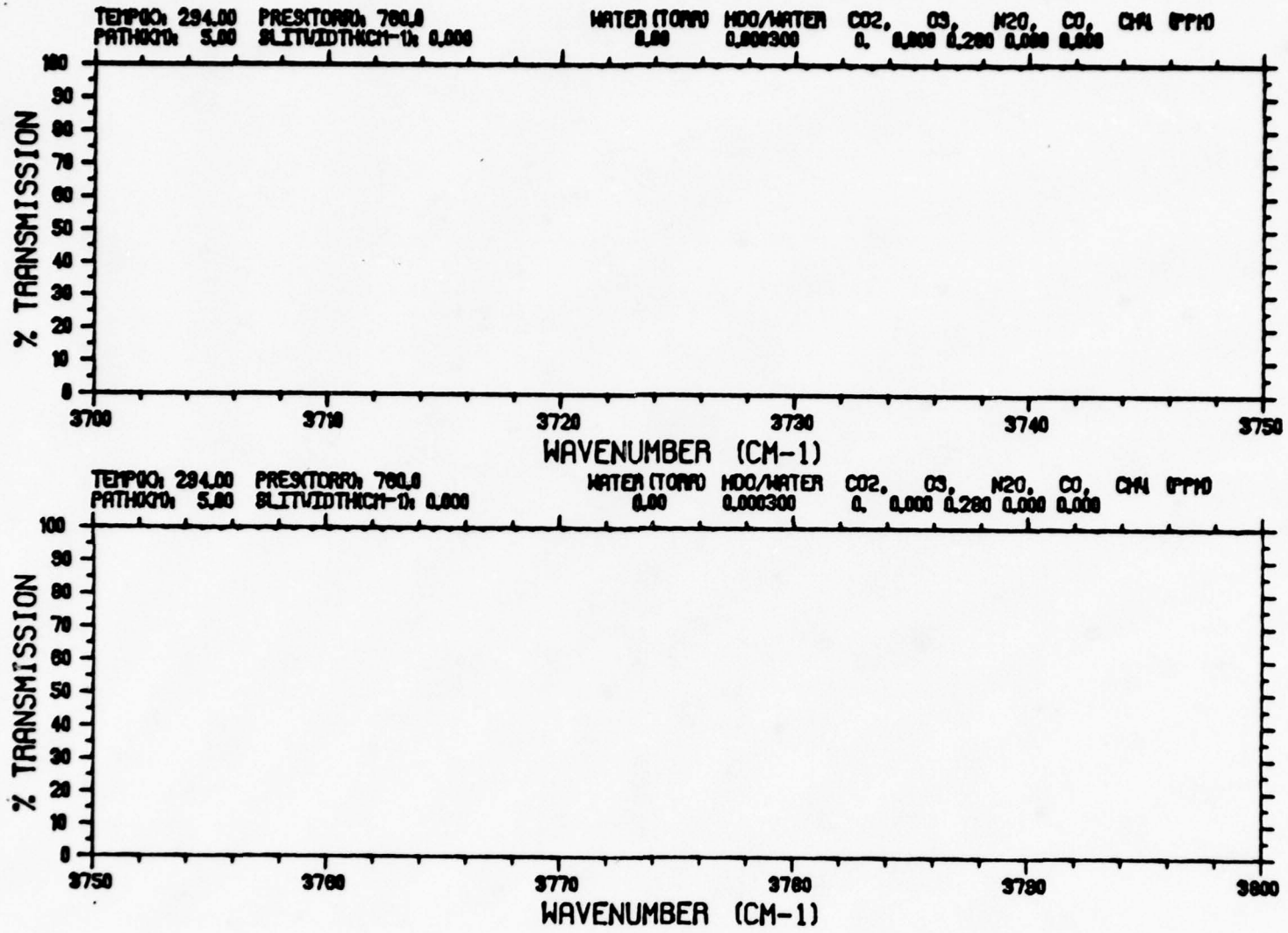

FIGURE 3j. FIGURE 3 CONTINUED

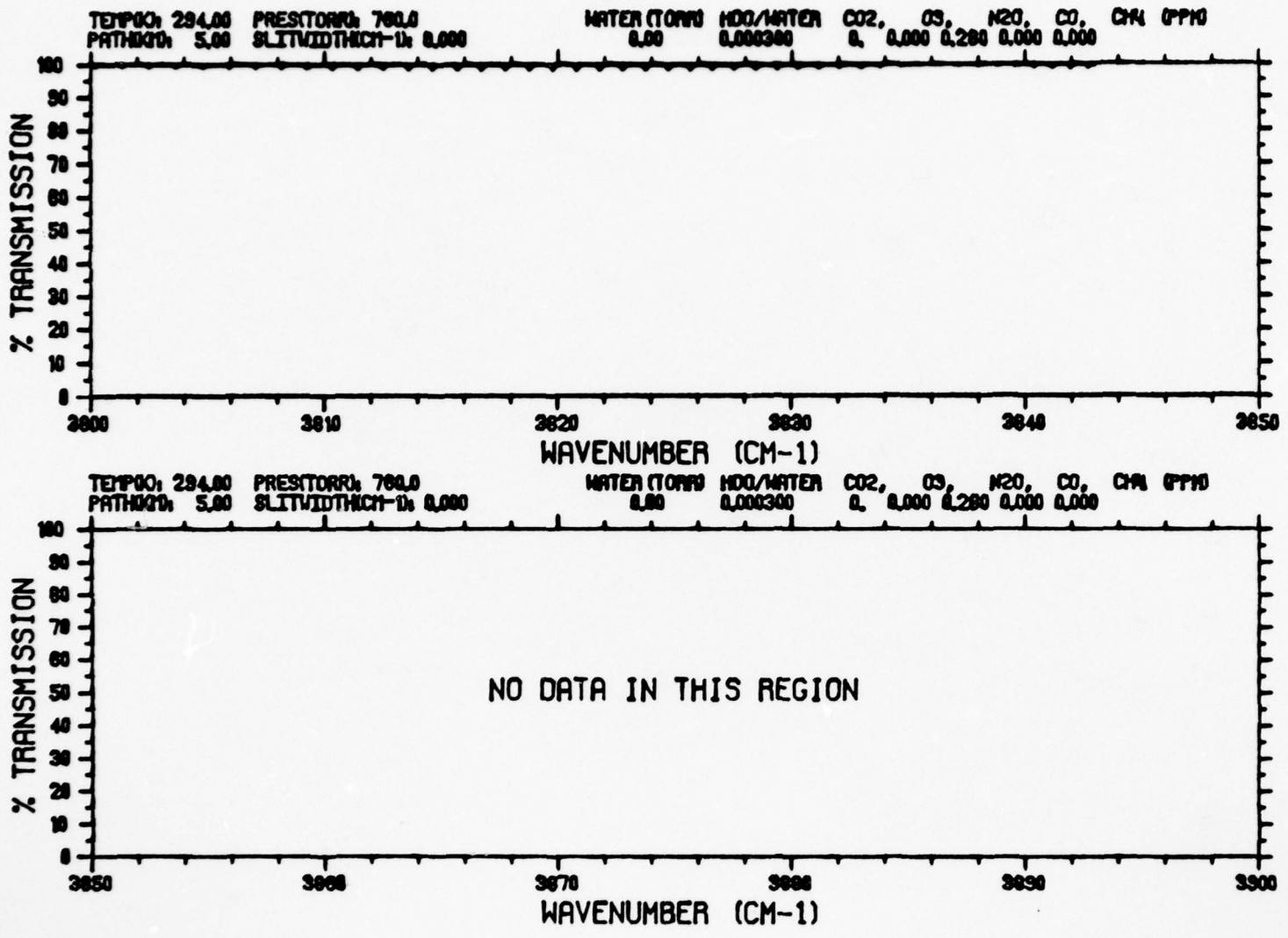

FIGURE 3k. FIGURE 3 CONTINUED

2.4 WATER VAPOR TRANSMISSION SPECTRA

The water vapor component (plus the N_2 continuum) of the atmospheric transmission plots shown in Figure 1 are given in Figures 4a - 4q. Three water vapor components are included: (1) H_2O lines, (2) HDO lines, and (3) water vapor continuum. The water continuum suggested by Burch is used, although more recent data soon will be available.

Inclusion of the N_2 continuum here provides a clear description of how the absorption components are modeled into the SYNSPC code (and typically in all such codes). Figure 4a shows the sharp cut-on of the N_2 continuum at $\sim$2389 cm^{-1}, and its merging with the HDO lines at shorter wavelengths. This artificial "step-function" modeling of the N_2 cut-on is simpler computationally, and it does not affect the transmission at longer wavelengths, since the CO_2 in the atmosphere is so strongly absorbing.

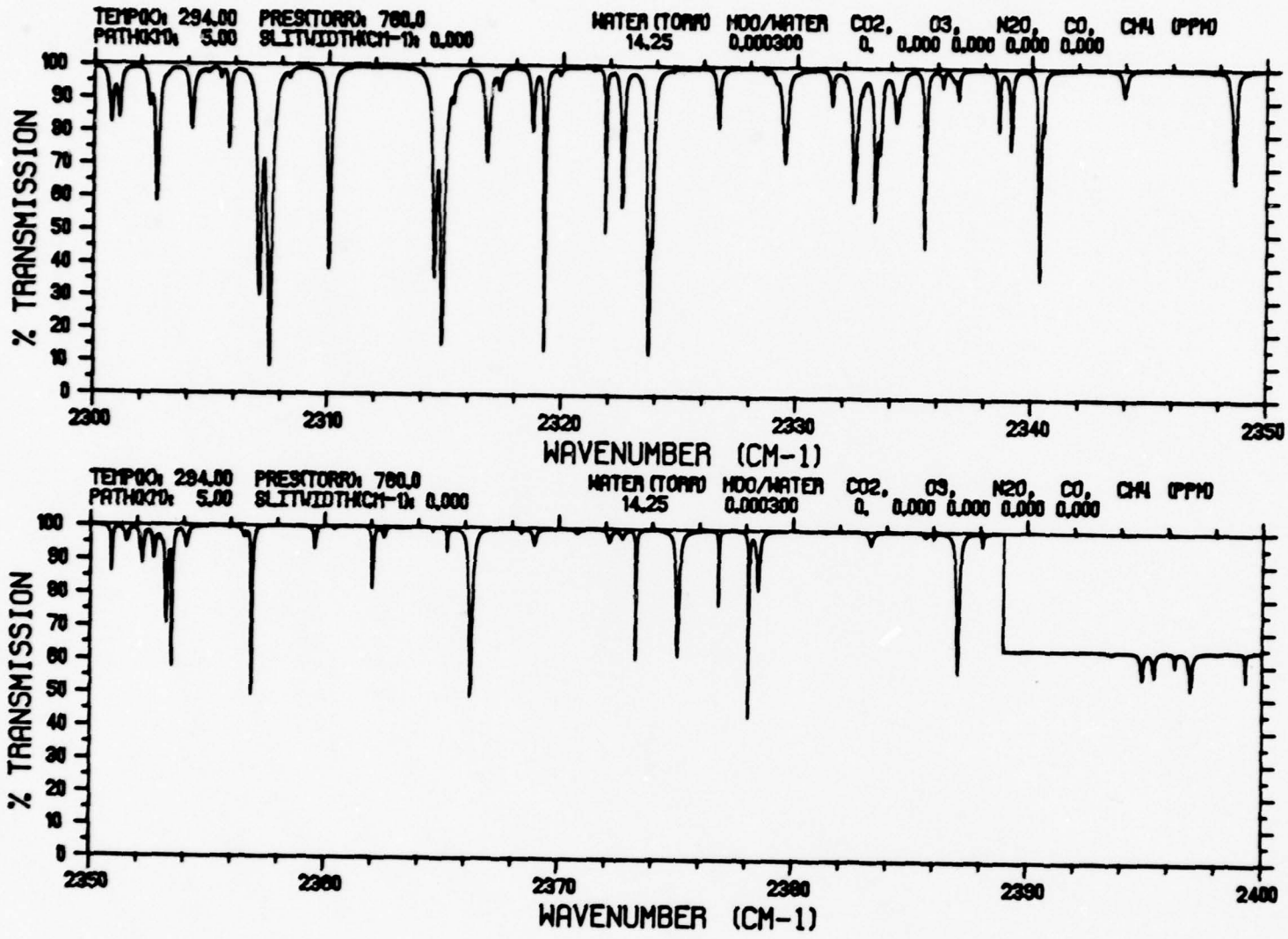

FIGURE 4a. ATMOSPHERIC TRANSMISSION FOR THE WATER VAPOR COMPONENT FOR THE INDICATED CONDITIONS

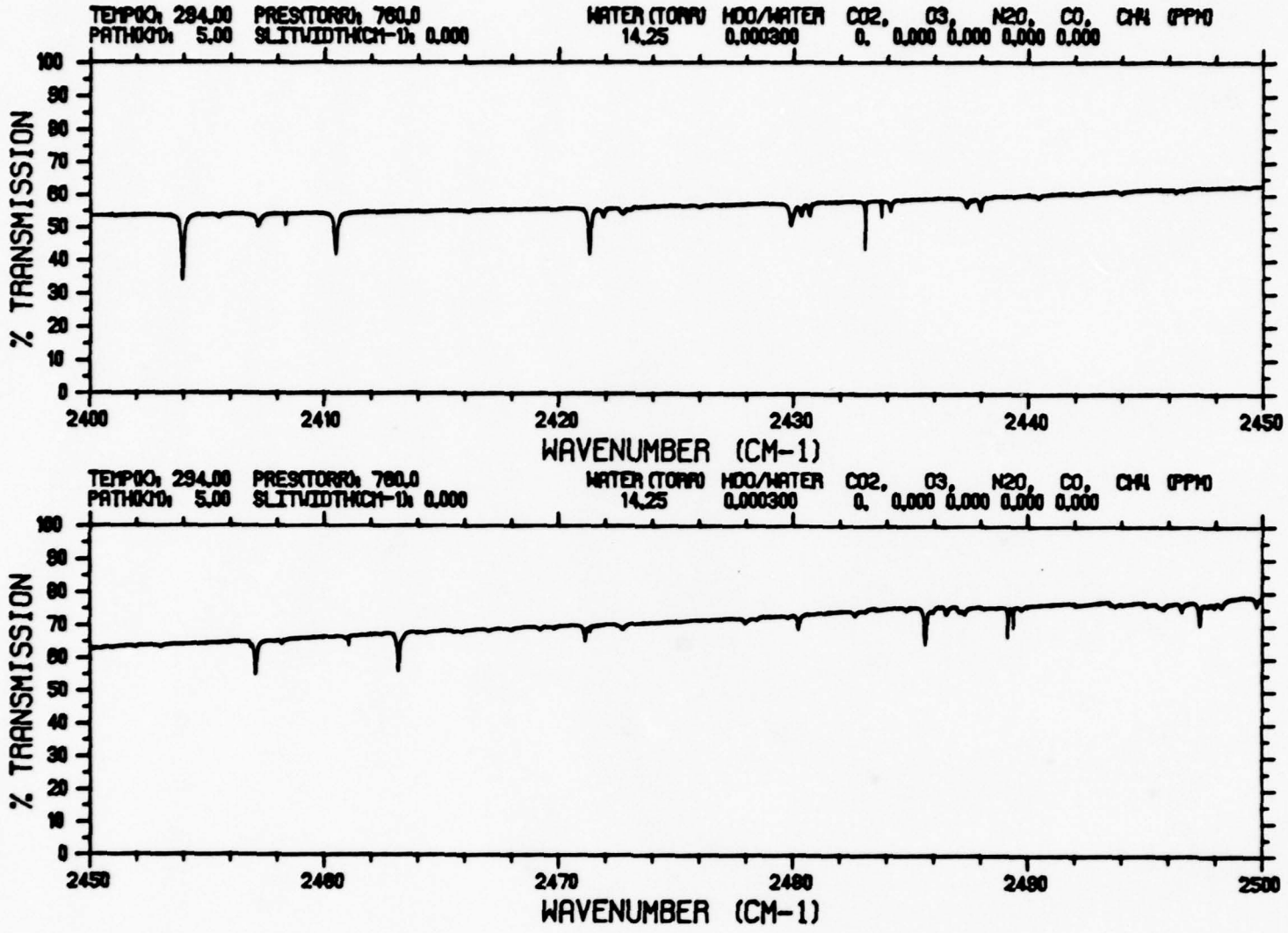

FIGURE 4b. FIGURE 4 CONTINUED

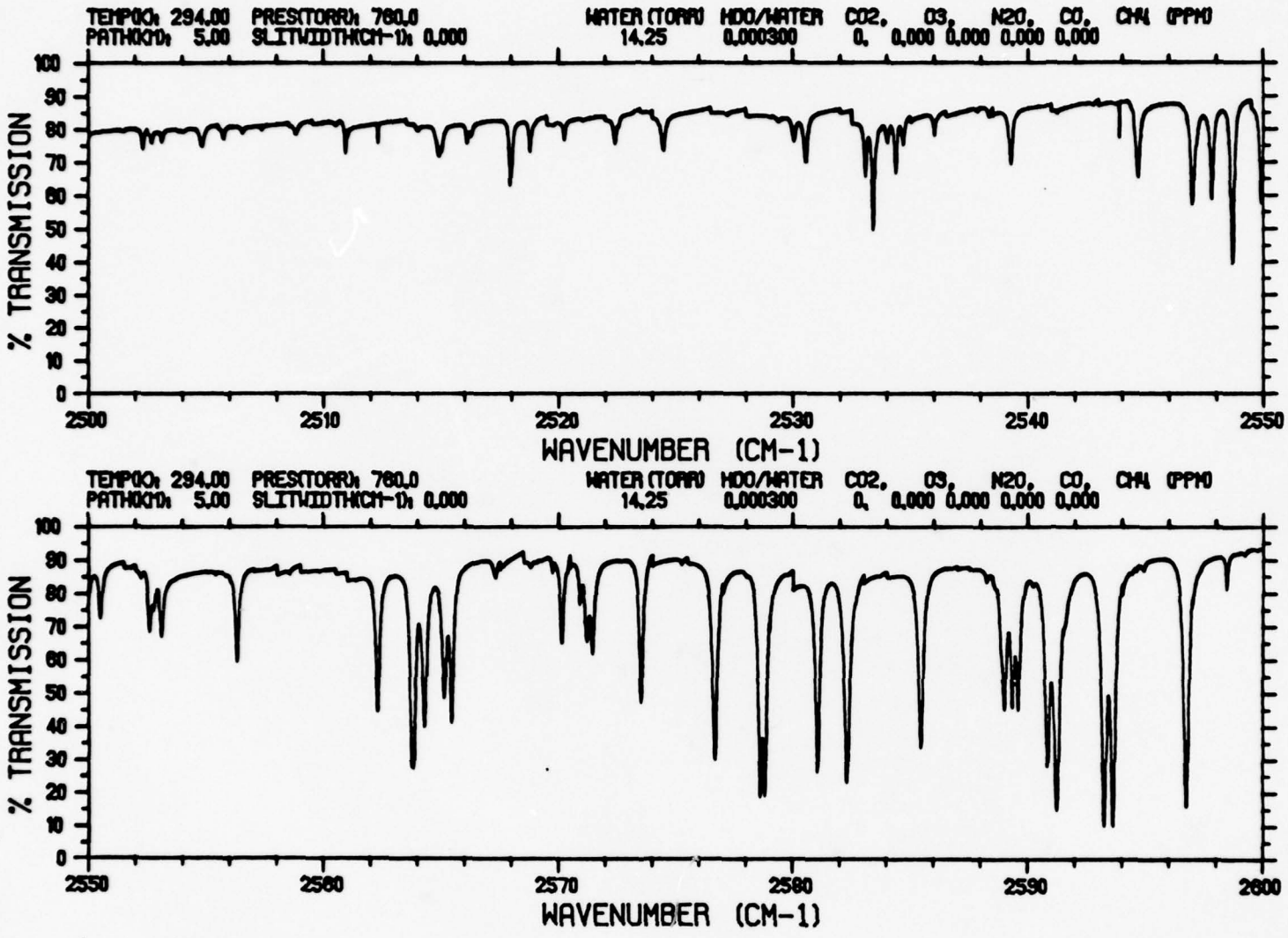

FIGURE 4c. FIGURE 4 CONTINUED

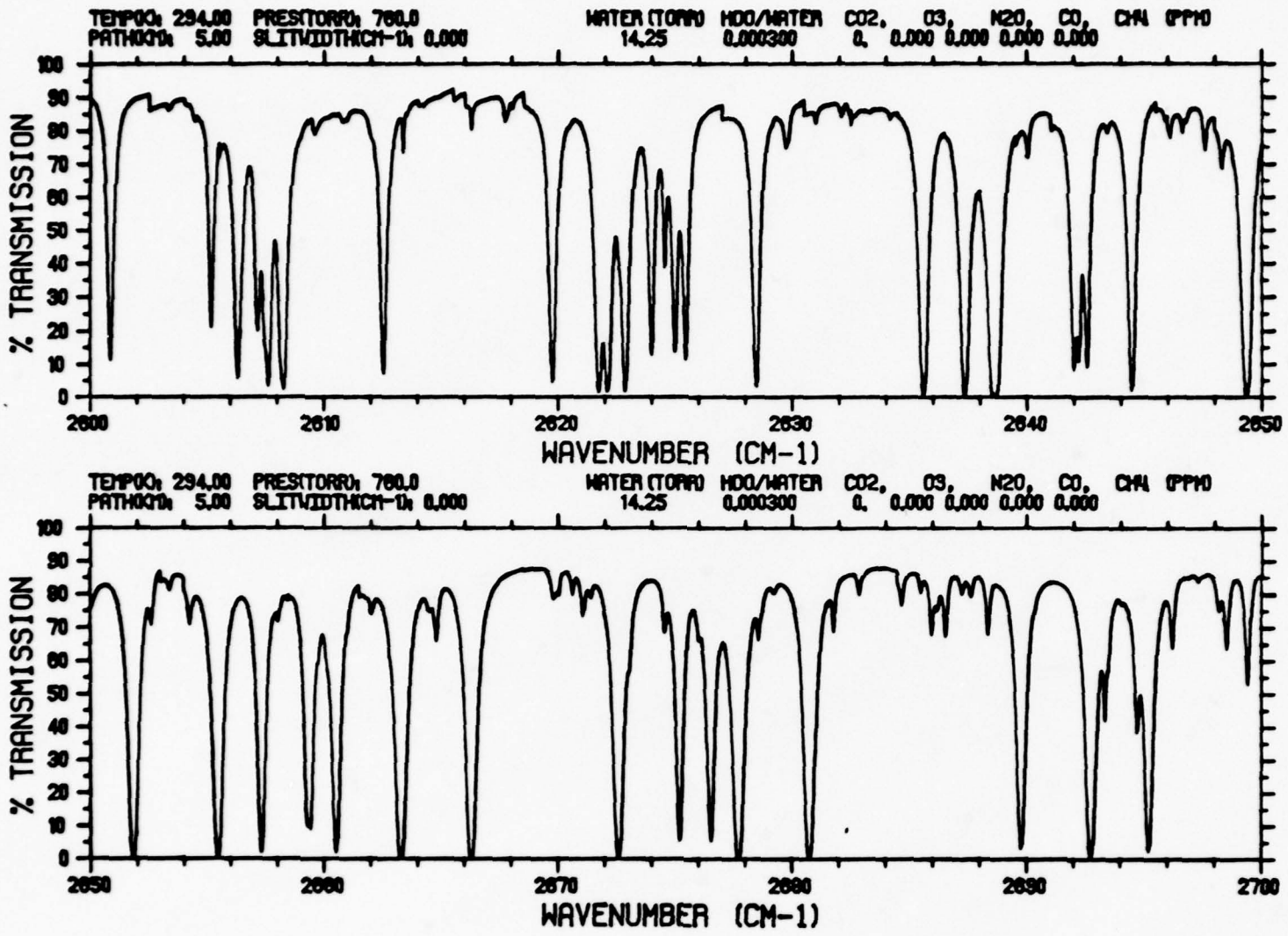

FIGURE 4d. FIGURE 4 CONTINUED

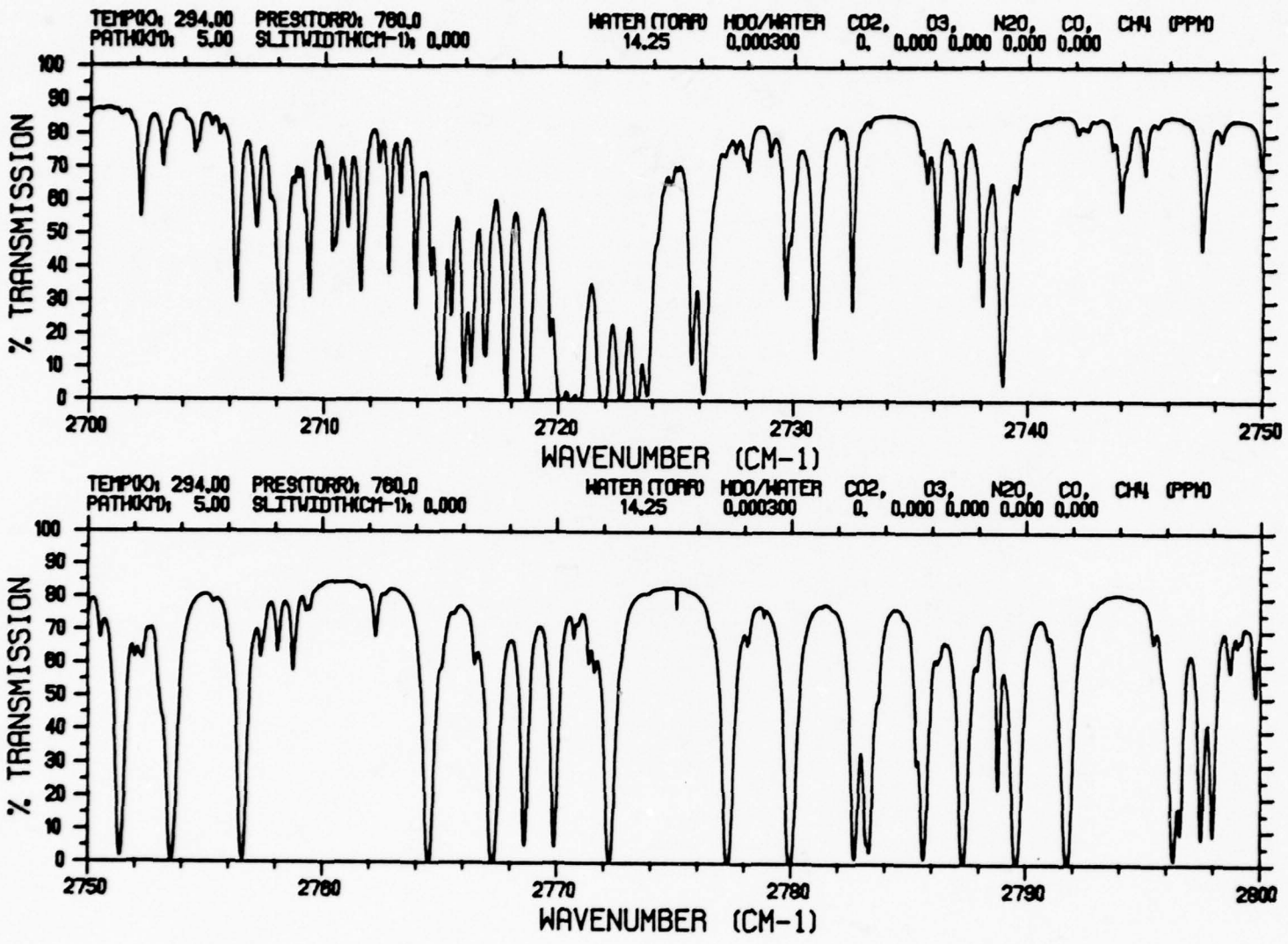

FIGURE 4e. FIGURE 4 CONTINUED

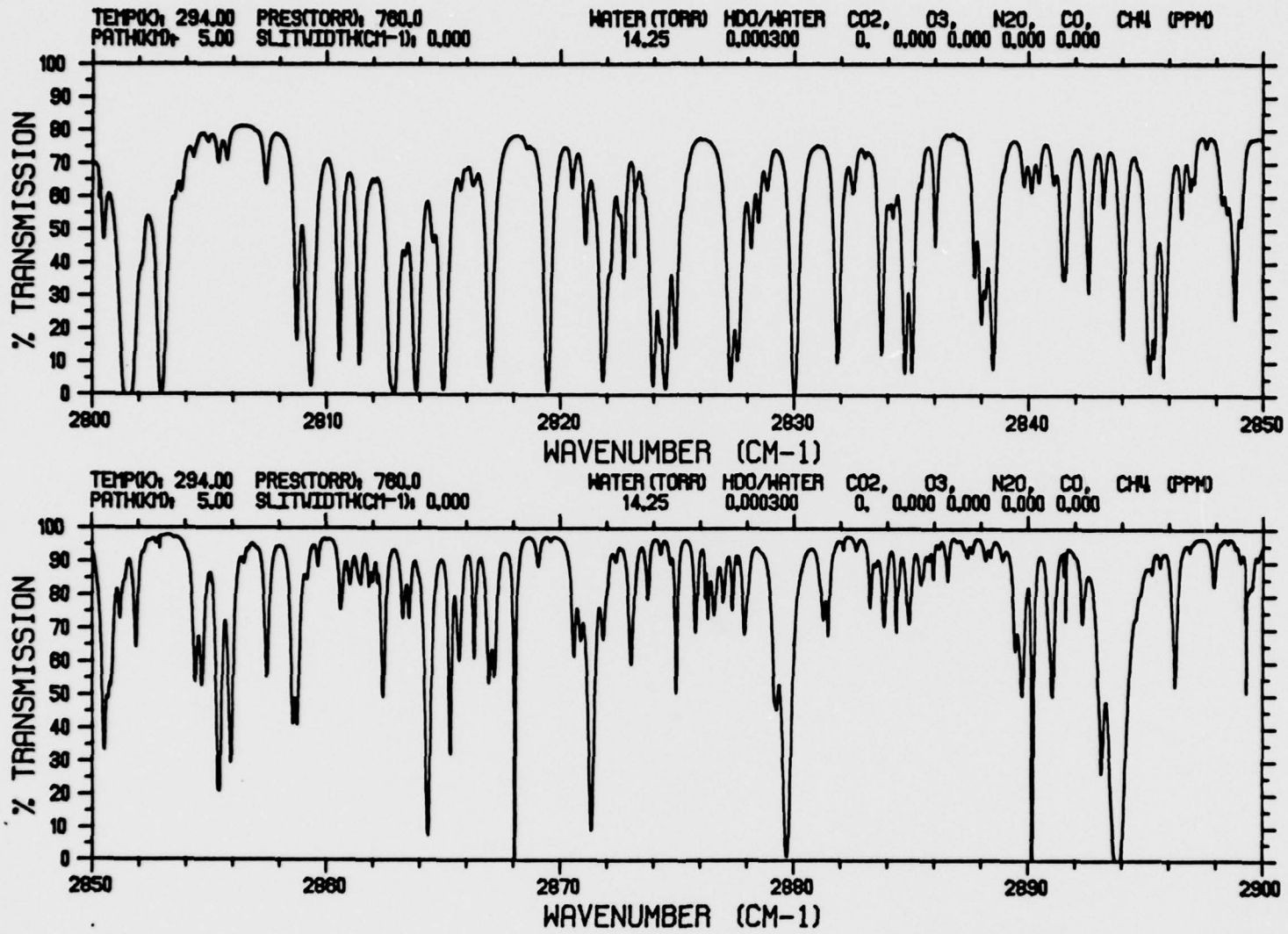

FIGURE 4f. FIGURE 4 CONTINUED

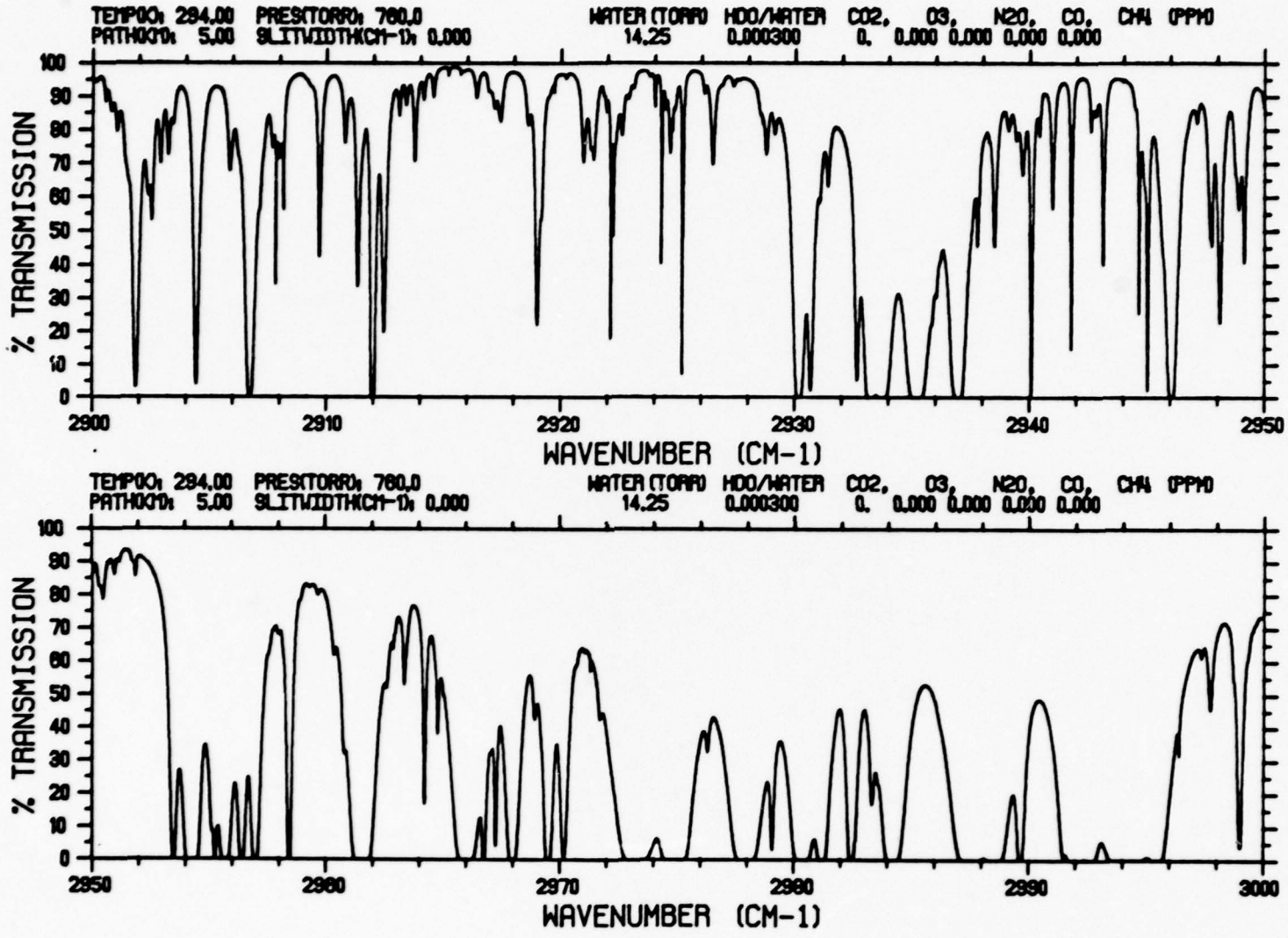

FIGURE 4g. FIGURE 4 CONTINUED

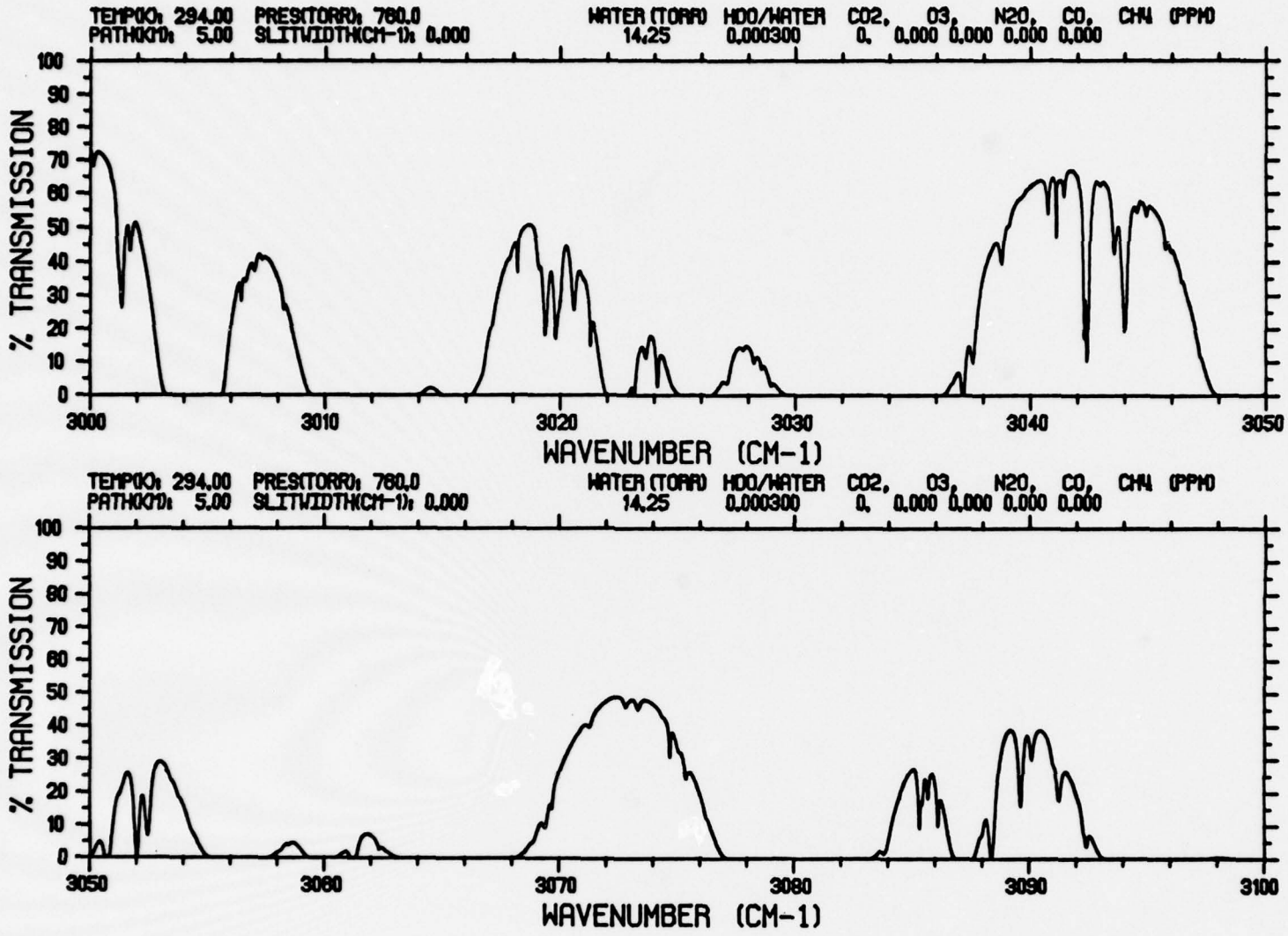

FIGURE 4h. FIGURE 4 CONTINUED

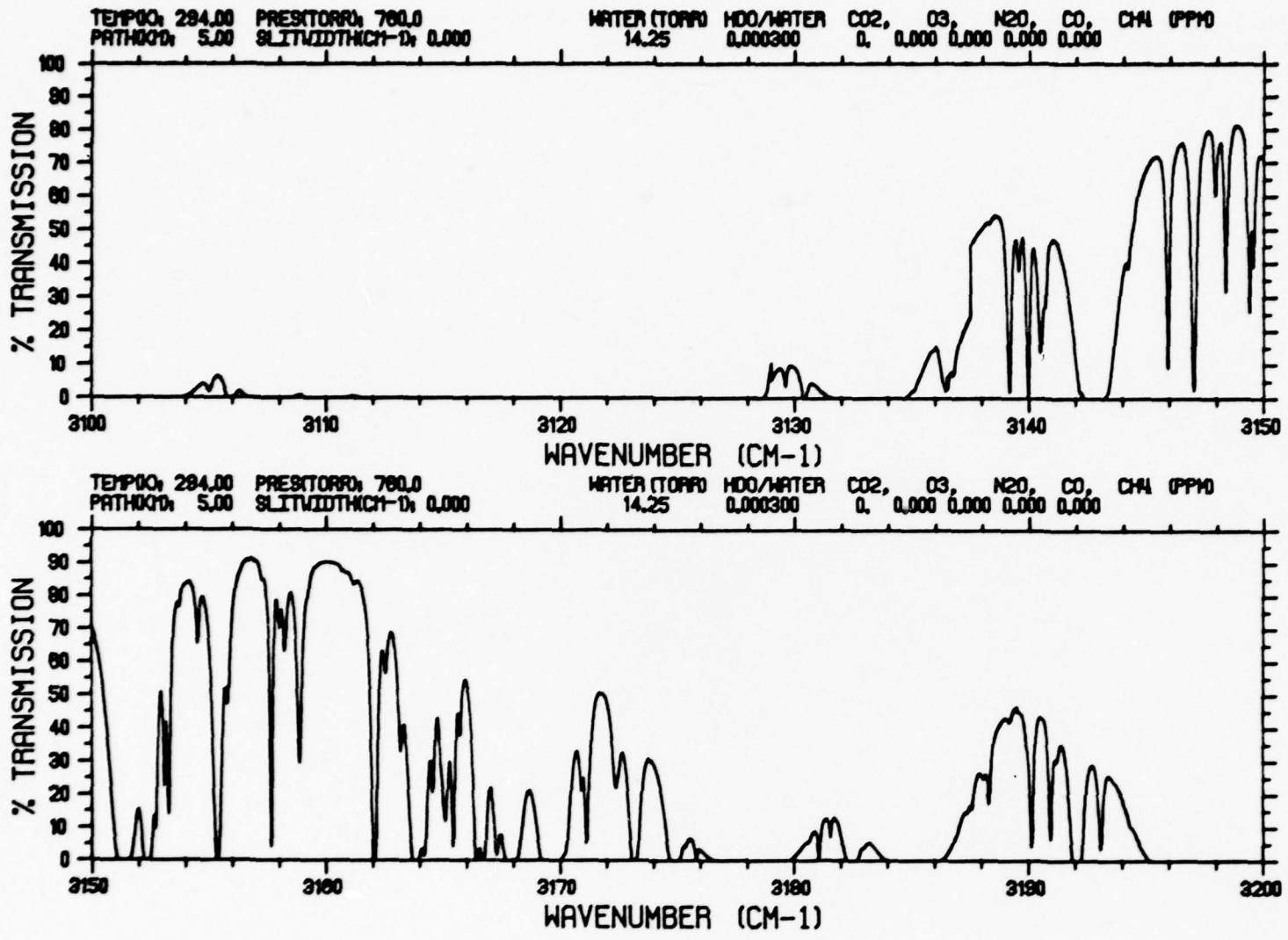

FIGURE 4i. FIGURE 4 CONTINUED

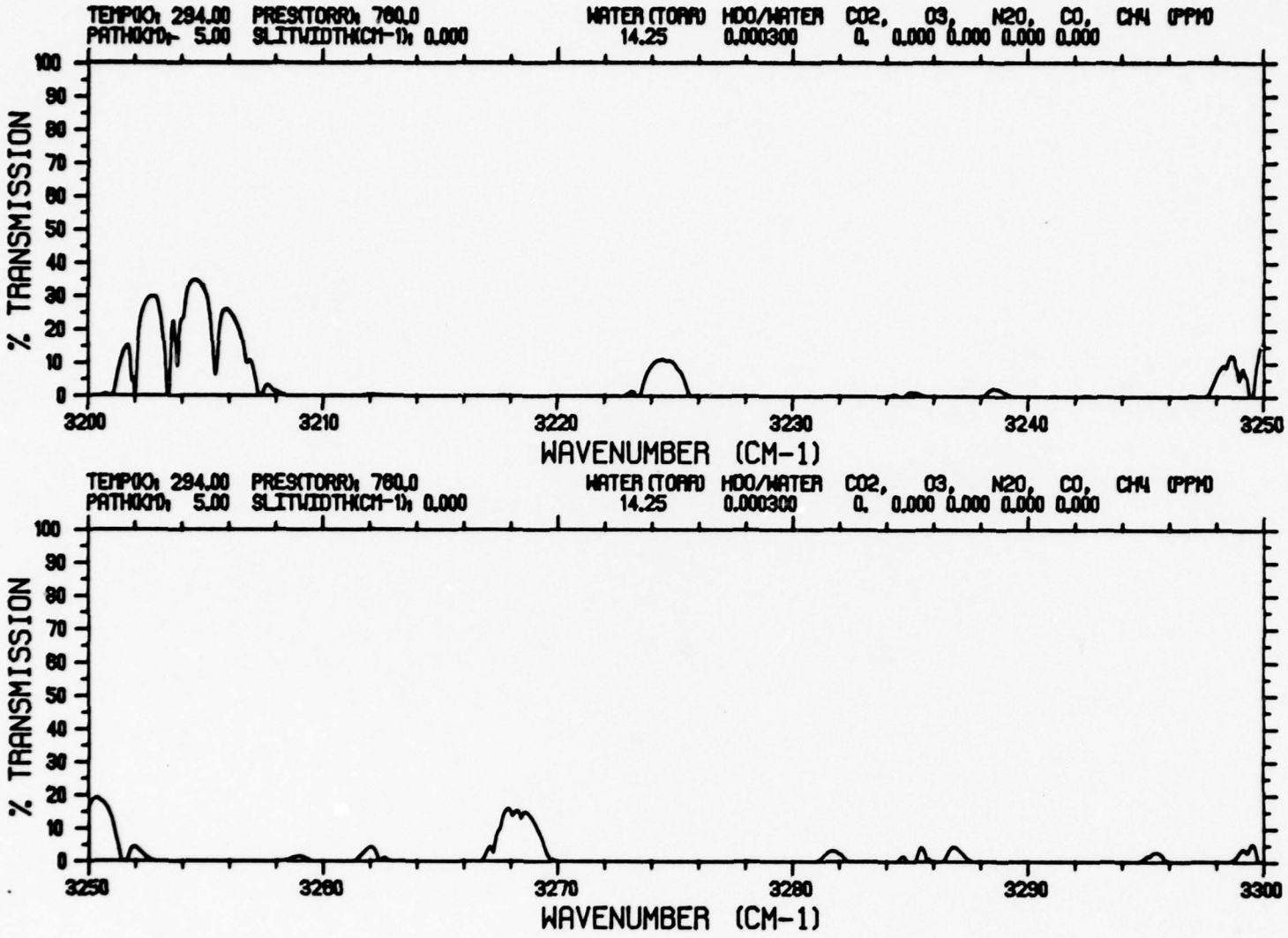

FIGURE 4j. FIGURE 4 CONTINUED

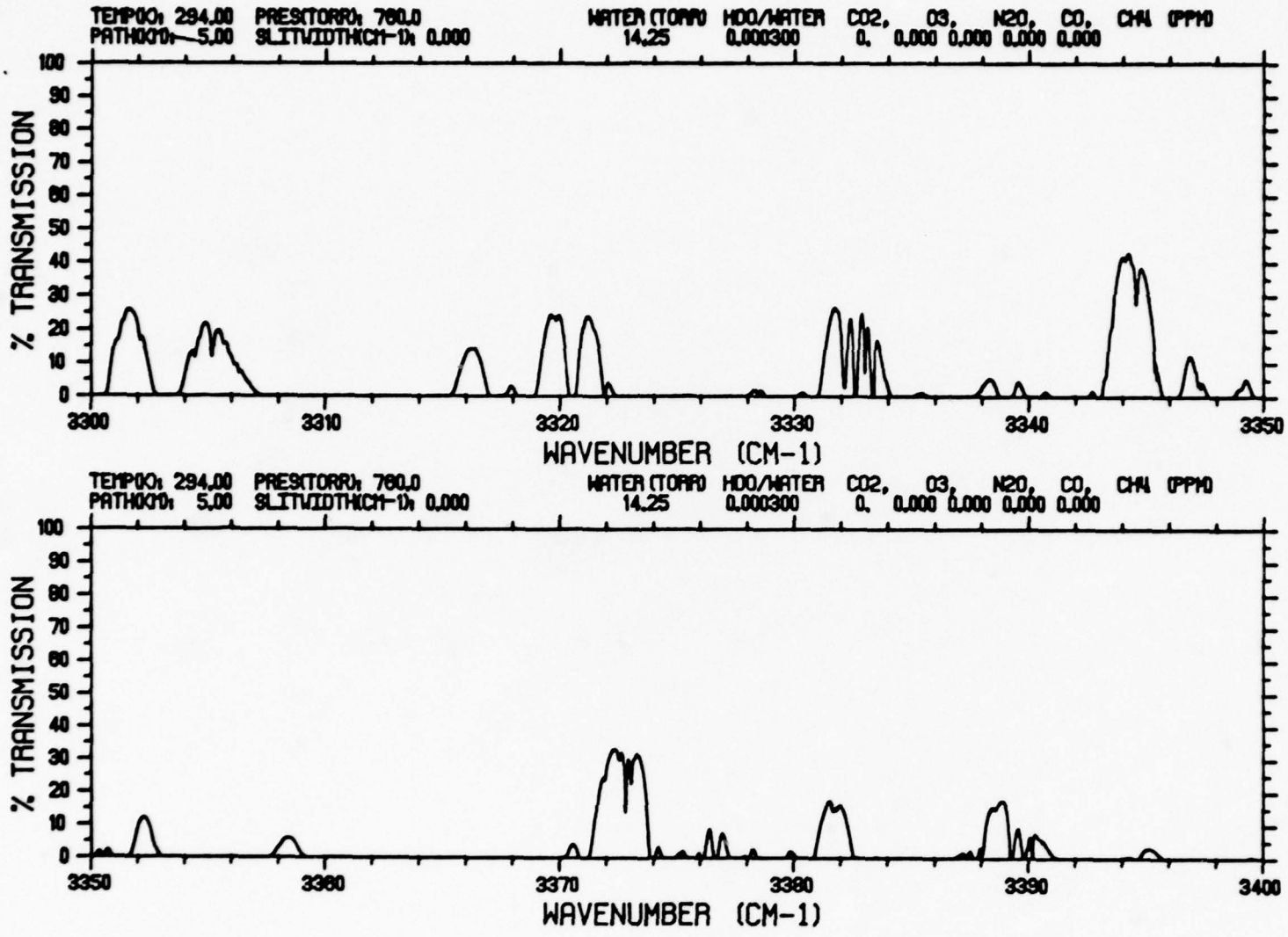

FIGURE 4k. FIGURE 4 CONTINUED

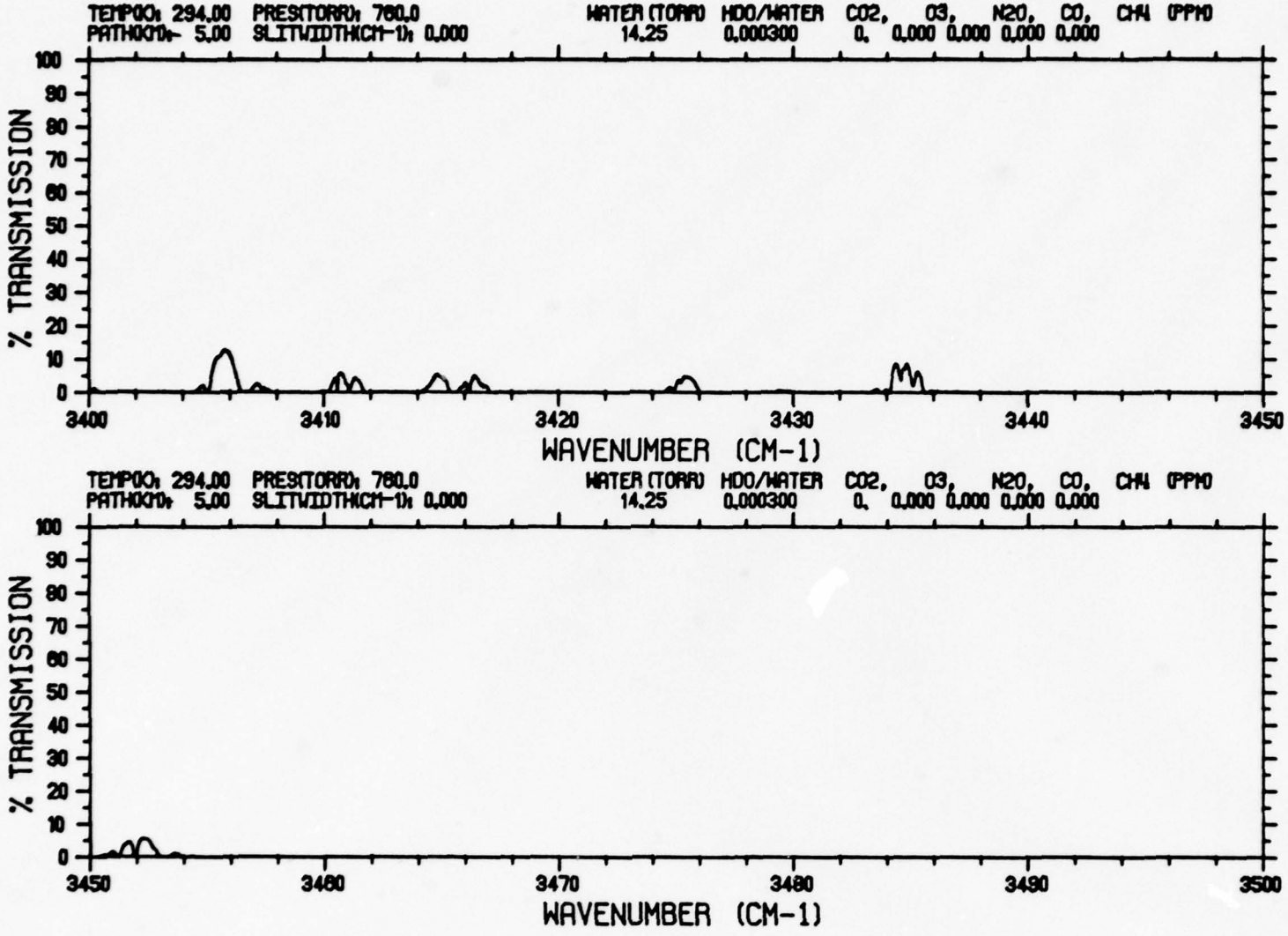

FIGURE 41. FIGURE 4 CONTINUED

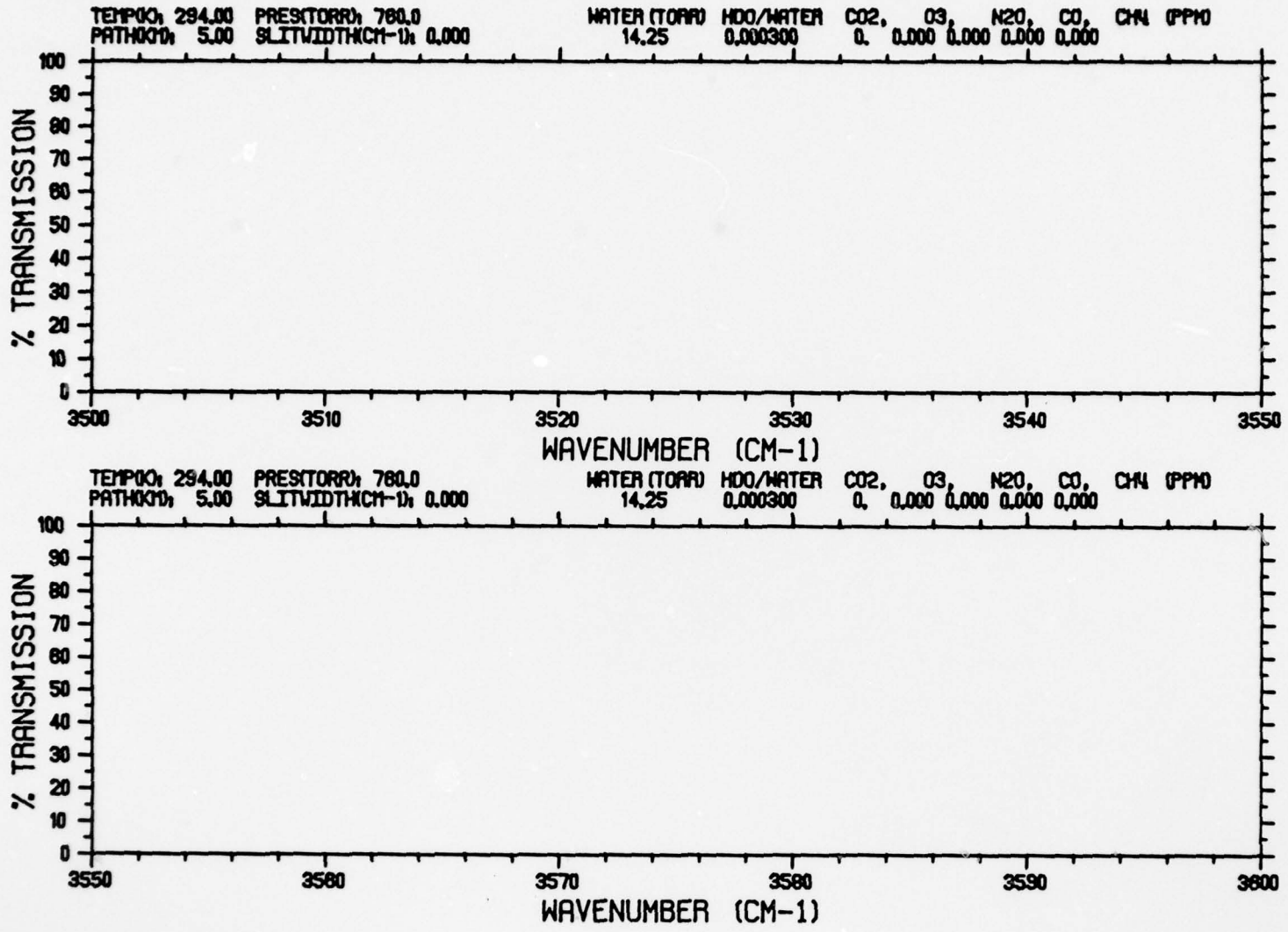

FIGURE 4m. FIGURE 4 CONTINUED

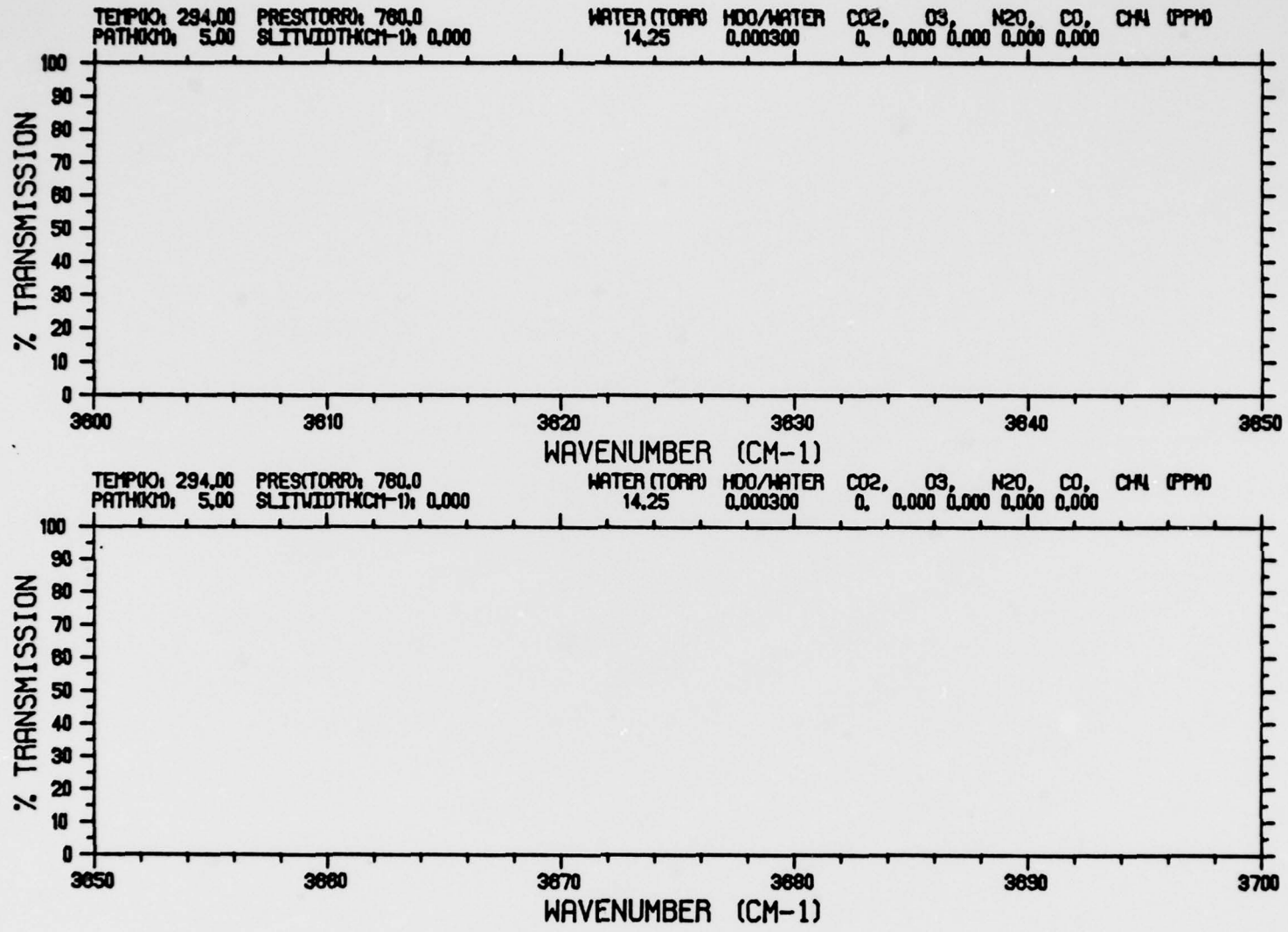

FIGURE 4n. FIGURE 4 CONTINUED

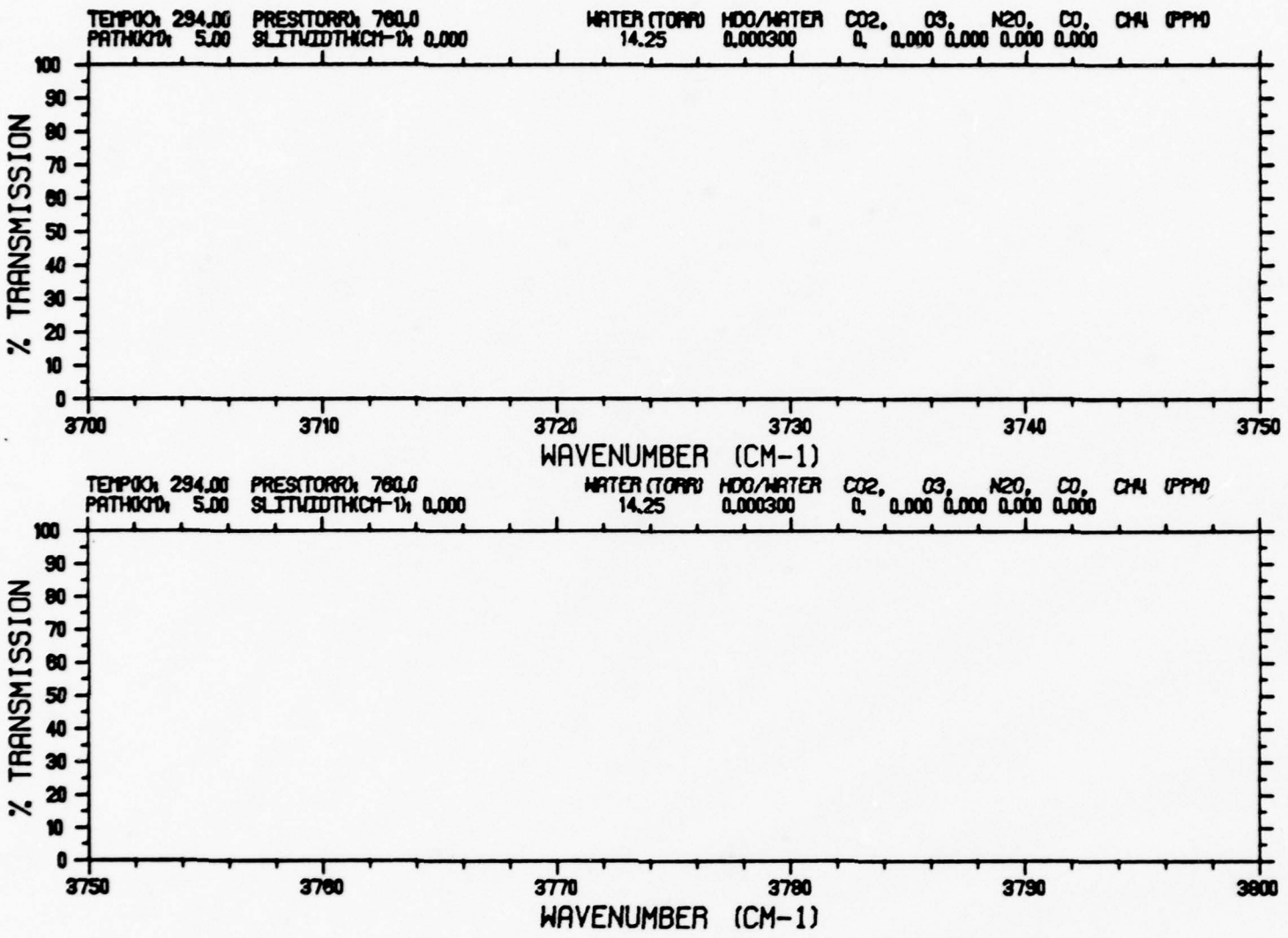

FIGURE 4o. FIGURE 4 CONTINUED

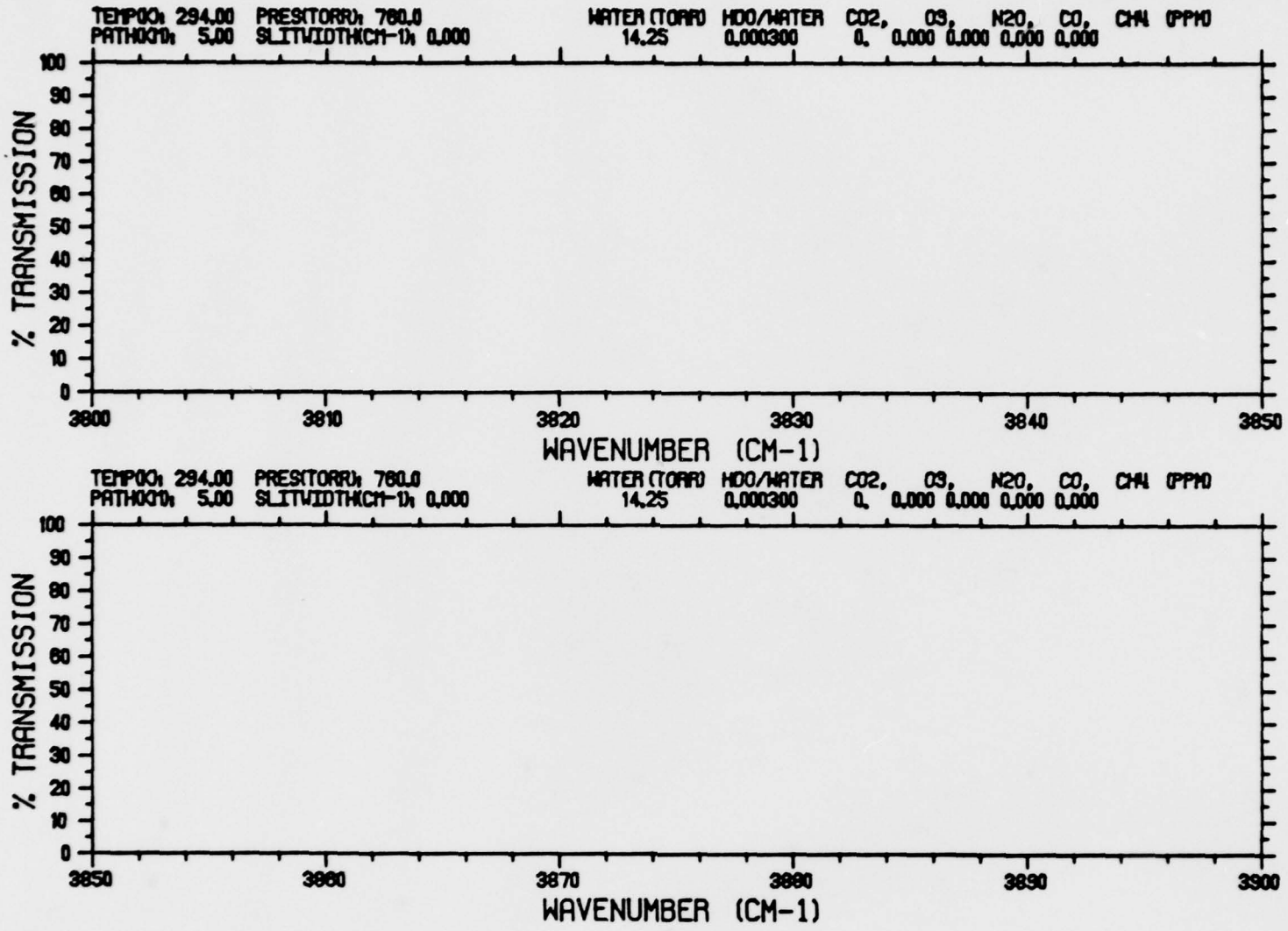

FIGURE 4p. FIGURE 4 CONTINUED

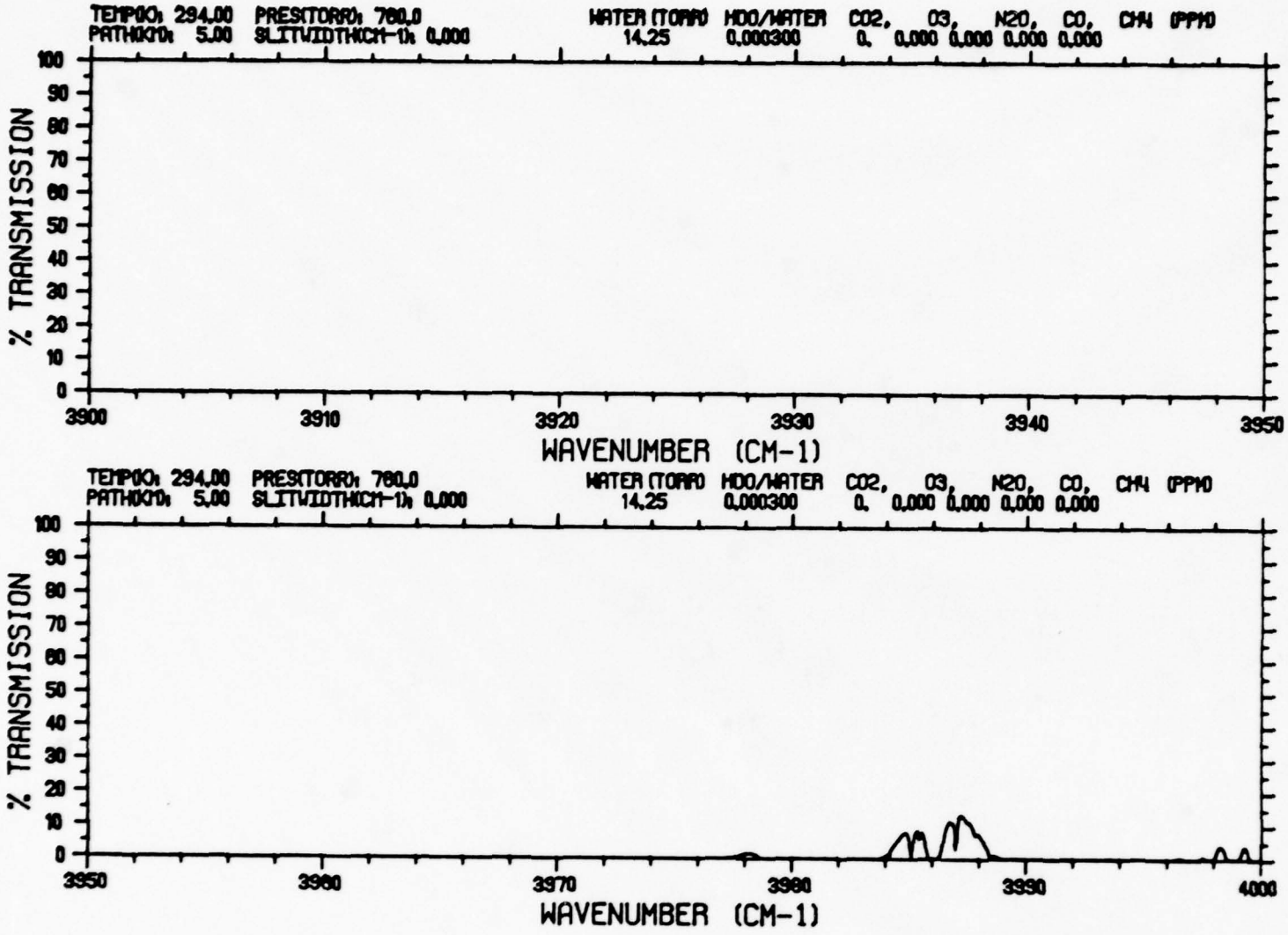

FIGURE 4q. FIGURE 4 CONTINUED

2.5 CH_4 TRANSMISSION SPECTRA

The transmission spectrum through CH_4 above is given in Figures 5a - 5f. The N_2 continuum is outside the spectral range of these plots. CH_4 is the only molecule for which there is serious discrepancy between the synthetic spectra and data [3]. The current plots were made using the January 1977 AFGL data compilation which includes a set of CH_4 parameters which is an improvement over those available earlier. Since CH_4 is of minor importance at sea level, laboratory measurements were not performed. However, the effect of CH_4 on laser transmission at higher altitudes or for long, slant paths is expected to be significant. The abrupt termination of CH_4 absorption in Figure 5f is caused by a lack of entries in the January 1977 version of the AFGL data compilation.

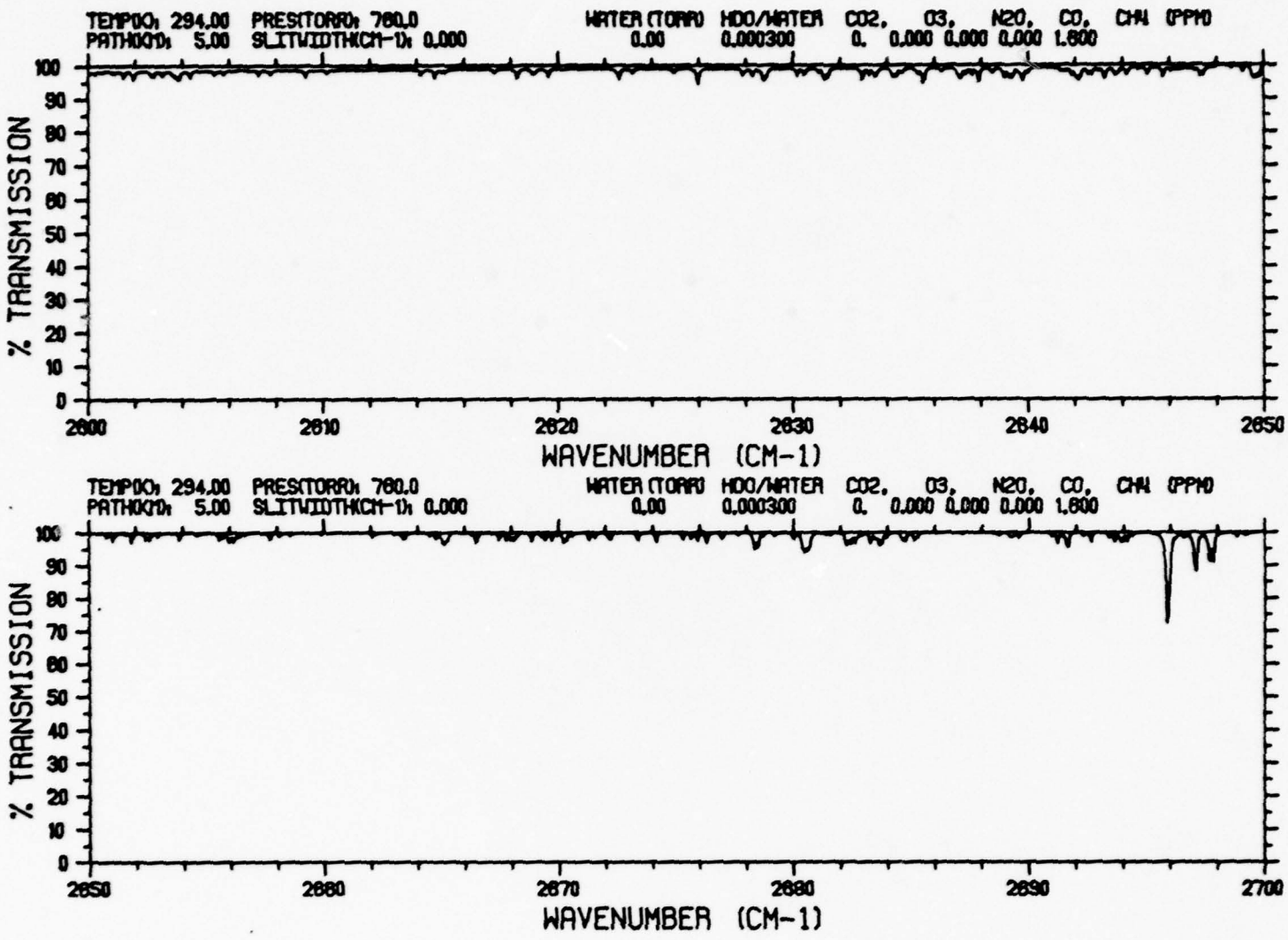

FIGURE 5a. ATMOSPHERIC TRANSMISSION FOR THE CH_4 COMPONENT FOR THE INDICATED CONDITIONS

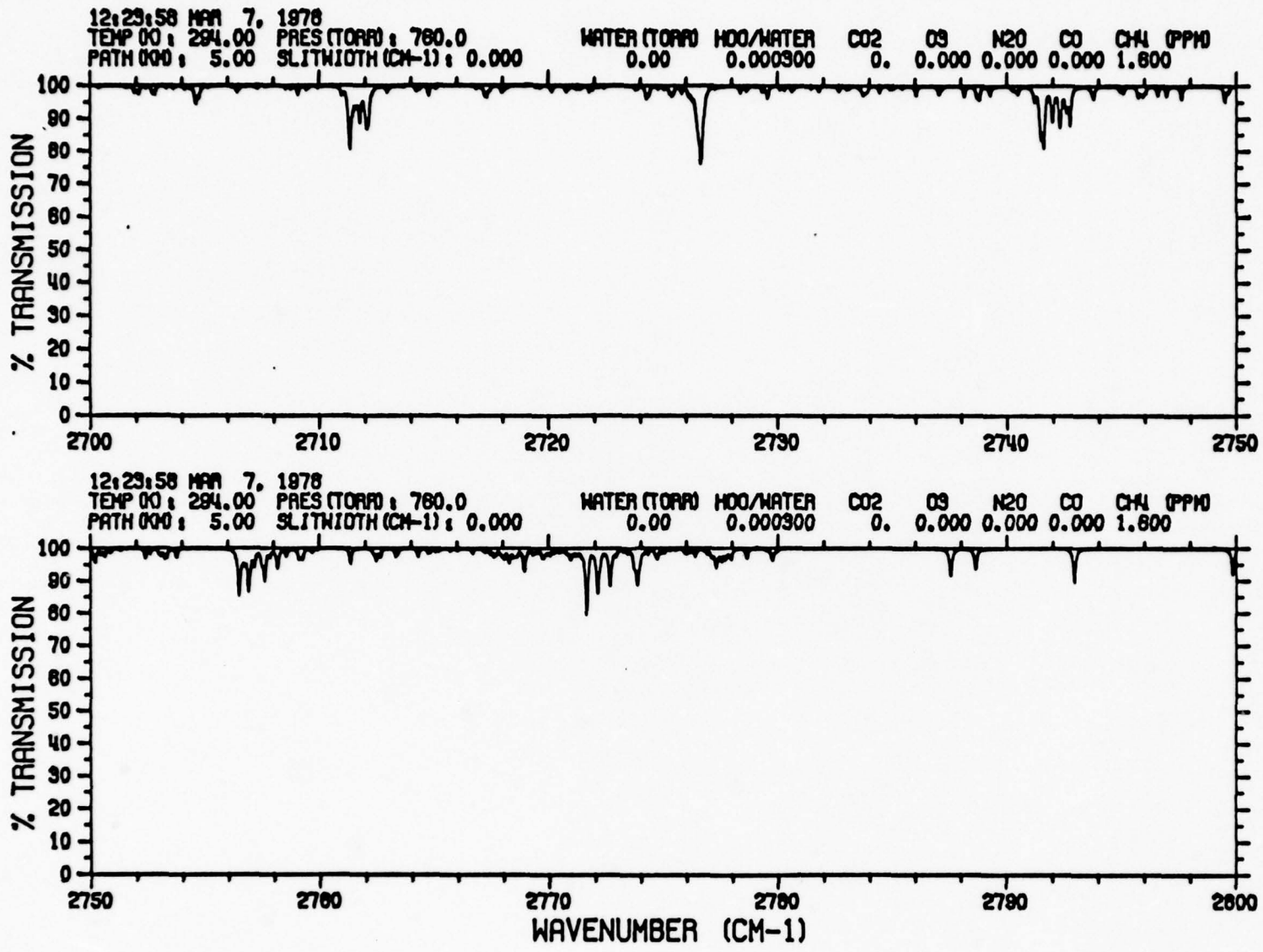

FIGURE 5b. FIGURE 5 CONTINUED

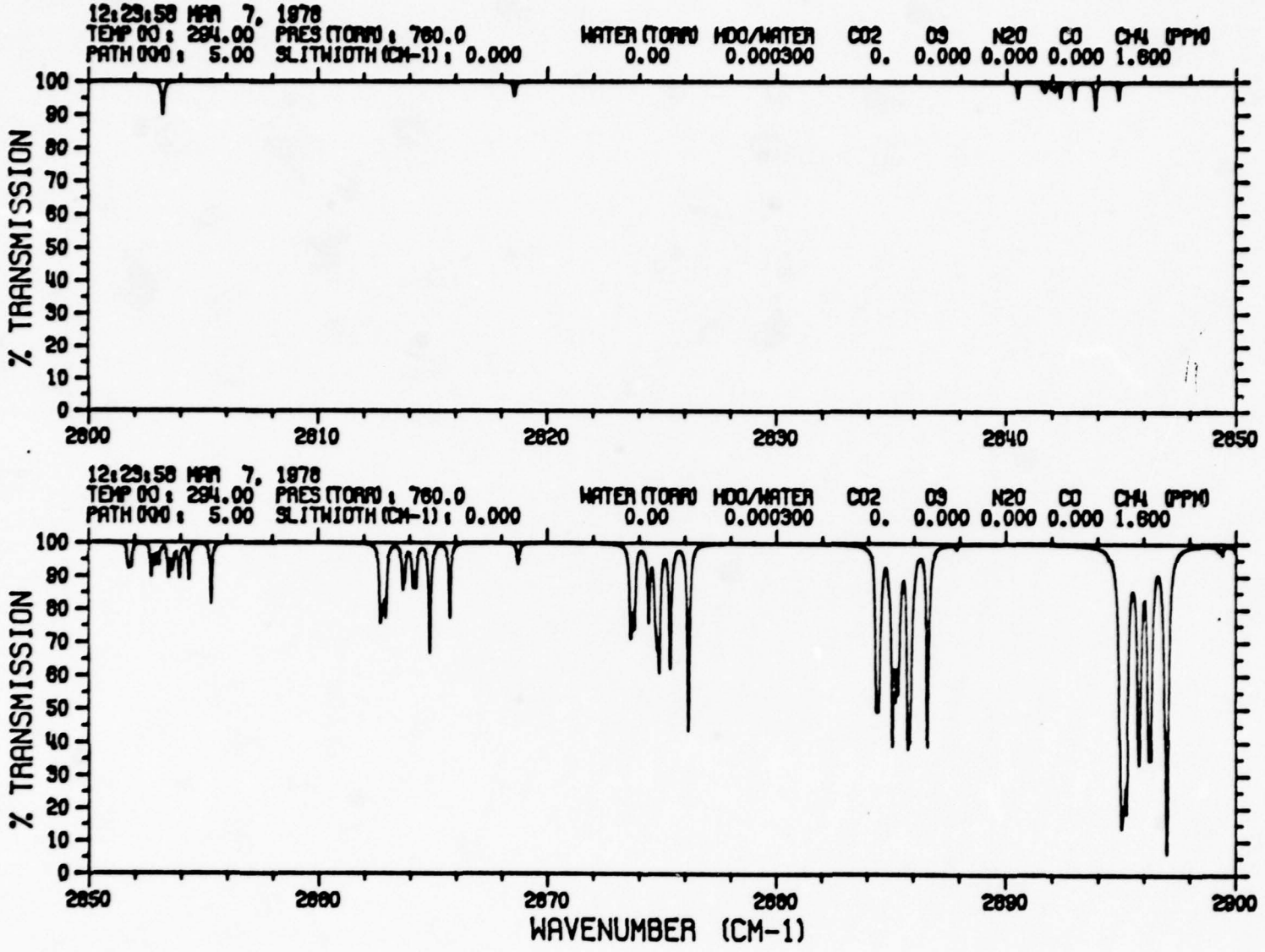

FIGURE 5c. FIGURE 5 CONTINUED

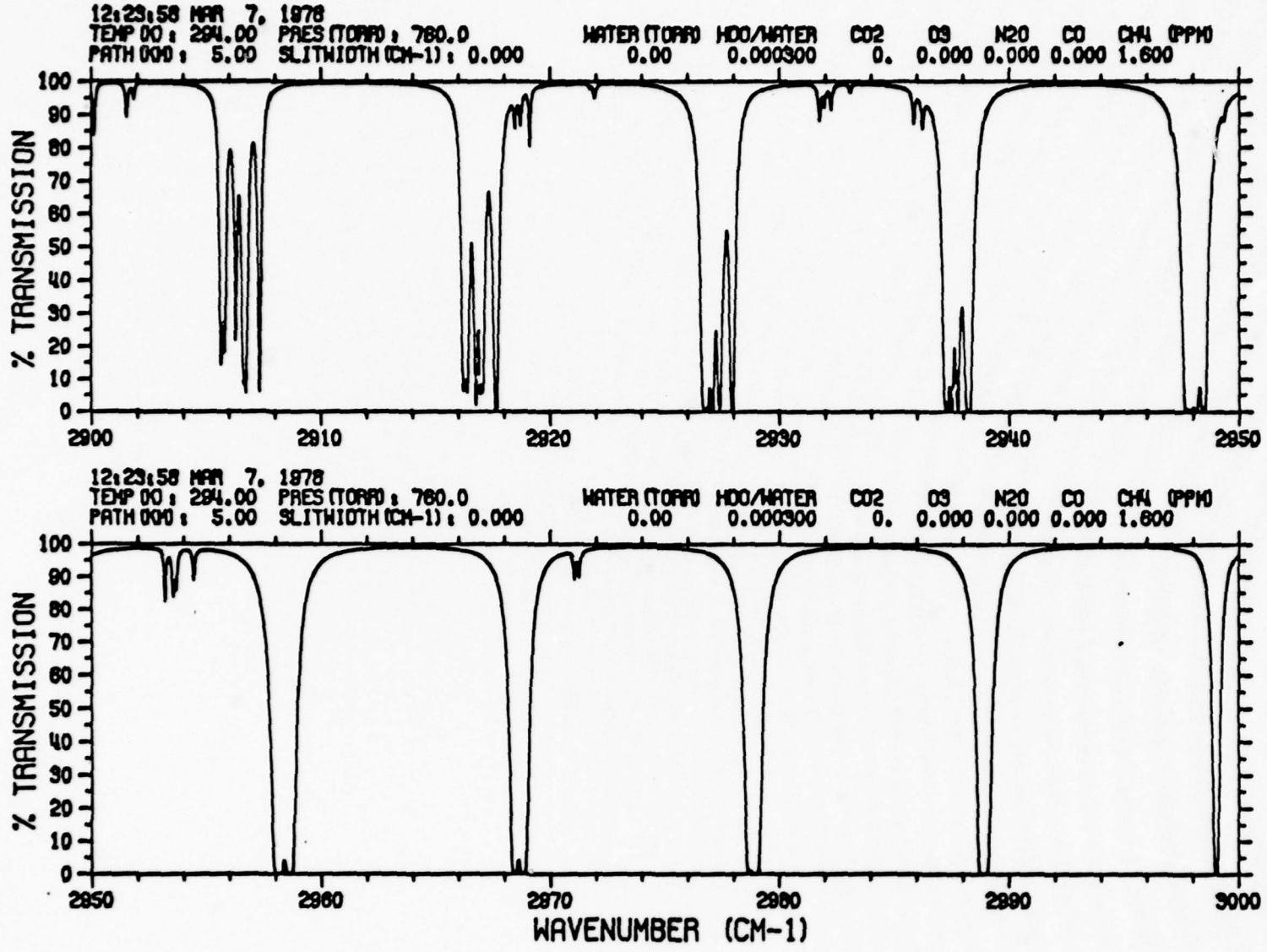

FIGURE 5d. FIGURE 5 CONTINUED

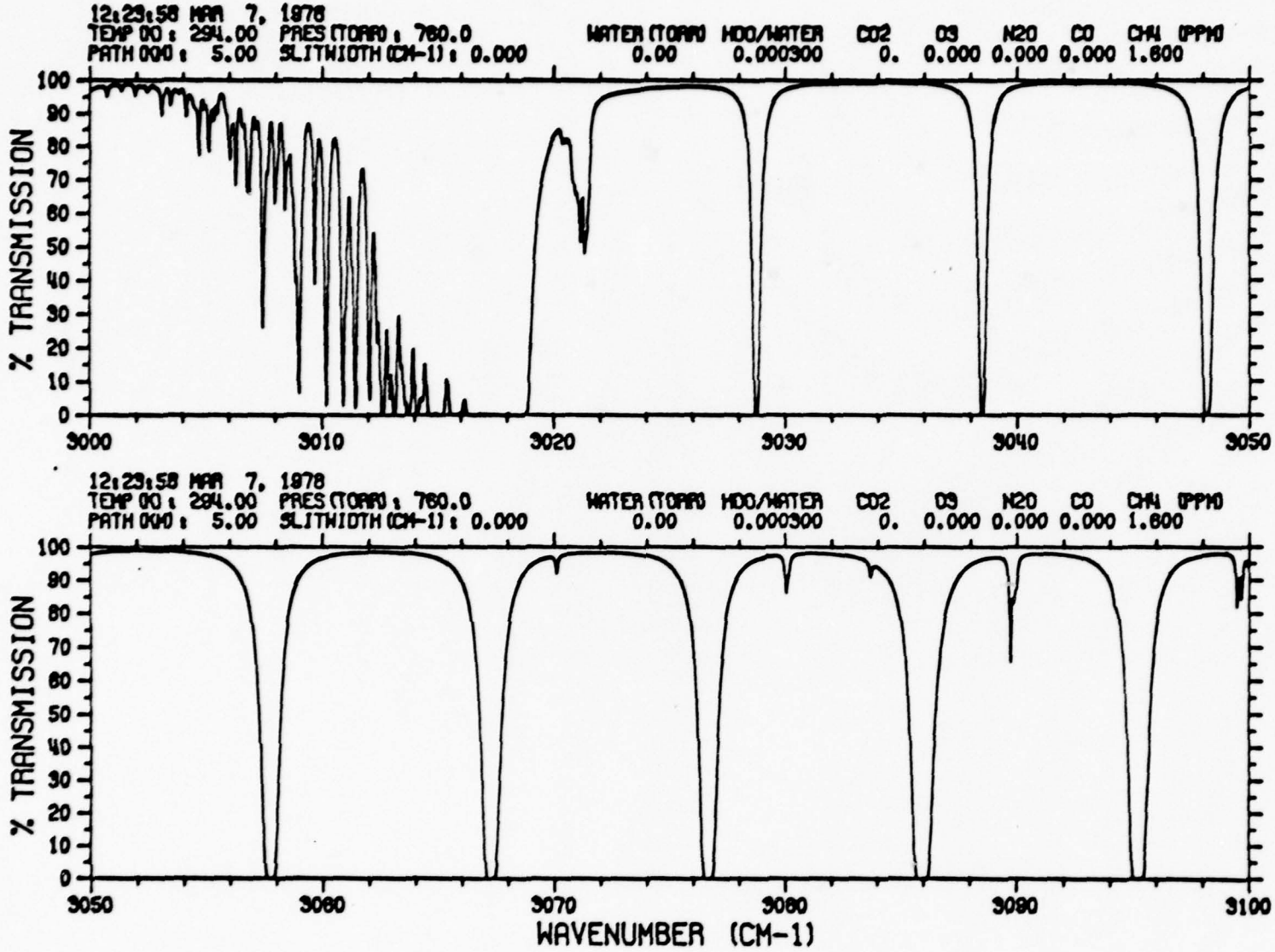

FIGURE 5e. FIGURE 5 CONTINUED

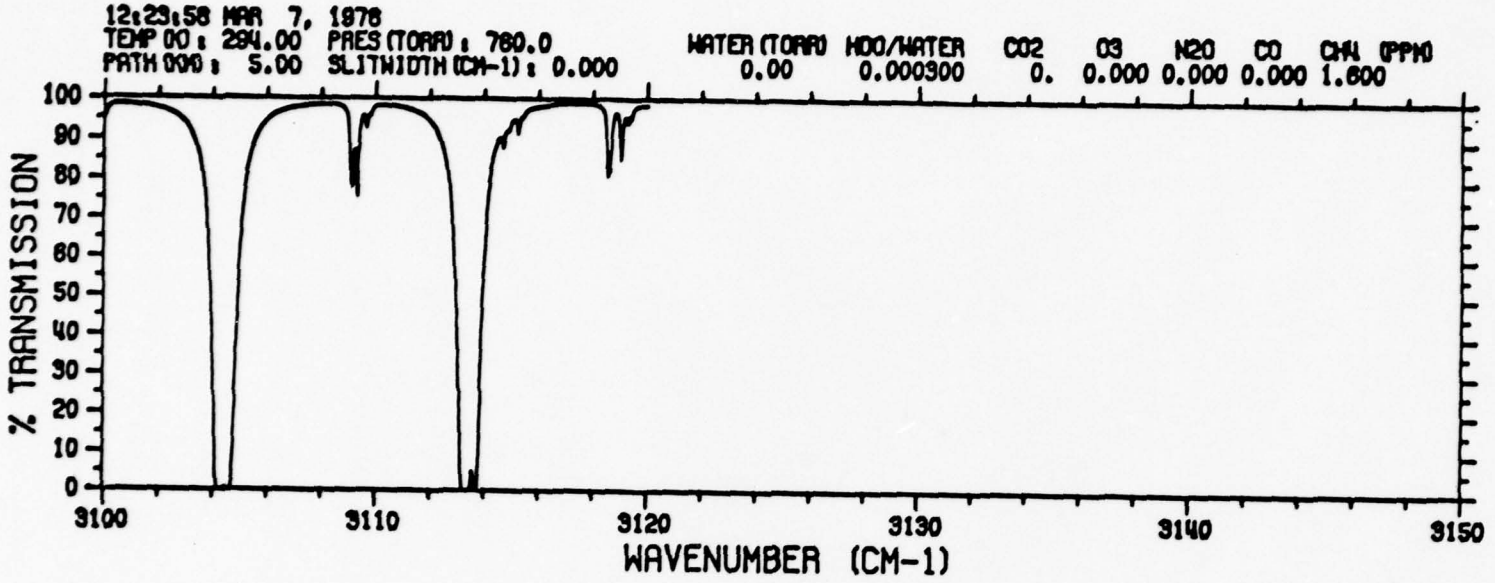

FIGURE 5f. FIGURE 5 CONTINUED

3
HIGH RESOLUTION HDO LINE PROFILE MEASUREMENTS

A large quantity of air broadened HDO data were obtained at several total pressures, water vapor partial pressures, and path lengths. All measurements were performed on the 3 meter focal length Ebert spectrometer located at the Physics Department of The University of Michigan. Details of the measurements apparatus and experimental procedures were explained in detail in an earlier report [2], and therefore they will not be repeated here. In the following paragraphs, the measurements plan will be described and the HDO data will be discussed.

3.1 HDO MEASUREMENTS PLAN

A total of 181 sets of data were obtained on HDO. Description of the 181 sets are included in the Appendix.

The data were taken to fulfill four requirements. These are as follows:

(1) Strength and width determination (S,γ). These are the basic data obtained at several pressure and path length conditions from which the strength and width values are obtained.

(2) Vacuum absorption cell measurements (EMPTY). This information is required for determining the cell mirror reflectivities.

(3) Low pressure data (SLIT). These data are required for determining the spectrometer slit function, for use in FITLINES.

(4) HDO calibration data (HDO cal). These data were obtained to verify that the H_2O + HDO + D_2O mixture had equilibriated with themselves and with the cell walls. When the cell was filled with different amounts of the D isotope, scans were made to verify that the HDO did not change with time, and that new fills were existent with old.

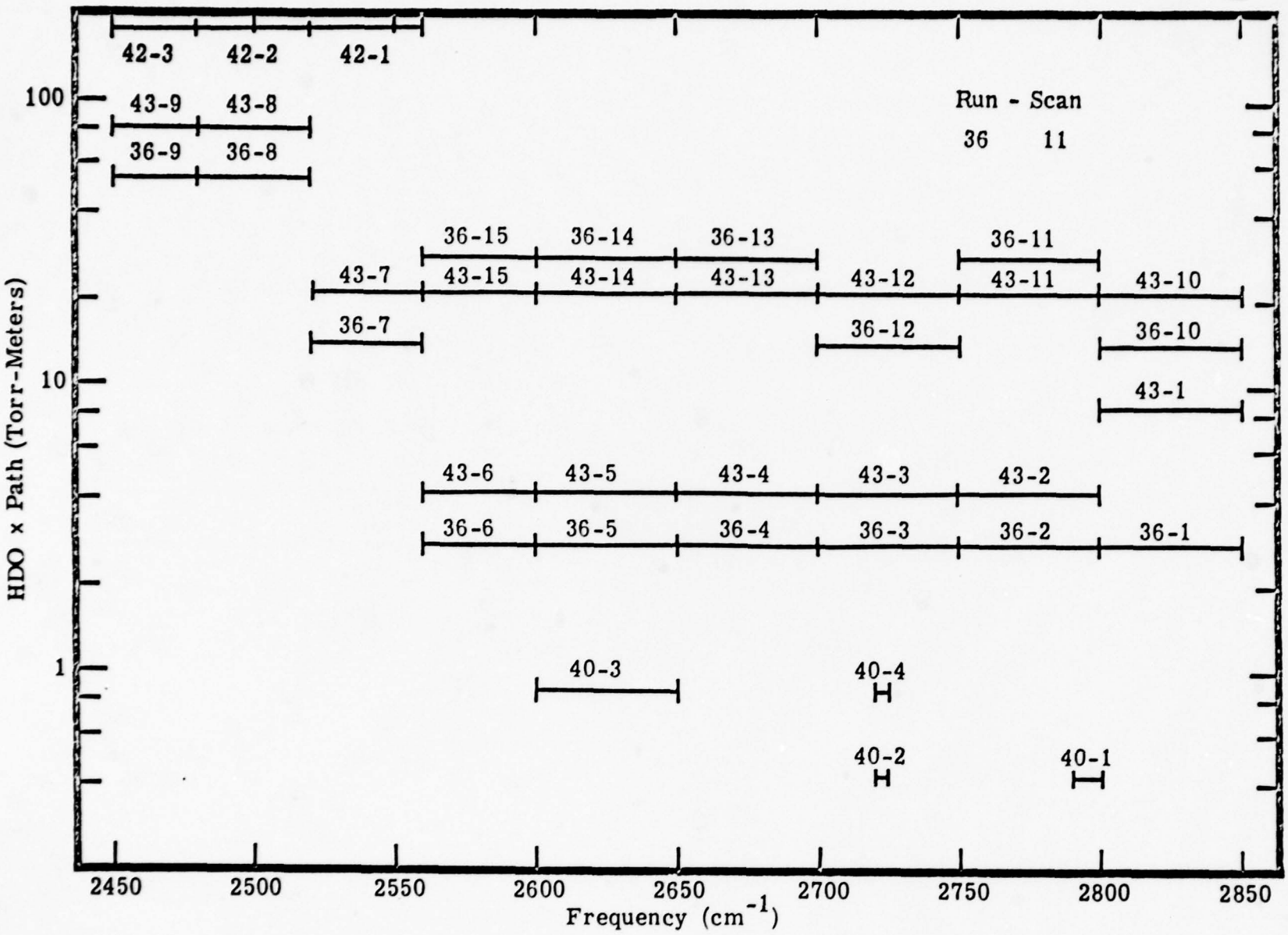

Figure 6. HDO Scan Index for 4 psi Dry Air Broadening

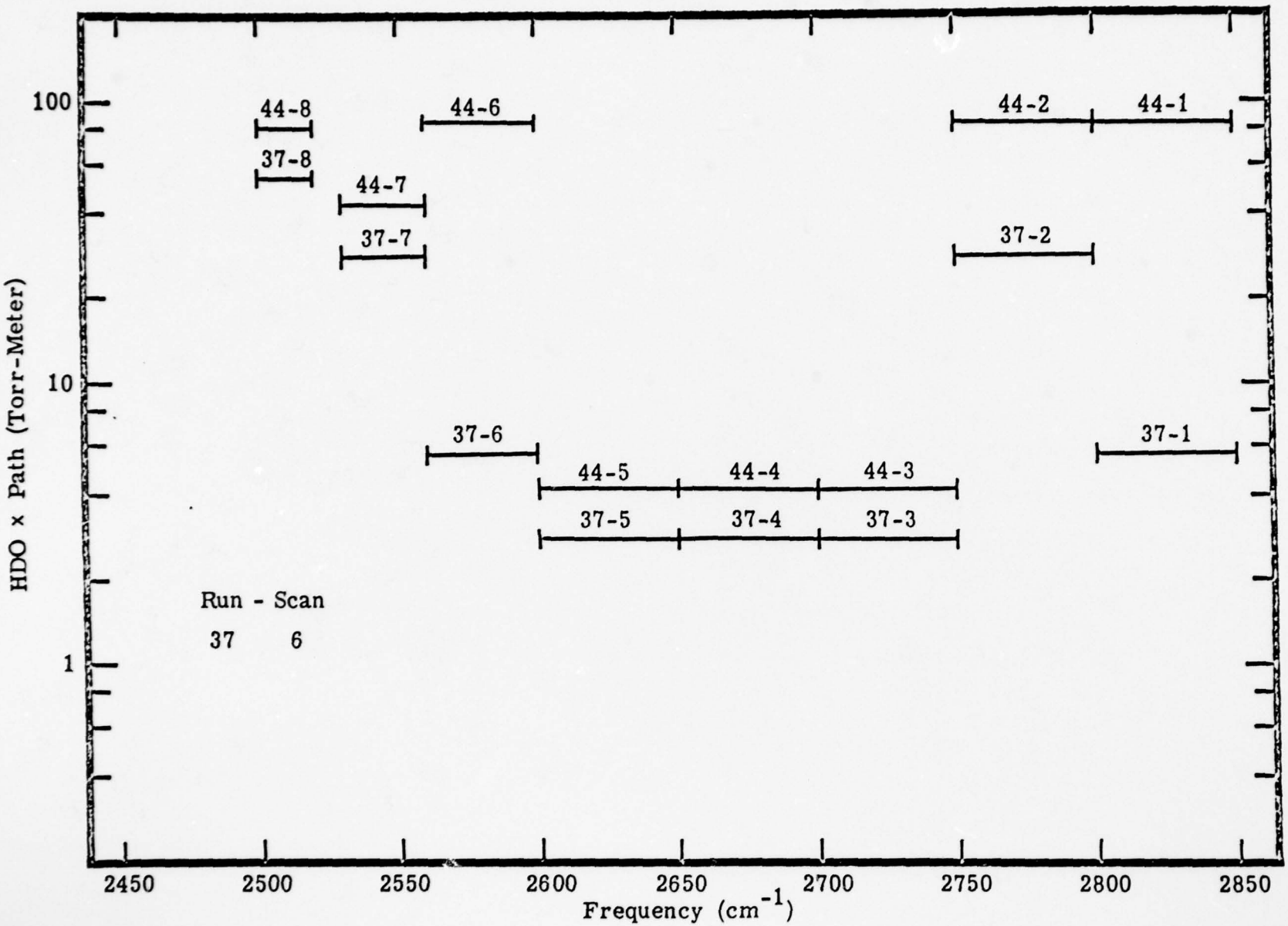

Figure 7. HDO Scan Index for 8 psi Dry Air Broadening

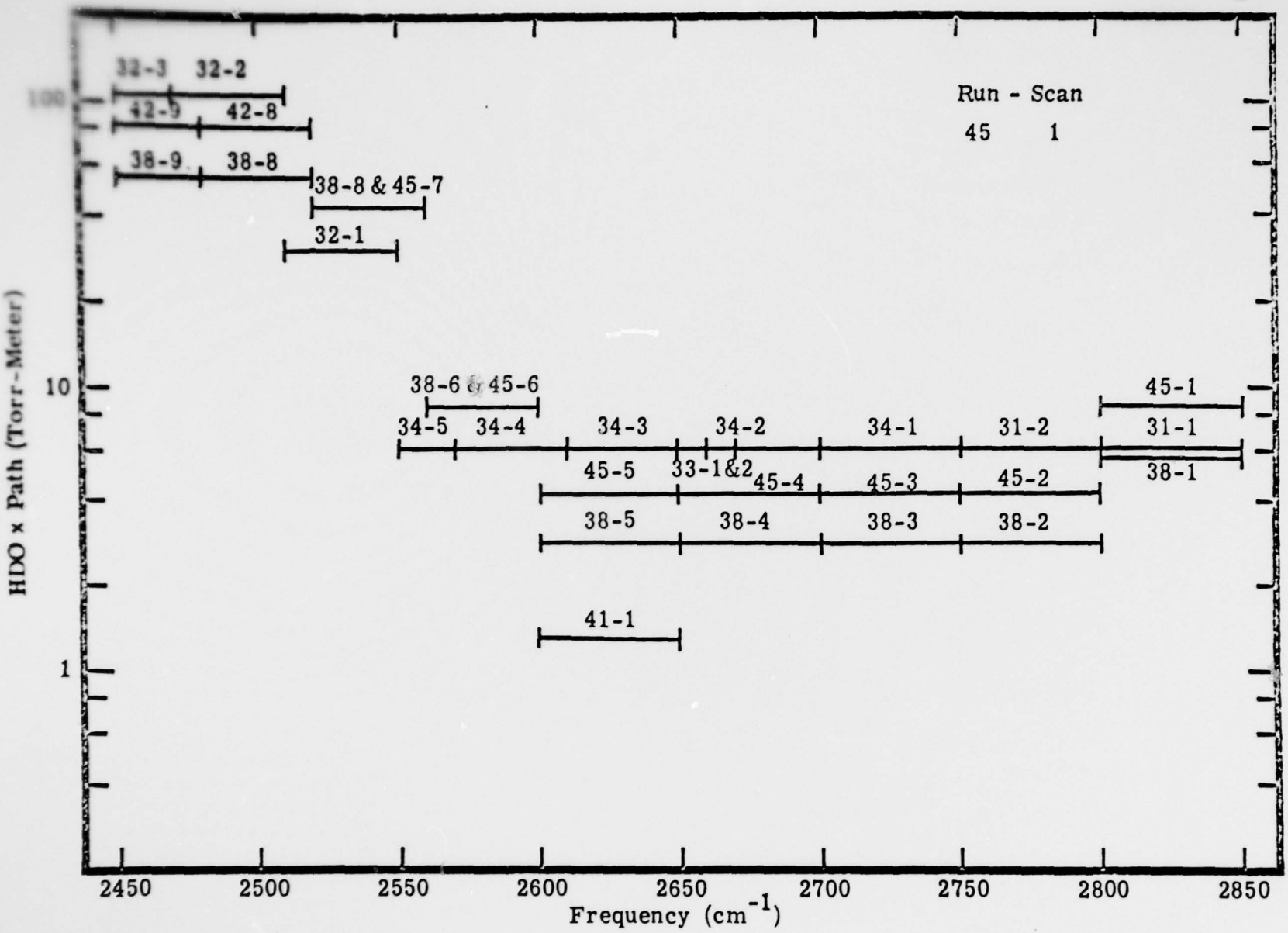

Figure 8. HDO Scan Index for 14.7 psi Dry Air Broadening

(5) Line position data ($\bar{\nu}$). This data was taken with the pulsed DF laser operating, to obtain HDO line center positions, relative to the DF laser lines. Data was taken for three total air pressures: 4 PSI, 8 PSI, and 14.7 PSI. A complete summary of the data is given in Figures 6, 7, and 8, respectively, for these cases.

A "run" is defined as a set of scans for which the cell fill is not changed. A "run" is an individual spectroscopic scan, usually limited by the data which could be obtained as a single tape cassette. A complete description of the individual runs and scans is given in the Appendix.

3.2 HDO MEASUREMENTS

Line profile measurements have been performed throughout the entire spectral region that it is a significant absorber of DF laser radiation. The entire data accumulation, for strength and width as well as for diagnostic requirements are summarized in the Appendix.

Reproduction of all the data in the form of transmission plots would be costly and extremely voluminous. Therefore, a smaller set of data has been selected for plotting in the SAI format. Only the spectra of samples having a total pressure of ~1 atm have been plotted. This choice is made since this condition is representative of the sea level propagation altitude most important to the Navy. Theoretical plots have been calculated for the same path length and pressure conditions as the data measured. Strength and width parameters for the theoretical plots were obtained from the AFGL data tape, January 1977 version. These plots are reproduced on the same page as measured data for easy comparison. The agreement is quite good relative to earlier comparisons. This is essentially because this data has been used to update HDO parameter modeling in the AFGL compilation prior to its publication [14].

The data selected for publication and the calculated plots are shown in Figures 9 - 14. Figures 9 and 10 represent an initial cell fill of 9.41 torr total water vapor, for path lengths of 380 m and 20 m respectively. Figures 11 and 12 describe initial cell fills of 6.61 torr total water vapor, for 20 m and 40 m path length respectively. Figures 13 and 14 are for initial cell fills of 4.37 torr total water vapor, for 380 m and 300 m path length, respectively. Identification of D_2O lines present in the spectra has not been attempted.

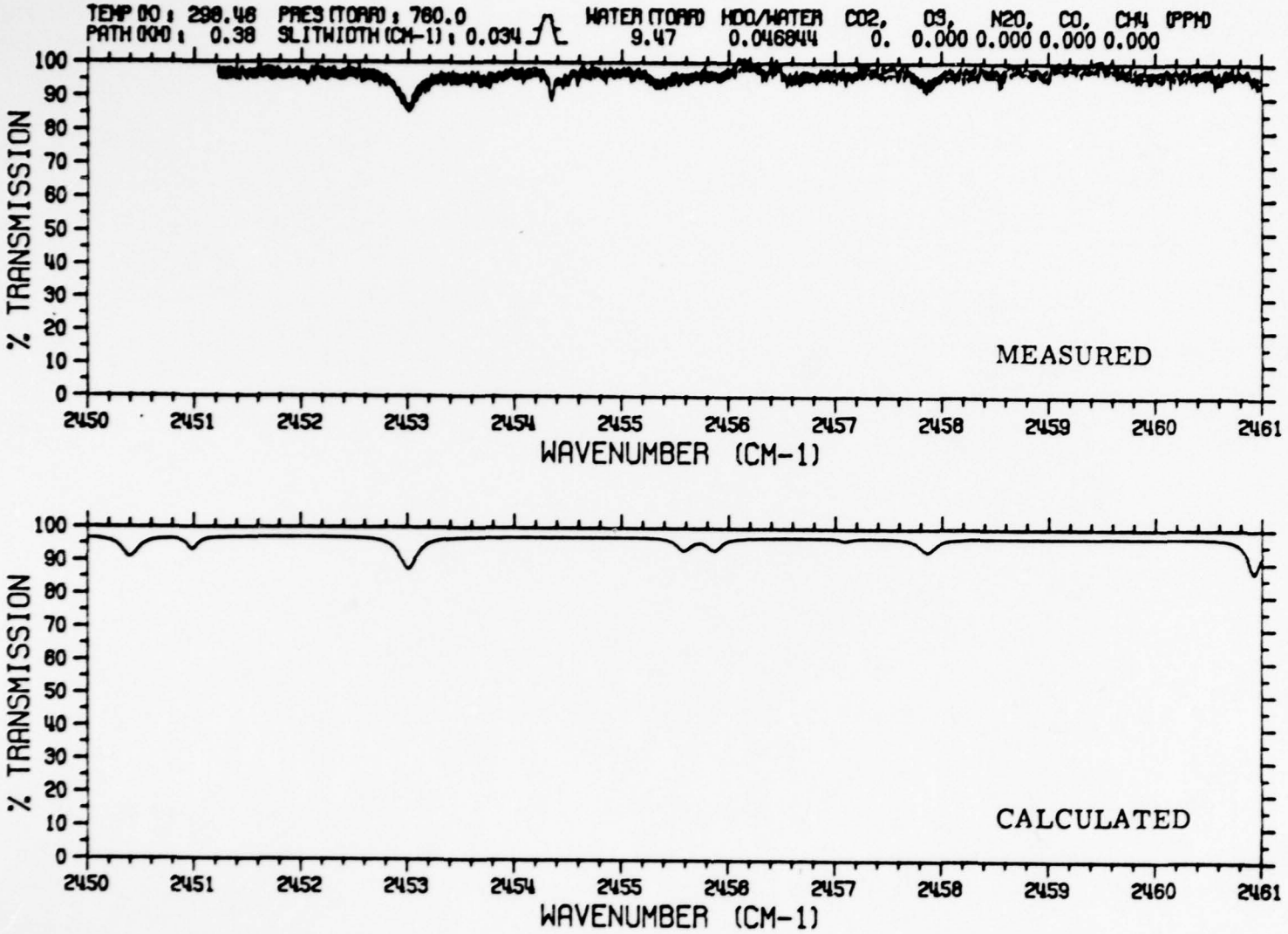

FIGURE 9a. HDO MEASUREMENTS AND COMPARISON PLOTS FOR 9.41 TORR TOTAL WATER VAPOR FILL PRESSURE, 380 M. PATH

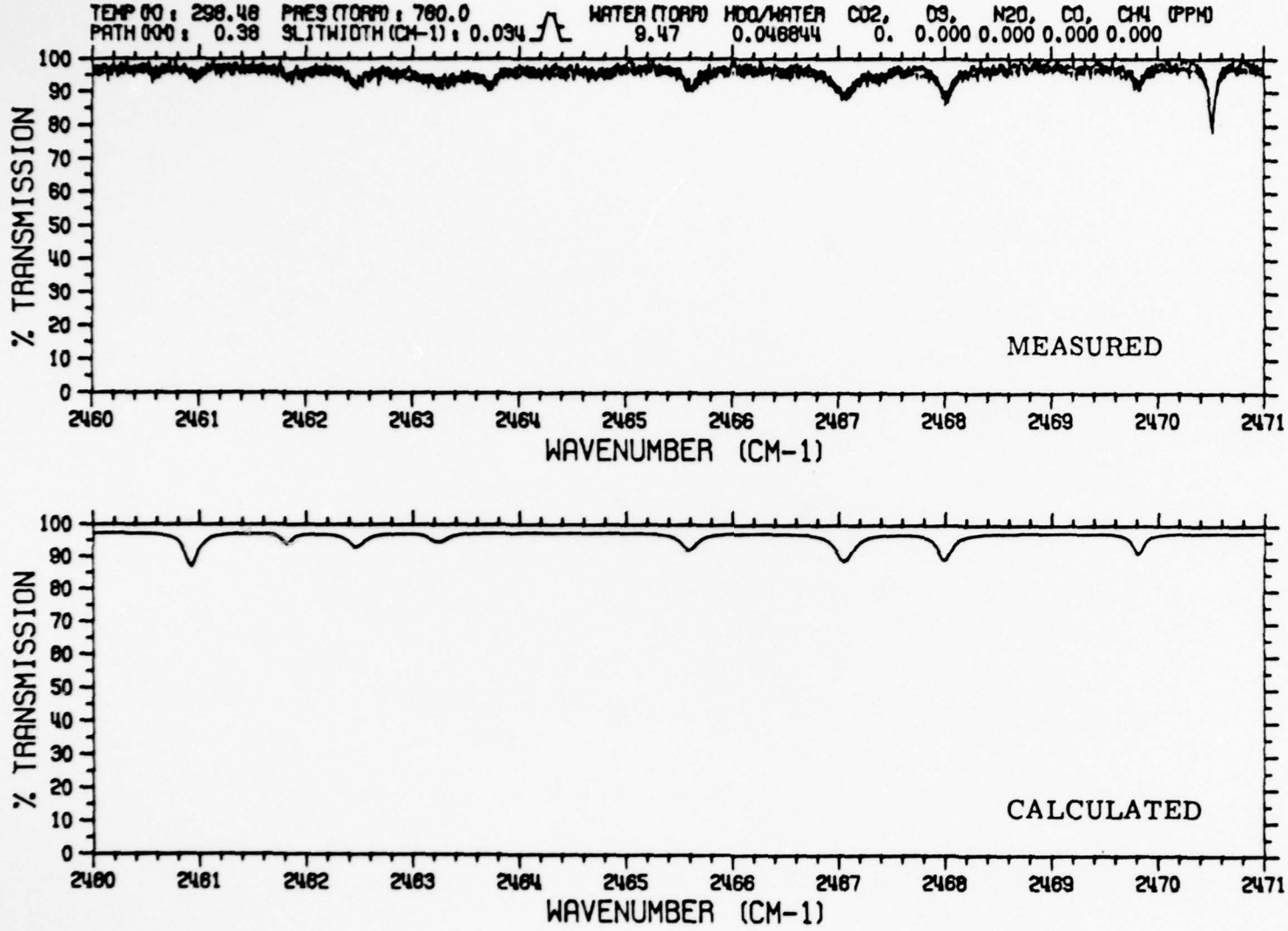

FIGURE 9b. FIGURE 9 CONTINUED

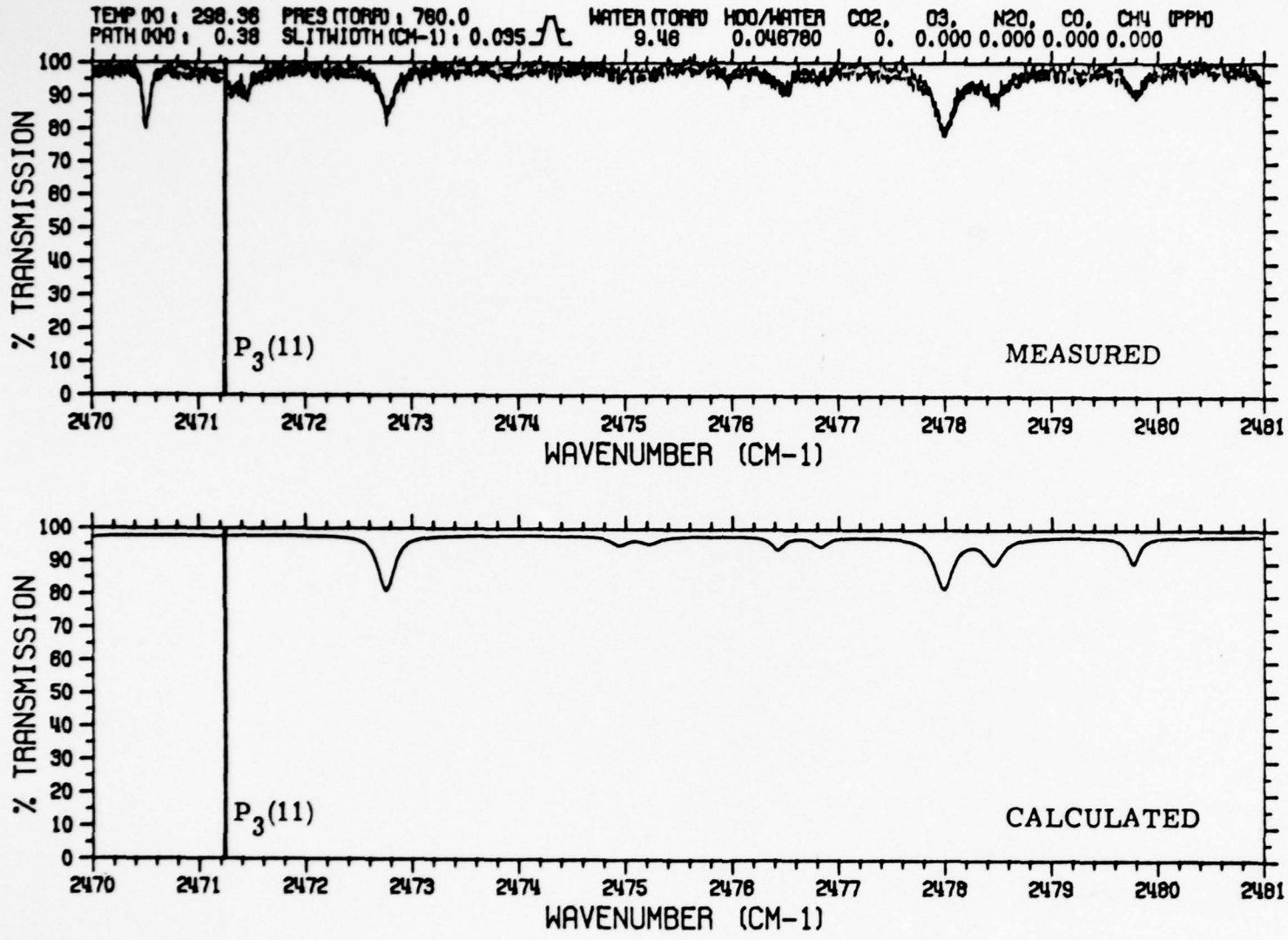

FIGURE 9c. FIGURE 9 CONTINUED

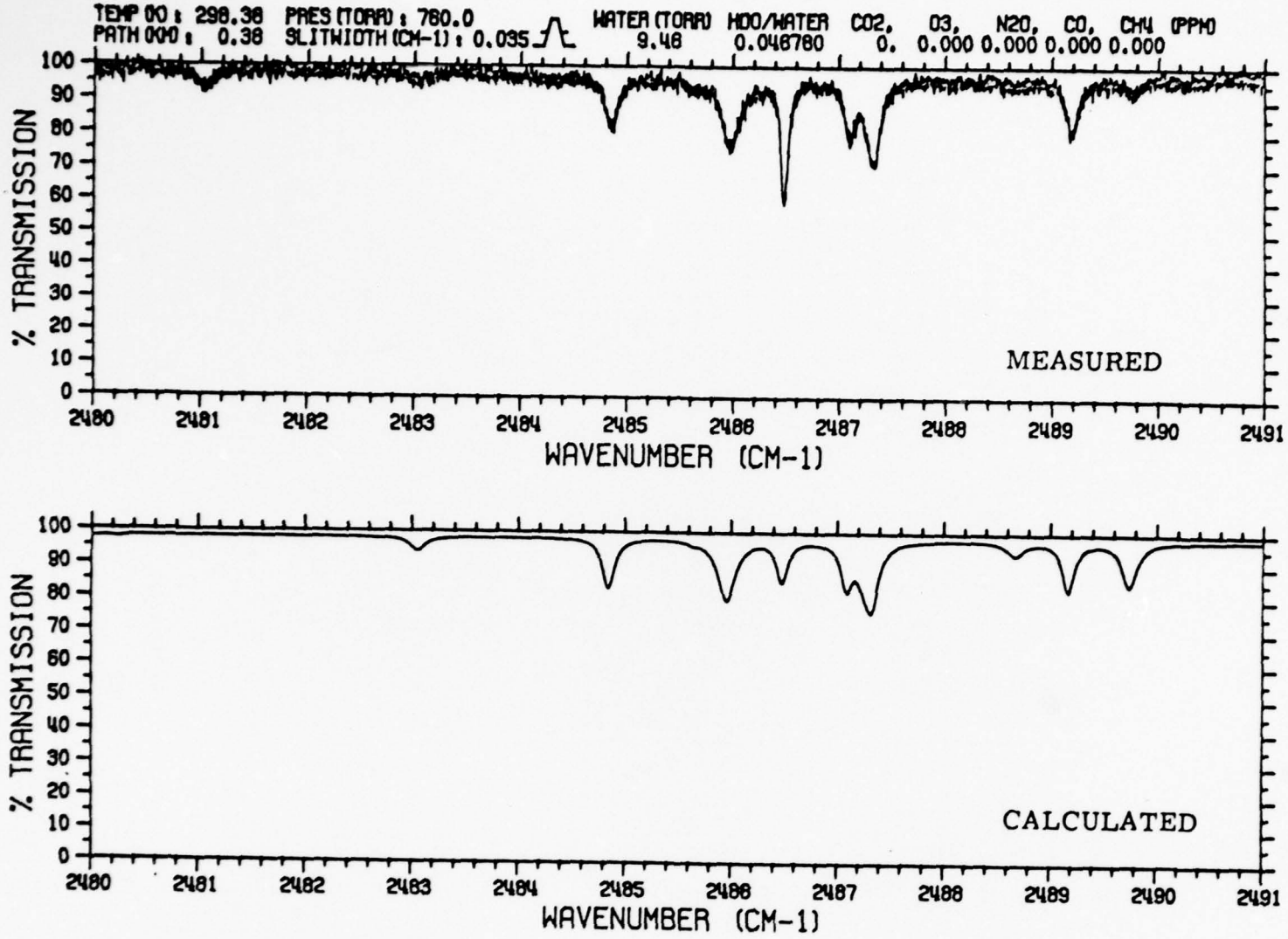

FIGURE 9d. FIGURE 9 CONTINUED

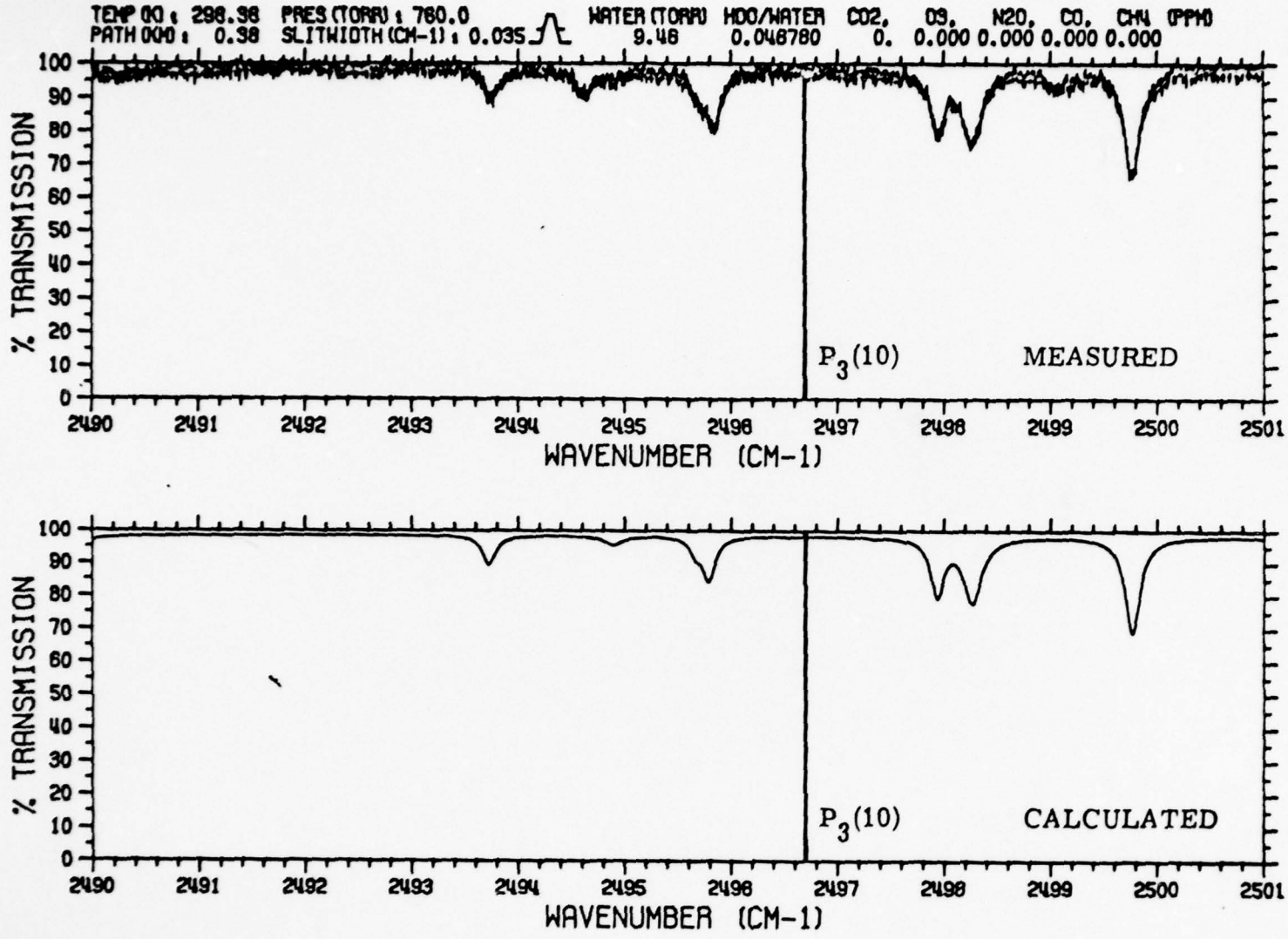

FIGURE 9e. FIGURE 9 CONTINUED

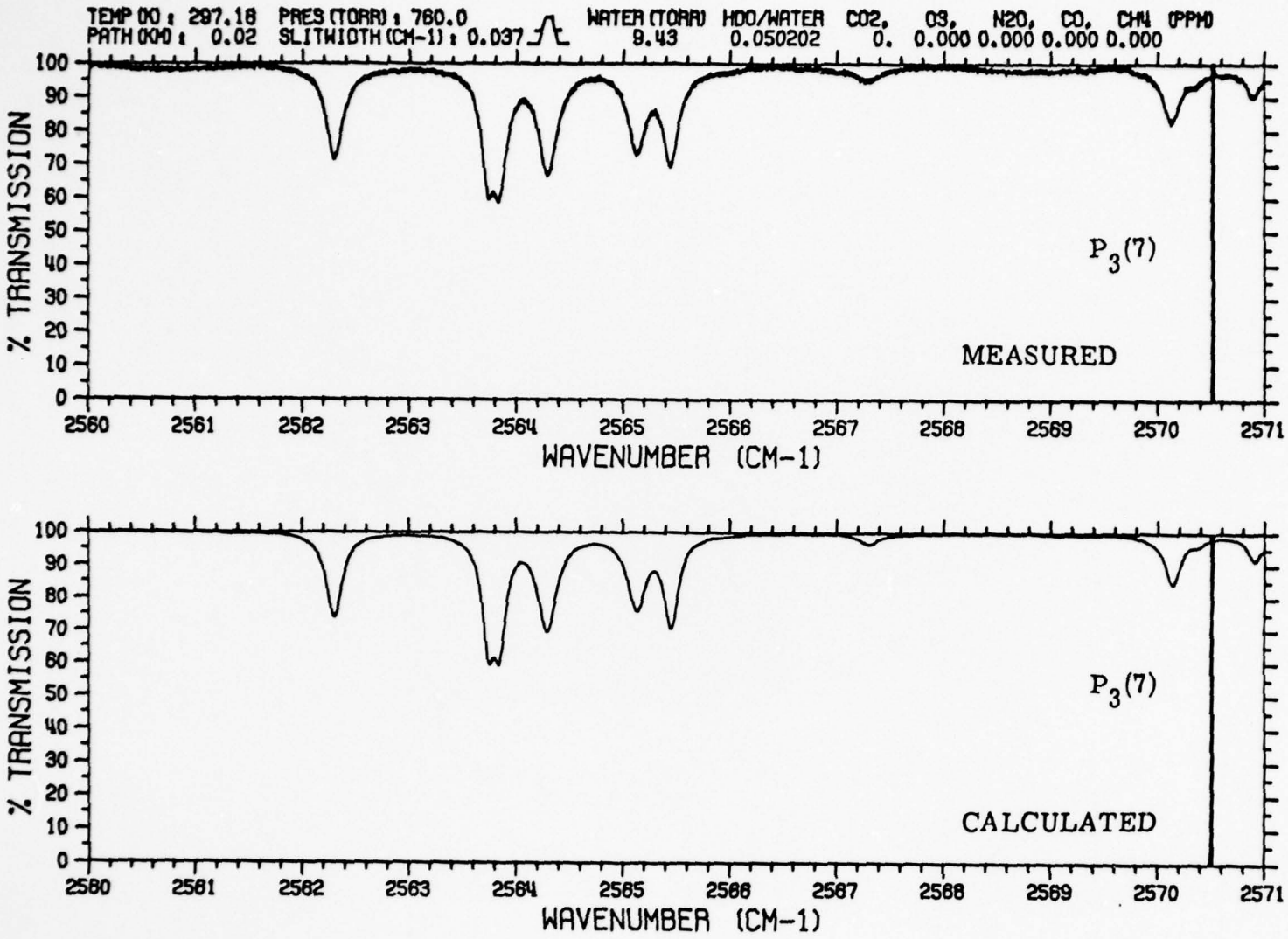

FIGURE 10a. HDO MEASUREMENTS AND COMPARISON PLOTS FOR 9.41 TORR TOTAL WATER VAPOR FILL PRESSURE, 20 M. PATH

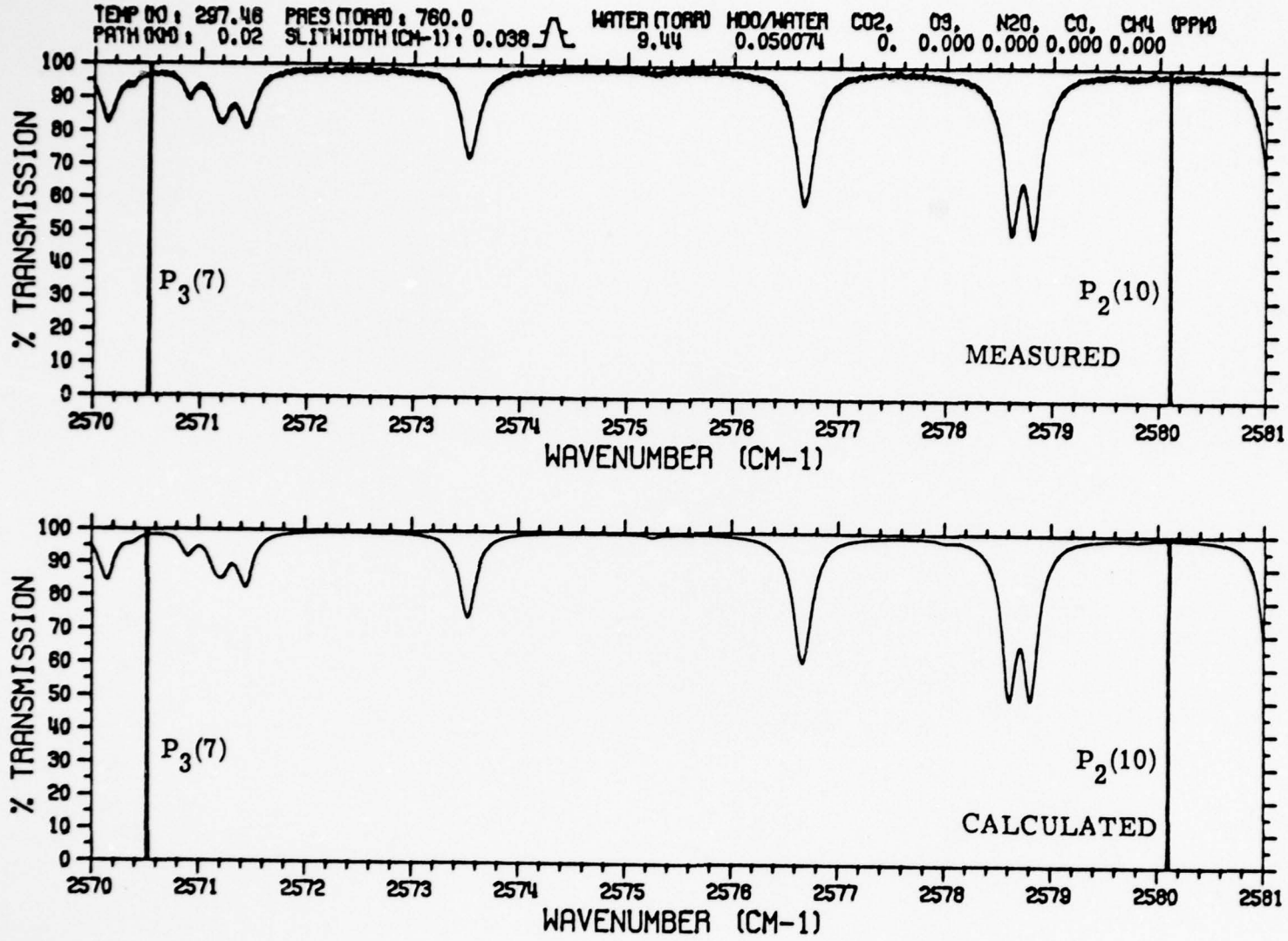

FIGURE 10b. FIGURE 10 CONTINUED

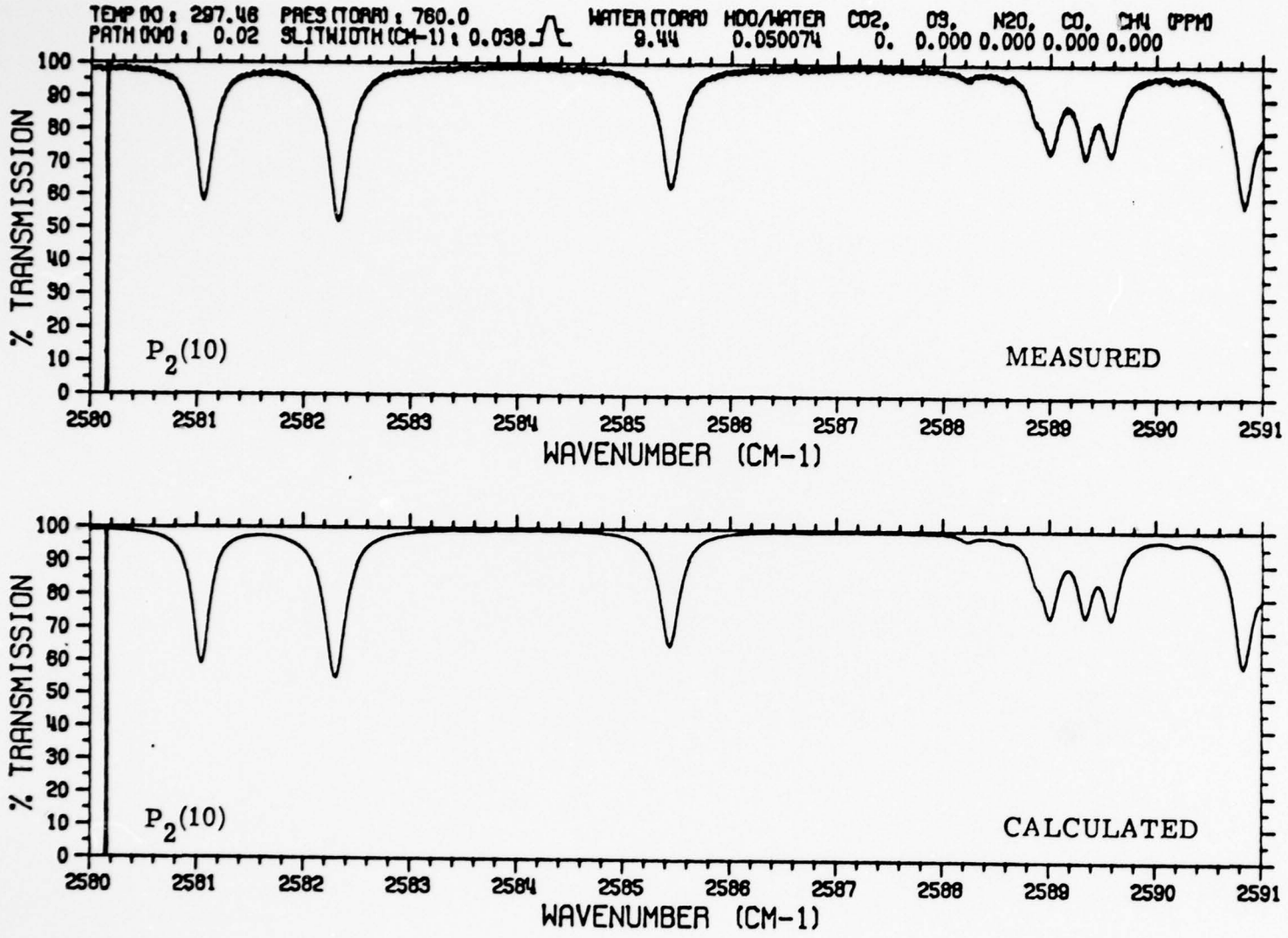

FIGURE 10c. FIGURE 10 CONTINUED

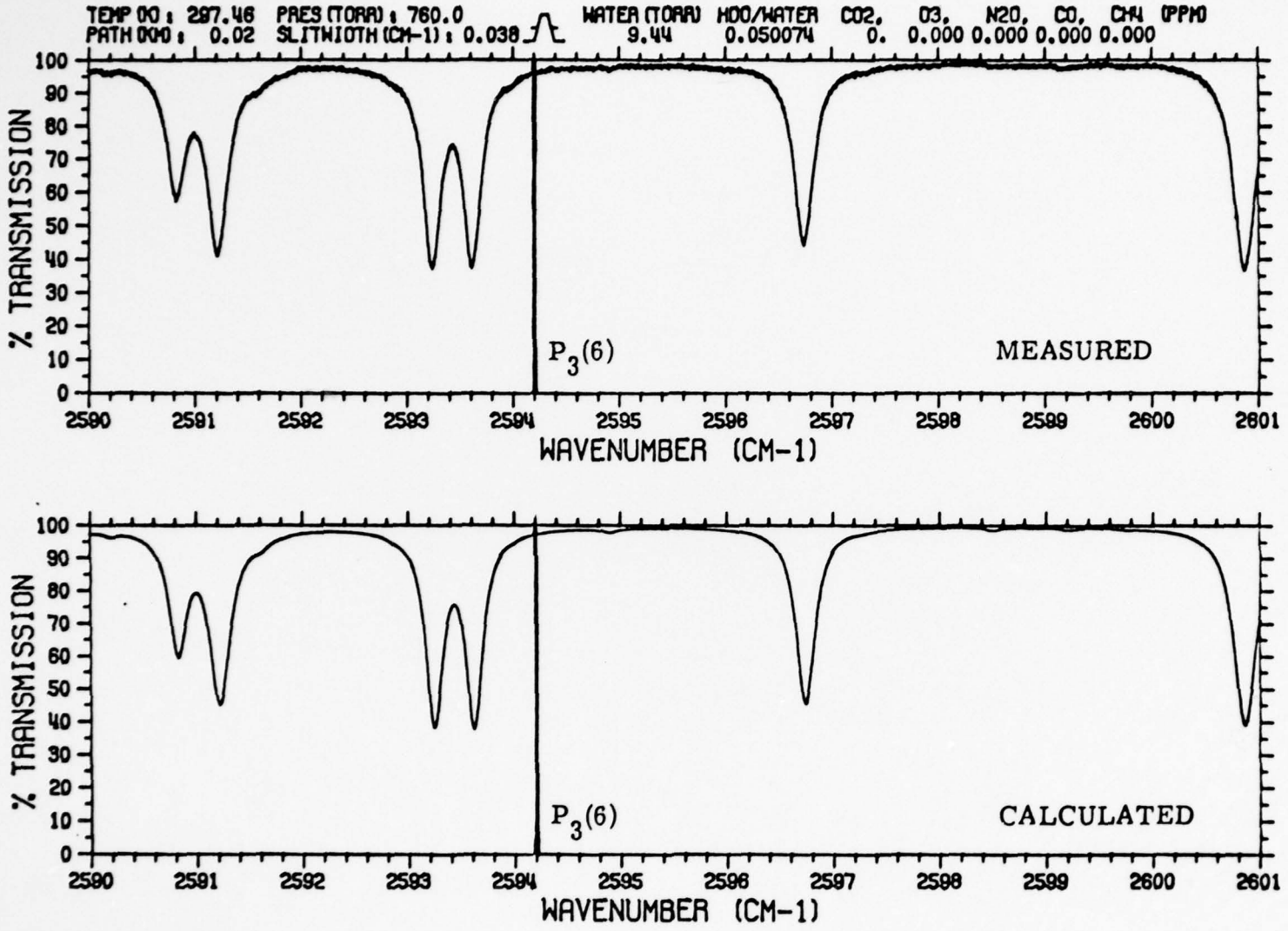

FIGURE 10d. FIGURE 10 CONTINUED

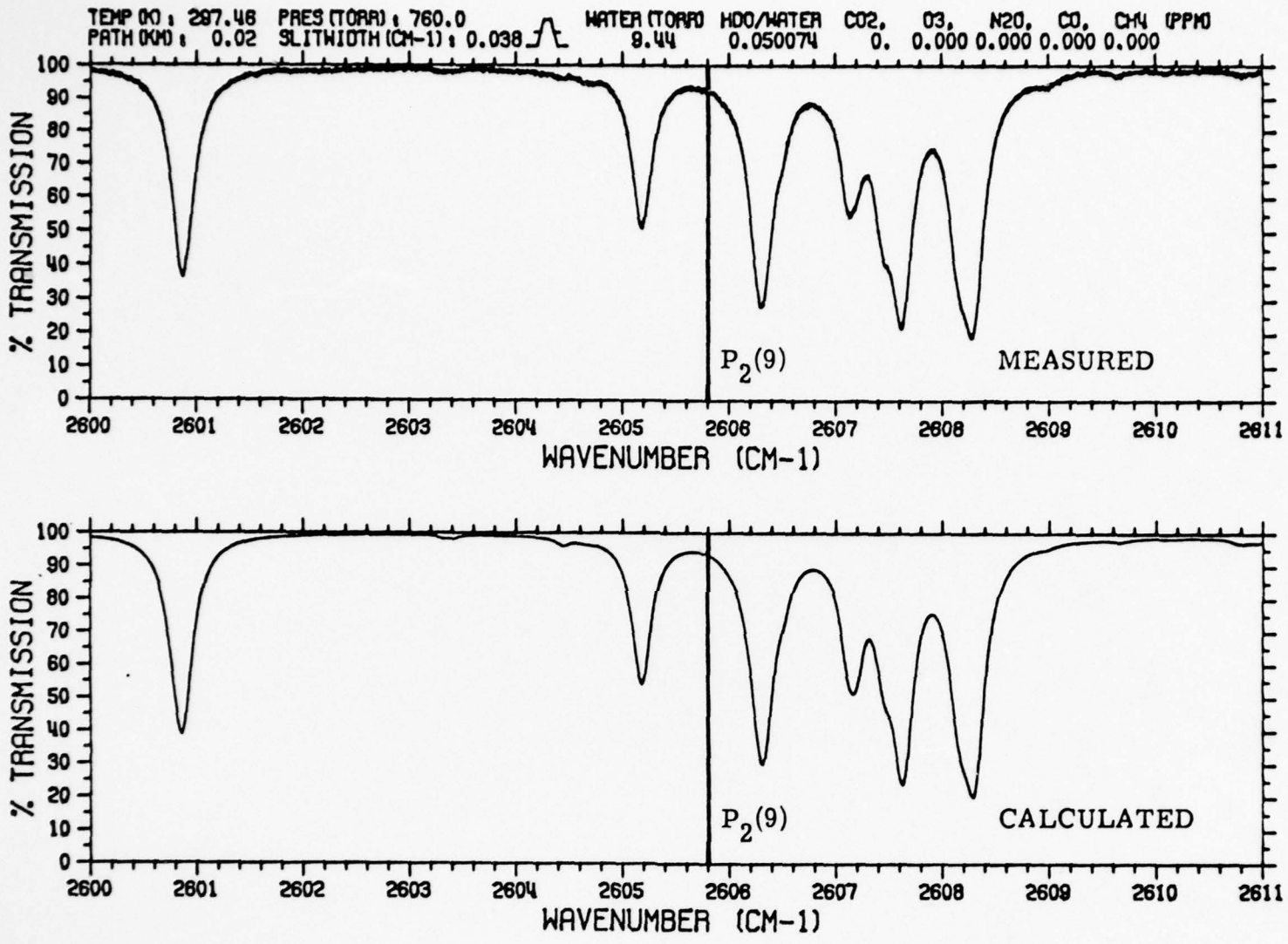

FIGURE 10e. FIGURE 10 CONTINUED

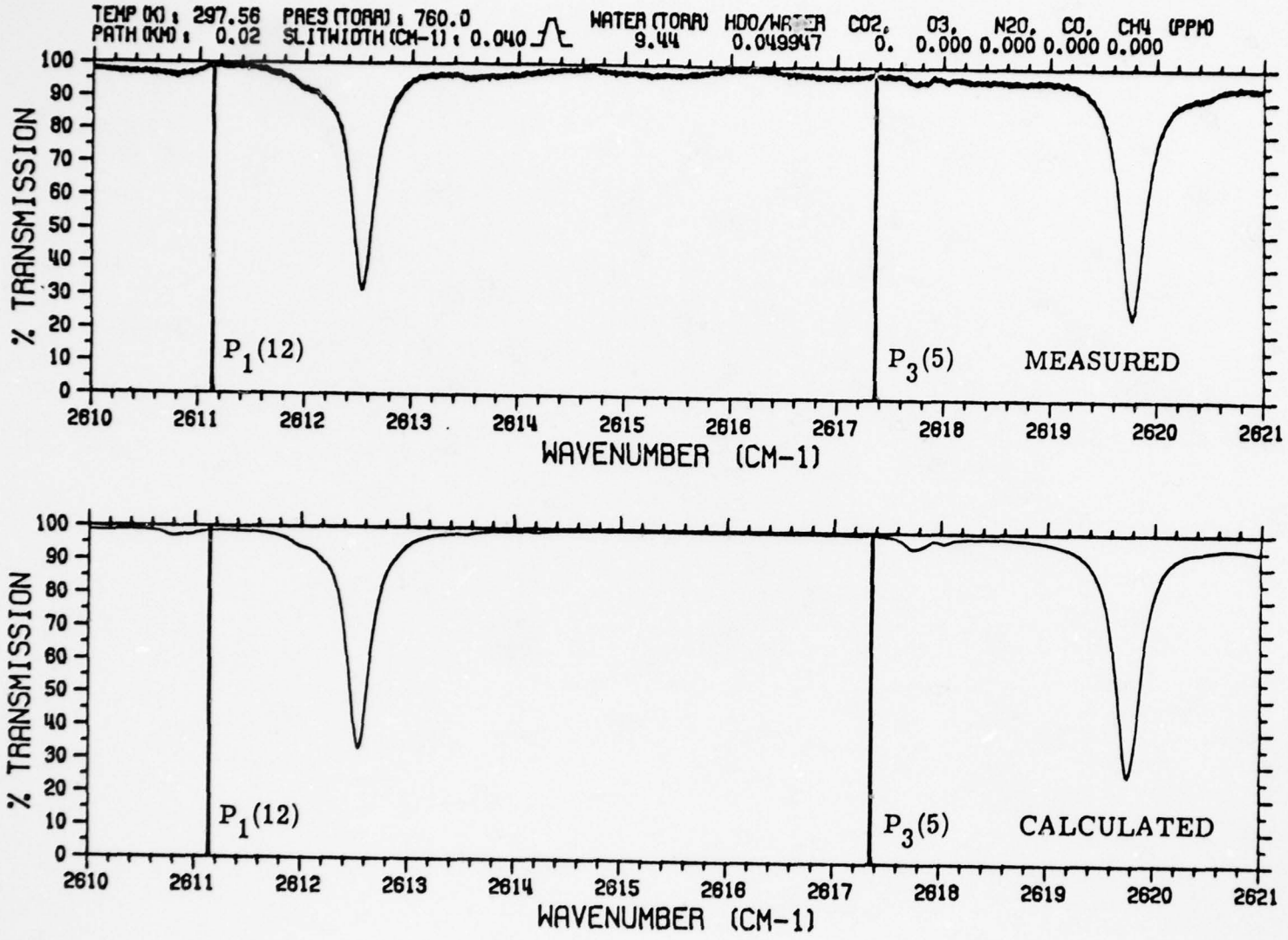

FIGURE 10f. FIGURE 10 CONTINUED

AD-A069 020 SCIENCE APPLICATIONS INC ANN ARBOR MICH F/G 20/6
SPECTROSCOPIC DATA BASE FOR DF LASER TRANSMISSION MODELING.(U)
DEC 77 D R WOODS, D H LESLIE, J L MANNING N00173-76-C-0152
UNCLASSIFIED SAI-77-918-AA NL

2 OF 2
AD A069020

END
DATE FILMED
6-79
DDC

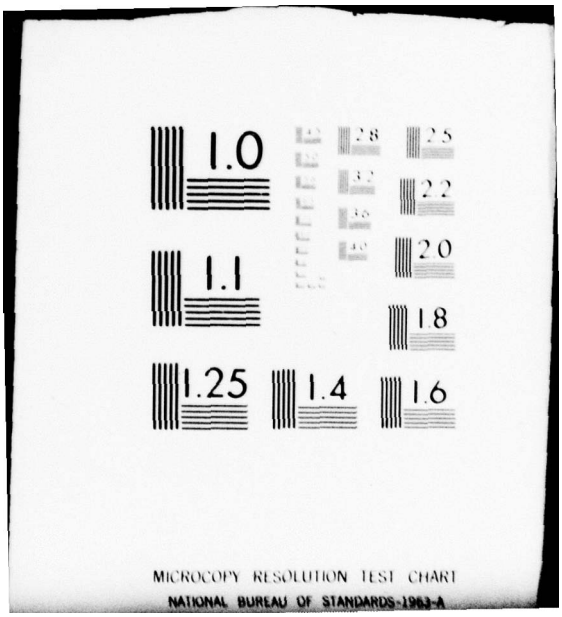
1.0
1.1
1.25
1.4
1.6
2.8
2.5
2.2
2.0
1.8
MICROCOPY RESOLUTION TEST CHART
NATIONAL BUREAU OF STANDARDS-1963-A

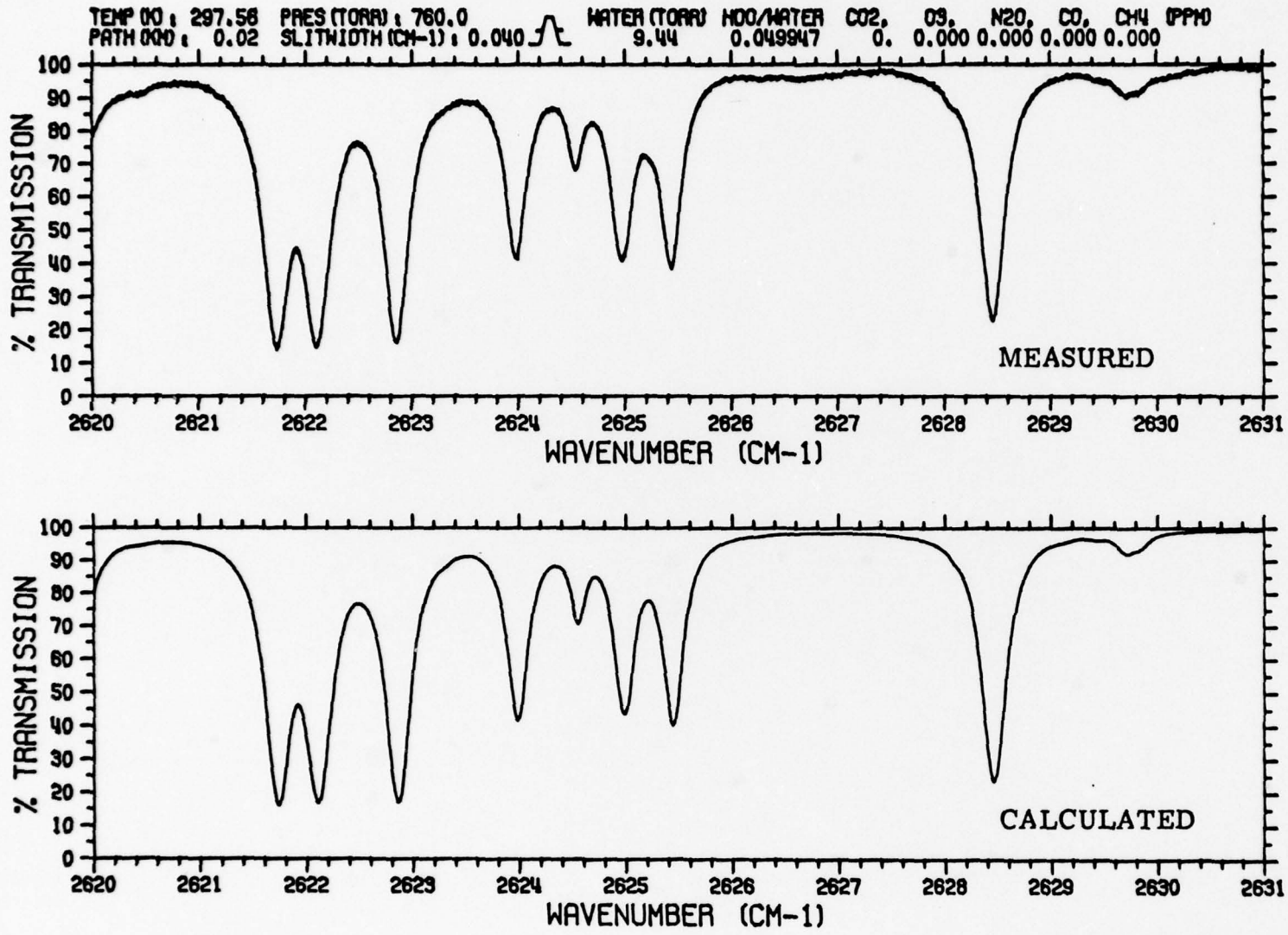

FIGURE 10g. FIGURE 10 CONTINUED

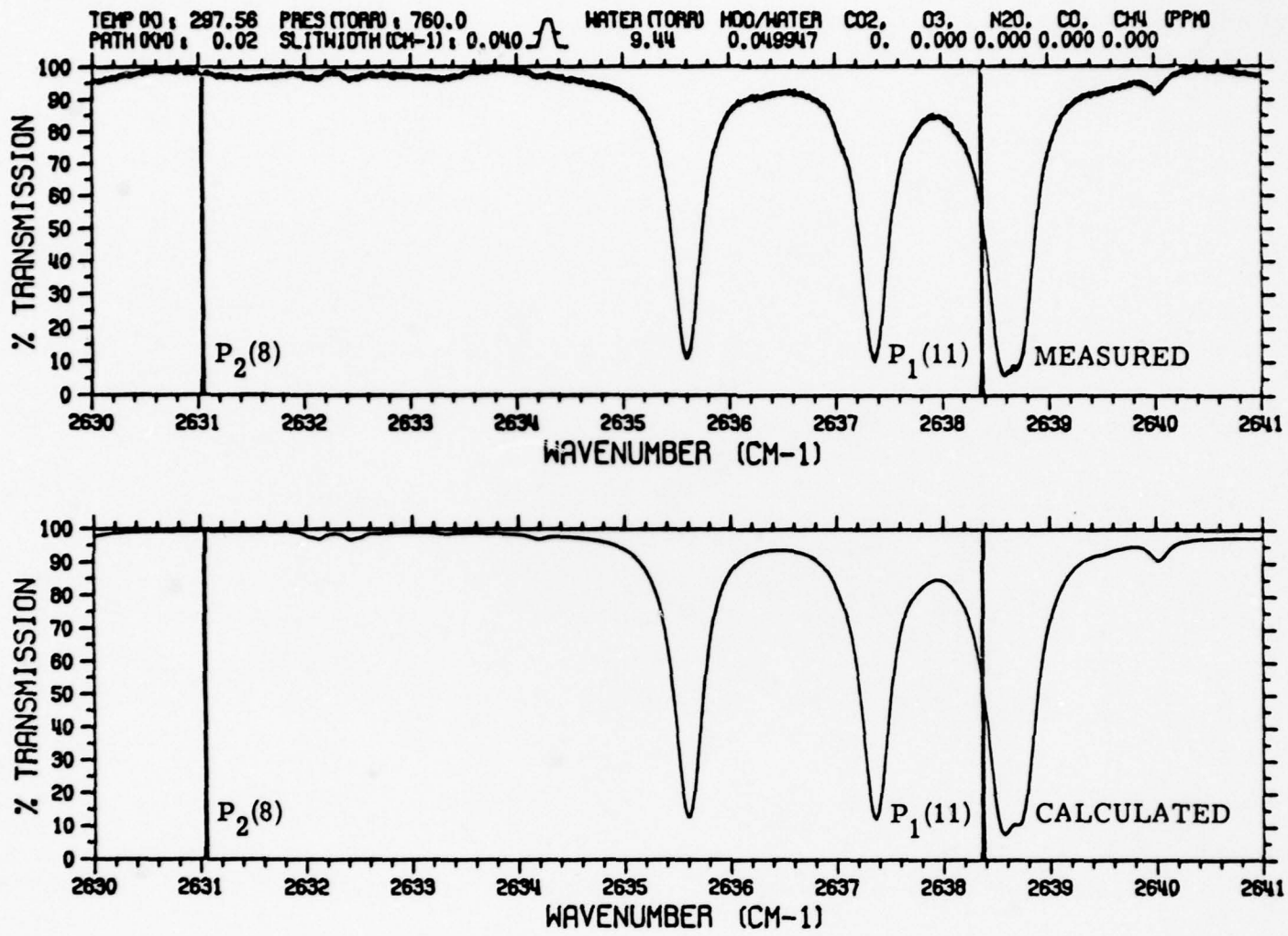

FIGURE 10h. FIGURE 10 CONTINUED

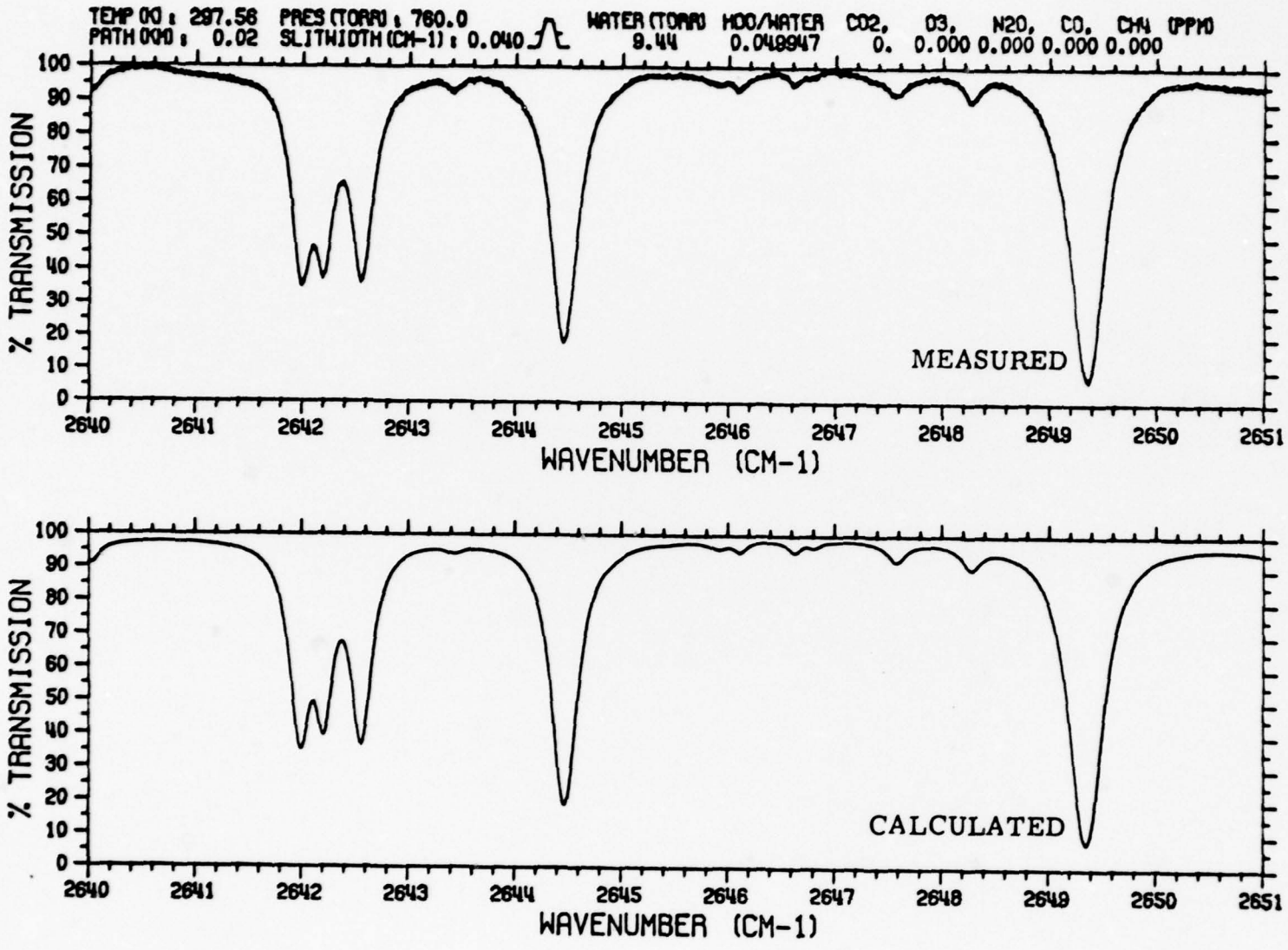

FIGURE 10i. FIGURE 10 CONTINUED

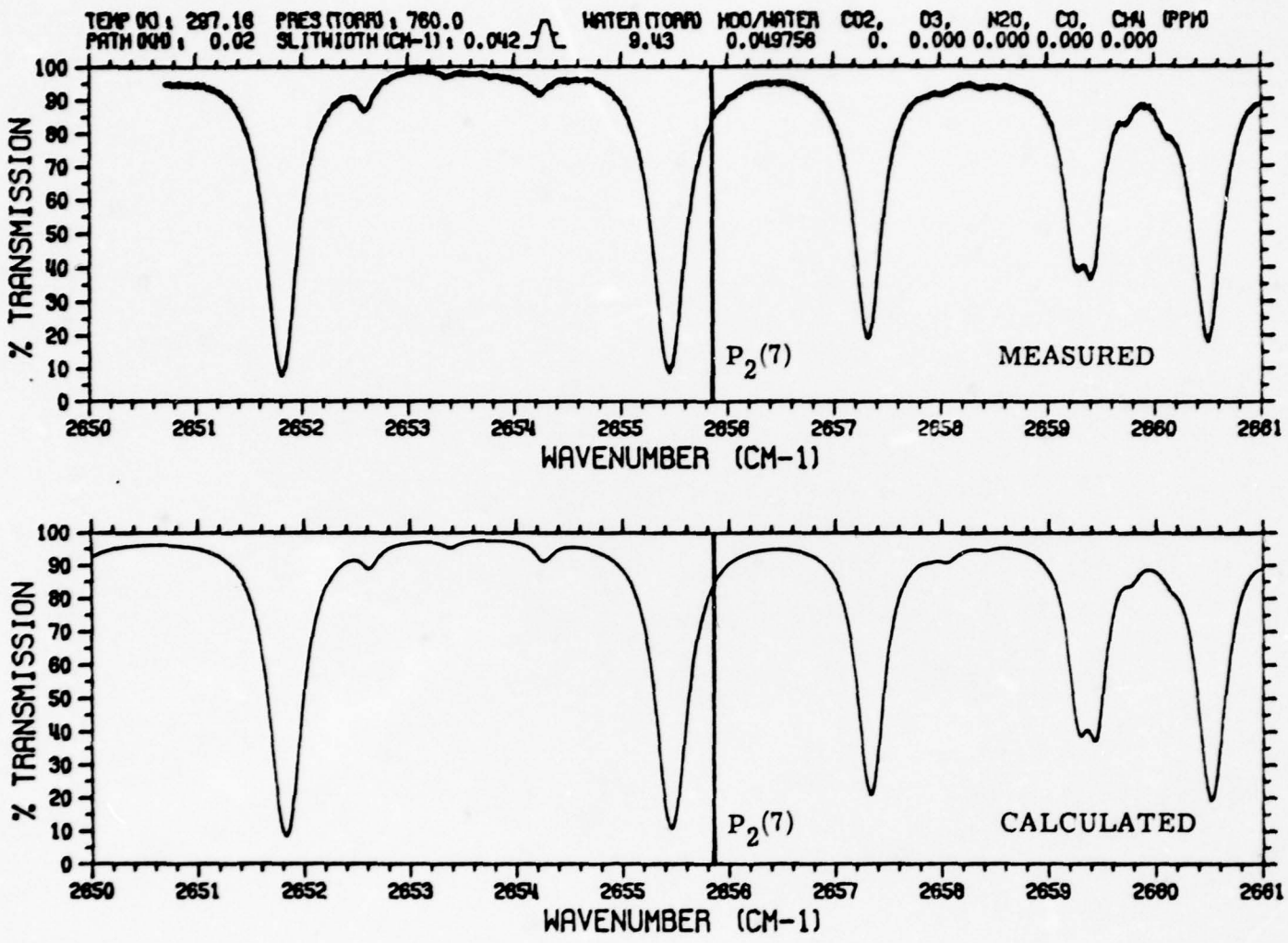

FIGURE 10j. FIGURE 10 CONTINUED

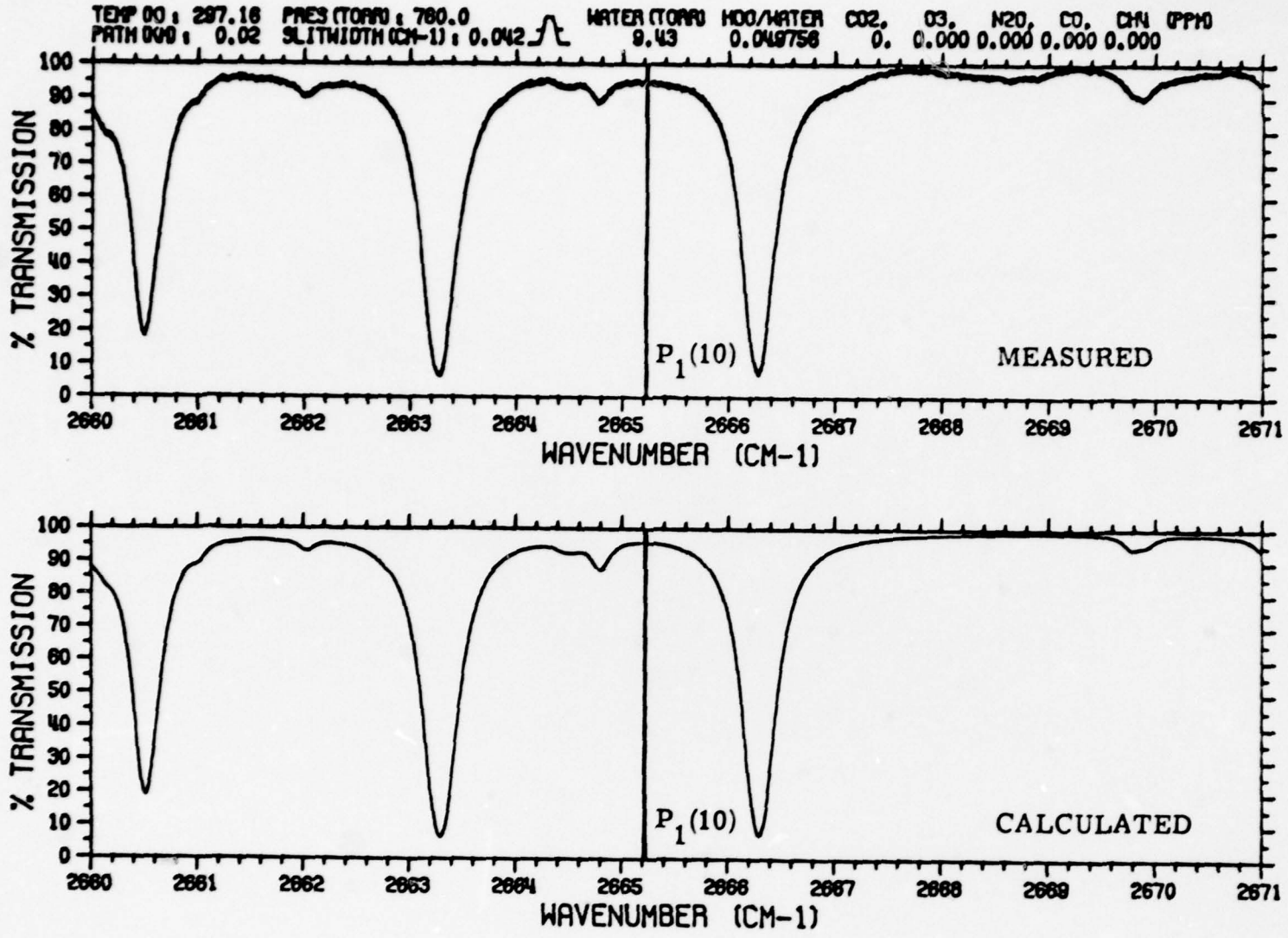

FIGURE 10k. FIGURE 10 CONTINUED

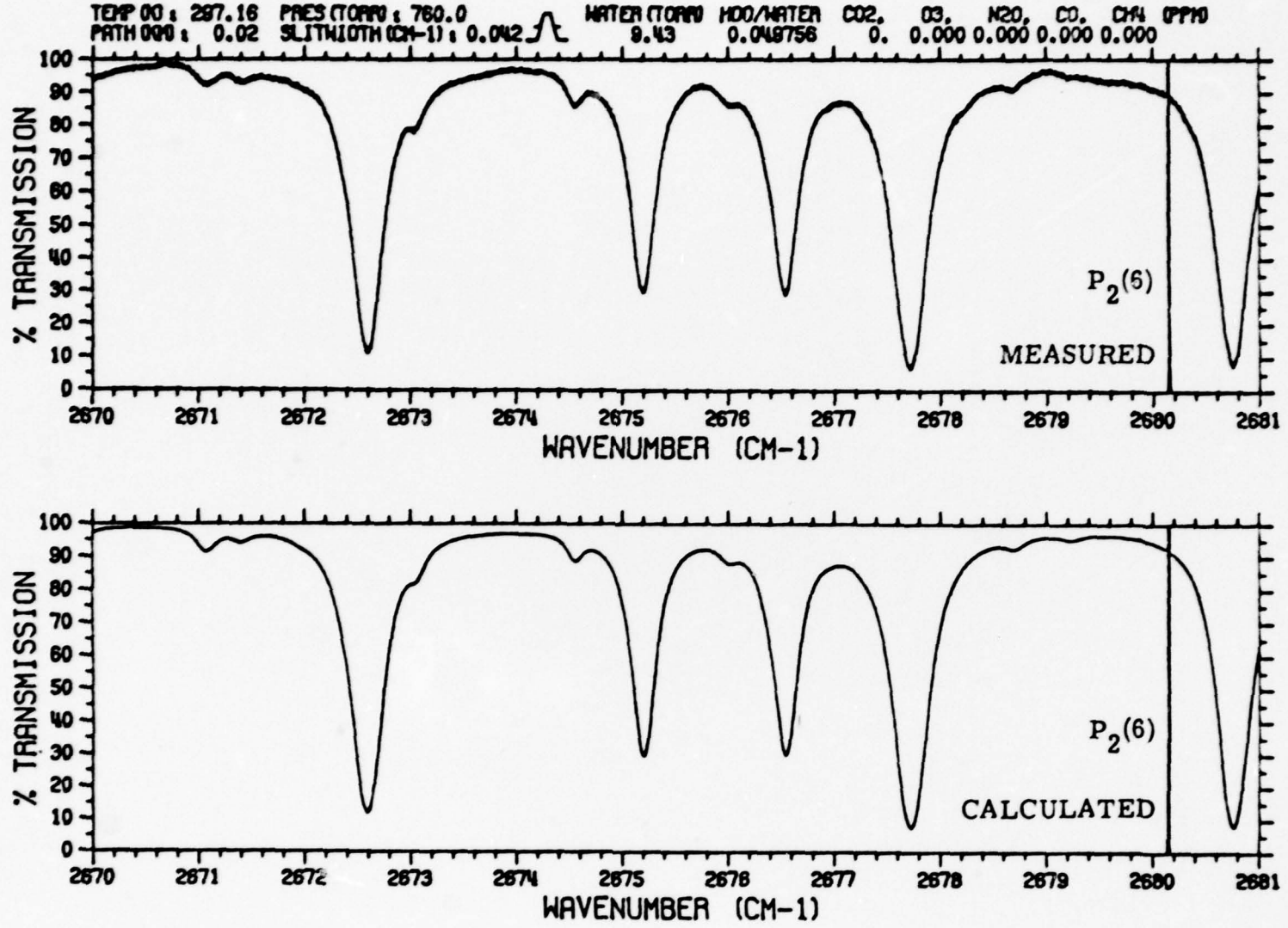

FIGURE 101. FIGURE 10 CONTINUED

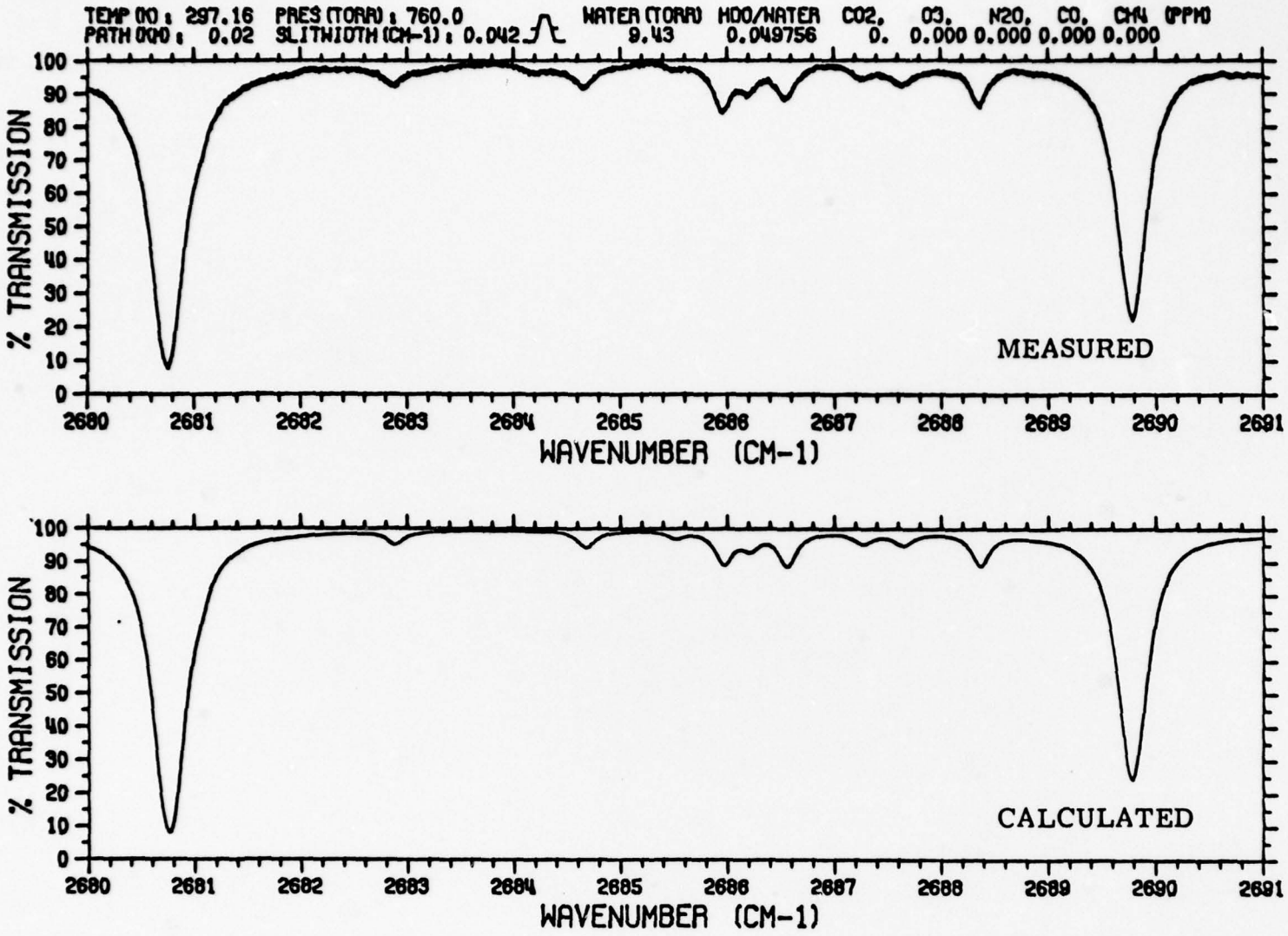

FIGURE 10m. FIGURE 10 CONTINUED

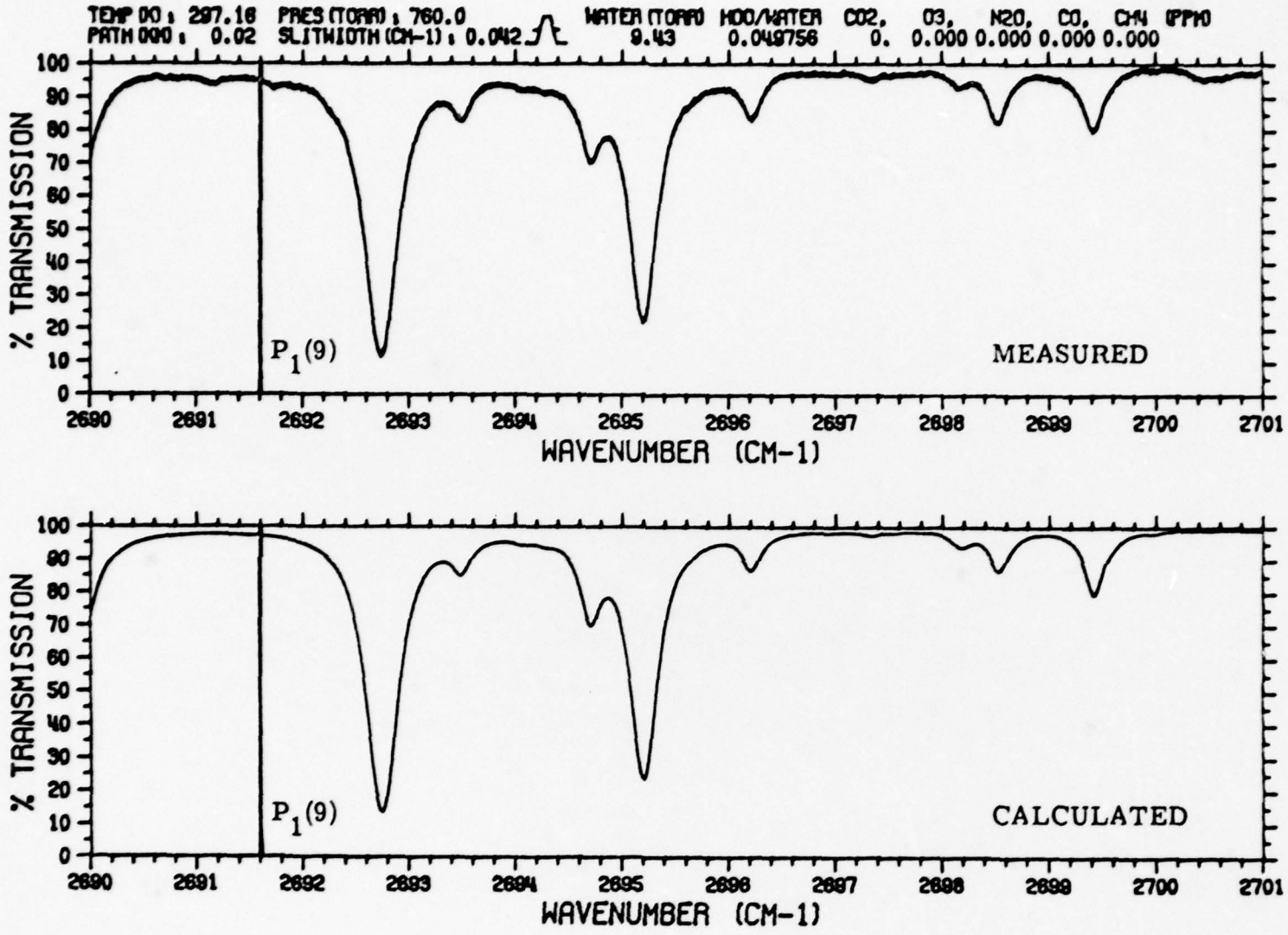

FIGURE 10n. FIGURE 10 CONTINUED

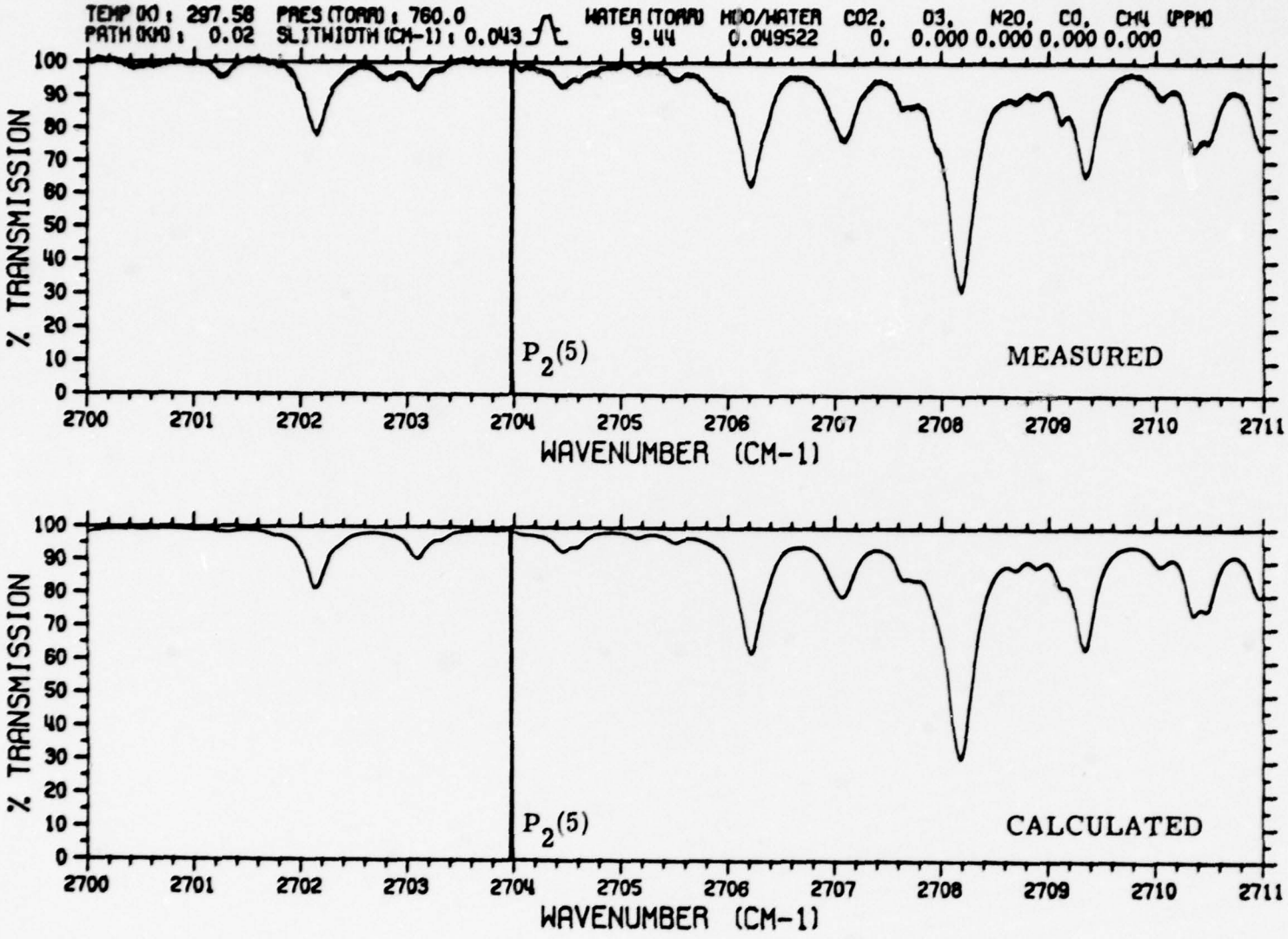

FIGURE 10o. FIGURE 10 CONTINUED

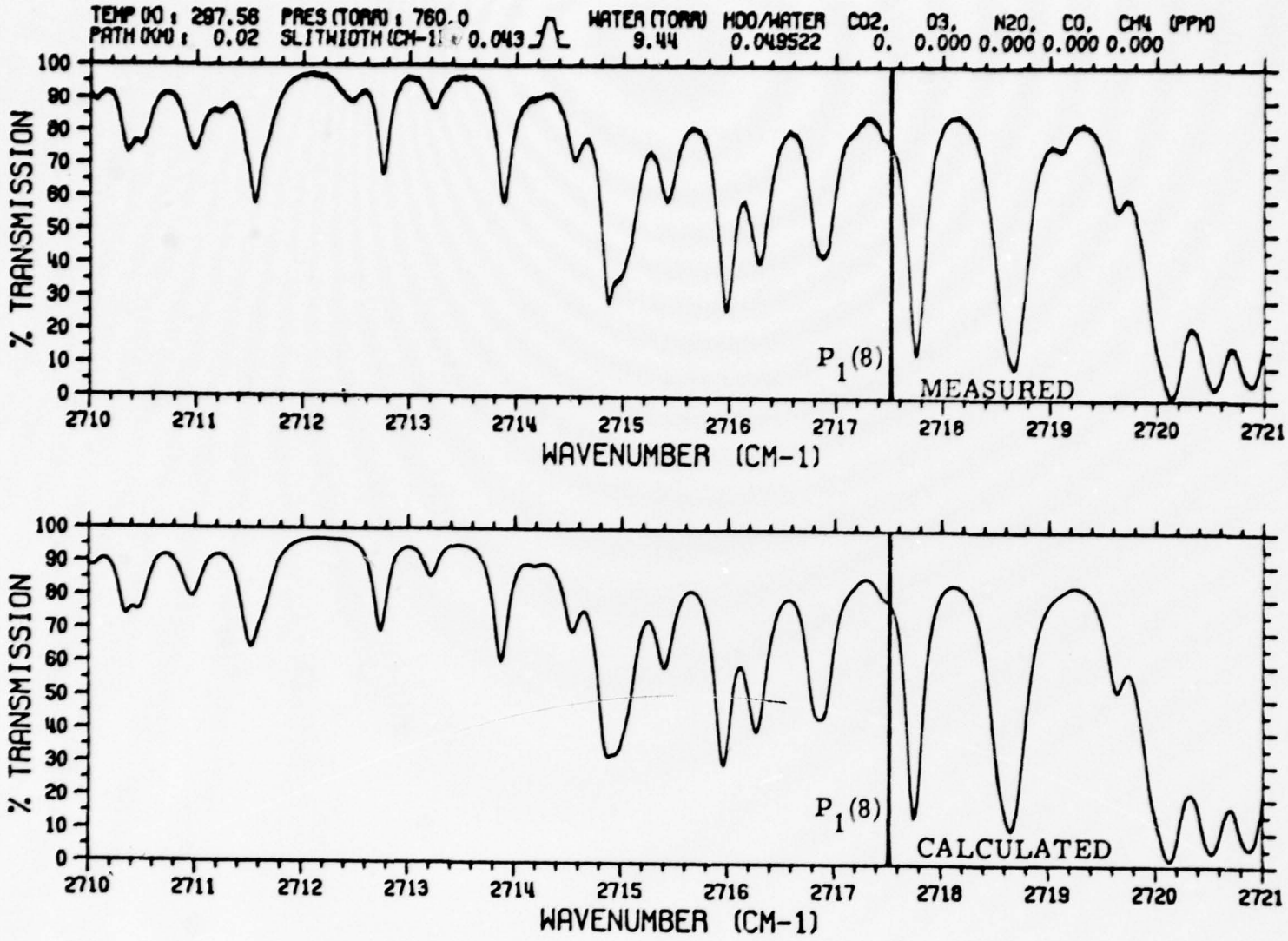

FIGURE 10p. FIGURE 10 CONTINUED

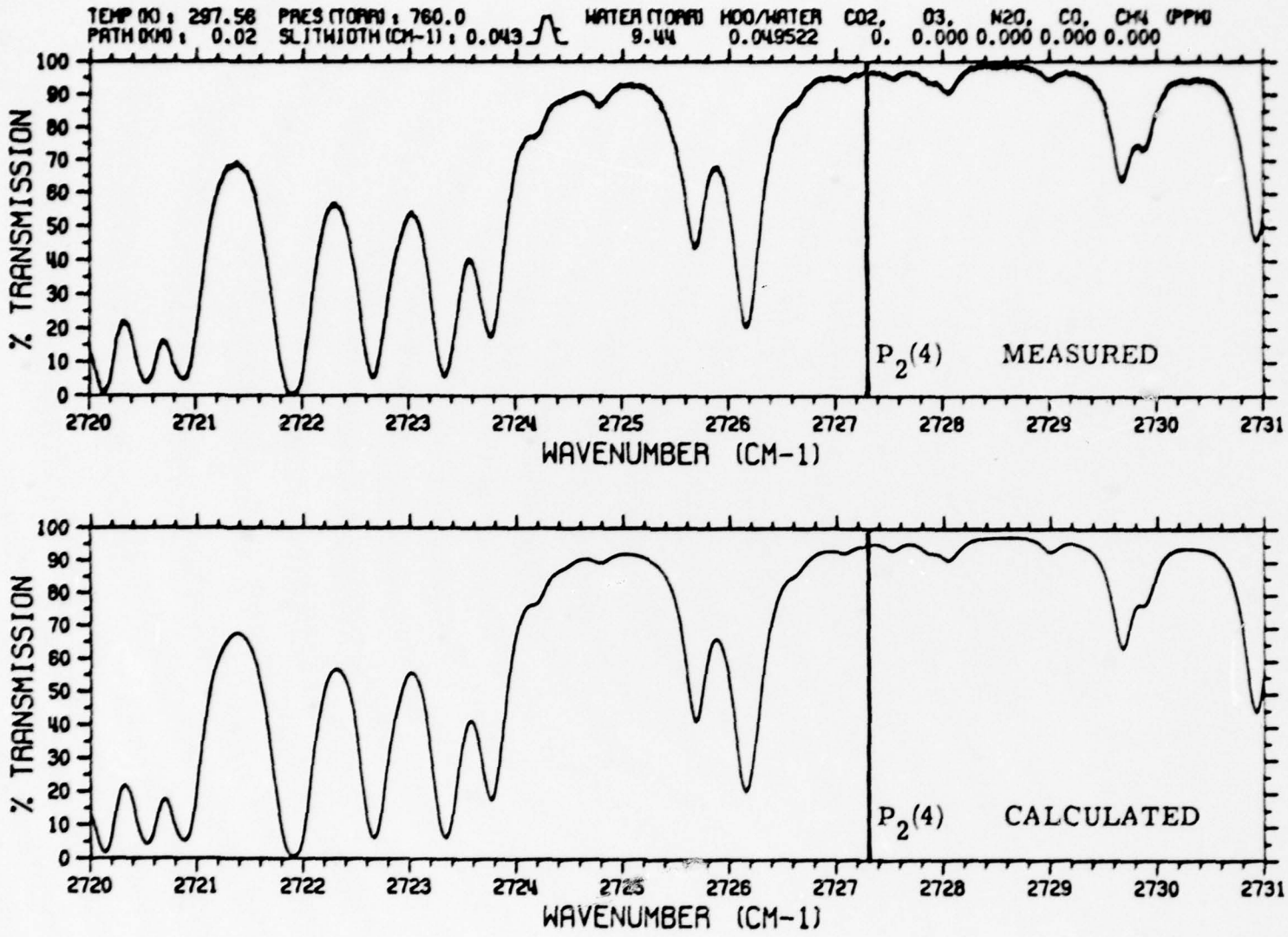

FIGURE 10q. FIGURE 10 CONTINUED

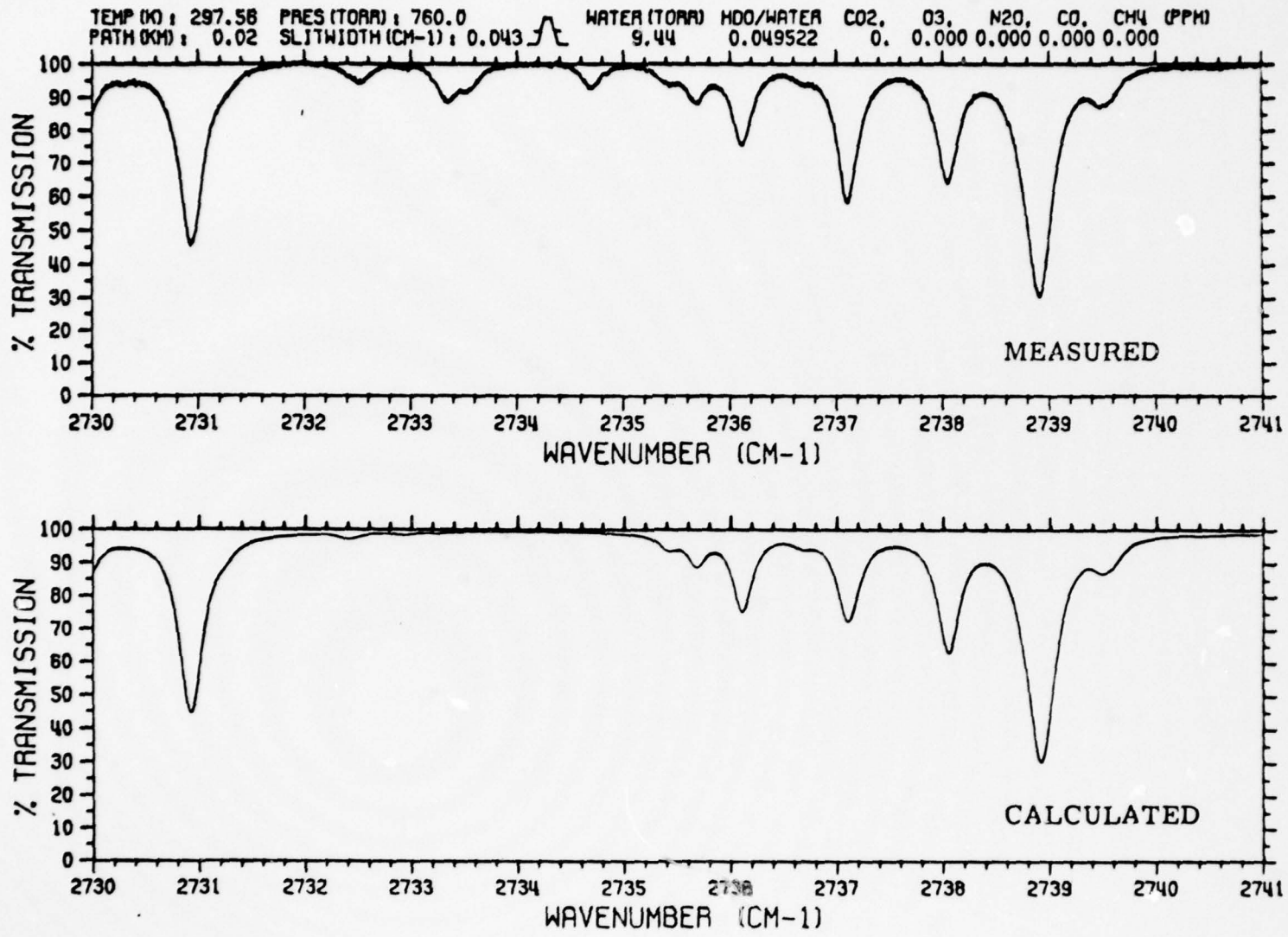

FIGURE 10r. FIGURE 10 CONTINUED

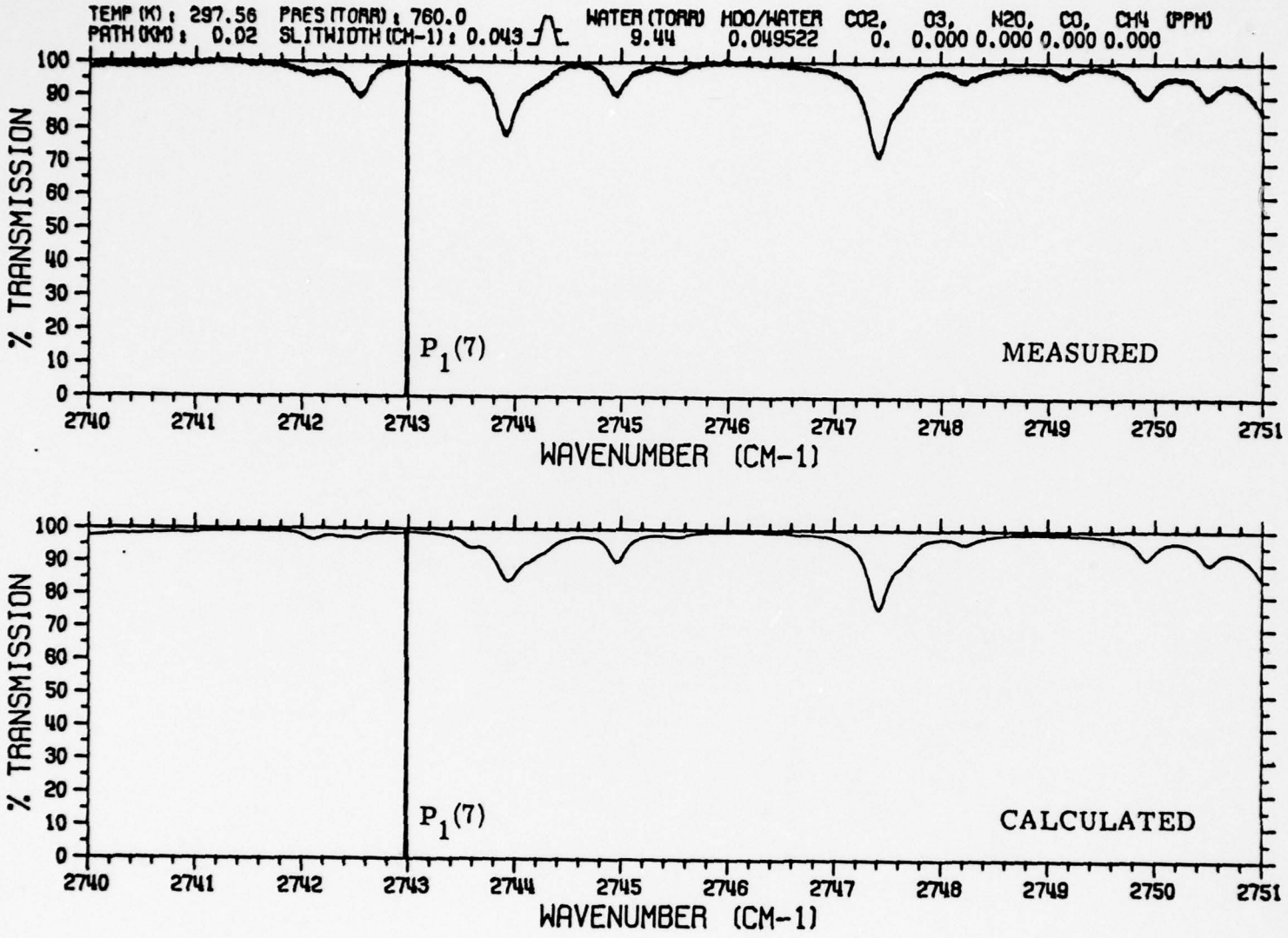

FIGURE 10s. FIGURE 10 CONTINUED

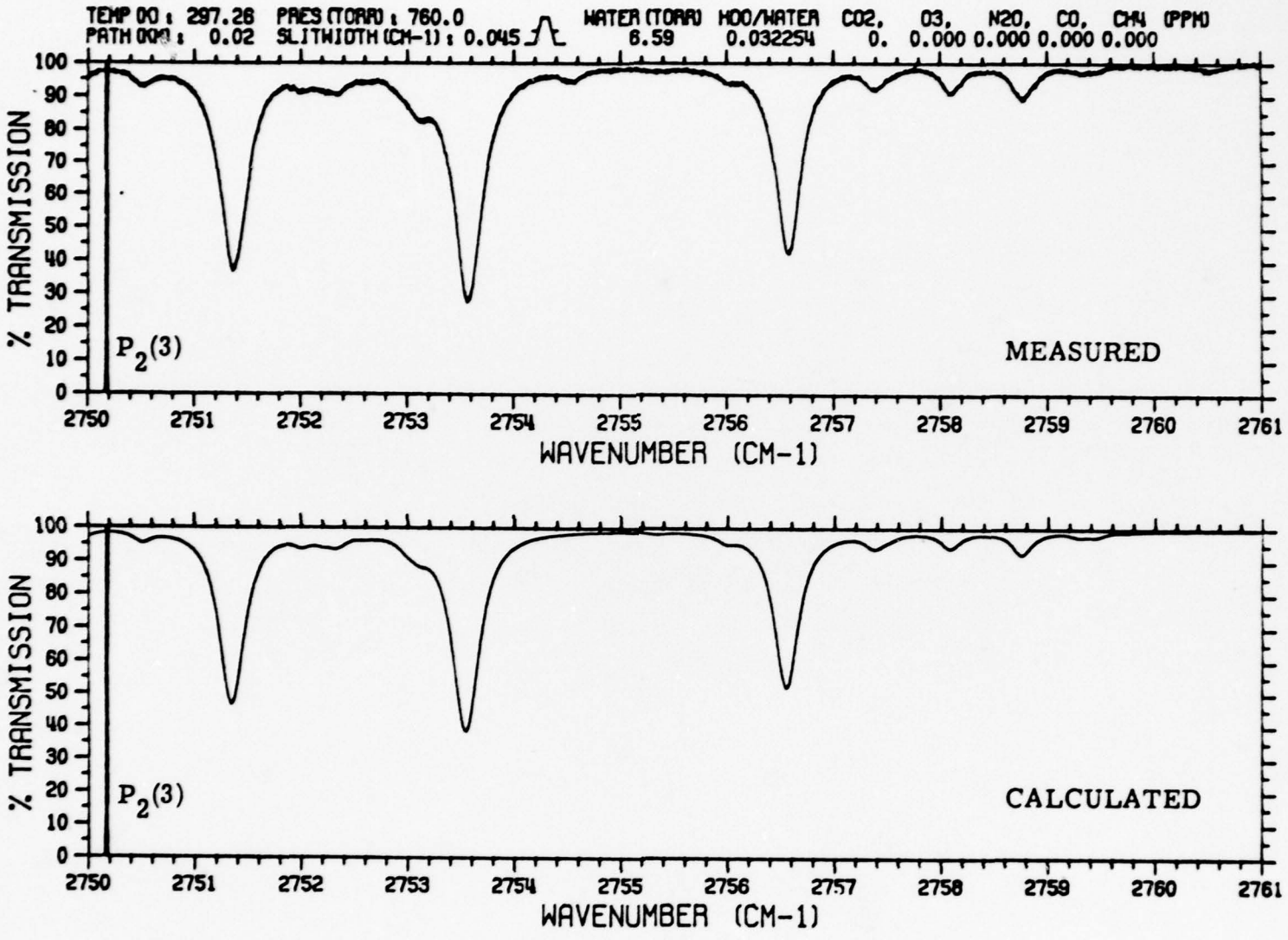

FIGURE 11a. HDO MEASUREMENTS AND COMPARISON PLOTS FOR 6.61 TORR TOTAL WATER VAPOR FILL PRESSURE, 20 M. PATH

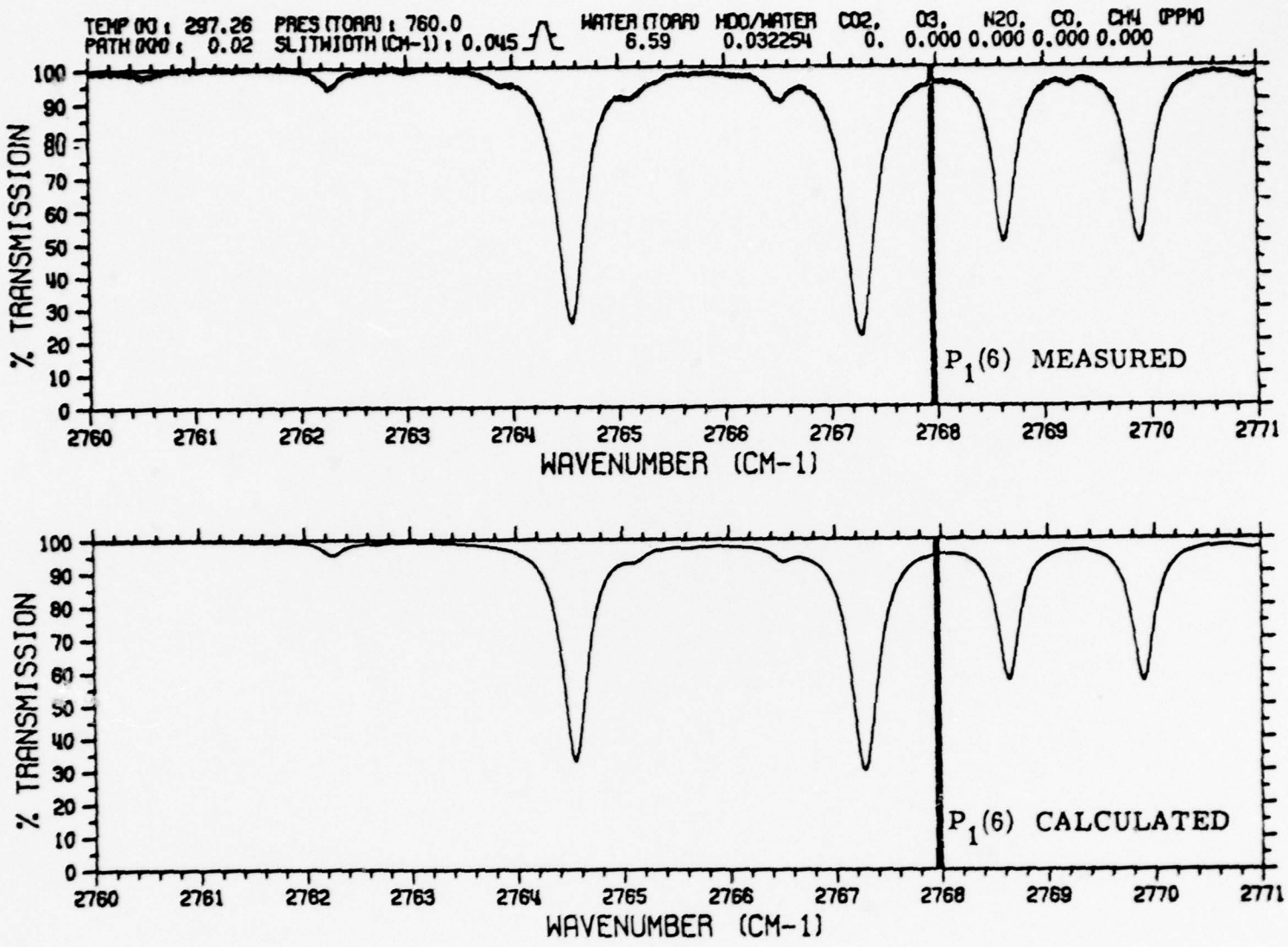

FIGURE 11b. FIGURE 11 CONTINUED

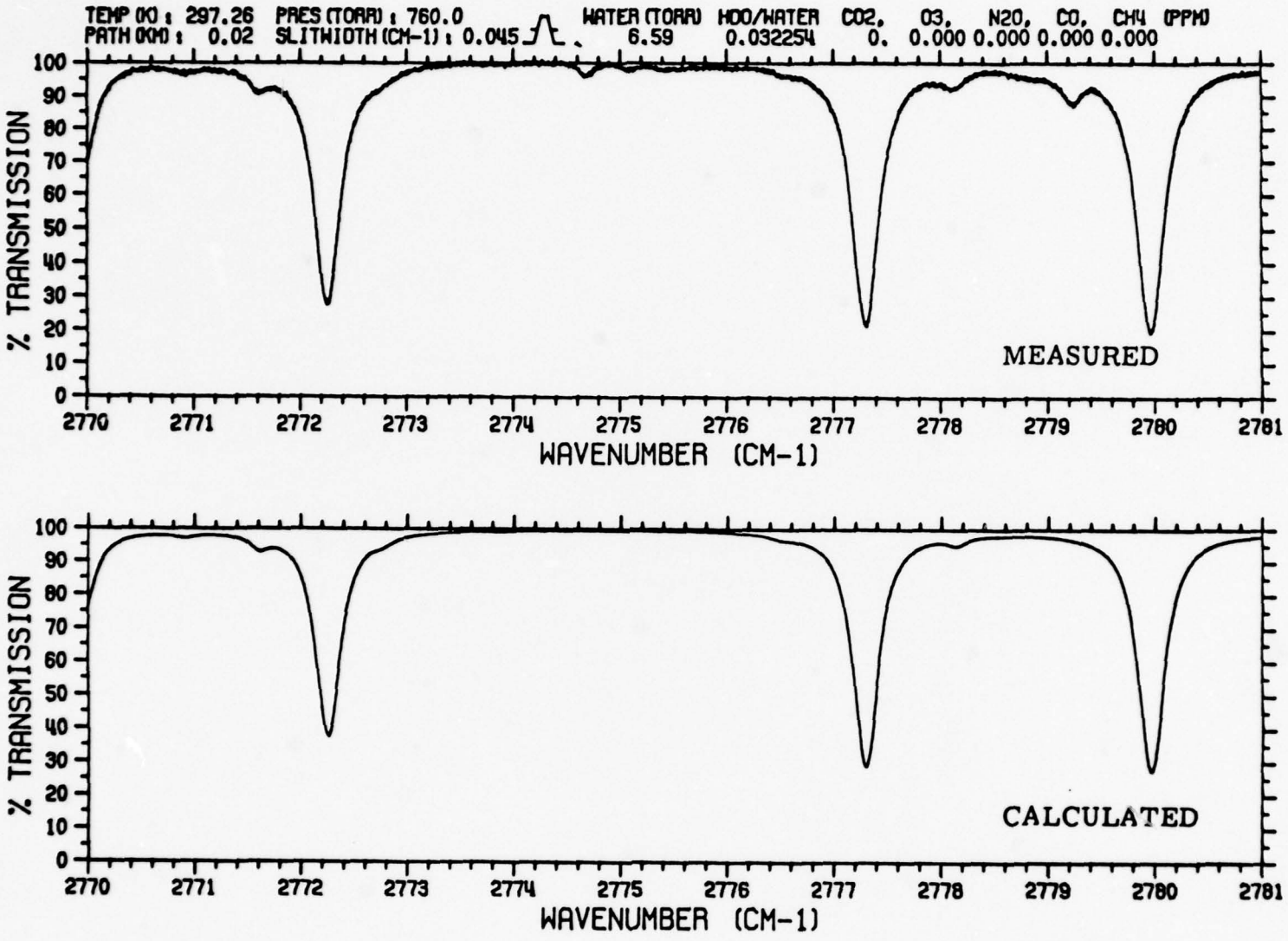

FIGURE 11c. FIGURE 11 CONTINUED

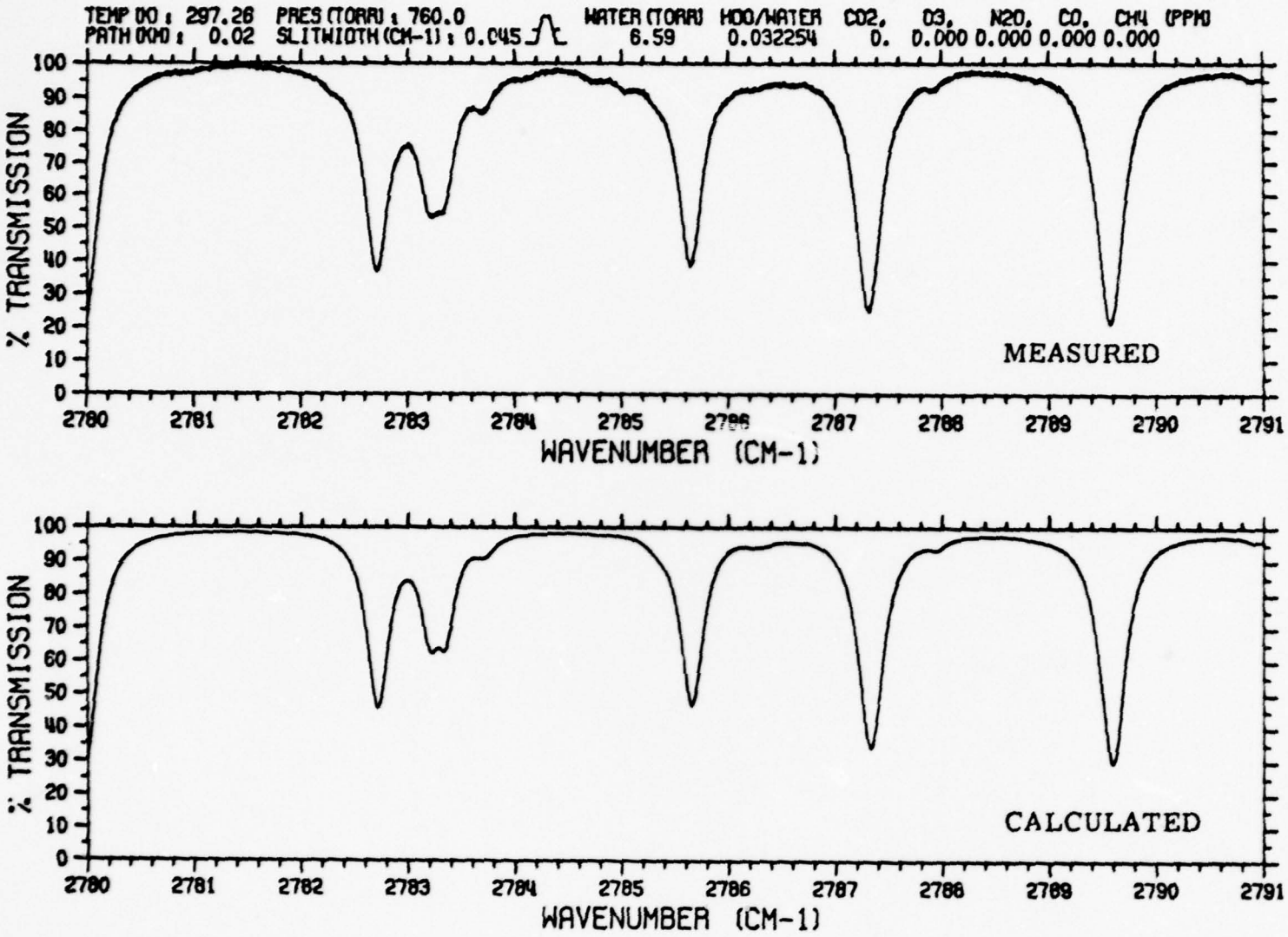

FIGURE 11d. FIGURE 11 CONTINUED

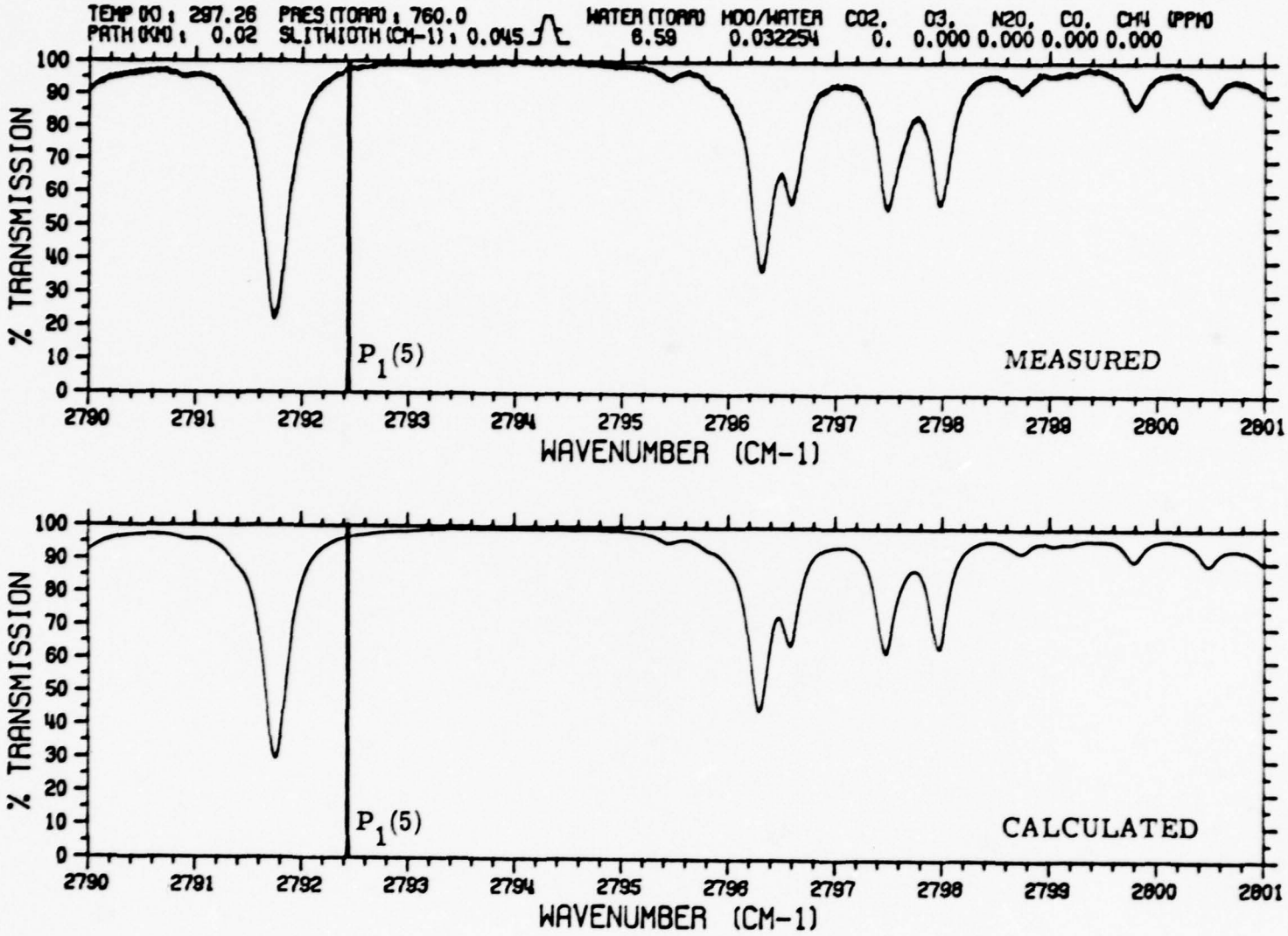

FIGURE 11e. FIGURE 11 CONTINUED

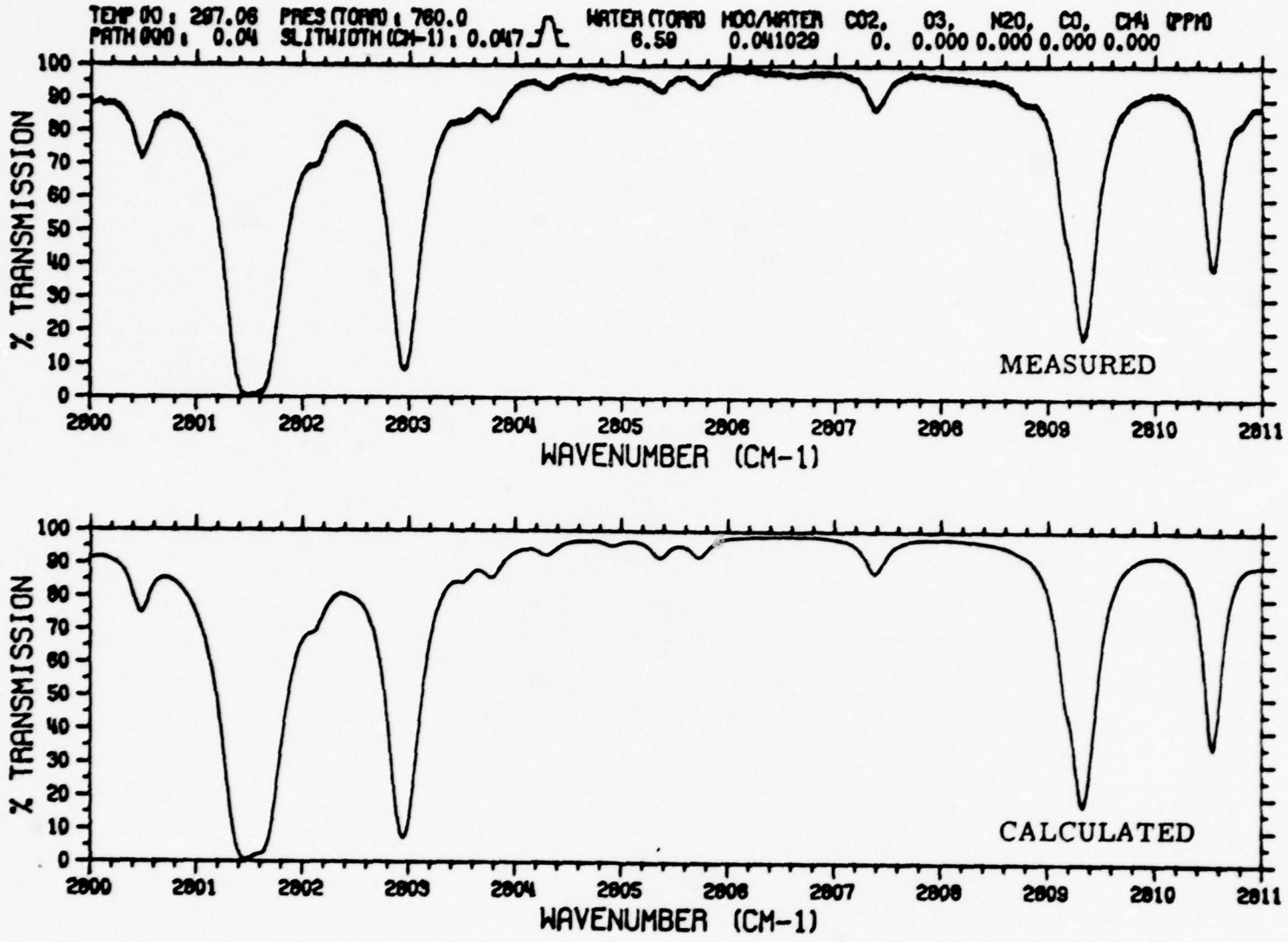

FIGURE 12a. HDO MEASUREMENTS AND COMPARISON PLOTS FOR 6.61 TORR TOTAL WATER VAPOR FILL PRESSURE, 40 M. PATH

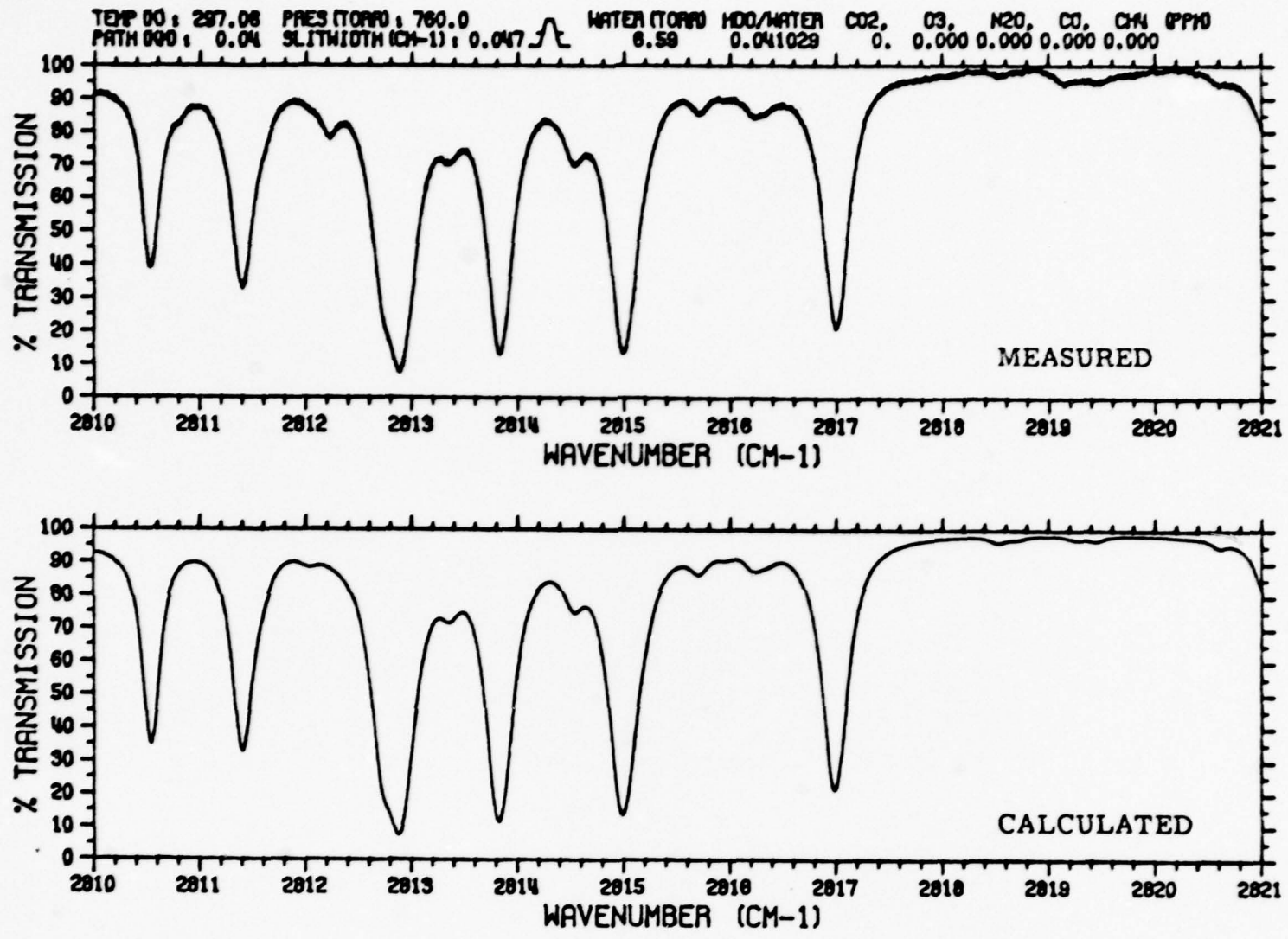

FIGURE 12b. FIGURE 12 CONTINUED

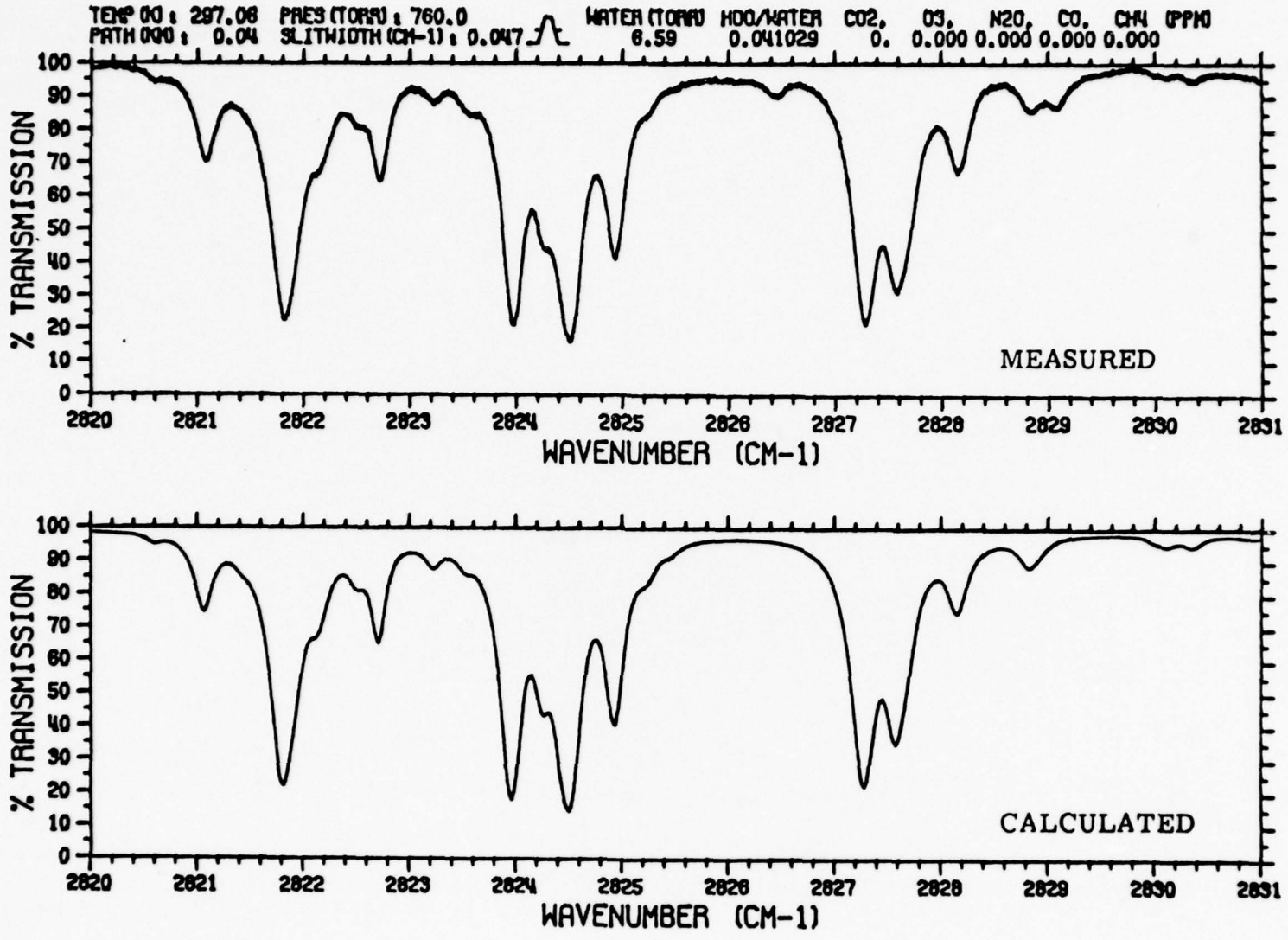

FIGURE 12c. FIGURE 12 CONTINUED

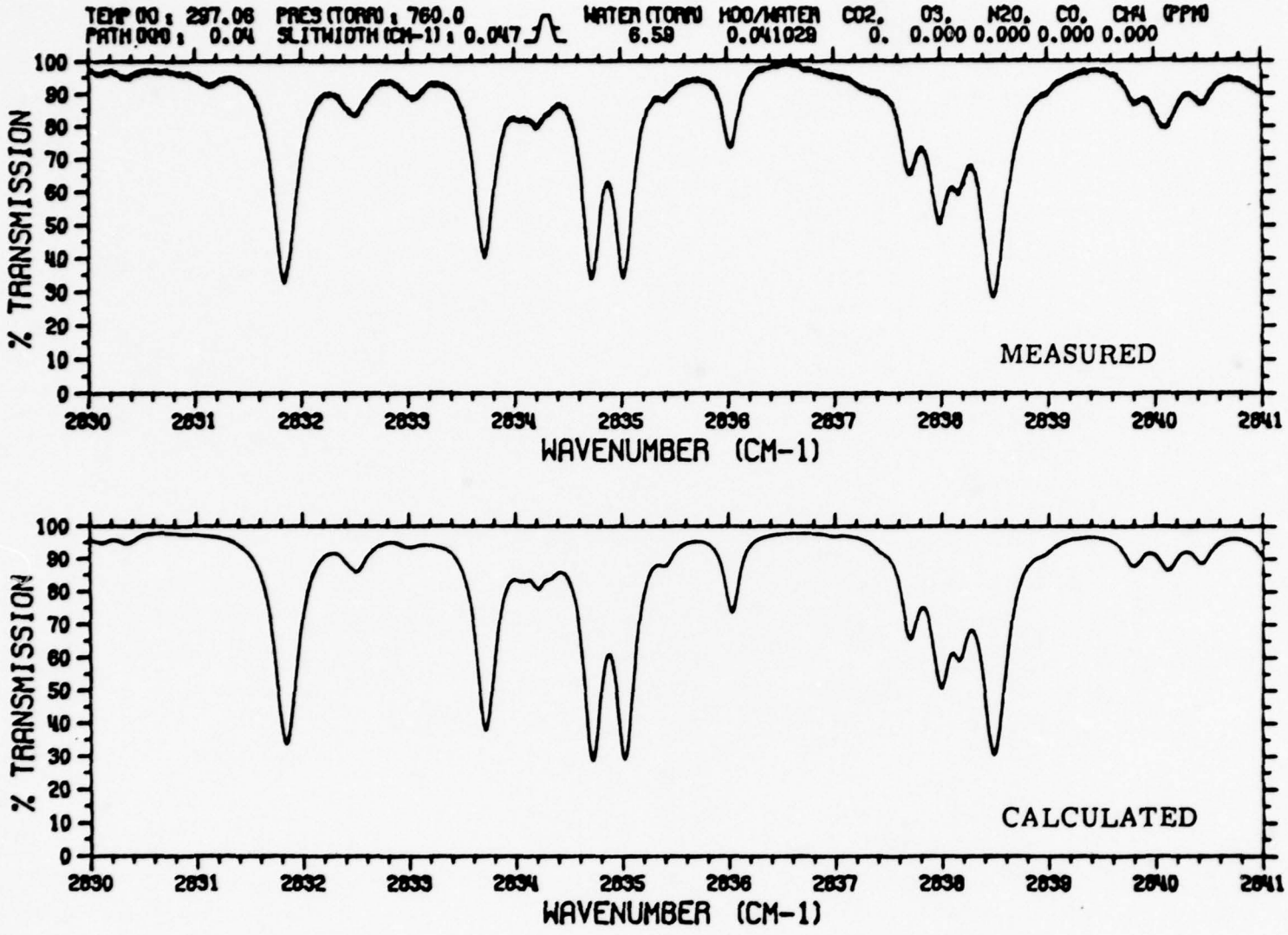

FIGURE 12d. FIGURE 12 CONTINUED

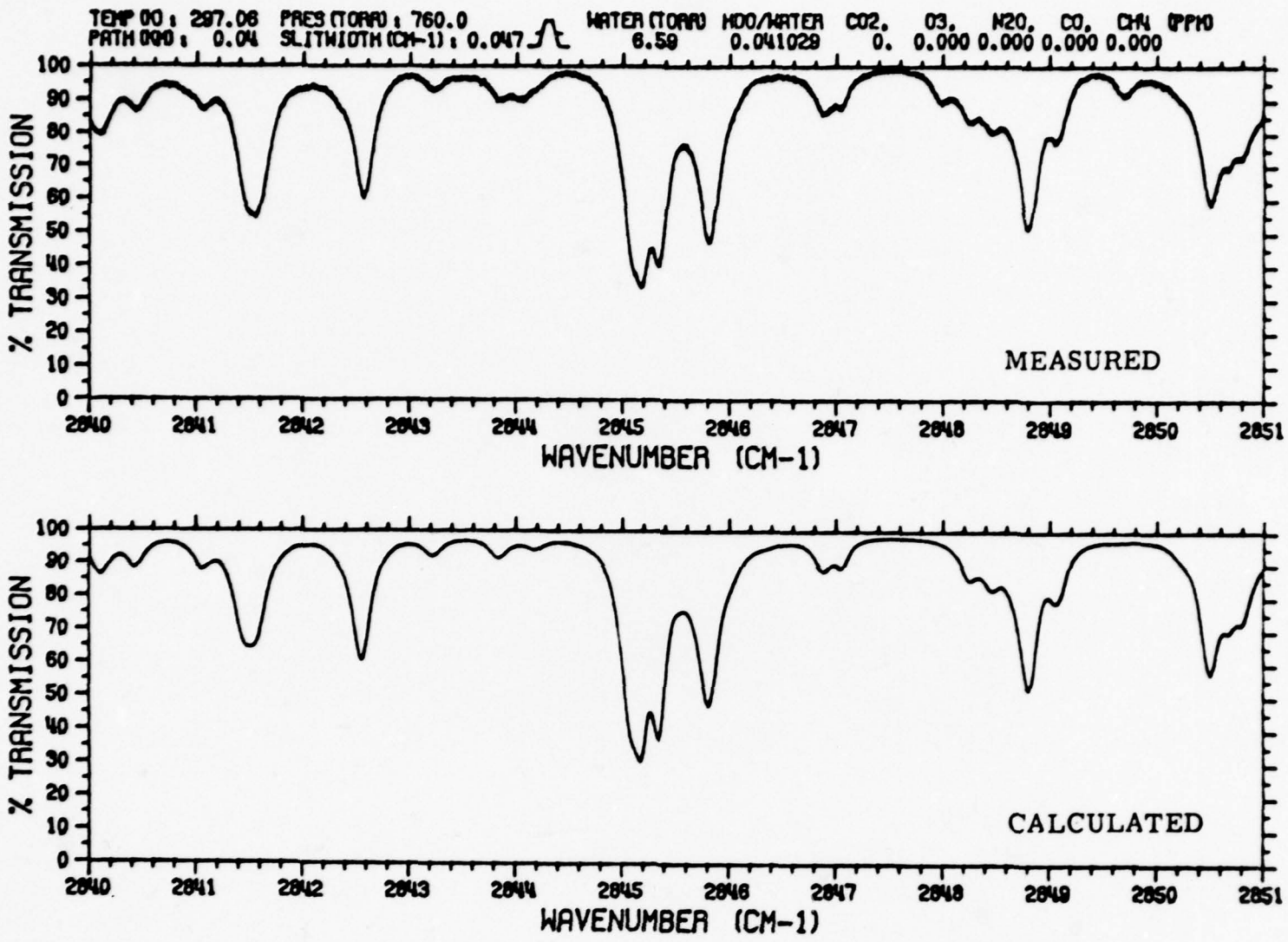

FIGURE 12e. FIGURE 12 CONTINUED

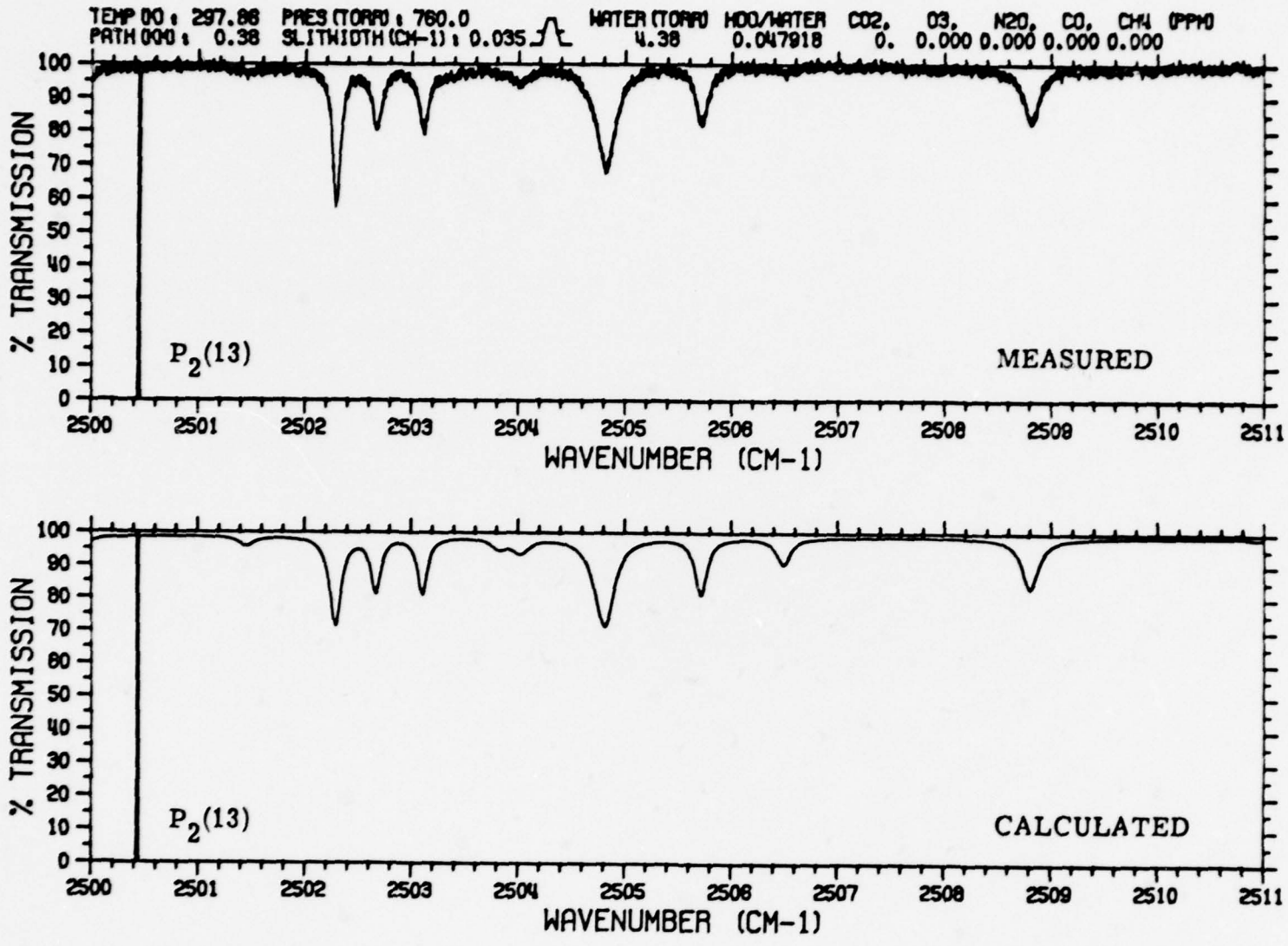

FIGURE 13a. HDO MEASUREMENTS AND COMPARISON PLOTS FOR 4.37 TORR WATER VAPOR FILL PRESSURE, 380 M. PATH

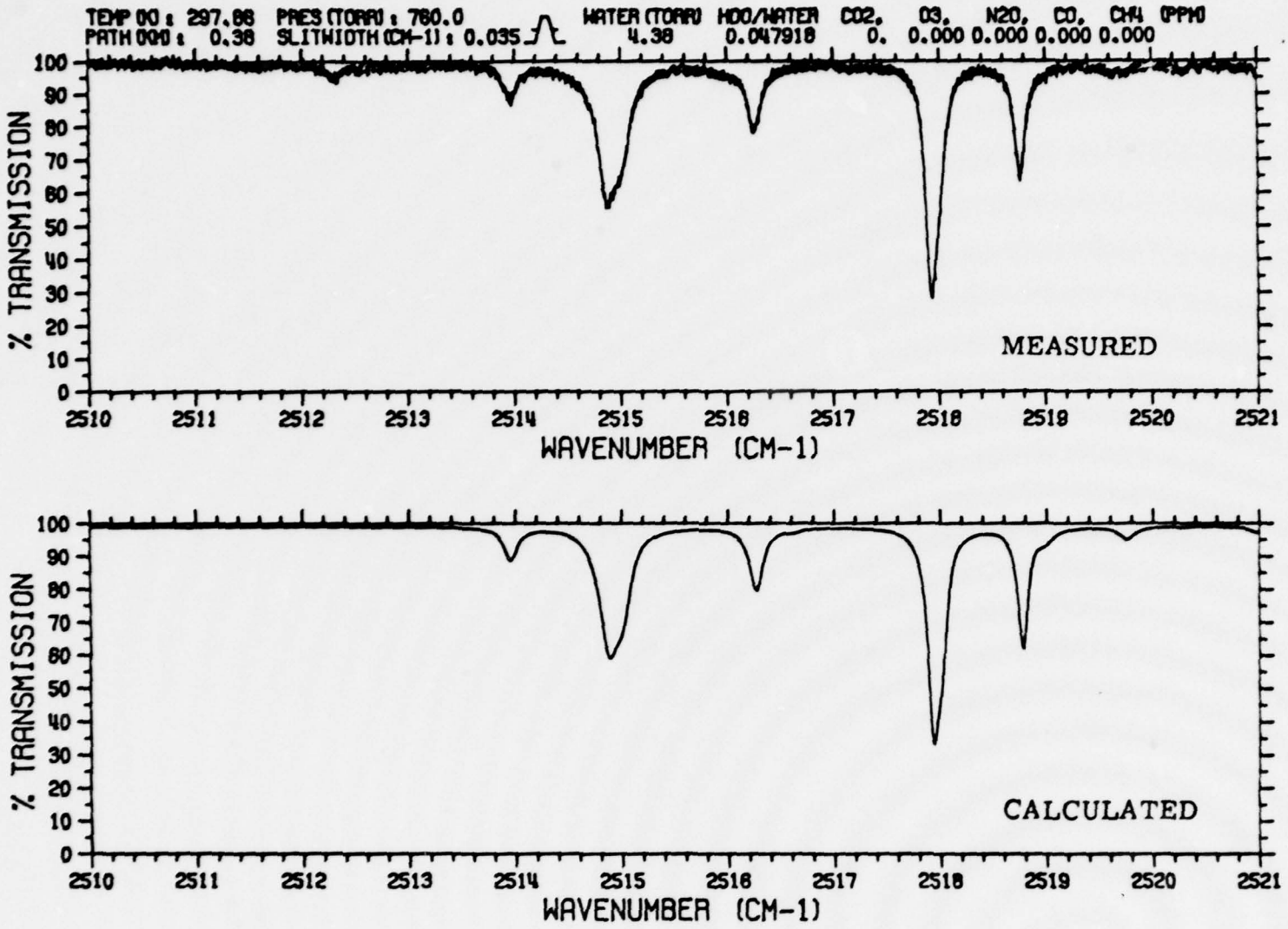

FIGURE 13b. FIGURE 13 CONTINUED

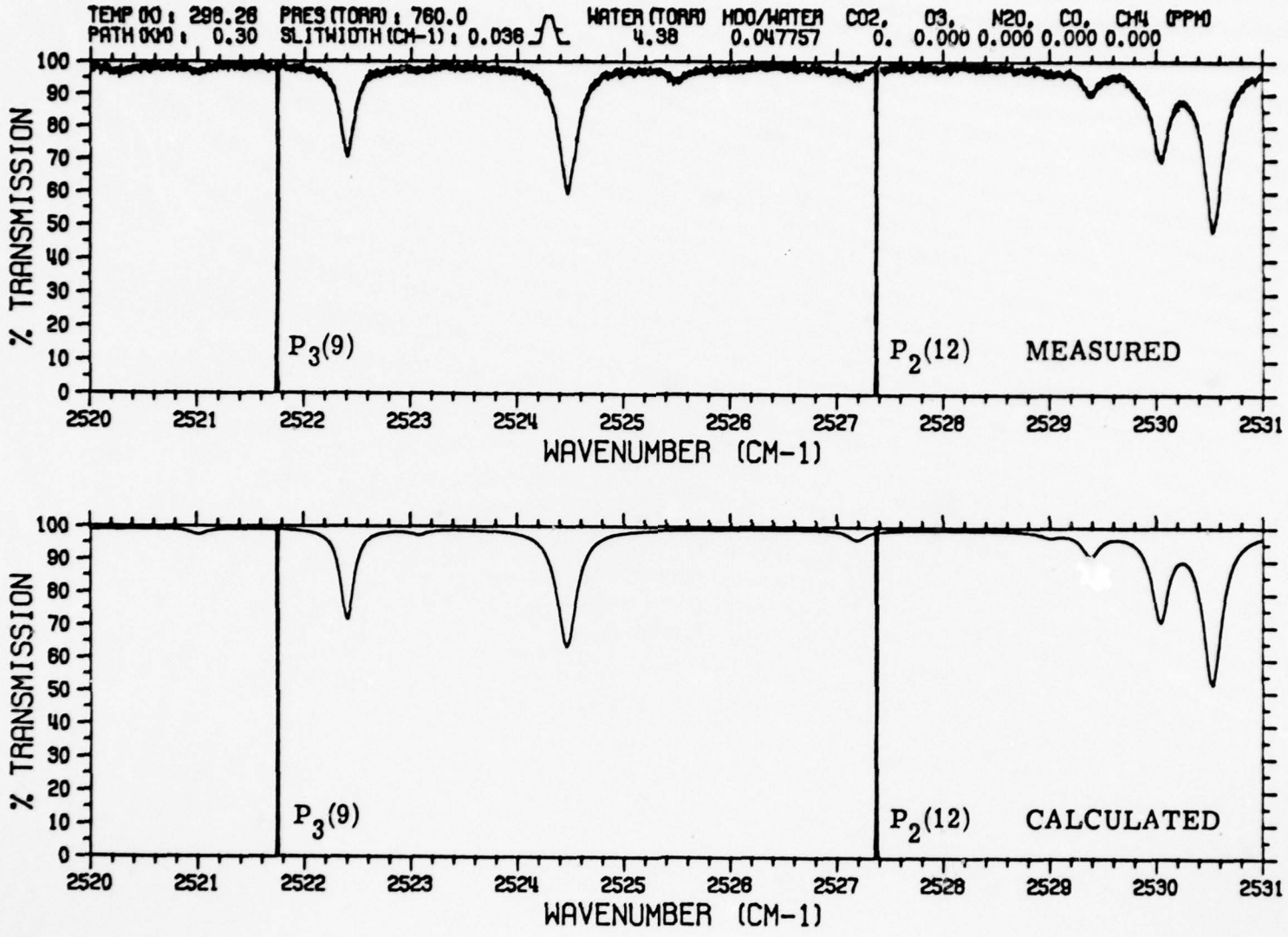

FIGURE 14a. HDO MEASUREMENTS AND COMPARISON PLOTS FOR 4.37 TORR WATER VAPOR FILL PRESSURE, 300 M. PATH

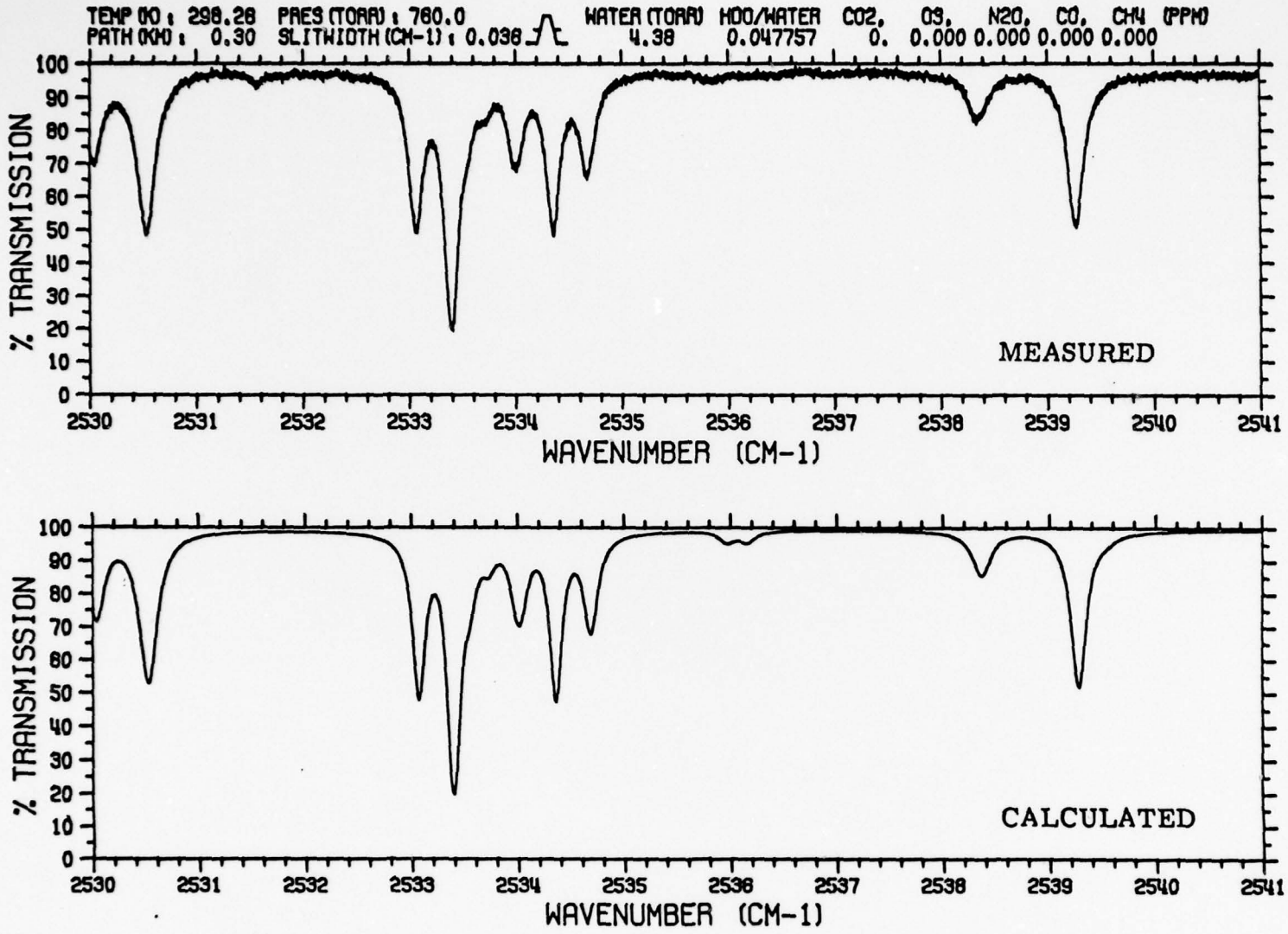

FIGURE 14b. FIGURE 14 CONTINUED

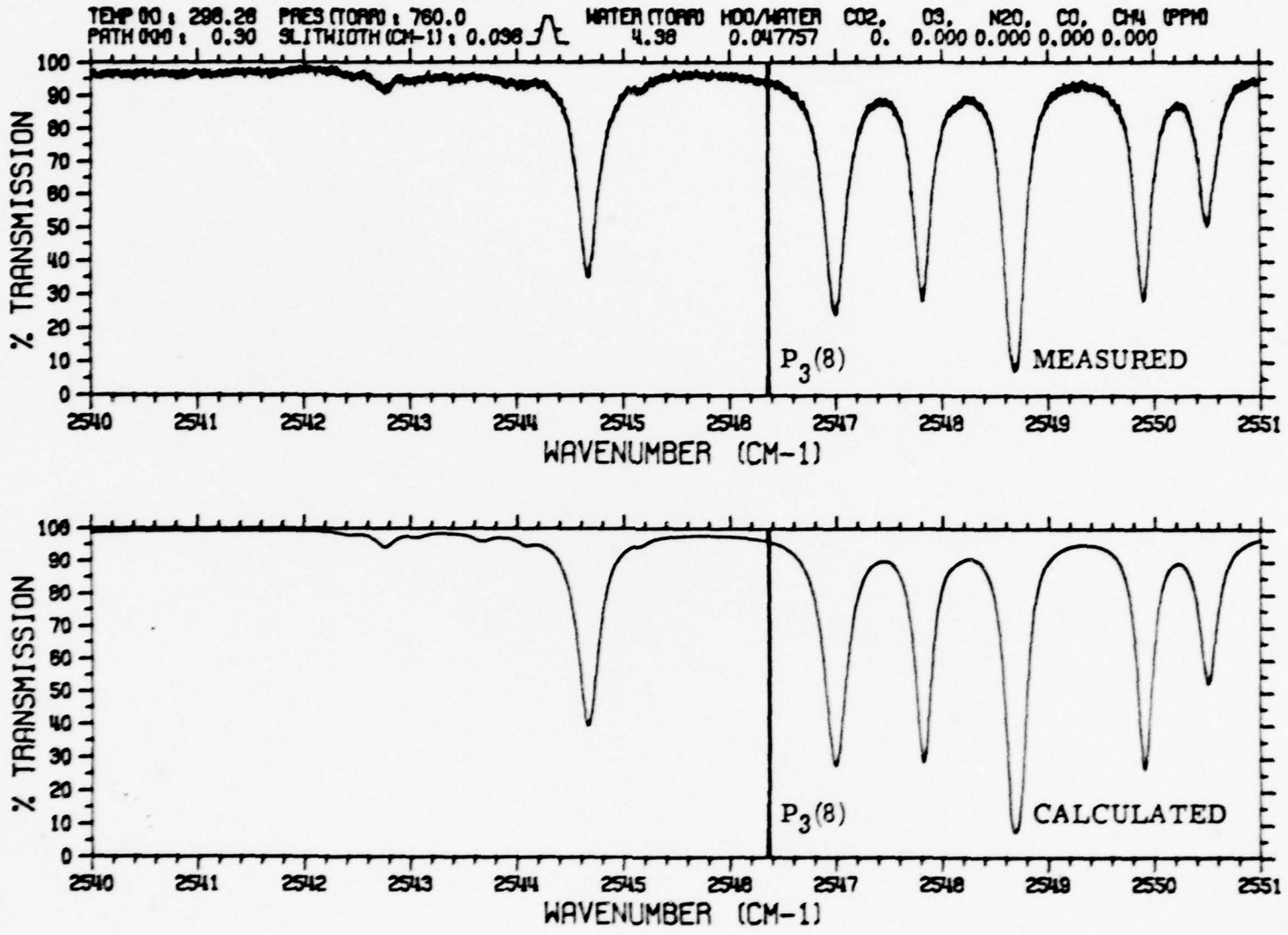

FIGURE 14c. FIGURE 14 CONTINUED

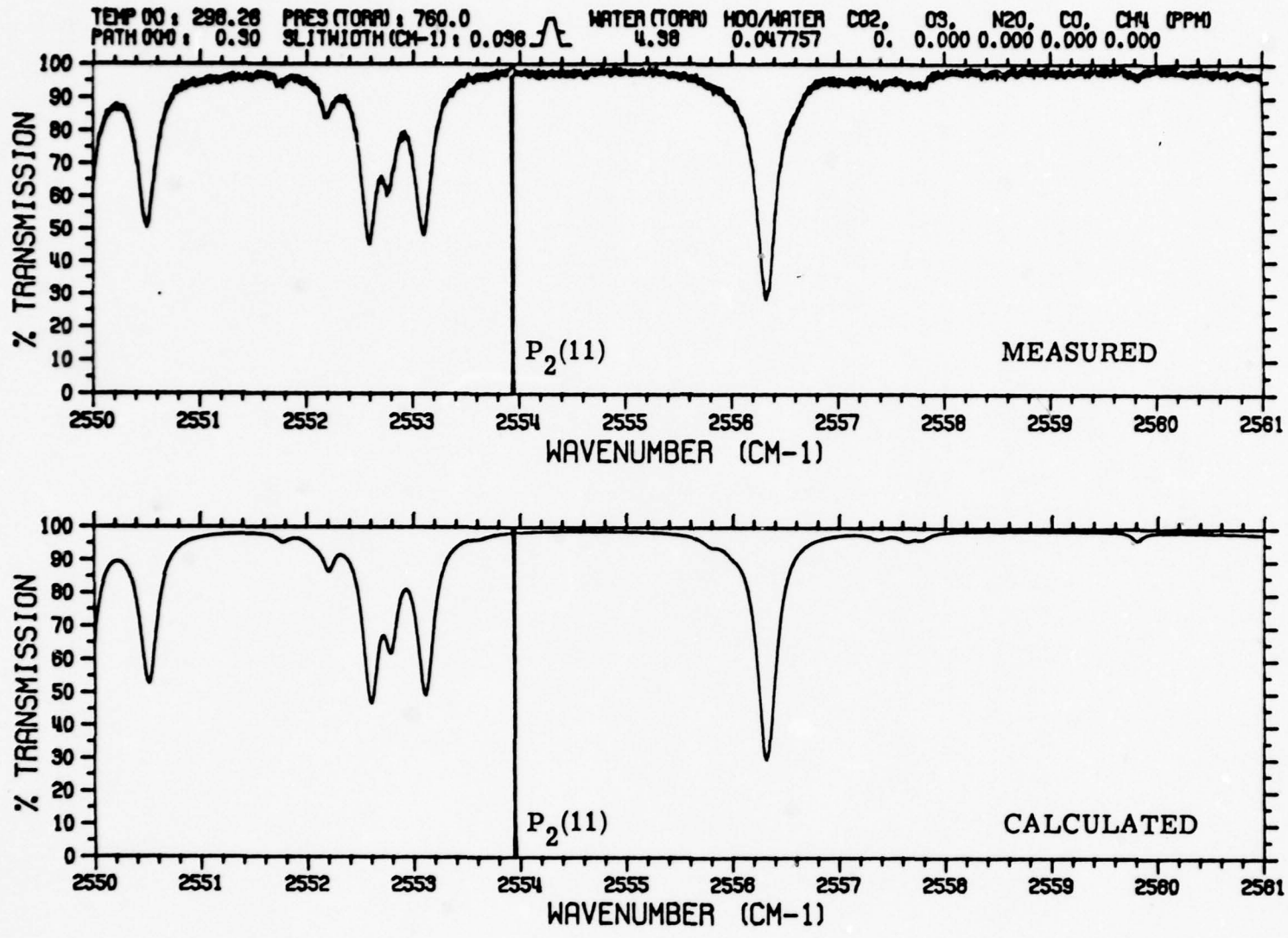

FIGURE 14d. FIGURE 14 CONTINUED

4
PLANNING AND ANALYSIS SUPPORT

Three kinds of planning and analysis support have been provided to NRL: (1) degraded resolution transmission calculations in support of NRL field Scanning Michelson Interferometer (SMI) measurements, (2) transmission measurements to support future NRL laser propagation measurements, (3) fixed frequency DF laser extinction calculations. These activities are discussed in the remainder of this section.

4.1 SMI CALCULATIONS AND COMPARISONS

Calculations for comparison with NRL SMI measurements have been performed during the NRL field measurements program. SAI has used the SYNSPC code for values of the variable parameters which correspond to the field measurements conditions. This primarily means selecting the spectral resolution (slit width in the plot formats) to match the SMI resolution, and to match the temperature total pressure, water vapor pressure, and path length. HDO quantity and concentrations of the non water vapor mixed gases were taken to be the values used in the AFGL data compilation.

A sample plot of NRL data and a comparison plot is shown in Figure 15 for the spectral region 2480 cm^{-1} - 2800 cm^{-1}. NRL data is on the lower panel, and the SAI calculation for the indicated conditions is shown in the upper panel. The comparisons are quite good, as viewed qualitatively. Laboratory compairsons have proven that the molecular line parameter data are now excellent, so discrepancies may be attributed to continuum extinction, both aerosol and molecular, and to number concentrations

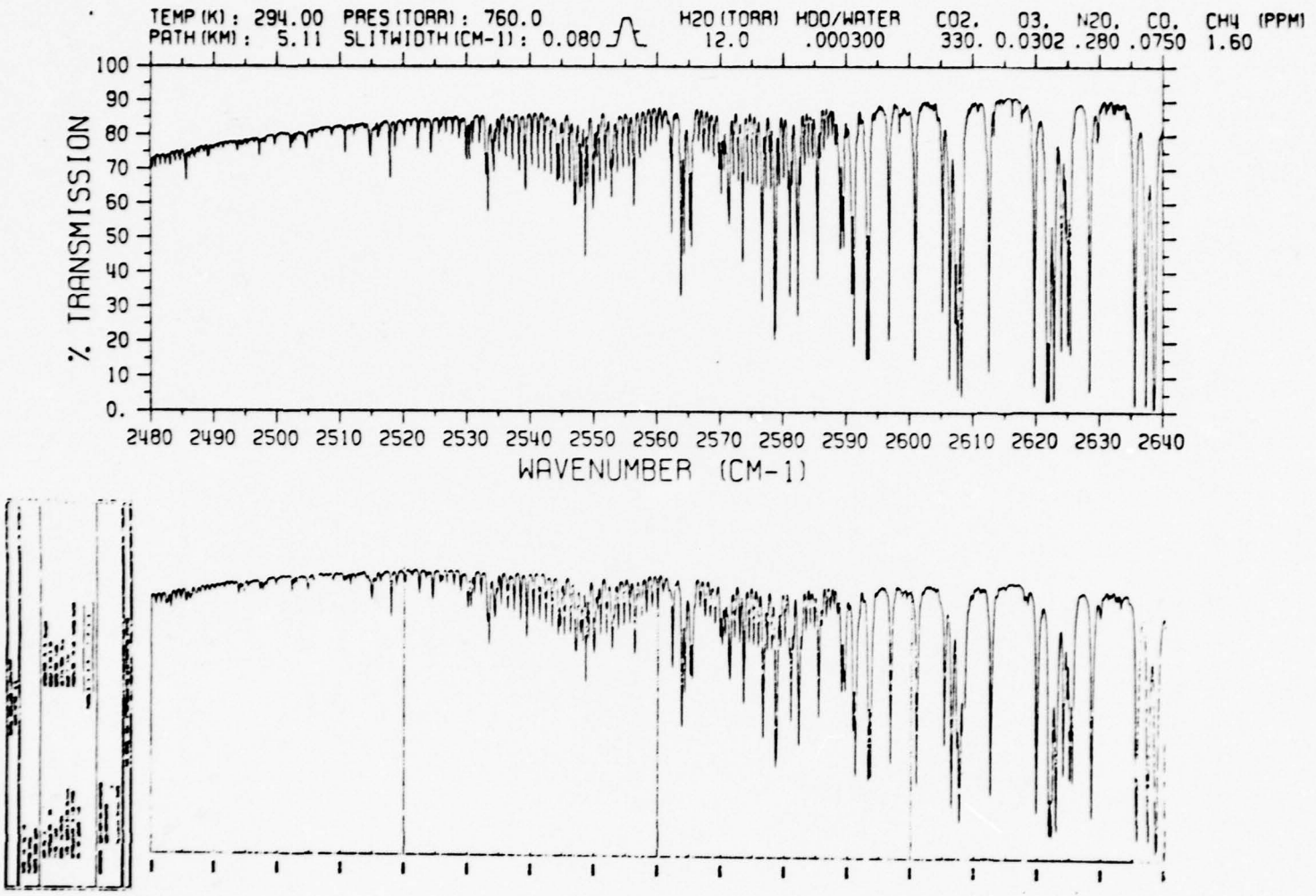

FIGURE 15a. A COMPARISON BETWEEN SAI SYNSPC PLOTS AND NRL

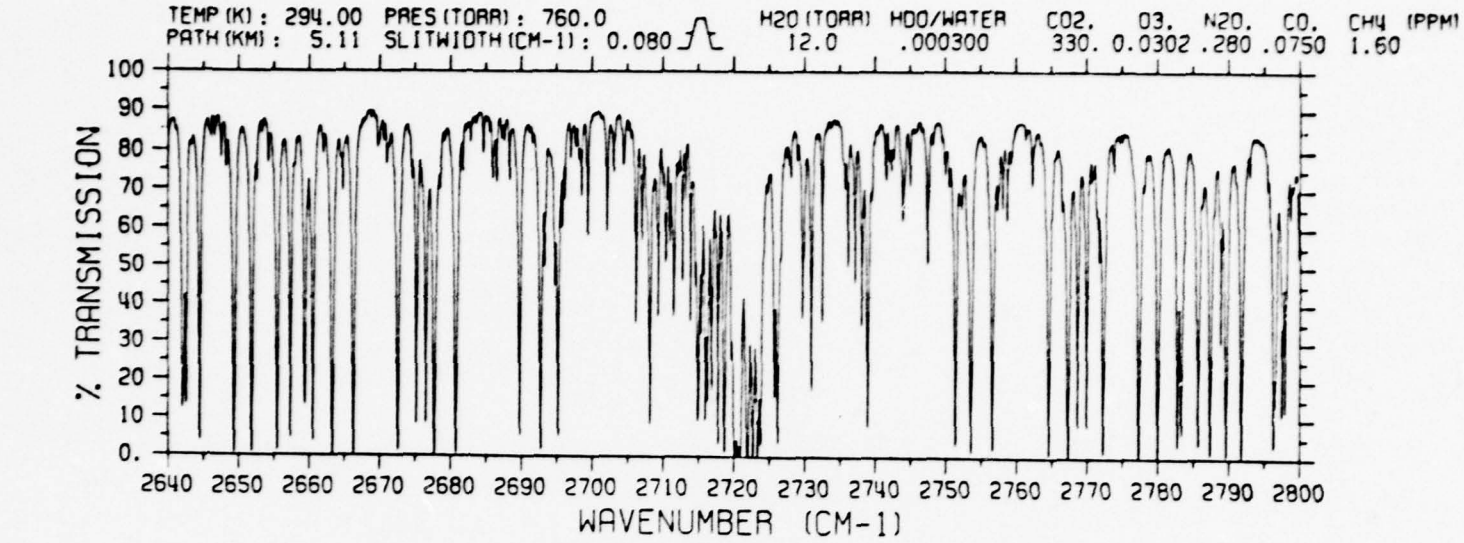

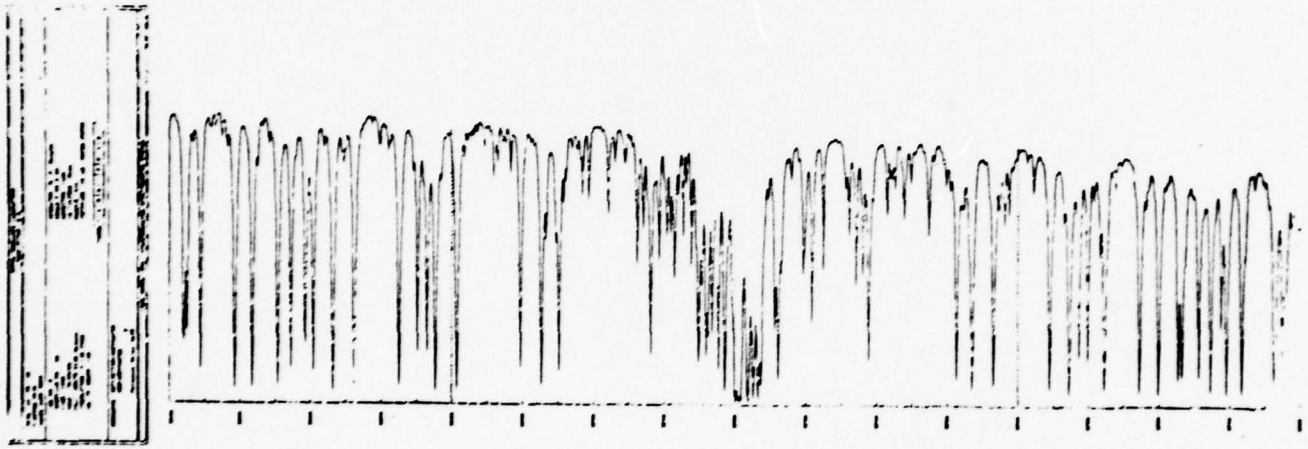

FIGURE 15b. FIGURE 15 CONTINUED

in the atmosphere. Recent NRL data on path integrated HDO measurements have shown that significantly less HDO is in the atmosphere, typically, than the assumed .03% HDO/HHO ratio [15]. This is apparent in Figure 15b only with careful scrutiny.

4.2 TRANSMISSION AT CO LASER FREQUENCIES

Transmission in the spectral region encompassing the lowest lying CO laser frequencies has been calculated for the Midlatitude Summer Model atmosphere, for three CO molecular concentrations. Values of .225 parts per million (PPM) .75 PPM and .075 PPM have been used. A synthetic spectrum is shown in Figure 16 for the lower CO bound. Tables 1, 2 and 3 gives the extinction value for the lower lying CO laser lines, and the absorption coefficient of each molecular absorber that is significant at the CO frequency.

4.3 DF EXTINCTION CALCULATIONS

DF extinction algorithms have been determined in detail from the measured HDO data, from earlier data and using values in the AFGL data compilation. These have been reported earlier [4]. However, during the course of this program, preliminary absorption coefficient values were determined, and power weighted absorption coefficiencies were calculated for a measured Baseline Demonstration Laser (BDL) power spectrum. This has been compared with estimates based on NRL measured extinction coefficients. The results are shown in Table 4.

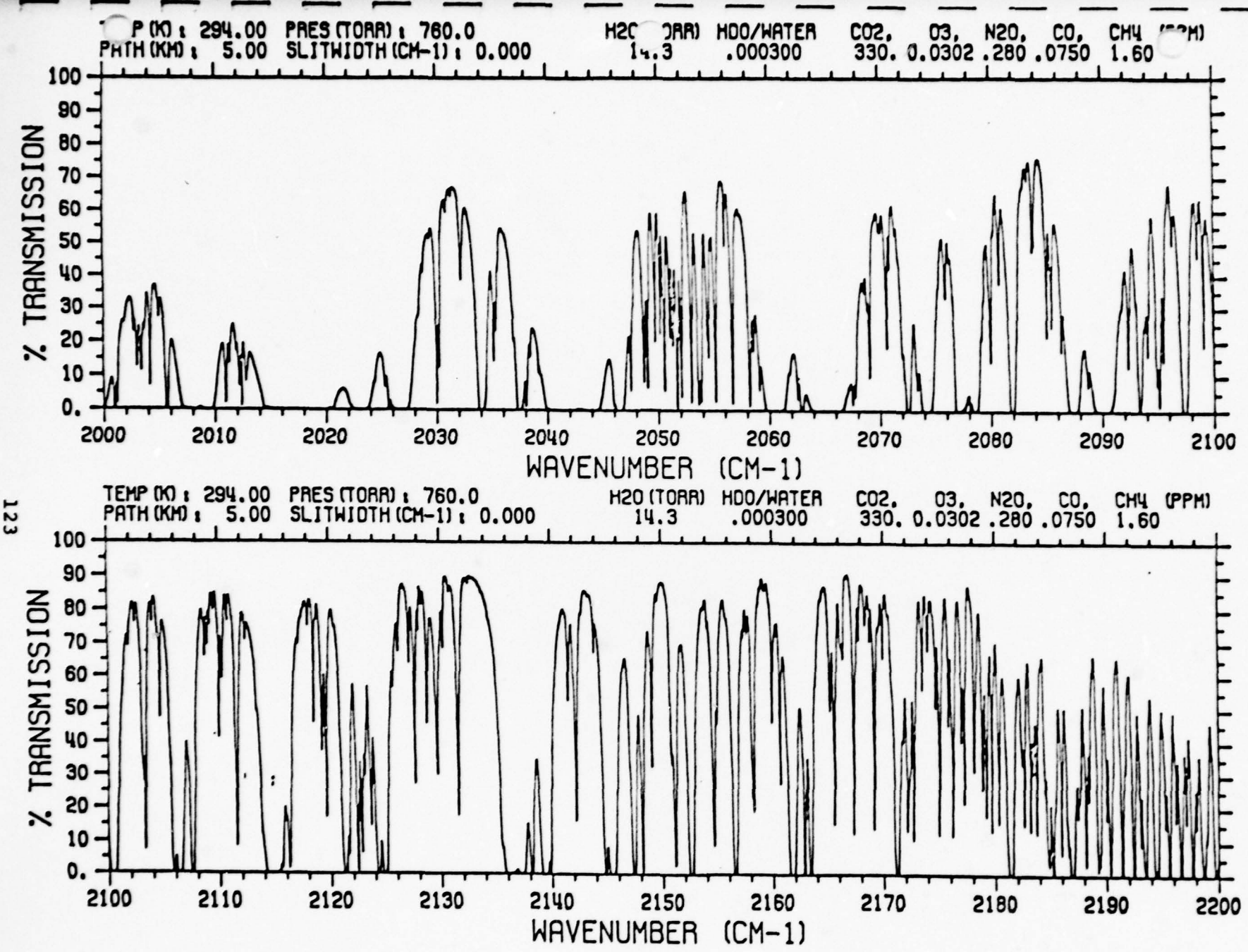

FIGURE 16. MONOCHROMATIC ATMOSPHERIC ABSORPTION IN THE CO LASER REGION

Table 1.
CO Laser Absorption Coefficients
Midlatitude Summer Sea Level with 0.075 ppm CO

SAI ABSORPTION COEFFICIENTS X 1000 (KM-1)
(6-18-76)

LASER LINES	FREQUENCY (CM-1)	H2O	CO2	O3	CO	TOTAL
P2(25)	2011.419	341.4	0.1	0.0	0.0	341.5
P2(24)	2016.025	5977.0	0.1	0.0	0.0	5977.1
P2(23)	2020.600	1687.0	0.7	0.0	0.1	1687.7
P2(22)	2025.143	435.4	0.5	0.0	0.2	436.1
P2(21)	2029.655	132.6	1.1	0.0	0.1	133.8
P2(20)	2034.134	5479.0	3.3	0.0	0.0	5482.4
P2(19)	2038.581	291.4	15.0	0.0	0.0	306.5
P2(18)	2042.996	1173.0	168.6	0.0	0.0	1341.6
P2(17)	2047.379	259.2	67.0	0.0	0.0	326.2
P2(16)	2051.729	847.2	22.5	0.0	0.1	869.9
P2(15)	2056.620	69.5	256.9	0.1	0.1	326.6
P2(14)	2060.332	15840.0	18.8	0.1	0.7	15859.5
P2(13)	2064.583	10380.0	112.3	0.2	4.2	10496.8
P2(12)	2068.802	150.7	31.5	0.3	39.3	221.9
P2(11)	2072.987	277.9	19.0	0.7	3.7	301.3
P2(10)	2077.139	155.5	1382.0	0.7	1.9	1540.0
(9)	2081.258	119.6	9.8	0.9	2.2	132.5
P2(8)	2085.343	137.6	19.8	0.9	0.9	159.2
P2(7)	2089.393	1279.0	6.1	1.4	0.8	1287.3
P2(6)	2093.410	628.3	260.0	1.3	0.7	890.2
P2(5)	2097.393	10390.0	3.3	2.5	0.6	10396.4
P2(4)	2101.342	91.3	7.9	1.5	0.6	101.4
P2(3)	2105.256	88.8	3.1	1.6	0.7	94.3
P2(2)	2108.768	44.4	8.7	1.8	1.1	56.1
P2(1)	2112.549	50.3	6.9	0.1	1.7	59.0
P1(25)	2037.027	327.1	22.0	0.0	5.8	354.9
P1(24)	2041.668	37720.0	14.2	0.0	10.3	37744.6
P1(23)	2046.278	1829.0	20.0	0.0	13.0	1862.0
P1(22)	2050.856	88.5	32.7	0.0	18.6	139.9
P1(21)	2055.402	57.5	63.2	0.1	26.4	147.2
P1(20)	2059.917	1567.0	188.1	0.1	36.6	1791.8
P1(19)	2064.399	4468.0	513.7	0.2	49.7	5031.6
P1(18)	2068.849	149.4	39.5	0.3	66.3	255.4
P1(17)	2073.267	395.2	25.5	0.5	86.5	507.6
P1(16)	2077.652	114.6	735.6	1.0	110.6	961.8
P1(15)	2082.005	2588.0	12.5	0.7	137.7	2738.9
P1(14)	2086.325	183.9	10.9	1.2	168.2	364.2
P1(13)	2090.611	1842.0	2.3	2.1	200.1	2046.5
P1(12)	2094.865	255.9	14.3	1.5	233.2	504.9
P1(11)	2099.085	69.1	2.6	2.0	265.6	339.4
P1(10)	2103.273	215.2	2.0	1.6	293.4	512.2
(9)	2107.426	1369.0	15.9	2.1	313.2	1700.2
P1(8)	2111.546	164.1	3.2	0.2	324.1	491.5
P1(7)	2115.632	490.9	8.2	1.2	323.5	823.8
P1(6)	2119.684	35.2	10.2	2.3	308.0	355.7

Table 2.
CO Laser Absorption Coefficients
Midlatitude Summer Sea Level with 0.225 ppm CO

SAI ABSORPTION COEFFICIENTS X 1000 (KM-1)
(6-18-76)

LASER LINES	FREQUENCY (CM-1)	H2O	CO2	O3	CO	TOTAL
P2(25)	2011.419	341.4	0.1	0.0	0.0	341.5
P2(24)	2016.025	5977.0	0.1	0.0	0.0	5977.2
P2(23)	2020.600	1687.0	0.7	0.0	0.2	1687.8
P2(22)	2025.143	435.4	0.5	0.0	0.5	436.4
P2(21)	2029.655	132.6	1.1	0.0	0.4	134.1
P2(20)	2034.134	5479.0	3.3	0.0	0.1	5482.4
P2(19)	2038.581	291.4	15.0	0.0	0.1	306.5
P2(18)	2042.996	1173.0	168.6	0.0	0.1	1341.7
P2(17)	2047.379	259.2	67.0	0.0	0.1	326.3
P2(16)	2051.729	847.2	22.5	0.0	0.3	870.0
P2(15)	2056.620	69.5	256.9	0.1	0.4	326.9
P2(14)	2060.332	15840.0	18.8	0.1	2.0	15860.9
P2(13)	2064.583	10380.0	112.3	0.2	12.7	10505.3
P2(12)	2068.802	150.7	31.5	0.3	118.0	300.6
P2(11)	2072.987	277.9	19.0	0.7	11.0	308.7
P2(10)	2077.139	155.5	1382.0	0.7	5.6	1543.8
P2(9)	2081.258	119.6	9.8	0.9	6.5	136.8
P2(8)	2085.343	137.6	19.8	0.9	2.8	161.1
P2(7)	2089.393	1279.0	6.1	1.4	2.3	1288.8
P2(6)	2093.410	628.3	260.0	1.3	2.0	891.5
P2(5)	2097.393	10390.0	3.3	2.5	1.9	10397.6
P2(4)	2101.342	91.3	7.9	1.5	1.9	102.7
P2(3)	2105.256	88.8	3.1	1.8	2.1	95.8
P2(2)	2108.768	44.4	8.7	1.8	3.3	58.2
P2(1)	2112.549	50.3	6.9	0.1	5.2	62.5
P1(25)	2037.027	327.1	22.0	0.0	17.5	366.6
P1(24)	2041.668	37720.0	14.2	0.0	30.9	37765.2
P1(23)	2046.278	1829.0	20.0	0.0	38.9	1888.0
P1(22)	2050.856	88.5	32.7	0.0	55.8	177.1
P1(21)	2055.402	57.5	63.2	0.1	79.2	200.0
P1(20)	2059.917	1567.0	188.1	0.1	109.7	1864.9
P1(19)	2064.399	4468.0	513.7	0.2	149.1	5131.0
P1(18)	2068.849	149.4	39.5	0.3	198.8	387.9
P1(17)	2073.267	395.2	25.5	0.5	259.5	680.6
P1(16)	2077.652	114.6	735.6	1.0	331.8	1183.0
P1(15)	2082.005	2588.0	12.5	0.7	413.1	3014.3
P1(14)	2086.325	183.9	10.9	1.2	504.6	700.6
P1(13)	2090.611	1842.0	2.3	2.1	600.3	2446.7
P1(12)	2094.865	255.9	14.3	1.5	699.6	971.3
P1(11)	2099.085	69.1	2.6	2.0	796.8	870.6
P1(10)	2103.273	215.2	2.0	1.6	880.2	1099.0
P1(9)	2107.426	1369.0	15.9	2.1	939.6	2326.6
P1(8)	2111.546	164.1	3.2	0.2	972.3	1139.7
P1(7)	2115.632	490.9	8.2	1.2	970.5	1470.8
P1(6)	2119.684	35.2	10.2	2.3	924.0	971.7

Table 3.
CO Laser Absorption Coefficients
Midlatitude Summer Sea Level with 0.75 ppm CO

SAI ABSORPTION COEFFICIENTS X 1000 (KM-1)
(6-18-76)

LASER LINES	FREQUENCY (CM-1)	H2O	CO2	O3	CO	TOTAL
P2(25)	2011.419	341.4	0.1	0.0	0.0	341.5
P2(24)	2016.025	5977.0	0.1	0.0	0.1	5977.2
P2(23)	2020.600	1687.0	0.7	0.0	0.5	1688.2
P2(22)	2025.143	435.4	0.5	0.0	1.7	437.7
P2(21)	2029.655	132.6	1.1	0.0	1.3	135.0
P2(20)	2034.134	5479.0	3.3	0.0	0.3	5482.6
P2(19)	2038.581	291.4	15.0	0.0	0.2	306.7
P2(18)	2042.996	1173.0	168.6	0.0	0.3	1341.9
P2(17)	2047.379	259.2	67.0	0.0	0.4	326.6
P2(16)	2051.729	847.2	22.5	0.0	0.9	870.6
P2(15)	2056.620	69.5	256.9	0.1	1.3	327.8
P2(14)	2060.332	15840.0	18.6	0.1	6.6	15865.5
P2(13)	2064.583	10380.0	112.3	0.2	42.4	10534.9
P2(12)	2068.802	150.7	31.5	0.3	393.5	576.1
P2(11)	2072.987	277.9	19.0	0.7	36.6	334.3
P2(10)	2077.139	155.5	1382.0	0.7	18.7	1556.9
P2(9)	2081.258	119.6	9.8	0.9	21.8	152.1
P2(8)	2085.343	137.6	19.8	0.9	9.2	167.5
P2(7)	2089.393	1279.0	6.1	1.4	7.7	1294.3
P2(6)	2093.410	628.3	260.0	1.3	6.5	896.1
P2(5)	2097.393	10390.0	3.3	2.5	6.3	10402.0
P2(4)	2101.342	91.3	7.9	1.5	6.5	107.3
P2(3)	2105.256	88.8	3.1	1.6	7.1	100.8
P2(2)	2108.768	44.4	8.7	1.8	10.9	65.8
P2(1)	2112.549	50.3	6.9	0.1	17.2	74.6
P1(25)	2037.027	327.1	22.0	0.0	58.2	407.3
P1(24)	2041.668	37720.0	14.2	0.0	103.1	37837.3
P1(23)	2046.278	1829.0	20.0	0.0	129.8	1978.8
P1(22)	2050.856	88.5	32.7	0.0	185.9	307.2
P1(21)	2055.402	57.5	63.2	0.1	264.0	384.8
P1(20)	2059.917	1567.0	188.1	0.1	365.7	2120.9
P1(19)	2064.399	4468.0	513.7	0.2	497.0	5478.9
P1(18)	2068.849	149.4	39.5	0.3	662.5	851.7
P1(17)	2073.267	395.2	25.5	0.5	865.0	1286.1
P1(16)	2077.652	114.6	735.6	1.0	1106.0	1957.2
P1(15)	2082.005	2588.0	12.5	0.7	1377.0	3978.2
P1(14)	2086.325	183.9	10.9	1.2	1682.0	1878.0
P1(13)	2090.611	1842.0	2.3	2.1	2001.0	3847.4
P1(12)	2094.865	255.9	14.3	1.5	2332.0	2603.7
P1(11)	2099.085	69.1	2.6	2.0	2656.0	2729.8
P1(10)	2103.273	215.2	2.0	1.6	2934.0	3152.8
P1(9)	2107.426	1369.0	15.9	2.1	3132.0	4519.0
P1(8)	2111.546	164.1	3.2	0.2	3241.0	3408.4
P1(7)	2115.632	490.9	8.2	1.2	3235.0	3735.3
P1(6)	2119.684	35.2	10.2	2.3	3080.0	3127.7

TABLE 4
BDL WEIGHTED α
COMPARISON OF CURRENT HI-TRAN WITH FIELD MEASUREMENT
$P(H_2O) \sim 14$ TORR

Line	% Power	Calc α	Measured α
P1-5	4.1	0.070	0.065
P1-6	6.1	0.087	0.074
P1-7	4.1	0.064	0.050
P1-8	14.8	0.140	0.152
P2-5	1.0	0.030	0.034
P1-9	0.5	0.040	0.038
P2-6	12.8	0.059	0.061
P2-7	11.3	0.100	0.114
P2-8	12.3	0.035	0.023
P3-5	0.8	0.023	0.019
P2-9	5.6	0.041	0.050
P3-6	4.3	0.030	0.032
P2-10	2.6	0.068	0.076
P3-7	12.8	0.065	0.068
P3-8	2.6	0.051	0.056
P3-9	3.6	0.036	0.033
P3-10	0.8	0.051	0.043

Measured $\bar{\alpha}$ = 0.074

Calc. $\bar{\alpha}$ = 0.071

Difference = 4.3 %

5
MODIFICATION OF THE HDO GFCS TO MEASURE CH_4, N_2O, $C^{13}O_2$, AND $C^{12}O_2$

NRL measurements of path integrated HDO vapor have demonstrated that the abundance of HDO relative to HHO is less than the generally accepted value of .03%, and that it varies significantly with local environmental conditions [15]. The dramatic effect of variations in molecular content on DF line absorption naturally leads one to question the reliability of accepted concentrations for the important "uniformly mixed" gases at specific sea level sites. For this reason, a study has been performed to determine the feasibility of modifying the NRL GFCS to measure the other gases important to DF propagation. These gases are: CH_4, $C^{13}O_2$, N_2O and $C^{12}O_2$.

The existing GFCS was designed and built under Contract N00173-75-C-9627 and delivered to NRL in October 1976. The instrument is completely described elsewhere [8] . It is an infrared instrument designed to measure the atmospheric water vapor content over a multi-kilometer path. The unit has been designed to operate in the NRL IMORL field measurement vans. A source unit is placed in the transmitter van. The GFCS unit (Fig. 17), a calibration source unit, and an electronics unit are placed in the receiver van which is 5 kilometers away from the transmitter van. The source unit provides an infrared signal which is sent through the 5 kilometer atmospheric path by the transmitter van optics to the receiver van optics. The GFCS unit then correlates the spectral structure of the received signal with the spectral structure of water vapor to determine the integrated atmospheric water vapor content.

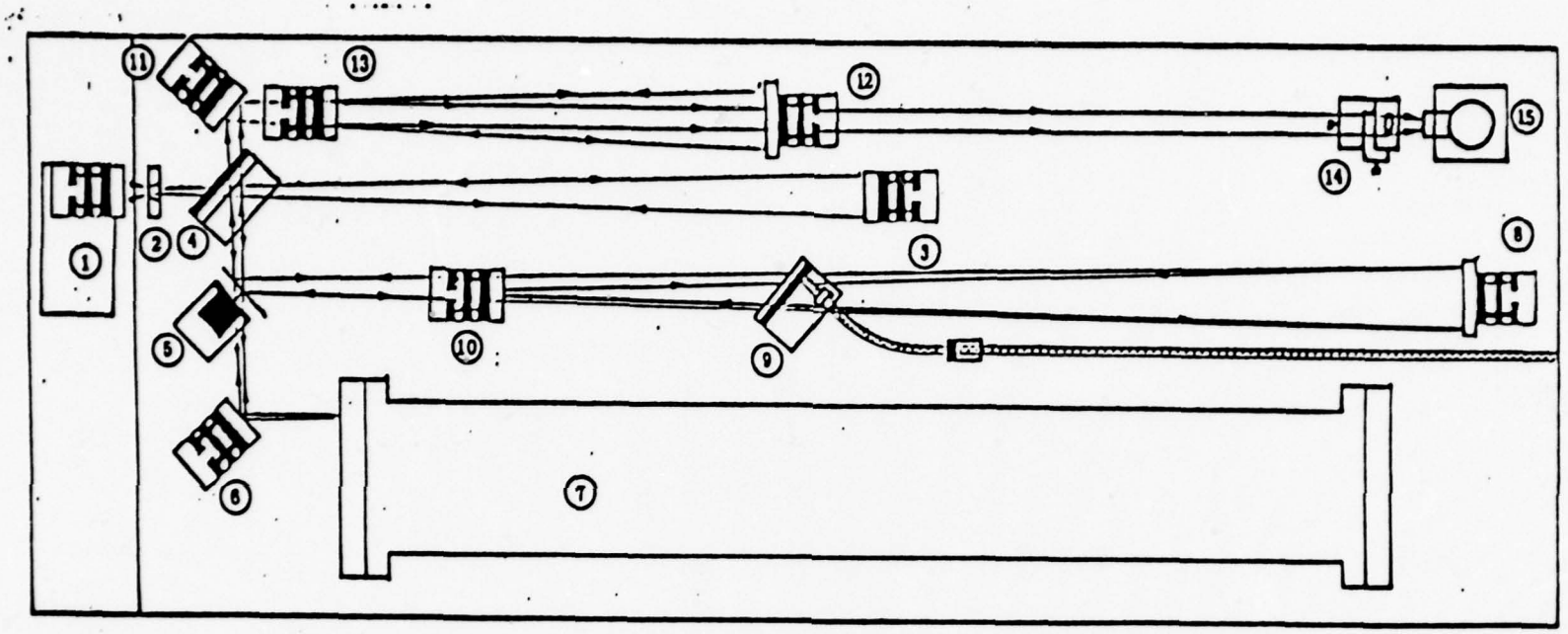

FIGURE 17. GAS FILTER CORRELATION SPECTROMETER

The suggested modification will permit the measurement of N_2O, CH_4, and CO_2 over the same 5 km path. The $C^{13}O_2$ measurement will be made over a short path of approximately 100 meters.

5.1 ANALYTICAL DESIGN STUDY

5.1.1 CONCEPT OF OPERATION

The GFCS concept was explained in the previous report describing the instrument and should be referred to for more detailed explanation. The term gas filter refers to the use of the complex infrared absorption spectra of a gas as an infrared filter. Correlation refers to the spectral correlation between the gas filter and the infrared absorption spectra of the same gas in the atmosphere. The principle of operation is given by Equation (1).

$$M = \frac{T_{ac} - T_a T_c}{T_{ac} + T_a T_c} \qquad (1)$$

where

- M is the instrument signal caused by the gas to be measured
- T_a is the average transmission of the measured gas over the infrared bandpass of the GFCS
- T_c is the average transmission of the GFCS sample cell over the infrared bandpass of the GFCS
- T_{ac} is the average transmission of a combination of the atmospheric gas transmission and the sample cell gas transmission over the infrared bandpass of the GFCS.

Equation (1) expresses the measurement signal in terms of the degree to which it modulates the source signal. The measurement signal M arises from the fact that the average transmission of the combination of atmosphere and sample

cell (T_{ac}) is greater than the product of individual average transmissions T_a and T_c

$$T_{ac} \geq T_a T_c \tag{2}$$

where

$$T_{ac} = \frac{1}{\Delta\nu} \int_{\Delta\nu} T_a(\nu) T_c(\nu) d\nu \tag{3}$$

$$T_a T_c = \frac{1}{\Delta\nu} \int_{\Delta\nu} T_A(\nu) d\nu \times \frac{1}{\Delta\nu} \int_{\Delta\nu} T_C(\nu) d\nu \tag{4}$$

In the actual GFCS, the source signal is initially chopped at 750 Hz to allow the signal processing electronics to discriminate between it and other signals. This beam is alternately passed through a sample cell to obtain the combined cell atmospheric path transmission T_{ac}, and passed through a reference attenuation path with a constant transmission adjusted to the average sample cell transmission $T_R = T_c$ to obtain the product $T_a T_c$. After the signal is modulated by this procedure it is imaged onto a detector.

The modulation M is of central importance because the primary limits to the accuracy of the measurements are manifested in terms of the modulation of the source signal rather than as a constant noise. The constant detector noise is small, less than the amount that would cause a 1% measurement error. However, errors which express themselves in terms of the modulation limit the measurement accuracy. The purpose of the analytical design studies are

to calculate the dependence of the modulation M on the various atmospheric and sample cell parameters: spectral region, interfering species, cell concentration, and path length.

5.1.2 SPECTRAL BAND SELECTION

A check was made of the spectral absorption bands of CH_4, H_2O and CO_2 which might be suitable for a GFCS instrument. The major bands considered are listed in Table 5. An asterisk has been placed next to the selected band.

Accuracy estimates for the selected bands were made based on line-by-line calculations. This information is given in Table 5.

The atmospheric transmission over long paths for the selected bands are shown in Figures 5, 3, and 18. It can be seen in Figure 5 that the CH_4 band is quite strong, but there are many water vapor lines in the same region. However, our calculations predict that the interference will be less than 2%. It should be noted in Figures 3 and 18 that there is very little interference in the N_2O band and virtually none in the CO_2 band.

The predicted modulation functions for these same bands as a function of the expected concentration is given in Figures 19 through 21. These can be compared with HDO modulation function given in Figure 22.

In addition to the gases included in the detailed analysis, it is proposed to measure $C^{13}O_2$. The spectral region selected for this measurement is 2240 - 2300 cm^{-1}. An atmospheric transmission path in this spectral region is shown in Figure 23. The absorption in the region is too strong to make measurements over a sea level 5 km horizontal path. Therefore, it is being proposed that a separate portable source be provided which can be set on a tripod at a con-

TABLE 5

GFC BANDS CONSIDERED FOR VARIOUS MOLECULES

Molecule	Band μm	Band cm^{-1}	Band Strength (atm^{-1} cm^{-2})	Comments
CH_4	1.665	6005	1.6	Too weak
	*3.312	3019	270.0 ($\bar{\alpha} = 0.30$)	H_2O interference 2860 - 2960 cm^{-1} Not bad.
	3.846	2600	3.07 (?)	Probably too weak.
	7.657	1306	204.0	No transmission because of H_2O and CO_2
N_2O	17.007	588.8	35	No transmission H_2O and CO_2
	8.561	1168.1	10	Weak interference
	7.782	1284.9	230	No transmission
	4.497	2223.8	1600	No good - badly overlapped with CO_2
	*3.755	2663.3	40 ($\bar{\alpha} = 0.09$)	Looks good, may be slightly weak
	2.873	3480.8	40	No transmission H_2O
CO_2	2.060	4853.6	0.217	Looks good if not too strong
	2.080	4807.7	0.018	Combination band, 4780-4804 fairly clear
	*1.606	6227.924	0.0137 ($\bar{\alpha} = 0.08$)	Clear, no interference
	1.576	6347.	0.0132	Clear, no interference

TABLE 6

ACCURACY ESTIMATES BASED ON LINE-BY-LINE CALCULATIONS FOR GFCS GAS CONCENTRATION MEASUREMENTS OVER A 10 KILOMETER PATH

Measured Gas	Measurement Range (ppm)	Accuracy
CO_2	50 - 500 No Interference	5%
N_2O	0.05 - 5 No Interference	10%
CH_4	0.4 - 4 H_2O Interference < 2% at 1.6 ppm	5%

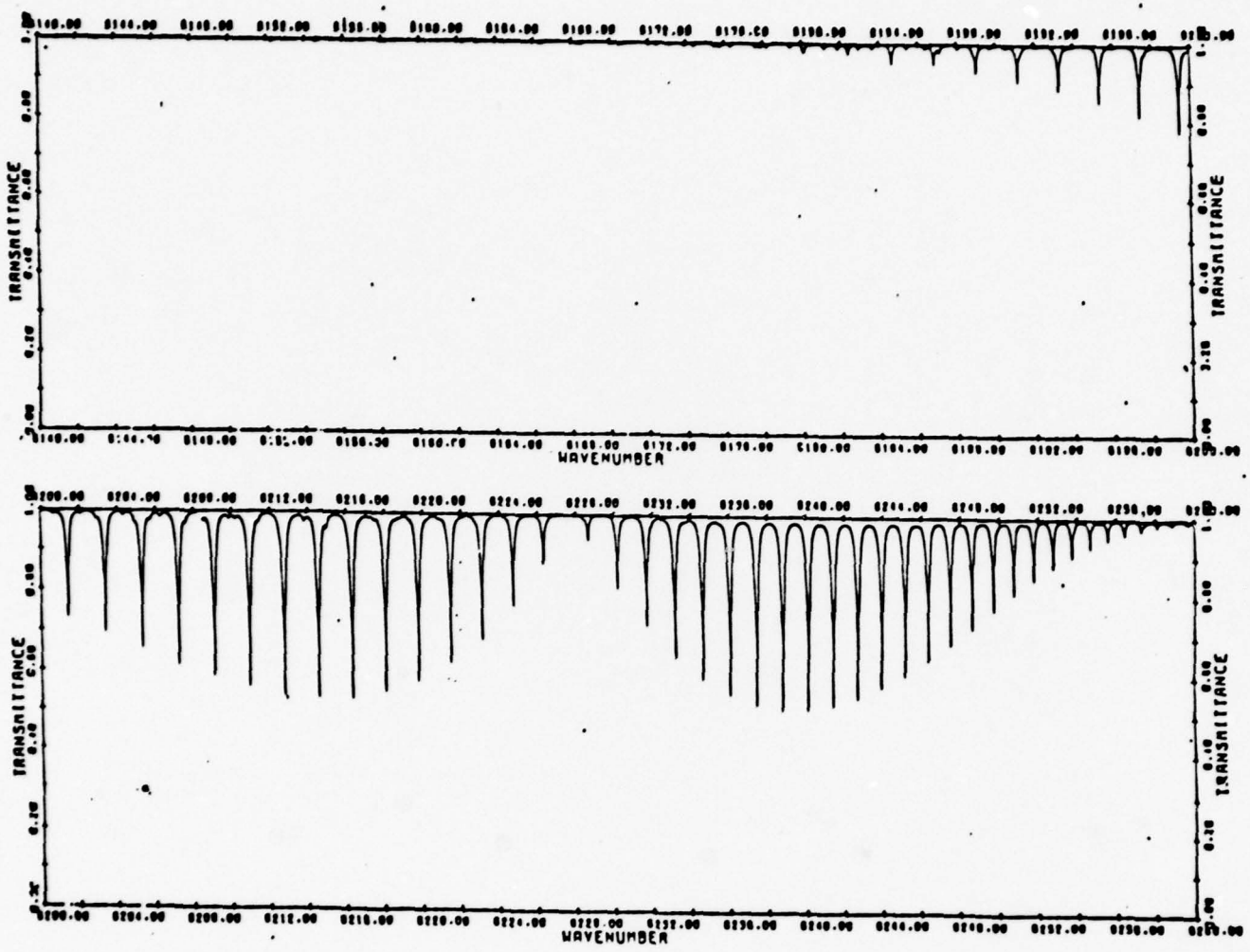

FIGURE 18. ATMOSPHERIC TRANSMITTANCE DUE TO MOLECULAR ABSORPTION THROUGH A 10 KM HORIZONTAL PATH AT SEA LEVEL SHOWING CO_2 ABSORPTION BANDS PROPOSED FOR GFCS (TAKEN FROM REFERENCE 15).

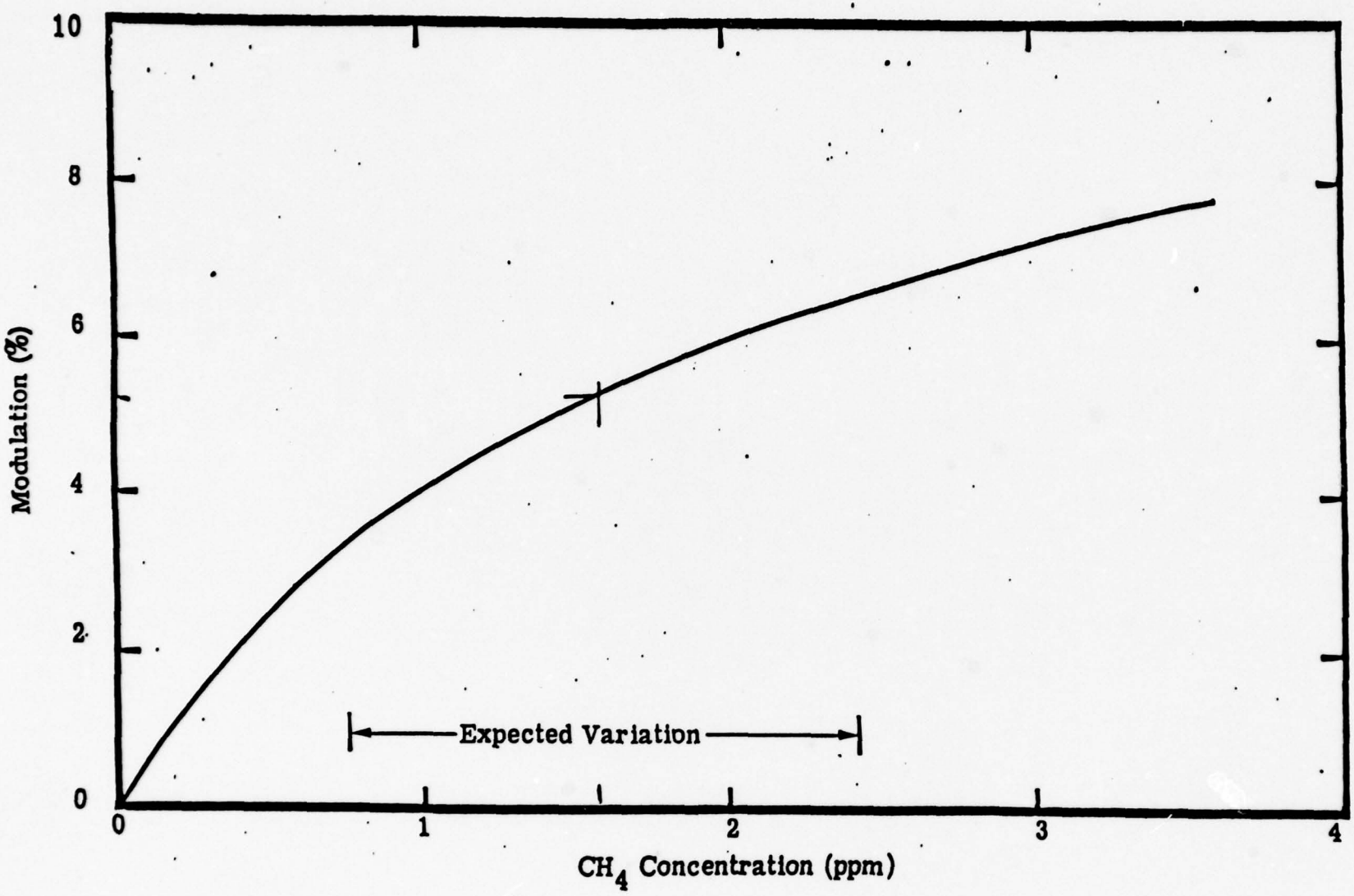

FIGURE 19. PREDICTED MODULATION FOR A CH_4 GFCS

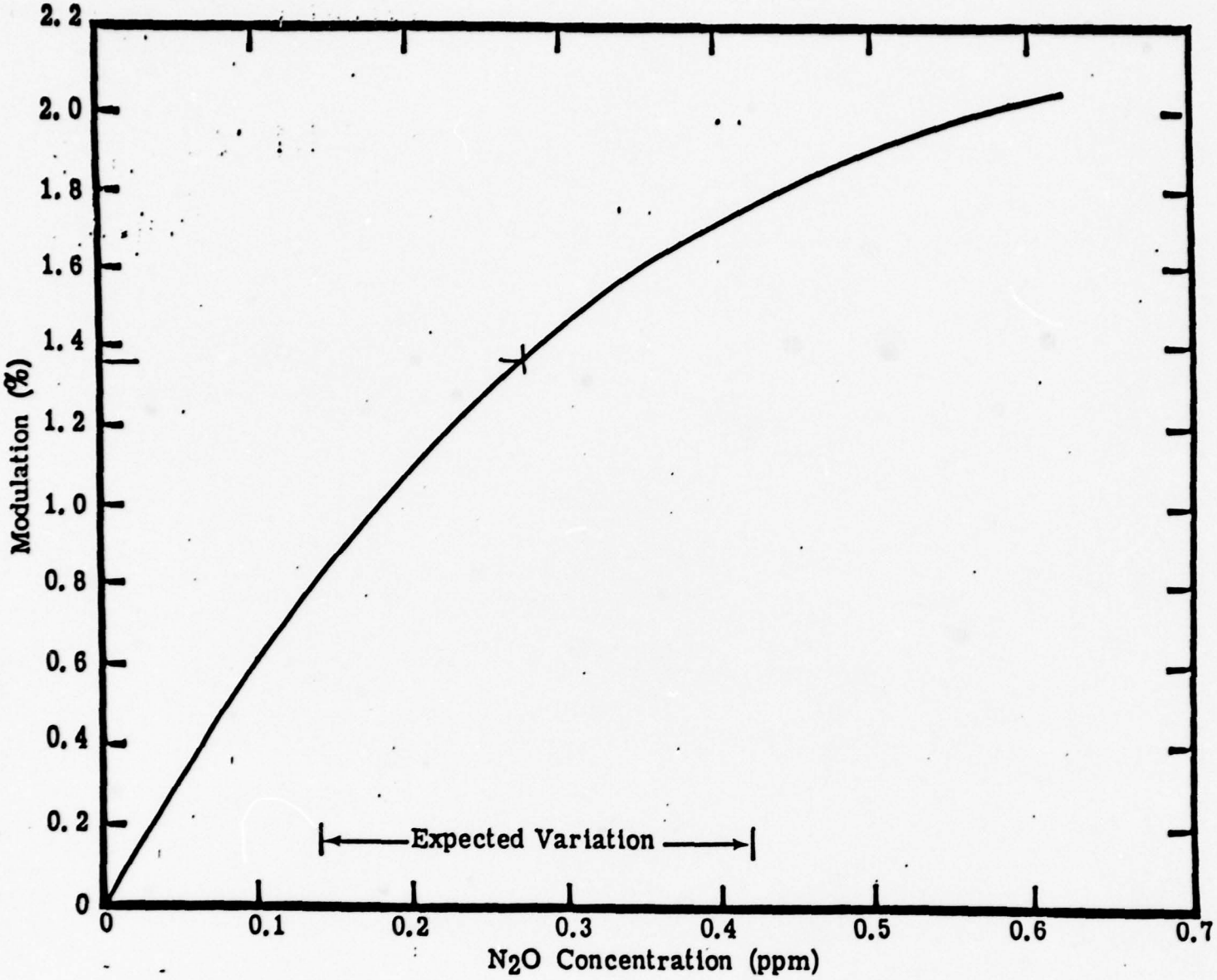

FIGURE 20. PREDICTED MODULATION FOR A N_2O GFCS OPERATING OVER A 10 KM PATH

venient distance from the receiver, about 100 meters for measurement. Calculations on single lines in this region indicate that this would be the approximate distance required.

5.1.3 DETERMINATION OF CELL CONCENTRATIONS

The modulation function M is dependent on the total amount of gas in the cell, the temperature and the pressure. Since we are making measurements at atmospheric pressure, the best correlation will occur with lines of approximately the same width. Hence, the first choice is to make the cell pressure equal to atmospheric pressure and maintain the temperature near ambient.

The modulation functions plotted in Figures 21 - 23 were done with the following selected cell concentration:

Molecule	Concentration
CH_4	5 atmos - cm
N_2O	3 atmos - cm
CO_2	1200 atmos - cm

The estimated concentration required for $C^{13}O_2$ is 0.25 atmos - cm.

Before the final cell depth is selected, the modulation function for a family of cell optical depths will be calculated similar to what was done for the HDO.

5.1.4 SELECTION OF MODULATION SYSTEM

As was pointed out in the introduction, the limits on the accuracy of measurement are set by the modulation M rather than detector noise. In the case of the HDO measurement, the nominal value of M is about 10% whereas in the case of N_2O, the nominal value is about 1%. This means that in order to achieve the same ultimate measurement

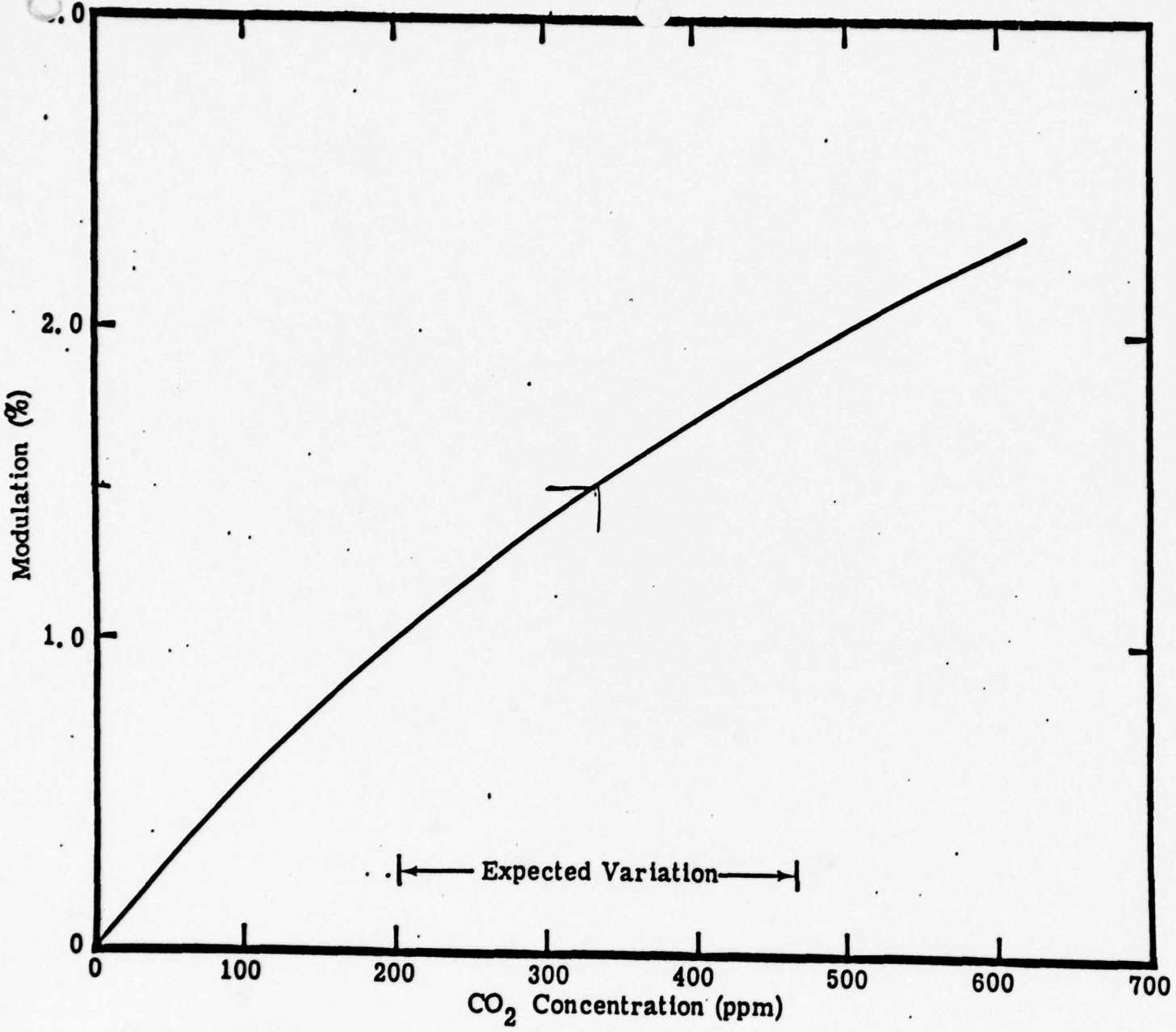

FIGURE 21. PREDICTED MODULATION FOR A CO_2 GFCS OPERATING OVER A 10 KM PATH

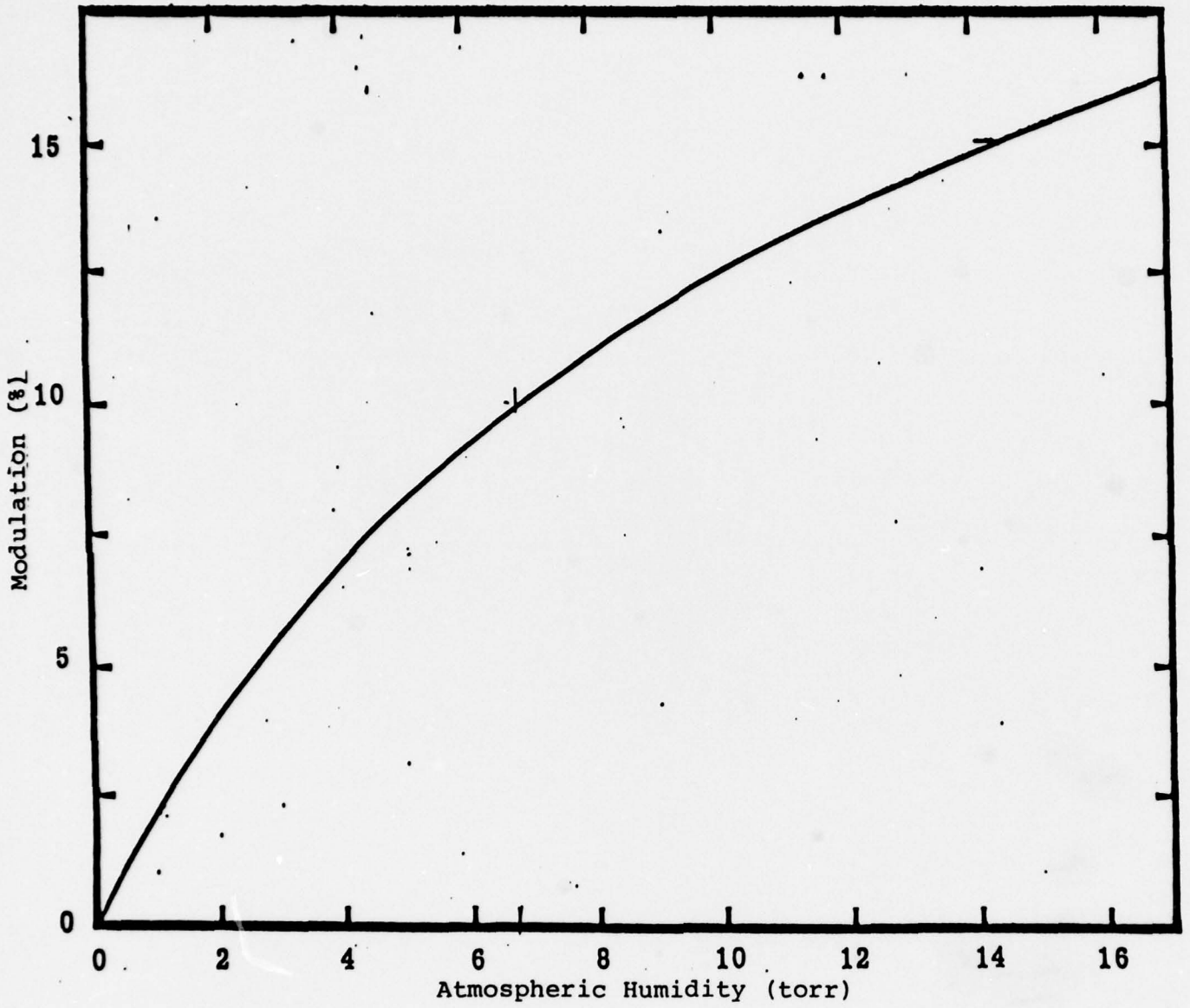

FIGURE 22. MODULATION FOR A WATER VAPOR GFCS OPERATING OVER A 10 KM PATH

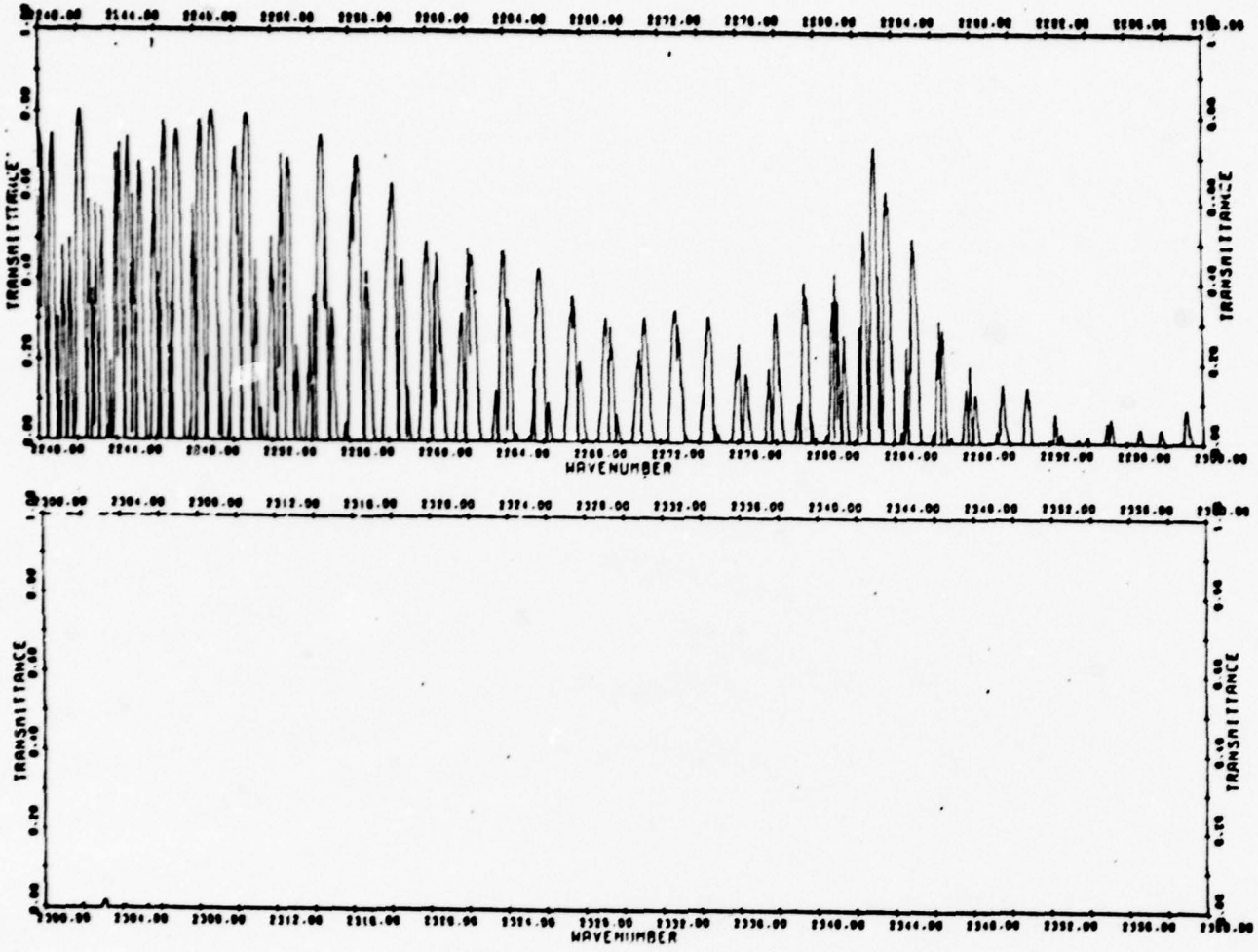

FIGURE 23. ATMOSPHERIC TRANSMITTANCE DUE TO MOLECULAR ABSORPTION THROUGH A 10 KM HORIZONTOL PATH AT 12 KM ALTITUDE

accuracy, the minimum value of M must be an order of magnitude lower. We have therefore given consideration to other modulation schemes in addition to the chopper modulation used in the current GFCS.

Two alternate modulation schemes were considered. The first splits the incoming radiation with a beamsplitter to make a reference and measurement path. The energy in each path is measured with a separate detector. The second scheme uses a reference cell and a measurement cell. Each cell is alternately placed in the measurement path. Both of these schemes are currently being used in existing instrumentation.

The beamsplitter approach is being used in a CO monitor designed for NASA-Langley by TRW to remotely measure the atmospheric CO concentration from an airplane. This system has the advantage of no moving parts and that the comparison between the two beams is made at the same time. The disadvantage is that a sophisticated amplifier gain and balance control are required. The minimum modulation which they report is .01%.

The second system is a rotating cell containing two sections, a reference and a balance, which are alternately rotated into the optical path. This system has the advantage over the current modulation scheme in that no energy is lost in the beamsplitter and the difference in the two optical paths is minimal. This scheme is used in several instruments built by Ford Aeronautics for EPA and based on the data collected on one of these instruments. The drift in M is less than 5% of the expected modulation from N_2O. Hence, we are reasonable assured that this scheme will provide satisfactory results. The disadvantage of this scheme will provide satisfactory results. The disadvantage of this scheme is that the rotating chopper would also have

to be provided for the HDO and CO_2 measurements. Based on our own experience and on information received from NASA-Langley, there is a reasonable expectation that with an improved chopper, the present chopper modulation scheme will give satisfactory results.

6
SUMMARY AND CONCLUSIONS

With the work reported here, the goal of developing a precise understanding of atmospheric molecular absorption of DF laser radiation has been attained for sea level paths. Some of the more important milestones reached during this two-year effort are the following:

(1) High resolution ($\lesssim .05$ cm^{-1}) survey spectra of HDO, N_2O, and CH_4 have been measured and compared with HI-TRAN calculations to identify inaccuracies or omissions in the AFGL data tape which should be important to molecular absorption of DF laser radiation. These spectra identified HDO and CH_4 as the two species for which the molecular line data base was inadequate for this application.

(2) Synthetic spectra were generated at the long wavelength end and the short wavelength end of the low power laser and BDL spectral region to quantify the important molecular absorbers for the high power DF devices (NACL and MIRACL) and for broad band E-O applications, respectively.

(3) A complete base of high resolution HDO measurements suitable for extracting HDO line strength, air broadened width, and position parameters has been established.

(4) Algorithms for predicting DF laser transmission, function of temperature and absolute humidity have been developed for sea level propagation paths.

(5) HI-TRAN modeling for predicting infinite and degraded resolution SMI spectra has been developed.

(6) Modeling of SMI spectra and DF laser transmission algorithms have been verified by NRL field data.

(7) HDO content in the atmosphere, relative to the most abundant isotopic variation has been found to be typically less than the heretofore assumed value of .03% HDO/HHO. This has been determined by NRL using a HDO GFCS designed and constructed by SAI.

(8) A design study for modifying the GFCS to monitor up to 5 gases important to DF laser transmission has been completed.

The work reported here and in the preceding DF work has not directly addressed aerosol and continuum extinction; nevertheless, a better understanding of these issues have been achieved since the modeling developed has allowed continuum extinction to be extracted from field data. Thus, a powerful tool for "backing out" aerosol and molecular continuum data, and for achieving predictive models for this extinction, has been developed. At the present time, however, it must be concluded that a verified predictive modeling of aerosol extinction has not been achieved.

The verification of the variability of HDO content as a function of the environmental condition (item 7) has identified the need for determining actual atmospheric number densities of the ambient as well as the variable gases, rather than relying on the accepted global average

values. Construction of the multi-channel GFCS (item 8) would permit monitoring all gases that are most relevant to DF HEL test and operational performance.

In addition to determining the actual atmospheric molecular content, short range and above sea level transmission remains as the unsolved linear propagation issues. Algorithms for molecular absorption for these scenarios have not been developed, nor have they been developed or verified even for sea level aerosol extinction.

REFERENCES

1. R.E. Meredith, T.S. Chang, F.G. Smith, D.R. Woods, "Investigations in Support of High Energy Laser Technology, Vol. I, Measured Molecular Absorption Line Parameters for CO_2 at 10.4 μm and Anomalous Parameters for H_2O at .93 μm and 10-14 μm", SAI-75-001-AA, February 1975.

2. D.R. Woods, R.E. Meredith, F.G. Smith and T.W. Tuer, "High Resolution Spectral Survey of Molecular Absorption in the DF Laser Region: Measurements and Calculations," RADC-TR-75-180, July 1975.

3. D.R. Woods and R.E. Meredith, "Application of High Resolution Spectroscopy to DF Laser Propagation," SAI-76-001-AA, January 1976.

4. D.R. Woods, W. Flowers, R.E. Meredith, T.W. Tuer, and J.P. Walker, "DF Laser Propagation Analysis," SAI-77-001-AA, January 1977.

5. A.C. Cron and K.N. Seeber, Proceedings of the Meeting "Absorption of Infrared Laser Radiation in the Atmosphere," M73-86, April 4-5, 1973.

6. T.H. Cosden, J.A. Curcio, J.A. Dowling, C.O. Gott, D.H. Garcia, S.T. Hanley, K.M. Haught, R.F. Horton, G.L. Trusty and W.L. Agambar, "Atmospheric Transmission Measurement Program Report for 1 July thru 30 September 1976 (TQ 1976), NRL Report 8104, Sept. 1977.

7. J.A. Dowling, K.M. Haught, R.F. Horton, S.T. Hanley, J.A. Curcio, D.H. Garcia, C.O. Gott and W.L. Agambar, "Atmospheric Transmission Measurements Using IR Lasers, Fourier Transform Spectroscopy and Gas Filter Correlation Techniques," Report of NRL Progress, March 1977 Reprint.

8. D.R. Woods, F.G. Smith, L.W. Chaney, W.L. Flowers, R.E. Meredith and J.P. Walker, "NRL Gas Filter Correlation Final Report, SAI-76-008-AA, October 1976.

9. R.A. McClatchey, R.W. Fenn, J.E.A. Selby, F.E. Volz and J.S. Garing, "Optical Properties of the Atmosphere," AFCRL-72-0496, 24 August 1972.

10. D.E. Burch, D.A. Gryvnak, and J.D. Pembrook, "Investigation of the Absorption of Infrared Radiation by Atmospheric Gases," Aeronutronic Report U-4829, June 1970.

11. D.E. Burch, D.A. Gryvnak and J.D. Pembrook, "Investigation of the Absorption of Infrared Radiation by Atmospheric Gases: Water, Nitrogen, Nitrous Oxide," Aeroneutronics Report U-4897, January 1971.

12. K.O. White, W.R. Watkins, C.W. Bruce, R.E. Meredith and F.G. Smith, "Water Vapor Continuum in the 3.5 to 4.0 μm Region," Accepted for publication in Applied Optics, September 1978.

13. R.A. McClatchey, W.S. Benedict, S.A. Clough, D.E. Burch, R.F. Calfee, K. Fox, L.S. Rothman, J.S. Garing, "AFCRL Atmospheric Absorption Line Parameters Compilation," AFCRL-TR-33-0096, January 1973.

14. W. Benedict, private communication.

15. R.A. McClatchey and J.E.A. Selby, "Atmospheric Attenuation of Laser Radiation from 0.76 to 31.25 μm," AFCRL-TR-74-0003, January 1974.

APPENDIX
HDO DATA LOG

A log of all 181 data sets obtained during the present program has been maintained. It is reproduced here as an Appendix to document the experimental conditions and other information relevant to its use. The log is described in Section 2.

RUN	SCAN	DATE	DATA TYPE	FILL TEMP.	PATH LENGTH	TOTAL H_2O V.P.	CALIB. HDO V.P.	AIR+H2O PRESSURE	CM-1 SCANNED
30	1	2/23/76	s+γ		20.				2893-2737
30	2	2/23/76	s+γ		200.				2893-2737
30	3	2/25/76	s+γ		380.				2871-2137
31	1	2/28/76	s+γ	23.5	20.	9.41	.319	760.1	2851-2799
31	2	2/29/76	s+γ	23.5	20.	9.41	.380	760.1	2801-2749
32	1	3/3/76	s+γ	23.5	100.	9.41	.429	760.	2551-2509
32	2	3/4/76	s+γ	23.5	380.	9.41	.440	760.	2511-2469
32	3	3/4/76	s+γ	23.5	380.	9.41	.441	760.	2471-2449
33	1	3/5/76	s+γ	23.5	20.	9.41	.447	760.	2671-2658
33	2	3/5/76	s+γ	23.5	20.	9.41	.447	760.	2673-2659
34	1	3/10/76	s+γ	23.5	20.	9.41	.466.	760.	2754-2701
34	2	3/11/76	s+γ	23.5	20.	9.41	.468	760.	2691-2638
34	3	3/12/76	s+γ	23.5	20.	9.41	.470	760.	2648-2604
34	4	3/13/76	s+γ	23.5	20.	9.41	.471.	760.	2612-2570

RUN	SCAN	DATE	DATA TYPE	FILL TEMP.	PATH LENGTH	TOTAL H_2O V.P.	CALIB. HDO V.P.	AIR+H2O PRESSURE	CM^{-1} SCANNED
34	5	3/14/76	S + γ	23.5	20.	9.41	.472	760.	2572-2550
35	1	3/16/76	slit functions	24.2	20.	4.37	.219	4,511	~2824-~2820
35	2	3/16/76	"	24.2	20.	4.37	.219	4.511	2826-2822
35	3	3/16/76	"	24.2	20.	4.37	.219	4.511	2801-
36	1	3/17/76	S + γ	24.2	20.	4.37	.158	206.8	2854-2799
36	2	3/17/76	S + γ	24.2	20.	4.37	.158	206.8	2803-2749
36	3	3/17/76	S + γ	24.2	20.	4.37	.158	206.8	2752-2699
36	4	3/18/76	S + γ	24.2	20.	4.37	.176	206.8	2702-2649
36	5	3/18/76	S + γ	24.2	20.	4.37	.176	206.8	2652-2599
36	6	3/19/76	S + γ	24.2	20.	4.37	.189	206.8	2602-2559
36	7	3/19/76	S + γ	24.2	100.	4.37	.189	206.8	2562-2519
36	8	3/20/76	S + γ	24.2	380.	4.37	.192	206.8	2522-2479
36	9	3/20/76	S + γ	24.2	380.	4.37	.192	206.8	2481-2449
36	10	3/25/76	S + γ	24.2	100.	4.37	.196	206.8	2854-2799

RUN	SCAN	DATE	DATA TYPE	FILL TEMP.	PATH LENGTH	TOTAL H_2O V.P.	CALIB. HDO V.P.	AIR+H2O PRESSURE	CM^{-1} SCANNED
36	11	3/26/76	s + γ	24.2	200.	4.37	.196	206.8	2803-2749
36	12	3/27/76	s + γ	24.2	100.	4.37	.198	206.8	2752-2699
36	13	3/28/76	s + γ	24.2	200.	4.37	.199	206.8	2702-2649
36	14	3/28/76	s + γ	24.2	200.	4.37	.199	206.8	2652-2599
36	15	3/29/76	s + γ	24.2	200.	4.37	.199	206.8	2602-2559
37	1	3/29/76	s + γ	24.2	40.	4.37	.199	413.6	2858-2803
37	2	3/30/76	s + γ	24.2	200.	4.37	.200	413.6	2803-2749
37	3	3/30/76	s + γ	24.2	20.	4.37	.200	413.6	2752-2699
37	4	3/31/76	s + γ	24.2	20.	4.37	.201	413.6	2662-2653
37	5	3/31/76	s + γ	24.2	20.	4.37	.201	413.6	2652-2600
37	6	3/31/76	s + γ	24.2	40.	4.37	.201	413.6	2604-2561
37	7	3/31/76	s + γ	24.2	200.	4.37	.201	413.6	2556-2532
37	8	4/1/76	s + γ	24.2	380.	4.37	.201	413.6	2522-2501
38	1	4/1/76	s + γ	24.2	40.	4.37	.202	760.	2854-2799

RUN	SCAN	DATE	DATA TYPE	FILL TEMP.	PATH LENGTH	TOTAL H_2O V.P.	CALIB. HDO V.P.	AIR+H2O PRESSURE	CM^{-1} SCANNED
51	2	10/5/76	HDO CALIBRATION CHECK		20.	1.98	.064	413.6	2660-2650
51	3	10/5/76	"		20.	1.98	.064	413.6	2660-2650
52	1	10/6/76	"		20.	1.99	.064	1.99	2660-2650
52	2	10/6/76	"		20.	1.99	.064	413.6	2660-2650
52	3	10/6/76	"		20.	1.99	.064	413.6	2660-2650
53	1	10/7/76	"		20.	2.0	.065	2.0	2660-2650
53	2	10/7/76	"		20.	2.0	.065	413.6	2660-2650
53	3	10/8/76	"		20.	2.0	.065	413.6	2660-2650
53	4	10/11/76	"		20.	2.0	.065	413.6	2660-2650
53	5	10/11/76	"		20.	2.0	.065	413.6	2660-2650
53	6	10/11/76	"		20.	2.0	.065	413.6	2660-2650
53	7	10/12/76	"		20.	2.0	.065	413.6	2660-2650
53	8	10/13/76	"		20.	2.0	.065	413.6	2660-2650
53	9	10/14/76	"		20.	2.0	.065	413.6	2660-2650

RUN	SCAN	DATE	DATA TYPE	FILL TEMP.	PATH LENGTH	TOTAL H_2O V.P.	CALIB. HDO V.P.	AIR+H2O PRESSURE	CM^{-1} SCANNED
53	10	10/25/76	HDO CALIBRATION CHECK		20.	2.0	.065	413.6	2660-2650
54	1	11/15/76	$\bar{\nu}$		20.	5.01	.162	5.01	2854-2748
54	2	11/16/76	$\bar{\nu}$		40.	5.01	.162	5.01	2757-2653
54	3	11/17/76	$\bar{\nu}$		40.	5.01	.162	5.01	2663-2545
54	4	11/18/76	$\bar{\nu}$		100.	5.01	.162	5.01	2551-2444
55	1	11/19/76	~~full-strength configuration~~ ↓	HDO calibration check	20.	5.01	.162	413.6	2660-
56	1	11/19/76	$\bar{\nu}$		40.	5.01	.162		2854-2766
56	2	11/22/76	$\bar{\nu}$		40.	5.01	.162		2779-2715
57	1	11/22/76	s+γ	25.5	20.	4.99	.161	206.8	2660-2654
57	2	11/22/76	s+γ	25.5	60.	4.99	.161	206.8	2546-2542
57	3	11/22/76	s+γ	25.5	20.	4.99	.161	206.8	2834-2828
57	4	11/22/76	s+γ	25.5	20.	4.99	.161	206.8	2766-2762
57	5	11/22/76	s+γ	25.5	20.	4.99	.161	206.8	2660-2654
58	1	11/23/76	s+γ	25.5	20.	4.99	.161	413.6	2660-2654

RUN	SCAN	DATE	DATA TYPE	FILL TEMP.	PATH LENGTH	TOTAL H_2O V.P.	CALIB. HDO V.P.	AIR+H2O PRESSURE	CM^{-1} SCANNED
58	2	11/23/76	s + γ	25.5	100.	4.99	.161	413.6	2546 - 2542
58	3	11/23/76	s + γ	25.5	20.	4.99	.161	413.6	2766 - 2762
58	4	11/23/76	s + γ	25.5	20.	4.99	.161	413.6	2660 - 2654
59	1	11/23/76	s + γ	25.5	20.	4.99	.161	760.1	2660 - 2654
59	2	11/23/76	s + γ	25.5	200.	4.99	.161	760.1	2546 - 2542
59	3	11/23/76	s + γ	25.5	40.	4.99	.161	760.1	2766 - 2762
59	4	11/23/76	s + γ	25.5	20.	4.99	.161	760.1	2639 - 2633
59	5	11/23/76	s + γ	25.5	20.	4.99	.161	760.1	2579 - 2575
59	6	11/23/76	s + γ	25.5	20.	4.99	.161	760.1	2660 - 2654
60	1	11/29/76	$\bar{\nu}$		40.	5.00	.161	5.0	2721 - 2627
60	2	11/30/76	$\bar{\nu}$		100.	5.00	.161	5.0	2636 - 2544
60	3	12/1/76	$\bar{\nu}$		200.	5.00	.161	5.0	2549 - 2443
61	1	12/3/76	$\bar{\nu}$	23.3	40.	4.96	.160	4.96	2854 - 2765
61	2	12/6/76	$\bar{\nu}$	23.3	40.	4.96	.160	4.96	2770 - 2677

RUN	SCAN	DATE	DATA TYPE	FILL TEMP.	PATH LENGTH	TOTAL H_2O V.P.	CALIB. HDO V.P.	AIR+H2O PRESSURE	CM^{-1} SCANNED
61	3	12/7/76	$\bar{\nu}$	23.3	40.	4.96	.160	4.96	2683-2575
61	4	12/8/76	$\bar{\nu}$	23.3	100.	4.96	.160	4.96	2583-2519
61	5	12/9/76	$\bar{\nu}$	23.3	300.	4.96	.160	4.96	2524-2441
62	1	12/10/76	$\bar{\nu}$	24.6	40.	4.98	.161	4.98	2853-2762
62	2	12/13/76	$\bar{\nu}$	24.6	40.	4.98	.161	4.98	2770-2685
62	3	12/14/76	$\bar{\nu}$	24.6	40.	4.98	.161	4.98	2693-2590
62	4	12/15/76	$\bar{\nu}$	24.6	100.	4.98	.161	4.98	2596-2522
62	5	12/16/76	$\bar{\nu}$	24.6	300.	4.98	.161	4.98	2531-2444
63	1	12/17/76	$\bar{\nu}$	25.1	40.	9.82	.317	9.82	2855-2764
63	2	12/20/76	$\bar{\nu}$	25.1	40.	9.82	.317	9.82	2770-2671
64	1	12/21/76	s+γ	25.7	20.	5.00	.161	413.6	2834-2828
64	2	12/21/76	s+γ	25.7	20.	5.00	.161	413.6	2766-2762
64	3	12/21/76	s+γ	25.7	20.	5.00	.161	413.6	2660-2654
64	4	12/21/76	s+γ	25.7	20.	5.00	.161	413.6	2639-2633

RUN	SCAN	DATE	DATA TYPE	FILL TEMP.	PATH LENGTH	TOTAL H_2O V.P.	CALIB. HDO V.P.	AIR+H2O PRESSURE	CM^{-1} SCANNED
64	5	12/21/76	s+γ	25.7	80.	5.00	.161	413.6	2578-2575
64	6	12/21/76	s+γ	25.7	200.	5.00	.161	413.6	2546-2542
65	1	12/22/76	s+γ	25.7	20.	5.00	.161	760.1	2834-2828
65	2	12/22/76	s+γ	25.7	20.	5.00	.161	760.1	2766-2762
65	3	12/22/76	s+γ	25.7	20.	5.00	.161	760.1	2660-2654
65	4	12/22/76	s+γ	25.7	20.	5.00	.161	760.1	2639-2633
65	5	12/22/76	s+γ	25.7	80.	5.00	.161	760.1	2578-2575
65	6	12/22/76	s+γ	25.7	200.	5.00	.161	760.1	2546-2547
69	1	1/7/77	D_2O		20.	sat'd	D_2O	230.	2875-2646
69	2	1/8/77	D_2O		20.	sat'd	D_2O	225.	2659-2306
69	3	1/10/77	D_2O			sat'd	D_2O	225.	2875-
72	1	2/12/77	$\bar{\nu}$		60.	10.0 Torr	60:1 HDO	no air	2605-2465
72	2	2/14/77	$\bar{\nu}$		100.	9.63 Torr + 3.00 Torr	60:1 HDO 50:1 N_2O	no air	2607-2492